Title
Effector Functions and Regulation of Host Antiviral Immunity

Author
Liu, Su-Yang

Publication Date
2012

Peer reviewed|Thesis/dissertation

UNIVERSITY OF CALIFORNIA
Los Angeles

Effector Functions and Regulation of Host Antiviral Immunity

A dissertation submitted in partial satisfaction of the requirements for the degree Doctor of Philosophy in Microbiology, Immunology, and Molecular Genetics

by

Su-Yang Liu

2012

ABSTRACT OF THE DISSERATION

Effector Functions and Regulation of Host Antiviral Immunity

By

Su-Yang Liu
Doctor of Philosophy in Microbiology, Immunology, and Molecular Genetics
University of California, Los Angeles, 2012
Professor Genhong Cheng, Chair

Interferons (IFNs) are essential anti-viral cytokines that suppress viral infections by upregulation of antiviral effectors, collectively called interferon-stimulated genes (ISGs). We identified ISGs by gene expression profiling and performed functional screen of 288 ISGs that have antiviral activity against vesicular stomatitis virus (VSV) and murine gammaherpes virus (MHV68). Validation of antiviral genes from the screen demonstrated ISGs have inhibitory effect on specific virus. In particular, BMP2 inhibited MHV68 but not VSV replication. Conversely, Tap1 overexpression and deficiency led to resistance and susceptibility to VSV infection, respectively, while having effect on MHV68 growth.

Initially identified by its antiviral activity against VSV and MHV68, cholesterol-25-hydroxylase (Ch25h) was found to be an ISG that cause antiviral effect by production of a soluble oxysterol, 25-hydroxycholesterol. Toll-like receptor agonists induced Ch25h in an IFN-dependent manner. Ch25h overexpression and 25HC treatment broadly inhibited replication of other enveloped RNA and DNA viruses, including HIV, HSV, RSSEV, RVFV, and EBOV. Ch25h and 25HC inhibited efficiency of viral fusion in VSV

and HIV. Administration of 25HC suppresses HIV replication in humanized mice, while functional loss of Ch25h lead to increased susceptibility to infections *in vitro* and *in vivo*.

Since interferons regulate many genes that can have profound impact on cellular homeostasis, regulation of IFN is tightly regulated. We have identified retinoid-X-receptors (RXR) to be a suppressor of type-I IFN response. Overexpression of RXR and activation of RXR with RXR-specific agonists led to increased viral susceptibility to viral infection in RAW264.7 cell lines. Functional loss of RXR in F9 embryonal caricoma cell lines led to increased resistance to viral infection. RXR agonists inhibited phosphorylation of upstream signaling activators of IFN, TBK and IRF3. Gene expression analyses show RXR inhibited many ISGs induced by dsRNA mimetic, polyI:C and partial suppression of genes induced by lipidA.

In effort to use virus as a tool to improve immunity, we developed an approach for live-attenuated vaccine development by genome-wide profiling. Using flu as a model, we generated high-density mutations in the influenza (WSN strain) M-gene and profiled the fitness of every mutation *in vivo* through time. By selecting mutants that exhibited an attenuated growth profile, we identified a mutant, W7-791, that grew *in vitro*, infected mice, and was not virulent. Vaccination of mice with W7-791 conferred protection against lethal infectious dose of two strains of H1N1 influenza and a phylogenetically disparate, H3N2 virus.

The dissertation of Su-Yang Liu is approved.

_____
Asim Dasgupta

_____
Peter Tontonoz

_____
Jerome Zack

_____
Genhong Cheng, Committee Chair

UNIVERSITY OF CALIFORNIA, Los Angeles
2012

To my mom, for teaching me,

There is a right time to do the right thing,

To my dad, for encouraging me,

Never will there be this time and opportunity,
To focus all your efforts on solving a problem.

TABLE OF CONTENTS

LIST OF FIGURES AND TABLES

ACKNOWLEDGEMENTS

I sincerely express my gratitude for my mentor, Genhong Cheng. Entering the lab with hardly an idea of what I would like to focus on, he provided vision and leadership. His enthusiasm for new ideas was inspiring and infectious, motivating me to explore fearlessly many research direction. As I became more focused on my projects, he became more a colleague. He was always enthusiastic to help interpret data and discuss future directions, whether it was in his office or in the hallway. Vision, ingenuity, and relentless enthusiasm for science are his qualities that I will continue to aspire to.

I would like to thank members of my committee. Dr. Peter Tontonoz was invaluable in the RXR project, providing advice and reagents. He also encouraged me to explore in Ch25h, which became my major work. Dr. Asim Dasgupta pushed me very early on to think about host-pathogen interaction from pathogen angle in addition to just from the perspective of the host. It helped me think about using molecular tools in virology to probe host antiviral mechanisms. Dr. Jerome Zack was helpful mentor and collaborator on HIV studies. I specially thank Dr. Benhur Lee for his mentorship and collaboration. His expertise and willingness has helped me address the hardest question of my project. His curiosity and constructive critiques have strengthened the quality of my work.

I am indebted to many wonderful colleagues in the Cheng lab for this work. Dr. David Sanchez was a great mentor, colleague, and friend. Through our frequent, random scientific discussions---although often unproductive—we found a way to screen for antiviral ISGs. Thanks to Dr. Roghiyari (Saba) Aliyari, who in a short one-year time, has helped our progress in understanding Ch25h antiviral mechanisms. Dr. Feng Ma is

a brilliant collaborator who has helped us gain deeper mechanistic understanding of RXR regulation of antiviral function. The flu project was initiated with Dr. Hsiang-Wen (Sharon) Chen, who performed flu M-gene mutagenesis and initial characterization of mutants *in vivo* and *in vitro*. Lulan Wang helped follow the work with modeling and genotyping study. Dr. Jane Deng and Dr. Xiaoli Tian helped perform mouse experiments, taught me how to do intratracheal injections, and helped develop the initial concept of the project. Dr. Yao Wang was tremendously helpful in my understanding of virology. She provided essential reagents for Ch25h and influenza studies as well as provided insight on the ISG work. Dr. Bahram Razani helped me start the RXR project and provided scientific guidance and encouragement throughout the years. My gratitude extends to all labmates; like family, they have unconditionally supported me throughout these memorable years.

For ISG project, Dr. Sun Lu and Genecopoeia Inc. provided ISG expression plasmids. Ting-ting Wu and Dr. Ren Sun provided MHV-68 and advice on methods. Iven Li helped me purify the plasmids. For the Ch25h project, I especially thank Kelechi Chikere and Olivier Pernet from Benhur Lee's lab for helping uncover the mechanism of 25HC inhibitory effect on HIV and viral entry. Thanks to our collaborators in UTMB, Jennifer Smith, Rebecca Nusbaum, and Dr. Alexander Freiberg, who tested the effect 25HC on various pathogenic viruses and provided understanding on the breadth of antiviral effect of 25HC. I thank Dr. Guangming Li and Dr. Lishan Su for testing the effect of 25HC on humanized mice. Dr. Matthew Marsden who initially helped me test 25HC on HIV in human PBMC that led to subsequent work on HIV. Dr. David Russell provided *Ch25h-/-* cells during the initial studies. Dr. Elizabeth Tarling and Dr. Peter

Edwards provided SREBP constructs. For the flu project, Dr. Vaithilingaraja Arumugaswami provided guidance on mutagenesis assay. Dr. Yuying Liang for providing the 8-plasmid reverse genetics system. Dr. Ioanna Skountzou and Dr. Joshy Jacobs for providing mouse-adapted H3N2/Victoria.

The work was supported by UCLA Medical Scientist Training Program, Tumor Immunology Training Grant (NRSA, NIH), and the Warsaw Fellowship.

BIOGRAPHICAL SKETCH

2002	Research student. American Cancer Society Fuller Fellowship. Massachusetts General Hospital, Boston, MA
2002	Genetics Teaching Assistant. Brown University, Providence, RI
2003-2004	Immunology Teaching Assistant. Brown University, Providence, RI
2003-2004	Research student. Howard Hughes Fellowship. Brown University, Providence, RI
2003-2004	Undergraduate Researcher. Dept. of Molecular Biology, Brown University, Providence, RI
2004	Bachelor of Science in Biochemistry, Brown University, Providence, RI
2004-2005	Research Assistant. Partner's AIDS Institute, Massachusetts General Hospital, Boston, MA
2005-present	Graduate Student. Medical Scientist Training Program, UCLA, Los Angeles, CA

PUBLICATIONS

Su-Yang Liu, David J. Sanchez, Rogiyarhi Aliyari, Genhong Cheng. Systematic Identification of Type I and II Interferon Induced Anti-Viral Effectors. *PNAS*. 109:11 4239-4244.

Su-Yang Liu, David J. Sanchez, Genhong Cheng. New Developments in the Induction and Antiviral Effectors of Type I Interferon. *Current Opinions in Immnology.* 2011. 23, 57-54. (PMCID: 257232)

Arash Shahangian, Edward K. Chow, Xiaoli Tian, Jason R. Kang, Amir Ghaffari, **Su-Yang Liu,** John A. Belperio, Genhong Cheng, Jane C. Deng, Type I IFNs mediate development of postinfluenza bacterial pneumonia in mice. *J. Clin. Invest.* 2009; 119(7):1910

Joshua J Blakeslee, Hong-Wei Zhou, Jeffrey T. Heath, Kyle R. Skottke, Jorge A. Rodriguez Barrios, **Su-Yang Liu**, Alison DeLong. Specificity of RCN1-mediated protein phosphatase 2A regulation in meristem organization and stress response in roots. *Plant Physiology* 2008 146:539-553

Supriya K Saha, Eric M Pietras, Jeannie Q He, Jason R Kang, **Su-Yang Liu**, Gagik Oganesyan, Arash Shahangian, Brian Zarnegar, Travis L Shiba, Yao Wang and Genhong Cheng. Regulation of antiviral responses by a direct and specific interaction between TRAF3 and Cardif. *The EMBO Journal* 2006. 25, 3257–3263.

William G. Tharp, R. Yadav, D. Irimia, A. Upadhyaya, A. Samadani, O. Hurtado, **Su-Yang Liu**, S. Munisamy, D. M. Brainard, M. J. Mahon, S. Nourshargh, A. van Oudenaarden, M. G. Toner, and Mark C. Poznansky. Neutrophil chemorepulsion in defined interleukin-8 gradients in vitro and in vivo. *J. Leukoc. Biol.* 2006 79: 539-554

Daniel Irimia, **Su-Yang Liu**, William G. Tharp, Azadeh Samadani, Mehmet Toner and Mark C. Poznansky. Microfluidic system for measuring neutrophil migratory responses to fast switches of chemical gradients. *Lab Chip*, 2006, 6, 191-198.

ABSTRACTS

Su-Yang Liu, Daniel Irimia, William G. Tharp, Azadeh Samadani, Mehmet Toner, Mark C. Poznansky. Microfluidics System for Measuring Neutrophil Migratory Responses to Rapid Changes of Chemokine Gradients. *Infectious Disease Society of America, poster. 2005*

INTRODUCTION

Viruses are obligatory pathogens that exploit host factors for its survival. In vertebrates, the innate and adaptive immune systems play unique roles in eliminating viral infections. Innate immunity rapidly responds to an infection by production of cellular factors that generate an antiviral state. Immune recognition by the adaptive immune system—consisting B and T cells—leads to targeted elimination of virus and establishment of immune memory. This series of studies describe functional effectors and metabolic regulation of innate antiviral factors as well as an approach to design live-attenuated vaccines to stimulate adaptive immunity.

In order to promptly respond to infection, a cell expresses multiple extracellular and intracellular sensors, called pattern-recognition receptors (PRRs), which recognize microbial components distinct from host cell. Toll-like receptors (TLRs), present on cell membrane or in endosomes, are innate sensors that sense bacterial or viral components. TLR1, TLR2, and TLR6 recognize a variety of microbial components. TLR5 senses the bacterial protein flagellin. TLR7 and TLR9 sense DNA with unmethylated CpG motifs common in bacteria. TLR3 are sensors for double-stranded RNA (dsRNA) produced by many viruses during their replication (Takeda et al., 2003). While TLRs are sensors for extracellular pathogenic components, a second line of sensory mechanism exists in the cytoplasm and is likely primary sensors for viruses. Rig-I (Ddx58) and Mda5 (Ifih1) were first identified to bind to double-stranded RNA (polyI:C) (Takeuchi and Akira, 2008). Subsequent studies have identified other intracellular receptors for DNA and RNA such as DDX41, DDX1, DDX21, and DDX36, suggesting that a wide array of viral sensors exist (Zhang et al., 2011a, 2011b).

TLRs and intracellular receptors signal through different molecular pathways, the subject has been extensively researched and reviewed (Seth et al.; Kawai and Akira, 2006a, 2006b). Despite the complexity of cellular signaling pathways, they activate a few common transcriptional factors, namely IRF3, NFκB, and AP-1, which induce the expression of important genes that determine the overall cellular response. PRRs that sense viral infections, TLR3, TLR4, RIG-I, and MDA5, activate these transcription factors to produce type-I interferon, an essential cytokine that establish the antiviral state.

Interferons (IFN), represented by different structural types, eliminate microbial infections by activation diverse set of IFN-stimulated genes (ISGs). Type I IFN consists of many isoforms, IFNα, β, ω, with α and β as the most broadly expressed and well characterized forms. In response to PRR activation, many cell types can secrete type-I IFNs, while dendritic and macrophages are believed to be dominant producers. On the other hand, only immune cells, particularly T and NK-cells, secrete the type-II IFN, IFNγ. While they have distinct physiological roles and anti-microbial effects---IFNγ associated as being anti-bacterial--both types of IFNs have antiviral functions.

Type I and II IFNs activate IFNα receptors (IFNAR) and IFNγ receptors (IFNGR), respectively, which are ubiquitously expressed. The heterodimeric IFNAR signals to through Janus kinases, Tyk2 and Jak1, to recruit of STAT1 and STAT2. Phosphorylation of STAT1 and STAT2 lead to heterodimer formation and migration to the nucleus, where they complex with transcription factor IRF9 (p48) to form a trimer called IFN-stimulated gene factor 3 (ISGF3). This active transcriptional complex binds to

upstream IFN-stimulated response elements (ISRE) and drive expression of many interferon-stimulated genes (ISGs) (Decker et al., 2005). IFNGR activation by IFNγ recruits predominantly STAT1 and lead to phosphorylation and homodimerization of STAT, which can bind to promoters with gamma-responsive elements (GAS) and induce expression of different ISGs. Importantly, IFNAR also causes STAT1 homodimer formation and activate similar IFNγ-induced genes. Many IFNγ-induced genes, however, are not responsive to type-I IFN, suggesting IFNGR activates other unique signaling pathways (Schroder et al., 2004).

The diverse functions of IFN-stimulated genes include, but are not limited to, amplification of IFN response, control of cell survival and metabolism, activation and recruitment of other immune cells, and direct inhibition of viral replication. Antiviral ISGs suppress growth of viruses by inhibiting particular stages of their lifecycle. For example, OAS1 proteins activate mechanisms to degrade viral RNA, PKR inhibits viral translation, and tetherin prevents release of virions from the cell. **Chapter 1** reviews current understanding of antiviral ISGs and their inhibitory mechanisms on viruses. In general, only a minor proportion of ISGs has been characterized and most of them remain elusive. Hence, **chapter 2** describes a study to systematically identify antiviral ISGs against a RNA and DNA virus. **Chapter 3** further explores a previously unidentified antiviral ISG, cholesterol-25-hydroxylase, in its mechanism of action and physiological importance.

While IFNs are critically important for the antiviral response, their expression is tightly regulated because they have profound effects on cellular homeostasis. Metabolic regulators, such as nuclear receptors, can affect immune processes. For

example, activation of glucocorticoid receptors, a steroid receptor, inhibits inflammatory gene activation through suppression of NFκB activity. Metabolic factors that regulate IFN production are less understood. **Chapter 4** details a study on the regulation of IFN and its ISGs by the nuclear receptor, Retinoid-X-Receptor, and the functional consequences of this regulatory pathway on viral infections.

The immune system has co-evolved with viruses in a competition for survival. Pathogenic viruses, such as influenza, have the ability to inhibit IFN production and mutate quickly enough to escape the host response. In some cases, both innate and adaptive immunity are insufficient for host protection. Vaccination, either using killed or attenuated viruses, is an effective way to generate immunological memory against pathogenic viruses. In particular, live-attenuated vaccines are more immunogenic, presumably because they stimulate a better immune response by establishing a real infection. Live-attenuated vaccine design, however, has been largely a trial-and-error process with little understanding of mutations that cause attenuation. Using influenza as a model, **chapter 5** outlines an unbiased approach to comprehensively find mutations that would cause viral attenuation for the purposes of vaccine development.

REFERENCES

Decker, T., Muller, M., and Stockinger, S. (2005). The Yin and Yang of type I interferon activity in bacterial infection. Nat Rev Immunol *5*, 675–687.

Kawai, T., and Akira, S. (2006a). Innate immune recognition of viral infection. Nat Immunol *7*, 131–137.

Kawai, T., and Akira, S. (2006b). TLR signaling. Cell Death Differ *13*, 816–825.

Schroder, K., Hertzog, P.J., Ravasi, T., and Hume, D.A. (2004). Interferon-γ: an overview of signals, mechanisms and functions. Journal of Leukocyte Biology *75*, 163 – 189.

Seth, R.B., Sun, L., and Chen, Z.J. Antiviral innate immunity pathways. Cell Res *16*, 141–147.

Takeda, K., Kaisho, T., and Akira, S. (2003). Toll-Like Receptors. Annu. Rev. Immunol. *21*, 335–376.

Takeuchi, O., and Akira, S. (2008). MDA5/RIG-I and virus recognition. Current Opinion in Immunology *20*, 17–22.

Zhang, Z., Kim, T., Bao, M., Facchinetti, V., Jung, S.Y., Ghaffari, A.A., Qin, J., Cheng, G., and Liu, Y.-J. (2011a). DDX1, DDX21, and DHX36 Helicases Form a Complex with the Adaptor Molecule TRIF to Sense dsRNA in Dendritic Cells. Immunity *34*, 866–878.

Zhang, Z., Yuan, B., Bao, M., Lu, N., Kim, T., and Liu, Y.-J. (2011b). The helicase DDX41 senses intracellular DNA mediated by the adaptor STING in dendritic cells. Nat Immunol *12*, 959–965.

CHAPTER 1

Antiviral Functions of Interferon-Stimulated Genes

Available online at www.sciencedirect.com
ScienceDirect
Current Opinion in Immunology

New developments in the induction and antiviral effectors of type I interferon

Su-Yang Liu, David Jesse Sanchez and Genhong Cheng

Type I interferons (IFNs) are cytokines of the innate immune system that induce antiviral protein expression in response to viral infection. Various proteins and pathways have been shown to recognize nucleic acid ligands especially from RNA viruses. Here, we will review recent developments including transcription of DNA virus genomes into RNA ligands, and the recognition of viruses by TLR2 for interferon induction. The induced IFNs activate many interferon stimulated genes (ISGs) that have direct antiviral effects. Recent studies have identified IFITM proteins as the first ISG to inhibit viral entry processes and revealed mechanistic understanding of known antiviral ISGs such as ISG15 and Viperin.

Address
Department of Microbiology, Immunology & Molecular Genetics, University of California, Los Angeles, CA 90095, USA

Corresponding author: Cheng, Genhong (gcheng@mednet.ucla.edu)

Current Opinion in Immunology 2011, **23**:57–64

This review comes from a themed issue on
Innate immunity
Edited by Robert Modlin and Laurie Glimcher

Available online 29th November 2010

0952-7915/$ – see front matter

DOI 10.1016/j.coi.2010.11.003

Introduction

Type I interferon (IFN) is a key innate immune cytokine produced by cells to combat viral infections. Intricate sensory mechanisms detect invading viruses and rapidly trigger interferon production. Recognition of distinctive viral nucleic acids as a pathogen associated molecular patterns (PAMPs) by cellular pattern recognition receptors (PRRs) will lead to IFN induction. While RNA virus recognition is well understood, new pathways are constantly being elucidated and the receptor for DNA viruses is a subject of intense research. The first part of this review will discuss recent advances in understanding how virus infection leads to IFN production.

Release of interferon after viral recognition signals to cells to induce the expression of a set of interferon stimulated genes (ISGs) that activate antiviral processes including amplification of interferon signaling, production of cytokines that activate adaptive immunity, and many factors that directly inhibit viruses. ISGs with direct antiviral functions remain poorly understood, largely because they are virus-specific and can have multiple mechanisms. The second part of this review will cover well-known and novel ISGs focusing on recent developments in understanding their antiviral function.

Old and new paths to IFN induction

The mechanism involved in how cells exposed to viruses or virion components 'know' to release IFN has not been well understood until recently. The discovery of the Toll like receptors (TLRs) as receptors for extracellular or endocytosed viral components was a major advance in understanding viral recognition in the IFN process [1]. Likewise, the recent discovery of the RIG-I-like RNA Helicases as RNA virus sensors has elucidated how a cell detects an active intracellular virus infection [2]. Signaling downstream of these receptors has been well studied and although some questions on the biochemical level remain, the signaling pathways generally converge on the activation of TANK-binding kinase 1 (TBK1) that phosphorylates and activates the interferon regulatory factors (IRFs 3 and/or 7) (Figure 1).

In addition, to TBK1 in this pathway, IFN induction through a LRRFIP1 mediated pathway was demonstrated in mouse peritoneal macrophages exposed to intracellular DNA or RNA. LRRFIP1 is a leucine rich repeat domain containing protein similar to the TLRs but cytoplasmic in localization [3•]. Intriguingly, induction of IFN-β by LRRFIP1 recognition of free nucleic acids is dependent on β-catenin, a well-known coactivator of transcription [4]. LRRFIP1 recognition of bacterial DNA or vesicular stomatitis virus (VSV) infection recruits β-catenin to the nucleus in an IRF-3 dependent manner (Figure 1). Nuclear β-catenin can function to activate CBP/p300 that enhances acetylation and activation of the IFN-β promoter. These findings show a novel IFN induction pathway that works with the canonical TBK1/IRF pathways. In fact, most of the recent advancements in understanding IFN induction underscore the need for critical examination of structured paradigms of innate immunity.

New players in recognition of DNA virus infection

A search for the primary DNA virus receptor has fueled much research over the past years. From the discovery of DAI, a protein that seemed critical for DNA induced IFN to the *in vivo* finding that DAI may be redundant, many groups have searched for the 'key' DNA receptor or

Figure 1

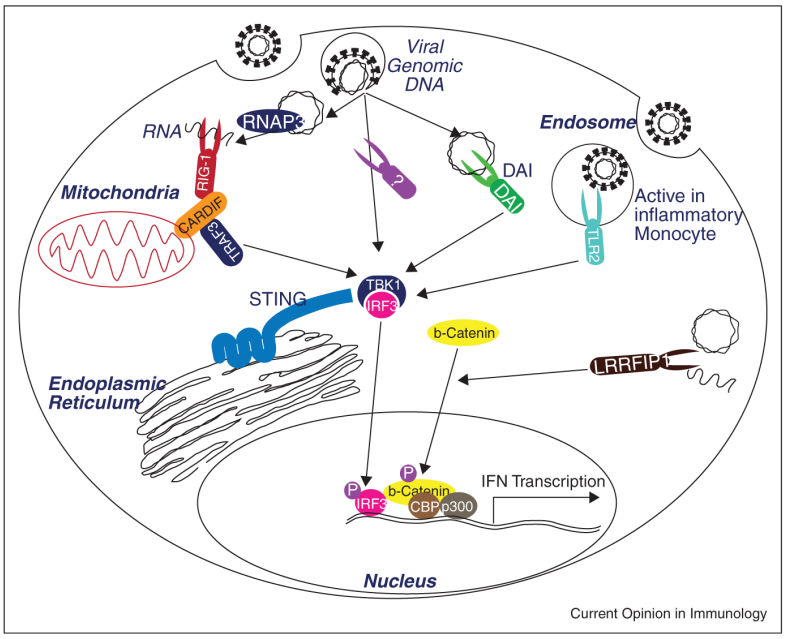

Old and new players in the induction of IFN. TANK-binding kinase-1 (TBK1) is the primary IRF3 activating kinase. IRF3 is activated by phosphorylation, after which is translocated to the nucleus and induce interferon gene transcription. DNA induction of this pathway may occur by RNA polymerase III (RNAP3) transcription of abundant DNA into RNA, which can then function as a RIG-I substrate. RIG-I is well known in RNA induction pathways to signal through CARDIF, a mitochondrial adaptor to TRAF3 and downstream to TBK1. In addition, DAI has been found to recognize DNA and induce signals downstream to TBK1. Further studies may reveal new receptors that are either parallel or a more primary receptor for DNA than either DAI or RNAP3. However, STING has recently been found to be an ER associated multi-membrane protein that is required for signaling by these nucleic acid receptors, potentially by serving as a signaling docking and coordination center. In addition, TLR2 has recently been found to induce IRF3 activation in inflammatory monocytes by signaling from endosomal compartments. Finally, LRRFIP1 has recently been found to respond to cytoplasmic nucleic acids and signal to induce β-catenin phosphorylation. Phosphorylated β-catenin translocates to the nucleus and is recruited to interferon promoters to activate CBP/p300 that then induces acetylation and activation of the interferon promoter in a mechanism whose importance is still being dissected.

sought to understand how DNA recognition occurs [5,6]. A major development is the discovery that the protein STING is necessary for IFN induction by exposure to B-DNA and the DNA virus HSV-1 [7••,8••]. STING is an ER-localized, multi-transmembrane domain protein that interacts with IRF-3, TBK1, CARDIF, and RIG-I, and seems to coordinate the signaling of IFN induction. Although, this protein is not a DNA receptor, STING deficient mice represent one of the first knockouts that are compromised in IFN induction capacity by all exogenous DNA or DNA viruses.

In the past year, the hypothesis that the DNA receptor directly binds to DNA was found to be insufficient. Two reports show that rather than DNA recognition, RNA transcribed from cytoplasmic DNA can function as a ligand for RIG-I induced IFN [9]. Here abundant cytoplasmic DNA containing AT-rich regions can be transcribed by RNA polymerase III (RNAP3) and the RNA transcripts are recognized by the RIG-I pathway, in effect turning viral DNA into RNA PAMPs. RNAP3 is important in cells transfected with B-DNA or infected at high MOI with HSV-1 [9]. Epstein-Barr virus (EBV) also transcribes small RNAs via RNAP3 from viral DNA into RIG-I ligands. Whether RNAP3 transcription of viral DNA is physiologically relevant remains a central question.

TLR2 as a virus receptor for interferon induction

The endosomal TLRs 3, 7, 8 recognize extracellular viral RNA PAMPs, while TLR9 recognizes CpG DNA and can lead to IFN production upon activation. Other TLRs were thought to primarily be inducers of inflammatory cytokines, none more so than TLR2.

However, in inflammatory monocytes, a small distinct fraction of bone marrow, TLR2 was found to be required for vaccinia virus induced IFN induction [10•]. Ablation of this cell type, which is not present in standard bone marrow derived macrophages or DCs, leads to increased susceptibility to vaccinia virus infection *in vivo*. TLR2

localizes to endosomal compartments in this cell type where it can induce IFN. This observation suggests that cellular localization of TLR2 can alter its downstream signaling potential. Classical bacterial ligands at the cell surface ligate to TLR2 where a distinct array of signaling adaptors induce inflammatory genes. However, signaling proteins localized to the endosome may be specialized to signal from TLR2 to induce IFN. As most of the nucleic acid sensing TLRs (3/7/8/9) are localized to the endosome, this model is consistent with the paradigm that the endosomal system represents a major hub of virus recognition and signaling.

Interferon stimulated genes

Viral recognition induces the release of IFN that signals to surrounding cells creating the 'antiviral state' that was described as far back as the original IFN studies. Expression array studies have shown that hundreds of genes are induced by IFN. While some ISGs such as protein kinase R (PKR), 2′5-oligoadenylate synthetase, and Mx GTPases have well described antiviral functions and mechanisms [11–13], functions of most ISGs are poorly characterized with little or no mechanistic understanding. Table 1 summarizes most of the known antiviral ISGs. Here, we review recent developments in ISG function (Figure 2).

IFITM3

The interferon induced transmembrane (IFITM) proteins 1, 2, and 3 were identified as the first host factors that restrict viral entry [14••]. Brass showed that overexpression of IFITM 2 and 3 significantly inhibited influenza, VSV, West Nile, and Dengue virus [14••]. Conversely, knockdown of IFITM3 or deletion of the *Ifitm* locus in murine embryonal fibroblast (MEF) increased susceptibility of the cells to viral infections. IFITM3 inhibited influenza pseudoviruses but not Machupo pseudoviruses, suggesting that IFITM3 inhibits viral entry processes because these pseudoviruses differ only in their envelopes. *Ifitm* deficient mice are viable, yet their susceptibility to viral infection is not known. Recently, IFITM3 was shown to be modified by S-palmitoylation, a post-translational modification that can regulate localization and function of membrane associated proteins. Interestingly, deletion of the palmitoylation site on IFITM3 abrogates its antiviral effect on influenza suggesting localization specific function [15].

The precise mechanism of the antiviral activity of IFITM3 awaits further studies. Overexpression and knockdown studies suggest that IFITM1, 2, and 3 may have non-redundant functions, but their effects on different viruses need to be further delineated. How IFITM3 affects entry steps, such as binding and fusion, is still unknown. Does it physically interact with influenza virions or does it recruit complexes to affect viral entry? IFITM3 may also have additional antiviral effects on assembly and budding.

ISG15

ISG15 is a 17 kDa ubiquitin-like protein that has been shown to inhibit replication of several viruses including influenza, sindbis, herpes, HIV, HPV, and Ebola. ISG15 modification, called ISGylation, occurs on over 100 cellular proteins and is catalyzed by the sequential action of the interferon-inducible E1, E2, and E3 ubiquitin ligases called UBE1L, UbcH8/Ube2L6, and Herc5, respectively [12,16]. Unlike canonical ubiquitination that targets proteins for degradation, ISGylation can have diverse effects. For example, ISGylation of IRF-3 inhibits its degradation and causes increase in its transcriptional activity [17]. ISGylation inhibits Ebola by blocking ubiquitin ligase Nedd4, which is required by viral budding [18].

One of the recent novel discoveries of the antiviral mechanism of ISG15 is the ISGylation of viral proteins. ISGylation of the influenza protein NS1 nuclear localization domain prevents its association with importin-alpha. Mutation of the ISGylation site conferred increased resistance of influenza virus in the presence of interferon [19,20•]. Other ISGylation sites have been found yet their functional significance is unclear. Interestingly, the amount of ISGylation of NS1 changes across different strains of influenza, which opens the question whether the propensity for ISGylation correlates with virulence [21]. While many proteins can be modified by ISG15, ISGylation seems to specifically modify newly synthesized host and viral proteins [16•]. This mechanism may help confer specific antiviral effects without causing global protein modifications in the cell.

Viperin

Viperin is an ER-associated ISG that inhibits HCV, HCMV, influenza, and HIV-1 through several mechanisms. Wang *et al.* showed that Viperin disrupts cell plasma membrane and lipid raft integrity and inhibits influenza virion budding [22]. Overexpression of farnesyl diphosphate synthase (FPPS), an enzyme required for isoprenoid synthesis and lipid metabolism, reversed this antiviral effect, suggesting that Viperin prevents viral budding through inhibition of FPPS [22].

Viperin may inhibit HCV replication through a different mechanism. HCV core and nonstructural (NS) proteins associate with lipid droplets, ER-associated organelles important for cellular protein and lipid trafficking that are thought to be a site of HCV replication in the cell [23]. Both Viperin and NS protein have an N-terminal amphipathic, alpha-helical domain required for localization to lipid droplets. More importantly, the N-terminal domain of Viperin is required for the inhibition of HCV [24]. Although these data suggest that Viperin can inhibit HCV in lipid droplets, it remains unclear whether there is direct association of Viperin with HCV proteins or whether the

Table 1

Summary of known antiviral functions of ISGs.

Interferon stimulated gene	Viruses inhibited and method of study	Antiviral mechanism
Protein kinase R	Overexpression of wild-type but not mutant PKR inhibits ECMV, vaccinia, HIV-1 [35–37]	*Translation inhibition*
	PKR deficient mice deleted are susceptible to VSV and influenza infections and increased HSV-1 susceptibility in neurons [38,39]	Binds to dsRNA and ssRNA and phosphorylates EIF2a, which prevents its guanine nucleotide exchange activity that is required for translational activity [12]
2′5-OAS and RNaseL	ssRNA viruses Picornaviridae, Reoviridae, Togaviridae, Paramyxoviridae, Orthomyxoviridae, Flaviviridae and Retroviridae [13,40,41]	*RNA degradation*
		Form short oligoadenylates from ATP, which activates RNaseL to degrade viral RNA [12]
TRIM5a	Stable expression of TRIM5a from Rhesus monkey in HeLa cells inhibits HIV-1 and SIV [42]	*Inhibition of viral cDNA synthesis and nuclear import* [43]
		Viral protein degradation
		Target HIV capsids and RT products proteosomal degradation [44]
APOBEC3G and APOBEC3F	Inhibits HIV-1, APOBEC3G and APOBEC3F deficient cell supports Vif-deficient HIV-1 [45]	*Mutation of HIV DNA*
	Expression inhibits parvoviruses and retrotransposons that is deaminase independent [45,46]	A cytidine deaminase that converts cytidine to uracil in the viral RNA, which subsequently leads to T/A hypermutation in the viral DNA after reverse transcription [47,48]. Catalytic activity not required for antiviral function [49]
		Inhibition of HIV-1 provirus formation
		A3G inhibits minus-strand to plus-strand step in reverse transcription [50]. A3F inhibits viral 3′ DNA processing [51]
		Inhibition of viral assembly
		A3G interacts with HIV RNA and Gag and packaged into viral particles [52]
ISG15	Influenza, Sinbis, HSV1, MHV68 [53,54]	*Modifying ubiquitination on many cellular and viral targets*
		ISGylation by ISG15 prevents IRF3 degradation [17]
		Indirectly prevents virion release
		Inhibits ubiquitination of HIV Gag and Tsg101 and prevents virion release [53]
ISG20	Overexpression inhibits VSV, EMCV, influenza, HIV [55,56]	A 3–5 exonuclease; mechanism is unclear [12]
IFITM1,2,3	Overexpression inhibits influenza, Dengue, West Niles virus, and VSV. Knockdown of IFITM3 increased susceptibility to influenza, WNV, and Dengue infection *in vitro* [14••]	*Inhibition of viral entry* [14••]
		Transmembrane protein. Antiviral mechanism unknown
Mx GTPases	Orthomyxoviruses, paramyxoviruses, rhabdoviruses, togaviruses, bunyaviruses including HBV, influenza, coxackie virus [11,26]	*Inhibition of vRNP trafficking*
		Human MxA targets viral necleocapsid structures and traps viral components [11,26]
		Inhibition of viral transcription
		MxA associates with influenza PB2 and prevents transcription of viral genome [11,26]
Viperin (Cig5)	Overexpression of Viperin inhibits hCMV [57] and HCV replication [24,58]	*Inhibition of budding*
		Disrupts lipid rafts [22]
	Induction of Viperin in HeLa cells inhibits influenza budding [22]	
	Viperin knockdown reduces TLR3 mediated inhibition of HIV-1 in astrocytes [59]	

Figure 2

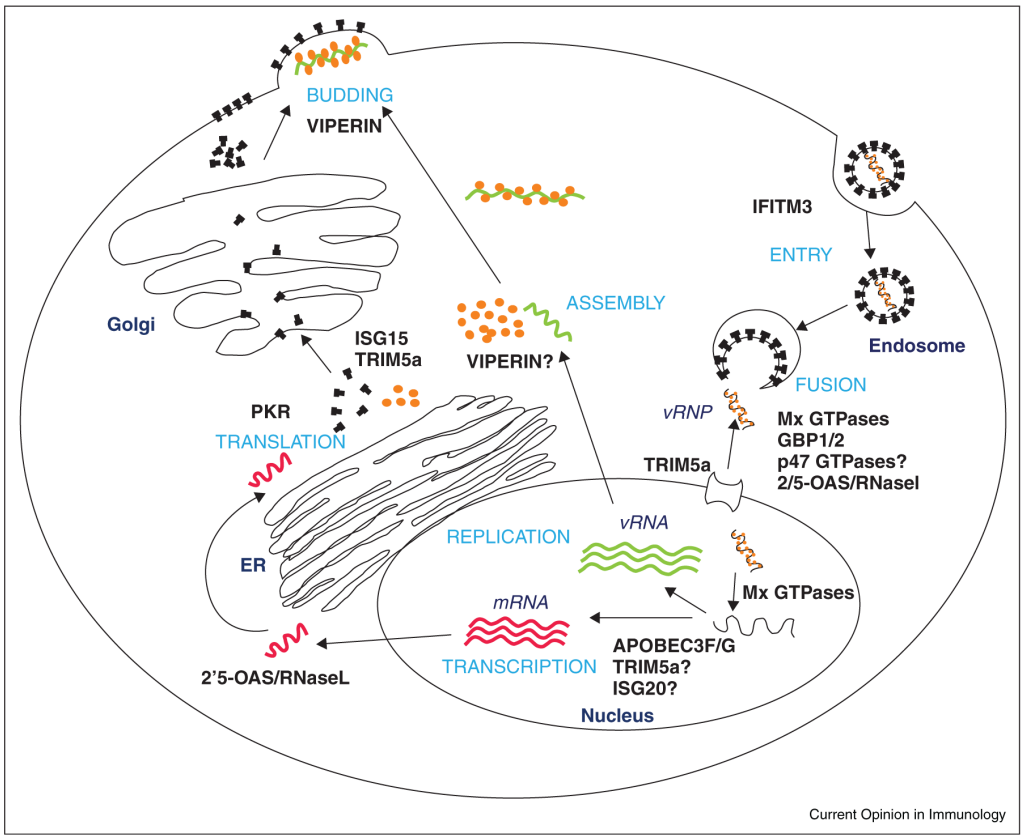

General antiviral mechanisms of interferon stimulated genes. The general lifecycle stages of an enveloped virus are depicted here (light blue letters). The virus binds to specific receptors on the cell surface and often enters the cell through endocytosis. Viral genetic material is released into the cytoplasm through pH-dependent or -independent fusion and may be subsequently transported to the nucleus. Replication of viral genetic material ensues along with mRNA transcription followed by transport to the ER for protein translation. Envelope proteins are transported to the cell surface while core viral proteins assemble with the viral genetic material. New virion particles are enveloped as they bud out of the plasma membrane. ISGs (in capital black bold letters) can inhibit viruses differently and at one or more stages of the viral lifecycle, see Table 1.

amphipathic sequence is necessary for its inhibitory activity.

Recent structural and biochemical studies identified Viperin is an S-adenosyl-L-methionine (SAM) enzyme that binds Fe–S clusters and catalyzes SAM to form 5′-deoxyadenosyl radicals [25]. The significance of this C-terminal catalytic domain is unknown and may be required for other cellular antiviral processes.

Interferon inducible GTPases

Both type I and type II interferon significantly induce expression of the Mx, p47, and p65 families of GTPases, which hydrolyze GTP and are well-known to confer resistance against a wide range of pathogens. The Mx proteins inhibit replication of orthomyxoviruses, Thogoto virus, bunyaviruses and rhabdoviruses [11,26]. The family of p47 GTPases, which consists of Iigp, Lrg47, Irg47, Tgtp, Iigp, and Gtpi, predominantly inhibits bacteria and protozoa growth [27]. Only Tgtp and Igtp overexpression *in vitro* have been shown to inhibit VSV [28] and coxackie viral replication [29], respectively. The family of p65 GTPases, also known as the guanylate-binding proteins (GBPs), is induced by all interferons, with more robust induction by interferon gamma. Overexpression of GBP-1 and GBP-2 inhibited VSV and encephalomyocarditis virus (EMCV) replication [30]. GBP-1 also reduces HCV replication, but replication competent HCV expresses NS5B that inhibit GBP-1 GTPase activity [31]. The functions of GBPs are largely unknown. GBP-2 can target to intracellular vesicles [32] and GBP-1 can form oligomers like Mx proteins [33], which may provide clues to their antiviral function. There may be more than one antiviral mechanism as exemplified by

the fact that GTP binding activity is required for the inhibition of EMCV but not VSV [34].

Concluding remarks

The complex host–virus interactions involved in mounting and executing an effective response to viral infections represent one of the major directions in innate immunity research. Although the general scheme for viral detection has been unraveled, much in terms of the actual ligands during an infection as well as the relative contribution of specific receptor signaling remains to be determined. One particularly important point will be defining the definitive detection pathway(s) for DNA viruses and testing whether detection through RNAP3 holds up in *in vivo* infections. While viral recognition remains an important subject of research, the elusive antiviral functions of ISGs against specific viruses are getting increased attention. Many studies have shown sufficiency of antiviral activity of ISGs, such as GBP-1, *in vitro*, but not necessity. The next level of studies will be to define physiological roles of such ISGs as is the case for IFITM3. Understanding of the interactions between ISGs and particular viral lifecycle processes will be particularly informative but not trivial. Nearly all the ISGs described here can inhibit viruses in more than one way and many of them may have redundant functions. In addition, how viruses have evolved ways to escape antiviral detection and effectors is equally important and lends another level of complexity to host–pathogen interactions. Elucidation of ISG and viral interaction may allow for the identification of susceptibility mutations and provide new approaches for viral therapy.

Acknowledgements

The authors were supported by funding from the National Institutes of Health (R01 AI069120, R01 AI078389 and PN2EY018228). We also thank the members of the Cheng laboratory for helpful discussions on the topic. We apologize for not recognizing authors who have made important contributions to the field of type I interferon induction and antiviral function due to reference limitation.

References and recommended reading

Papers of particular interest, published within the period of review, have been highlighted as:

- • of special interest
- •• of outstanding interest

1. Kawai T, Akira S: **Toll-like receptor and RIG-1-like receptor signaling**. *Ann N Y Acad Sci* 2008, **1143**:1-20.

2. Baum A, García-Sastre A: **Induction of type I interferon by RNA viruses: cellular receptors and their substrates**. *Amino Acids* 2010, **38**:1283-1299.

3. • Yang P, An H, Liu X, Wen M, Zheng Y, Rui Y, Cao X: **The cytosolic nucleic acid sensor LRRFIP1 mediates the production of type I interferon via a [beta]-catenin-dependent pathway**. *Nat Immunol* 2010, **11**:487-494.
In addition to the importance of LRRFIP1 in IFN induction, this paper strengthens the key role of β-catenin in IFN induction.

4. Stadeli R, Hoffmans R, Basler K: **Transcription under the control of nuclear arm/[beta]-catenin**. *Curr Biol* 2006, **16**:R378-R385.

5. Takaoka A, Wang Z, Choi MK, Yanai H, Negishi H, Ban T, Lu Y, Miyagishi M, Kodama T, Honda K *et al.*: **DAI (DLM-1/ZBP1) is a cytosolic DNA sensor and an activator of innate immune response**. *Nature* 2007, **448**:501-505.

6. Wang Z, Choi MK, Ban T, Yanai H, Negishi H, Lu Y, Tamura T, Takaoka A, Nishikura K, Taniguchi T: **Regulation of innate immune responses by DAI (DLM-1/ZBP1) and other DNA-sensing molecules**. In *Proceedings of the National Academy of Sciences* 2008, **105**:5477-5482.

7. •• Ishikawa H, Barber GN: **STING is an endoplasmic reticulum adaptor that facilitates innate immune signalling**. *Nature* 2008, **455**:674-678.
See annotation to Ref. [8••].

8. •• Ishikawa H, Ma Z, Barber GN: **STING regulates intracellular DNA-mediated, type I interferon-dependent innate immunity**. *Nature* 2009, **461**:788-792.
This study and Ref. [7••] define and study STING as a key molecule in DNA induced IFN.

9. Chiu Y, MacMillan JB, Chen ZJ: **RNA polymerase III detects cytosolic DNA and induces type I interferons through the RIG-I pathway**. *Cell* 2009, **138**:576-591.

10. • Barbalat R, Lau L, Locksley RM, Barton GM: **Toll-like receptor 2 on inflammatory monocytes induces type I interferon in response to viral but not bacterial ligands**. *Nat Immunol* 2009, **10**:1200-1207.
Although TLR2 is canonically inflammatory, here we see that TLR2 can induce IFN and protect from vaccinia virus infection by trafficking to the endosomes of inflammatory monocytes.

11. Haller O, Staeheli P, Kochs G: **Interferon-induced Mx proteins in antiviral host defense**. *Biochimie* 2007, **89**:812-818.

12. Sadler AJ, Williams BRG: **Interferon-inducible antiviral effectors**. *Nat Rev Immunol* 2008, **8**:559-568.

13. Hovanessian AG: **On the discovery of interferon-inducible, double-stranded RNA activated enzymes: The 2'-5'oligoadenylate synthetases and the protein kinase PKR**. *Cytokine & Growth Factor Reviews* 2007, **18**:351-361.

14. •• Brass AL, Huang I, Benita Y, John SP, Krishnan MN, Feeley EM, Ryan BJ, Weyer JL, van der Weyden L, Fikrig E *et al.*: **The IFITM proteins mediate cellular resistance to influenza A H1N1 virus, West Nile virus, and Dengue virus**. *Cell* 2009, **139**:1243-1254.
This is the first study that demonstrates IFITM family of proteins that inhibit entry processes of several RNA viruses.

15. Yount JS, Moltedo B, Yang Y, Charron G, Moran TM, López CB, Hang HC: **Palmitoylome profiling reveals S-palmitoylation-dependent antiviral activity of IFITM3**. *Nat Chem Biol* 2010, **6**:610-614.

16. • Durfee LA, Lyon N, Seo K, Huibregtse JM: **The ISG15 conjugation system broadly targets newly synthesized proteins: implications for the antiviral function of ISG15**. *Mol Cell* 2010, **38**:722-732.
This study provides insight on how specificity is conferred by ISGylation. The authors show ISGylation occurs only on newly synthesized host protein and HPV L1 protein.

17. Shi H, Yang K, Liu X, Liu X, Wei B, Shan Y, Zhu L, Wang C: **Positive regulation of interferon regulatory factor 3 activation by Herc5 via ISG15 modification**. *Mol Cell Biol* 2010, **30**:2424-2436.

18. Okumura A, Pitha PM, Harty RN: **ISG15 inhibits Ebola VP40 VLP budding in an L-domain-dependent manner by blocking Nedd4 ligase activity**. *Proc Natl Acad Sci USA* 2008, **105**:3974-3979.

19. Hsiang T, Zhao C, Krug RM: **Interferon-induced ISG15 conjugation inhibits influenza A virus gene expression and replication in human cells**. *J Virol* 2009, **83**:5971-5977.

20. • Zhao C, Hsiang T, Kuo R, Krug RM: **ISG15 conjugation system targets the viral NS1 protein in influenza A virus-infected cells**. *Proc Natl Acad Sci USA* 2010, **107**:2253-2258.
This study demonstrated ISGylation on NS1 of influenza in lysine 41 is partially responsible for its direct inhibitory effect on the virus.

21. Tang Y, Zhong G, Zhu L, Liu X, Shan Y, Feng H, Bu Z, Chen H, Wang C: **Herc5 attenuates influenza A virus by catalyzing ISGylation of viral NS1 protein**. *J Immunol* 2010, **184**:5777-5790.

22. Wang X, Hinson ER, Cresswell P: **The interferon-inducible protein Viperin inhibits influenza virus release by perturbing lipid rafts**. *Cell Host Microbe* 2007, **2**:96-105 This study to show mechanism of Viperin inhibition on influenza through changes in membrane integrity..

23. Miyanari Y, Atsuzawa K, Usuda N, Watashi K, Hishiki T, Zayas M, Bartenschlager R, Wakita T, Hijikata M, Shimotohno K: **The lipid droplet is an important organelle for hepatitis C virus production**. *Nat Cell Biol* 2007, **9**:1089-1097.

24. Jiang D, Guo H, Xu C, Chang J, Gu B, Wang L, Block TM, Guo J: **Identification of three interferon-inducible cellular enzymes that inhibit the replication of hepatitis C virus**. *J Virol* 2008, **82**:1665-1678.

25. Shaveta G, Shi J, Chow VT, Song J: **Structural characterization reveals that viperin is a radical S-adenosyl-l-methionine (SAM) enzyme**. *Biochem Biophys Res Commun* 2010, **391**:1390-1395.

26. Haller O, Stertz S, Kochs G: **The Mx GTPase family of interferon-induced antiviral proteins**. *Microbes and Infection* 2007, **9**: 1636-1643.

27. Taylor GA, Feng CG, Sher A: **p47 GTPases: regulators of immunity to intracellular pathogens**. *Nat Rev Immunol* 2004, **4**:100-109.

28. Carlow DA, Teh S, Teh H: **Specific antiviral activity demonstrated by TGTP, a member of a new family of interferon-induced GTPases**. *J Immunol* 1998, **161**:2348-2355.

29. Zhang HM, Yuan J, Cheung P, Luo H, Yanagawa B, Chau D, Stephan-Tozy N, Wong BW, Zhang J, Wilson JE *et al.*: **Overexpression of interferon-γ-inducible GTPase inhibits coxsackievirus B3-induced apoptosis through the activation of the phosphatidylinositol 3-kinase/akt pathway and inhibition of viral replication**. *J Biol Chem* 2003, **278**:33011-33019.

30. Anderson SL, Carton JM, Lou J, Xing L, Rubin BY: **Interferon-induced guanylate binding protein-1 (GBP-1) mediates an antiviral effect against vesicular stomatitis virus and encephalomyocarditis virus**. *Virology* 1999, **256**:8-14.

31. Itsui Y, Sakamoto N, Kakinuma S, Nakagawa M, Sekine-Osajima Y, Tasaka-Fujita M, Nishimura-Sakurai Y, Suda G, Karakama Y, Mishima K *et al.*: **Antiviral effects of the interferon-induced protein guanylate binding protein 1 and its interaction with the hepatitis C virus NS5B protein**. *Hepatology* 2009, **50**:1727-1737.

32. Gorbacheva VY, Lindner D, Sen GC, Vestal DJ: **The interferon (IFN)-induced GTPase, mGBP-2**. *J Biol Chem* 2002, **277**:6080-6087.

33. Prakash B, Praefcke GJK, Renault L, Wittinghofer A, Herrmann C: **Structure of human guanylate-binding protein 1 representing a unique class of GTP-binding proteins**. *Nature* 2000, **403**:567-571.

34. Carter CC, Gorbacheva VY, Vestal DJ: **Inhibition of VSV and EMCV replication by the interferon-induced GTPase, mGBP-2: differential requirement for wild-type GTP binding domain**. *Arch Virol* 2005, **150**:1213-1220.

35. Meurs EF, Watanabe Y, Kadereit S, Barber GN, Katze MG, Chong K, Williams BR, Hovanessian AG: **Constitutive expression of human double-stranded RNA-activated p68 kinase in murine cells mediates phosphorylation of eukaryotic initiation factor 2 and partial resistance to encephalomyocarditis virus growth**. *J Virol* 1992, **66**:5805-5814.

36. Lee SB, Esteban M: **The interferon-induced double-stranded RNA-activated human p68 protein kinase inhibits the replication of vaccinia virus**. *Virology* 1993, **193**: 1037-1041.

37. Muto NF, Martinand-Mari C, Adelson ME, Suhadolnik RJ: **Inhibition of replication of reactivated human immunodeficiency virus type 1 (HIV-1) in latently infected U1 cells transduced with an HIV-1 long terminal repeat-driven PKR cDNA construct**. *J Virol* 1999, **73**:9021-9028.

38. Balachandran S, Roberts PC, Brown LE, Truong H, Pattnaik AK, Archer DR, Barber GN: **Essential role for the dsRNA-dependent protein kinase PKR in innate immunity to viral infection**. *Immunity* 2000, **13**:129-141.

39. Leib DA, Machalek MA, Williams BRG, Silverman RH, Virgin HW: **Specific phenotypic restoration of an attenuated virus by knockout of a host resistance gene**. *Proc Natl Acad Sci USA* 2000, **97**:6097-6101.

40. Lin R, Yu H, Chang B, Tang W, Liao C, Lin Y: **Distinct antiviral roles for human 2′,5′-oligoadenylate synthetase family members against dengue virus infection**. *J Immunol* 2009, **183**:8035-8043.

41. Silverman RH: **Viral encounters with 2′,5′-oligoadenylate synthetase and RNase L during the interferon antiviral response**. *J Virol* 2007, **81**:12720-12729.

42. Stremlau M, Owens CM, Perron MJ, Kiessling M, Autissier P, Sodroski J: **The cytoplasmic body component TRIM5[alpha] restricts HIV-1 infection in Old World monkeys**. *Nature* 2004, **427**:848-853.

43. Berthoux L, Sebastian S, Sokolskaja E, Luban J: **Lv1 inhibition of human immunodeficiency virus type 1 is counteracted by factors that stimulate synthesis or nuclear translocation of viral cDNA**. *J Virol* 2004, **78**: 11739-11750.

44. Wu X, Anderson JL, Campbell EM, Joseph AM, Hope TJ: **Proteasome inhibitors uncouple rhesus TRIM5α restriction of HIV-1 reverse transcription and infection**. *Proc Natl Acad Sci USA* 2006, **103**:7465-7470.

45. Pion M, Granelli-Piperno A, Mangeat B, Stalder R, Correa R, Steinman RM, Piguet V: **APOBEC3G/3F mediates intrinsic resistance of monocyte-derived dendritic cells to HIV-1 infection**. *J Exp Med* 2006, **203**:2887-2893.

46. Bogerd HP, Wiegand HL, Doehle BP, Lueders KK, Cullen BR: **APOBEC3A and APOBEC3B are potent inhibitors of LTR-retrotransposon function in human cells**. *Nucleic Acids Res* 2006, **34**:89-95.

47. Harris RS, Bishop KN, Sheehy AM, Craig HM, Petersen-Mahrt SK, Watt IN, Neuberger MS, Malim MH: **DNA deamination mediates innate immunity to retroviral infection**. *Cell* 2003, **113**:803-809.

48. Strebel K, Luban J, Jeang K: **Human cellular restriction factors that target HIV-1 replication**. *BMC Med* 2009, **7**:48.

49. Bishop KN, Holmes RK, Malim MH: **Antiviral potency of APOBEC proteins does not correlate with cytidine deamination**. *J Virol* 2006, **80**:8450-8458.

50. Li X, Guo F, Zhang L, Kleiman L, Cen S: **APOBEC3G inhibits DNA strand transfer during HIV-1 reverse transcription**. *J Biol Chem* 2007, **282**:32065-32074.

51. Mbisa JL, Bu W, Pathak VK: **APOBEC3F and APOBEC3G inhibit HIV-1 DNA integration by different mechanisms**. *J Virol* 2010, **84**:5250-5259.

52. Strebel K, Khan M: **APOBEC3G encapsidation into HIV-1 virions: which RNA is it?** *Retrovirology* 2008, **5**:55.

53. Okumura A, Lu G, Pitha-Rowe I, Pitha PM: **Innate antiviral response targets HIV-1 release by the induction of ubiquitin-like protein ISG15**. *Proc Natl Acad Sci USA* 2006, **103**:1440-1445.

54. Lenschow DJ, Lai C, Frias-Staheli N, Giannakopoulos NV, Lutz A, Wolff T, Osiak A, Levine B, Schmidt RE, García-Sastre A *et al.*: **IFN-stimulated gene 15 functions as a critical antiviral molecule against influenza, herpes, and Sindbis viruses**. *Proc Natl Acad Sci USA* 2007, **104**:1371-1376.

55. Espert L, Degols G, Lin Y, Vincent T, Benkirane M, Mechti N: **Interferon-induced exonuclease ISG20 exhibits an antiviral activity against human immunodeficiency virus type 1**. *J Gen Virol* 2005, **86**:2221-2229.

56. Espert L, Degols G, Gongora C, Blondel D, Williams BR, Silverman RH, Mechti N: **ISG20, a new interferon-induced RNase specific for single-stranded RNA, defines an**

alternative antiviral pathway against RNA genomic viruses. *J Biol Chem* 2003, **278**:16151-16158.

57. Chin K, Cresswell P: **Viperin (cig5), an IFN-inducible antiviral protein directly induced by human cytomegalovirus**. *Proc Natl Acad Sci USA* 2001, **98**:15125-15130.

58. Helbig KJ, Lau DT, Semendric L, Harley HAJ, Beard MR: **Analysis of ISG expression in chronic hepatitis C identifies viperin as a potential antiviral effector**. *Hepatology* 2005, **42**:702-710.

59. Rivieccio MA, Suh H, Zhao Y, Zhao M, Chin KC, Lee SC, Brosnan CF: **TLR3 ligation activates an antiviral response in human fetal astrocytes: a role for viperin/cig5**. *J Immunol* 2006, **177**:4735-4741.

CHAPTER 2

Systematic Identification of Type I and II Interferon-Induced Antiviral Factors

Systematic identification of type I and type II interferon-induced antiviral factors

Su-Yang Liu[a], David Jesse Sanchez[b], Roghiyh Aliyari[a], Sun Lu[c], and Genhong Cheng[a,1]

[a]Department of Microbiology, Immunology, and Molecular Genetics, University of California, Los Angeles, CA 90095; [b]Department of Pharmaceutical Sciences, Western University of Health Sciences, Pomona, CA 91766; and [c]Guangzhou FulenGen Co. Ltd., Guangzhou City 510663, China

Edited by Owen N. Witte, University of California, Los Angeles, CA, and approved January 24, 2012 (received for review September 21, 2011)

Type I and type II interferons (IFNs) are cytokines that establish the cellular antiviral state through the induction of IFN-stimulated genes (ISGs). We sought to understand the basis of the antiviral activity induced by type I and II IFNs in relation to the functions of their ISGs. Based on gene expression studies, we systematically identified antiviral ISGs by performing blinded, functional screens on 288 type I and type II ISGs. We assessed and validated the antiviral activity of these ISGs against an RNA virus, vesicular stomatitis virus (VSV), and a DNA virus, murine gammaherpes virus (MHV-68). Overall, we identified 34 ISGs that elicited an antiviral effect on the replication of either one or both viruses. Fourteen ISGs have uncharacterized antiviral functions. We further defined ISGs that affect critical life-cycle processes in expression of VSV protein and MHV-68 immediate-early genes. Two previously undescribed antiviral ISGs, TAP1 and BMP2, were further validated. TAP1-deficient fibroblasts were more susceptible to VSV infection but less so to MHV-68 infection. On the other hand, exogenous BMP2 inhibits MHV-68 lytic growth but did not affect VSV growth. These results delineate common and distinct sets of type I and type II IFN-induced genes as well as identify unique ISGs that have either broad or specific antiviral effects on these viruses.

interferon stimulated genes | antiviral effectors | murine gammaherpes virus 68

The immune system inhibits viral growth through expression of a diverse set of antiviral genes. Interferons (IFNs) are potent activators of these antiviral factors. Type I IFNs, which include IFNα, -β, and -ω, are rapidly activated during viral infection and considered "antiviral" partly because IFNα receptor-deficient mice are highly susceptible to viral infections (1). Type II IFN, which is represented only by IFNγ, also inhibits growth of viral and other pathogenic infections. Both types of IFN induce expression of IFN-stimulated genes (ISGs) that have a variety of functions ranging from direct inhibition of viral components to activation of other immune cell types.

Type I and type II IFNs have distinct physiological roles, but they both can activate the cellular antiviral response. Many cell types, particularly macrophages and dendritic cells, secrete type I IFN through the activation of intracellular and extracellular sensors of viral components. Type I IFN acts in paracrine and autocrine fashion to activate IFN receptors (IFNARs) present on most cell types. Upon receptor ligation, IFNAR is phosphorylated by the kinases JAK1 and TYK2, which recruit and phosphorylate STAT1 and STAT2 proteins. STAT1 can homodimerize or heterodimerize with STAT2 and translocate into the nucleus to activate specific target promoters (2). Type II IFN is largely secreted by T and natural killer cells and is induced predominantly by IL-12 and IL-18 (3). IFNγ receptor (IFNGR) activation leads to phosphorylation and homodimerization of STAT1 and target gene expression (3).

IFN-stimulated genes have diverse effects on different viruses and operate through distinct mechanisms. A comparison of ISGs that inhibit various RNA viruses shows that there are some that broadly inhibit RNA virus growth and others that are specific for particular viruses (4). We sought to identify and compare ISGs that inhibit growth of vesicular stomatitis virus (VSV), a negative-strand RNA virus, and murine gammaherpes virus 68 (MHV-68), a DNA virus. VSV is a neurotropic virus in the *Rhabdoviridae* family, which includes rabies virus. It infects most cell types and replicates lytically in the cytoplasm. MHV-68 is a member of the gammaherpes virus family that includes Kaposi sarcoma-associated herpes virus and Epstein–Barr virus. They can infect particular cell types and are thought to predominantly establish latency in B cells (5). These viruses are models for virology and several human-related diseases, yet a systematic identification of ISGs that inhibit these viruses has not been done.

In this study, we sought to compare IFNα and IFNγ induction of ISGs under an equivalent signaling input and systematically screened their effects on VSV and MHV-68 growth. We identified and validated known and unique ISGs that have broad and specific antiviral activity against these viruses.

Results

Both type I and type II IFNs broadly inhibit many types of viruses and elicit antiviral responses in various cell types. We hypothesized that IFNα and IFNγ can activate distinct and common ISGs that govern their antiviral effects. Because IFNα and IFNγ are structurally distinct cytokines that activate different receptors, we normalized IFNα and IFNγ concentrations based on phosphorylation of the shared and obligatory signaling factor STAT1 (6). Titration of both IFNs showed IFNγ phosphorylates STAT1 more than IFNα at equivalent units; for example, 1 U/mL of IFNγ phosphorylates STAT1 to an equivalent level as 62 U/mL of IFNα (Fig. S1 *A* and *B*). Based on this equivalent biological input, primary bone marrow-derived macrophages (BMMs) were stimulated with IFNα or IFNγ for 2.5 h in biological triplicates and processed for gene expression profiling by microarray (Fig. 1). Overall, IFNα and IFNγ regulated a common set of genes that had a significant correlation coefficient of 0.59. There were more ISGs induced by IFNα than IFNγ over untreated controls. Genes that were induced by IFNα threefold over IFNγ were classified as "IFNα-specific," and genes that were induced by IFNγ threefold more than IFNα were classified as "IFNγ-specific." Based on this categorization, 165 ISGs were IFNα-specific, 17 were IFNγ-specific, and 203 ISGs were commonly induced by both IFNs (Fig. 1, *Inset* and Table S1). These results suggest that under an equivalent signaling input, IFNα is a more efficient activator of gene expression than IFNγ.

To further understand the basis of type I and type II antiviral activity, we next sought to identify IFNα- and IFNγ-induced ISGs that inhibit replication of VSV and MHV-68. The ISGs identified in Fig. 1 and Table S1 were used to generate a list of human ISGs based on homology for study in HEK293T cells. ISGs in the same family were included, and some genes were omitted because they were not found in the human genome. We obtained 288 genes in pCMV-driven expression constructs. First, we per-

Author contributions: S.-Y.L., D.J.S., and G.C. designed research; S.-Y.L. and R.A. performed research; S.L. contributed new reagents/analytic tools; S.-Y.L. and G.C. analyzed data; and S.-Y.L. and D.J.S. wrote the paper.

The authors declare no conflict of interest.

This article is a PNAS Direct Submission.

Freely available online through the PNAS open access option.

Data deposition: The microarray data reported in this paper have been deposited in the Gene Expression Omnibus (GEO) database, www.ncbi.nlm.nih.gov/geo (accession no. GSE35825).

[1]To whom correspondence should be addressed. E-mail: gcheng@mednet.ucla.edu.

This article contains supporting information online at www.pnas.org/lookup/suppl/doi:10.1073/pnas.1114981109/-/DCSupplemental.

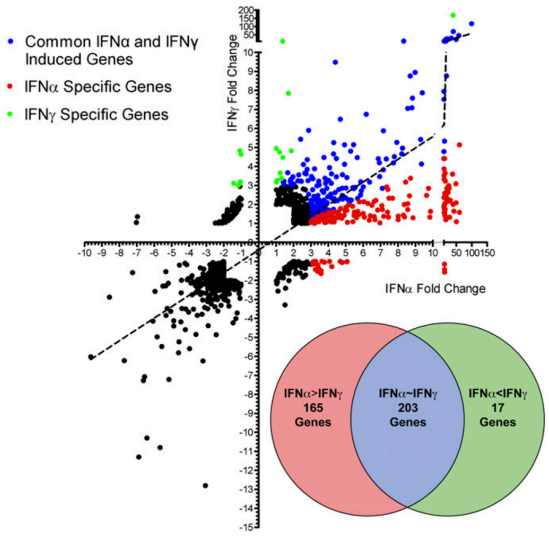

Fig. 1. Gene expression profile of BMMs treated for 2.5 h with IFNα and IFNγ at 62 U/mL and 1 U/mL, respectively. Axes represent fold change in response to IFNα or IFNγ over untreated cells. IFNα- and IFNγ-specific and commonly induced genes were categorized (see text) and are represented in a Venn diagram (*Inset*).

formed a blinded screen to identify ISGs that inhibit VSV coexpressing GFP (VSV-GFP) using a FACS-based approach. Individual ISGs in expression plasmids were cotransfected with red fluorescent construct (DsRed) in HEK293T cells. Empirical studies with a GFP construct and DsRed construct transfected at a 3:1 ratio show that >99% of DsRed-positive cells were also GFP-positive, which has been supported by other studies (7). Hence, DsRed-positive cells transfected under a 3:1 ratio of a gene of interest to DsRed would largely express the gene of interest. Using these conditions, HEK293T cells were cotransfected with individual ISGs and DsRed for 36 h and subsequently infected with VSV-GFP for 9 h and analyzed by FACS. Active viral replication was indirectly measured by GFP fluorescence in the cells. Tank-binding kinase 1 (TBK-1), which is a strong activator of IFN production, was used as positive control for the screen. The amount of infection was normalized to cells cotransfected with DsRed and a control gene, protein-tyrosine sulfotransferase 1 (TPST1), which had no effect on viral infection. As this screen was blinded, we sequenced the plasmids that inhibited viral growth to identify the gene.

For the initial large-scale screen, we measured VSV-GFP expression in the DsRed-positive population, which should be cells that highly coexpressed individual ISGs. We quantified VSV-GFP expression by the product of the percent VSV-GFP–positive, which should reflect the degree of viral infection across the population, and the geometric mean of the fluorescence intensity (MFI), which would reflect intensity of viral replication within a particular cell (Fig. 2 *A* and *B*). Next, we verified our approach with several known antiviral genes, such as IFITM3, ISG20, and OAS1, to serve as positive controls (Fig. 2*C*). Screening results demonstrated that expression of many of the ISGs inhibited VSV replication. Approximately 30 genes displayed greater than 50% inhibition of VSV-GFP expression, and the median VSV-GFP was 77% of cells transfected with control (Fig. 2 *D* and *E*). Known antiviral ISGs identified were IRF1, OAS1 variant 1 (OAS1-1), OAS1 variant 2 (OAS1-2), ISG20, IFIH (MDA5), IFITM3, TRIM25, RIG-I (DDX58), APOBEC3F, APOBEC3G, and OASL. ISGs that have uncharacterized antiviral activity were PARP11, PARP12, PVRL4, MGAT1, LY6E, CASP2, SERPAINA5, PML, SP110, SLFN12, SERPINA10, GPR146, MITD1, TAP1, RHOH, TRIM62, and FCGR1A (Table S2).

Twenty-four candidate genes that demonstrated high antiviral activity were chosen for further verification with biological triplicates. The amounts of VSV-GFP infection in total, DsRed-positive ($DsRed^+$), and DsRed-negative ($DsRed^-$) populations were measured for these ISGs and normalized to the control transfected cells of the respective populations (Fig. 2*F*). The DsRed-positive population should have high expression of the particular ISG that is cotransfected with DsRed, whereas the DsRed-negative population should have very low or no expression of the ISG. Comparison of both populations should indicate whether a particular ISG has an antiviral effect intrinsic to the cell expressing the gene or whether the ISG can confer protection *in trans* for cells expressing the gene. Genes that had the most pronounced inhibitory effect were IRF1, IFIH1 (MDA5), CH25H, and DDX58 (RIG-I). These genes inhibited VSV-GFP expression in all populations, suggesting that they amplify antiviral response to confer resistance on cells that do not express or express low levels of the ISG (DsRed-negative population), likely through induction of IFN (8, 9). On the other hand, ISGs such as ISG20, IFITM3, OAS1, MGAT1, GPR146, PARP12, LY6E, APOBEC proteins, TAP1, MX2, CD64, TRIM62, OASL, and others inhibited VSV-GFP expression in DsRed-positive cells but had little effect in DsRed-negative cells. These ISGs likely inhibit viral growth within the cell but not in surrounding cells. To validate this idea, we collected conditioned media from the supernatants of HEK293T cells transfected with IRF1, IFIH1, ISG20, and TBK and transferred them onto freshly plated HEK293T cells. The cells were infected with VSV after 4 h of treatment. Cells that were treated with MDA5, TBK, or IRF1 conditioned media were protective against VSV infection compared with control and ISG20-transfected conditioned media (Fig. S2). These results confirm that MDA5, TBK, and IRF1 can confer protection *in trans* to surrounding cells, whereas most other ISGs, such as ISG20, mediate their antiviral functions intrinsically. Taken together, this functional screen has identified known and unique antiviral ISGs against VSV (Table S3).

We next explored whether antiviral ISGs could be defined in similar or distinct sets based on their effect on growth of the DNA virus MHV-68. Individual ISGs were screened for their antiviral effect on MHV-68 coexpressing a luciferase reporter with the early-late gene, M3 (MHV-68-Luc) (10). HEK293T cells were transfected in quadruplicate with individual ISGs for 36 h and infected with MHV-68-Luc for 9 h, which was about the linear range for luciferase expression after infection. MHV-68 luciferase activity was measured and normalized to infected cells that expressed the control gene TPST1, which had no effect on MHV-68 replication (Fig. 3*A* and Table S4). The median reduction inhibition was about 10% (Fig. 3*B*). Eight genes that inhibited MHV-68-Luc production by ~50% were verified in quadruplicate in independent experiments (Fig. 3*C*). We found that IRF1, MX2, DDX58, BMP2, SPRY2, MNDA, OAS1-1, and ADAR significantly inhibited MHV-68-Luc production (Table S5).

The screening approaches described thus far used indirect readouts using a marker, such as GFP or luciferase, coexpressed with a virally encoded protein. They are not a direct measure of infectious virions. Viral plaque assay is quantitative for live virions even though they are less sensitive than GFP or luciferase assays. Nonetheless, as a separate validation, we tested 34 selected ISGs from the previous two screens (Figs. 2*F* and 3*C*) and measured their effects on VSV or MHV-68 by plaque assay. Supernatants were collected at 9 h postinfection (hpi) for VSV and 24 hpi for MHV-68 and titered individually (Fig. 4 *A* and *B*). We considered ISGs that significantly inhibited viral growth ($P \leq 0.05$ by Student's *t* test with unpaired, two-tailed hypothesis). IRF1, IFIH1, CH25H, ISG20, and DDX58 significantly inhibited growth of both viruses. ISGs that significantly antagonized VSV replication more strongly than MHV-68 were GPR146, APOBEC3G, APOBEC3F, TAP1, CD64, IFITM3, TRIM62, and LY6E. Conversely, ISGs that were more antiviral against MHV-68 than VSV were MNDA, BMP2, SPRY2, MAFK, OAS1-1, and ADAR (Fig. 4*C*). These results were significant and consistent in at least two independent experiments with biological triplicates. PARP12, GPR146, and

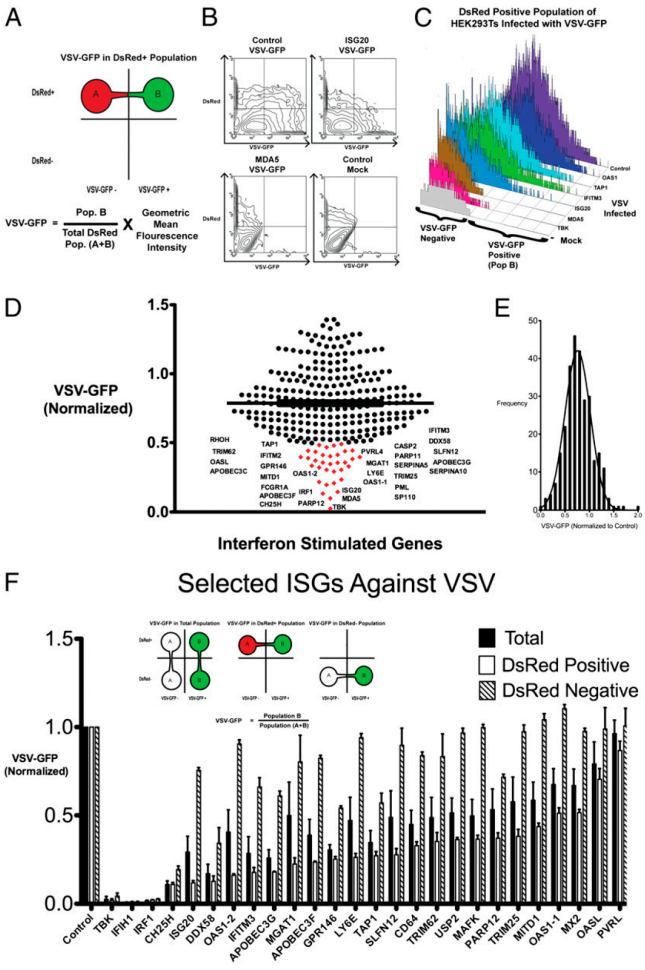

Fig. 2. (*A*) Schematic of FACS-based assay to identify ISGs against VSV-GFP. HEK293T cells were transfected with individual ISGs with DsRed plasmid at a 3:1 ratio. DsRed-positive cells indicate cells that highly express the ISG. VSV growth (VSV-GFP) was calculated by the product of the percent GFP-positive cells and the geometric mean fluorescence intensity (MFI) of GFP in the DsRed-positive cells. (*B*) Contour maps of VSV-GFP in HEK293T cells transfected with the indicated ISGs and DsRed. (*C*) VSV-GFP was measured in the DsRed-positive population of selected ISGs transfected in HEK293T cells. TBK-1 was used as a positive control. (*D*) All 288 ISGs were screened by a FACS-based method. Each dot represents an ISG, and its effect on VSV-GFP expression is normalized to VSV-GFP in control transfected cells. ISGs that inhibited VSV-GFP expression over 50% are labeled and indicated in red. Values represent mean of duplicates. (*E*) Histogram of all ISGs and their effect on VSV-GFP normalized to VSV-GFP in control transfected cells. (*F*) Effect of individual ISGs on VSV-GFP expression in total population, DsRed-positive population, and DsRed-negative population was calculated. Values represent mean ± SEM from biological triplicates.

SLFN12 demonstrated an inhibitory effect against the two viruses, but the results did not always meet the significance criteria ($P < 0.05$) in replicate experiments, indicating that they may have moderate inhibitory effects on viral replication. There were some ISGs such as PARP12, MITD1, ISG20, and MAFK that inhibited MHV-68 in plaque assays but did not affect luciferase expression, indicating that these ISGs may affect other viral life-cycle steps but not necessarily the activity of the MHV-68 M3 promoter of luciferase. Taken together, the plaque assay results provided additional validation of common and distinct sets of antiviral ISGs against VSV and MHV-68.

The selected antiviral ISGs were compared with their respective type I and type II IFN-mediated gene expression based on the initial microarray study. Many antiviral ISGs were commonly induced by IFNα and IFNγ. IFNα induced most ISGs to higher levels than the correlation of all IFNα and IFNγ ISGs that were found to be antiviral (Fig. 4*D*, dotted line). Only IRF1 and GPR146 were induced by IFNγ higher than IFNα. These results provide an explanation for stronger inhibitory activity of IFNα against VSV and MHV-68 than IFNγ. The antiviral effect of IFNγ may be mediated by activation of fewer yet highly effective antiviral ISGs such as IRF1 or by activation of IFNα through an autocrine loop, as suggested in other studies (11–13).

To better understand the effect of selected ISGs on inhibition of these viruses, we determined whether certain ISGs inhibited early critical life-cycle processes in VSV and MHV-68. As a negative-strand RNA virus, VSV undergoes primary transcription by its packaged polymerases to form positive-stranded mRNA; the process is independent of host protein synthesis after entry. Protein expression occurs in the sequential order N, P, M, G, and L, and is required for the switch from primary transcription to replication and downstream transcript amplification (14, 15). Hence, we tested whether the 30 most inhibitory ISGs against VSV from Fig. 4*A* could inhibit VSV protein expression. We used a VSV pseudovirus that has the receptor-binding G protein (VSV-G) replaced by the luciferase reporter (VSVΔG-Luc) enveloped inside VSV-G, called VSVΔG-Luc/G (16). This pseudovirus can undergo VSV-G–mediated entry but cannot produce its own VSV-G envelope, and hence is only capable of a single-round infection. Quantification of luciferase activity is indicative of viral life-cycle processes from entry to protein synthesis. MNDA and BMP2, which did not affect VSV replication, were used as negative controls. Of the 34 ISGs that inhibited

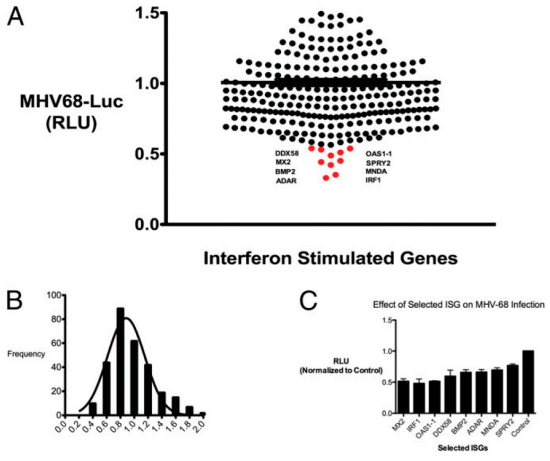

Fig. 3. (*A*) Individual ISGs expressed in HEK293T cells and infected with MHV-68 at 0.25 MOI in quadruplicates. Cells were lysed at 9 hpi and luciferase activity was measured. Mean relative luminescence unit (RLU) are presented. (*B*) Histogram of all ISGs, and their effects on MHV-68-Luc were normalized to MHV-Luc in control transfected cells. (*C*) Selected ISGs from the screen were verified in two experiments in quadruplicate and normalized to control. Values are expressed as mean ± SEM.

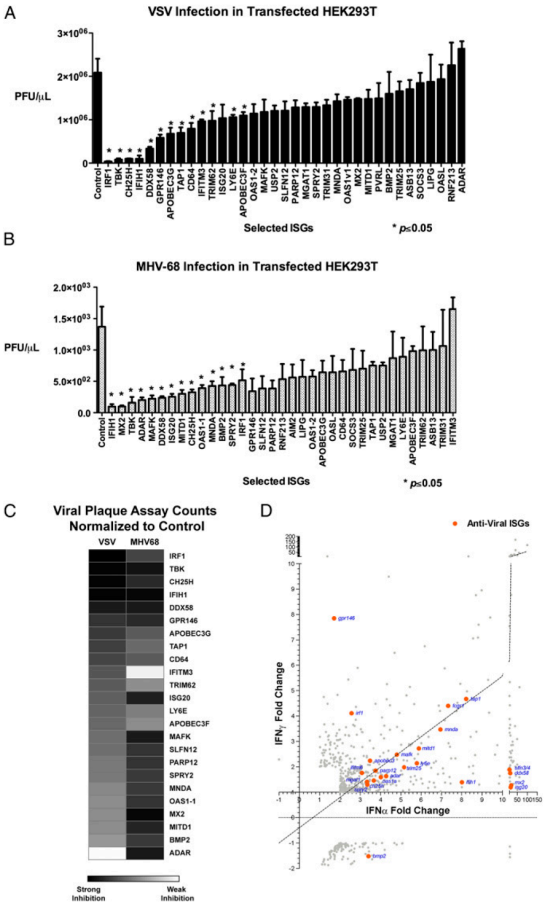

Fig. 4. (*A* and *B*) The inhibitory effects of 34 ISGs selected from previous screens against VSV (*A*) and MHV-68 (*B*) were measured by plaque assay. Values represent mean ± SEM. Data represent 1 of 3 experiments. Asterisks indicate significant difference compared with control by Student's *t* test ($P < 0.05$). (*C*) Heat map showing the inhibitory effect of selected ISGs on VSV and MHV-68 based on plaque assay. (*D*) Antiviral ISGs (orange) was graphed with respect to their fold induction by IFNα and IFNγ in microarray analyses (Fig. 1).

VSV, only IRF1, CH25H, IFITM3, GPR146, TAP1, DDX58, PARP12, TRIM25, and IFIH1 inhibited VSVΔG-Luc expression at 8 hpi (Fig. 5*A*). Thus, these ISGs inhibited steps before viral protein expression. Other ISGs that antagonized VSV, such as OAS1, ISG20, TRIM62, APOBEC3G, and CD64, did not reduce VSVΔG-Luc activity, suggesting they inhibited subsequent steps in replication, secondary transcription, assembly, or budding. These results demonstrate antiviral ISGs that inhibit stages up to or after VSV protein expression.

For ISGs that inhibited replication of MHV-68, we determined whether critical early life-cycle processes were inhibited by the selected 11 ISGs in Fig. 4*B* (MNDA, IRF1, MX2, BMP2, MITD1, IFIH1, MAFK, CH25H, OAS1-1, ADAR, SPRY2). As a DNA virus, MHV-68 first expresses essential genes after entry into the cell independent of host protein synthesis, called immediate-early (IE) genes. The replication and transactivator protein RTA is an IE gene that activates subsequent MHV-68 gene expression and is required for lytic replication and reactivation from latency (17). Hence, we tested the effect of expression of selected ISGs on RTA expression in HEK293T cells. BMP2, MX2, IRF1, IFIH1, CH25H, MITD1, MNDA, and OAS1-1 significantly inhibited RTA expression at 4 hpi ($P < 0.01$) (Fig. 5*B*). IFITM3, which did not inhibit MHV-68 replication, served as a negative control. As a separate validation, MNDA, IRF1, BMP2, MX2, and MITD1 also inhibited another IE gene, ORF57, at 4 hpi with $P < 0.01$ (Fig. S3). SPRY2, ADAR, and MAFK did not inhibit RTA or ORF57 expression, indicating they might affect early or late MHV-68 gene expression or other late life-cycle processes. Taken together, these results delineate inhibitory ISGs against MHV-68 that affect stages up to or after expression of critical immediate-early genes.

As a way to independently confirm our screening results, we sought to characterize two ISGs, TAP1 and BMP2, that have not been described as antiviral and had differential inhibitory effects on VSV and MHV-68 replication. Transporter associated with antigen processing 1 (TAP1) is well-described for its role in antigen presentation with MHC class I but has not been described to play a role in innate antiviral response. TAP1 expression significantly inhibited VSV replication but not MHV-68 replication. We hypothesized that deficiency in *tap1* would adversely affect innate immune response against VSV. Hence, we infected tail-derived fibroblasts from $tap1^{+/+}$ and $tap1^{-/-}$ mice with VSV and MHV-68. VSV growth in $tap1^{-/-}$ fibroblasts was significantly higher compared with $tap1^{+/+}$ fibroblasts as assessed by plaque assay and FACS (Fig. 6*A* and Fig. S4*A*). There was no difference in MHV-68 replication by plaque assay or MHV-68-Luc expression (Fig. 6*B* and Fig. S4*B*). These results show that TAP1 is sufficient and may be a required factor for cellular immune response against VSV.

Bone morphogenic protein 2 (BMP2) is well-studied in development, but its role in control of viral infection is unclear. Overexpression of *bmp2* inhibited MHV-68-Luc expression and replication by 40% by plaque assay, but did not significantly affect VSV. Addition of the recombinant, active form of human human BMP2 (hBMP2) to HEK293T and murine pre-B-cells inhibited MHV-68-Luc expression in a dose-dependent manner (Fig. 6*C* and Fig. S4*C*). Exogenous addition of hBMP2 had no effect on VSV-GFP infection in HEK293T cells or B-cells (Fig. 6*D* and Fig. S4*D*). In addition, hBMP2 treatment of HEK293T inhibited RTA expression (Fig. S5). These results demonstrate BMP2 to be a sufficient inhibitory factor against MHV-68 but not VSV.

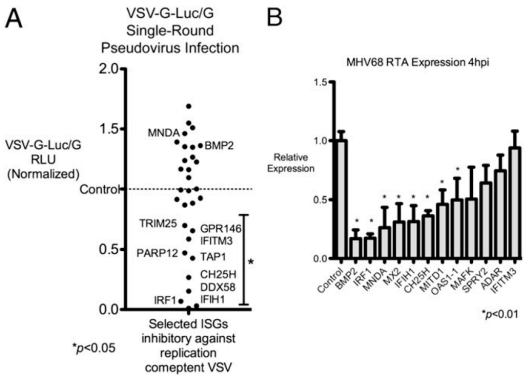

Fig. 5. (*A*) ISGs that were most inhibitory against VSV in Fig. 4*A* were transfected in HEK293T cells for 36 h in triplicate and infected with VSVΔG-Luc reporter within a VSV-G envelope. Cells were lysed 10 hpi and luciferase activity was measured. BMP2 and MNDA, which did not inhibit VSV replication, were used as negative controls. Mean RLU are presented; data are representative of two independent experiments. (*B*) Eleven ISGs that were most inhibitory against MHV-68 were expressed in HEK293T cells for 36 h and infected with 0.2 MOI of MHV-68. Expression of the immediate-early gene RTA was measured by quantitative PCR at 4 hpi. IFITM3, which has no inhibitory effect on MHV-68, was used as a negative control. Data are representative of three independent experiments.

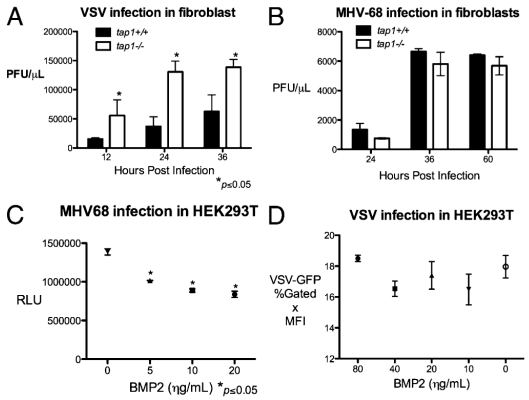

Fig. 6. (*A*) $tap1^{+/+}$ and $tap1^{-/-}$ tail-derived fibroblasts were infected with VSV at 0.1 MOI for the indicated time, and the supernatants were titered by plaque assay. Values represent mean ± SEM. (*B*) $tap1^{+/+}$ and $tap1^{-/-}$ fibroblasts were infected the MHV-68 at 0.25 MOI, and the supernatants were collected at the indicated times and titered by plaque assay. Values represent mean ± SEM. (*C*) HEK293T were treated with hBMP2 at the indicated concentration for 12 h and infected with MHV-68-Luc at 0.25 MOI. Luciferase activity in the cell lysates was quantified at 9 hpi. Values represent mean ± SEM. RLU, relative luminescence unit. (*D*) HEK293T were treated with BMP2 at increasing concentrations for 12 h and infected with VSV at 0.01. VSV-GFP expression was measured by FACS at 9 hpi. Values represent mean ± SEM. MFI, geometric mean of fluorescence index.

Discussion

In this study, we sought to understand the basis of the antiviral activity of type I and type II IFNs. IFNs induce a large group of ISGs, each of which is presumed to have important roles in innate immunity against different families of microorganisms. We performed functional screens of 288 type I and type II ISGs for their antiviral activity against VSV and MHV-68, which are RNA and DNA viruses, respectively. We found distinct and common sets of ISGs that inhibited VSV and MHV-68, including 14 ISGs that were not previously described as having antiviral activity. Of these newly identified antiviral ISGs, some inhibited critical early viral life-cycle processes in VSV protein expression and MHV-68 transcription. TAP1 and BMP2 were further functionally validated and shown to have specific, unique antiviral functions on these disparate viruses.

The large-scale functional screens identified more ISGs that inhibited VSV than MHV-68. This may be a reason that wild-type mice, which have a robust IFN response, are completely resistant to VSV but not to MHV-68 infection (1). IFNα is also a stronger inducer of antiviral ISGs than IFNγ, which is consistent with studies showing that type I IFN plays a dominant antiviral role. For example, $ifnar^{-/-}$ mice are very sensitive to VSV infection, whereas $ifngr^{-/-}$ mice are resistant (1). Immune-mediated inhibition of acute MHV-68 infection also requires type I but not type II IFNs (18, 19).

Interestingly, most antiviral ISGs inhibited these viruses moderately when expressed individually, suggesting that IFN-stimulated cells express a large group of ISGs that play a cumulative antiviral effect. Indeed, expression of various combinations of ISGs has an additive inhibitory effect on viruses (4). Expression of an array of antiviral effectors may be an effective method for the host to defend against the various viruses as well as counteract viral inhibition of any one or group of ISGs. Moreover, gene profiling suggests that many antiviral ISGs are induced only a few fold above basal levels (Fig. 4*D*). Expression of several ISGs at low levels may create less detrimental cellular changes while still achieving a global antiviral effect.

Many ISGs such as IRF1 and IFIH1 (MDA5) have broad antiviral activity, which can be attributed to amplification of IFN production. IRF1 is a well-studied transcription factor that induces IFN expression (20), and IFIH1 acts as an intracellular RNA receptor that activates IFN. Indeed, some studies support that this IFN amplification loop is a mechanism by which IFNγ mediates its antiviral effect. For example, IFNGR signaling is dependent on IFNAR activity (12), and STAT2, which is primarily activated by IFNAR, is required for IFNGR-mediated antiviral effect (11). Our data show that IFNγ is less efficient at activating most ISGs than IFNα, but induces IRF1 to higher levels than IFNα. IRF1 can directly induce ISGs as well as expression of type I IFN, implying that the antiviral activity of IFNγ may be mediated by the induction of IRF1 and type I IFN. In addition to positive feedback mechanisms, there may be other feedback mechanisms that may differentiate the gene expression programs and physiological effects of type I and II IFNs.

Several ISGs inhibited growth of VSV more than MHV-68, such as TAP1 IFITM3, GPR146, APOBEC proteins, CD64 (FCGR1A), TRIM62, and LY6E. Of these, GPR146, CH25H, PARP12, and TAP1 are unique antiviral proteins that inhibit VSV-G protein expression. It is likely that these ISGs inhibit steps before replication and secondary transcription, because sufficient protein translation is required before these steps.

To verify one of these genes, we showed that TAP1 is sufficient and required for inhibition of VSV in fibroblasts but not MHV-68, introducing a unique role of TAP1 in innate immune defense. This endoplasmic ATP-Binding Cassette (ABC) transporter facilitates transport of proteosomal-degraded proteins into the lumen onto MHC class I receptors. Interestingly, many viruses evade host immune response by inhibiting TAP1, which most studies attribute to be a method to block adaptive immune presentation to T cells. However, our work shows that there may be an antiviral function of TAP1 independent of its association with adaptive immune presentation. Its inhibitory effect on VSV-G-Luc expression suggests a potential role in posttranslational processing and degradation of viral proteins. A possible reason TAP1 did not play a significant role in inhibition of MHV-68 is that the viral mK3 protein of MHV-68 interacts with TAP1 and promotes its proteosomal degradation (21, 22).

ISGs that significantly inhibited MHV-68 more strongly than VSV include MX2, MNDA, SPRY2, BMP2, and ADAR1. BMP2 and MNDA are unique antiviral ISGs that strongly

inhibited expression of the immediate-early gene RTA at 4 hpi. Expression of RTA directly affects expression of other MHV-68 genes required for lytic replication. We further showed that addition of recombinant BMP2 inhibits MHV-68 replication and RTA expression. One possible mechanism is that BMP2 can activate TGFβ-activating kinase 1 and subsequent activation of NF-κB, which prevents MHV-68 lytic growth (23, 24). This result introduces the possibility of unique IFN-inducible soluble factors that can inhibit growth of specific viruses.

Although more studies need to be done to elucidate the mechanisms of action and breadth of antiviral activity of the antiviral ISGs defined here, further understanding of these ISGs may provide future direction for antiviral therapies. Comprehensive understanding of ISG antiviral activity may introduce other avenues for targeted antiviral therapy that would bypass the need for IFN treatment as well as viral evasion strategies that inhibit IFN activation.

Materials and Methods

Cells and Reagents. RAW and HEK293T cells were obtained from the American Type Culture Collection and grown in standard DMEM with 5% FBS, 1% penicillin/streptomycin (GIBCO). Glen Barber (University of Miami, Miami, FL) provided VSV-GFP. MHV-68 coexpressing luciferase reporter was provided by Ren Sun (University of California, Los Angeles, CA). Luciferase activity was measured using a firefly luciferase substrate kit (Promega). Human recombinant BMP2 was purchased from R&D Laboratories.

Bone marrow macrophages were harvested from 6- to 8-wk-old C57B/L6 mice (The Jackson Laboratory) and differentiated with 10 ng/mL of M-CSF in DMEM, 10% FBS for 7 d. On day 6 the media were replaced, and on day 7 the cells were stimulated with IFNα or IFNγ (PBL InterferonSource). The cells were treated for 2.5 h and harvested in TRIzol (Invitrogen). RNA was isolated by isopropanol precipitation for microarray analysis. For immunoblots, BMMs were treated with IFNα and IFNγ for 30 min and separated by SDS/PAGE as described previously (26) and blotted with phospho-STAT1 antibody (Cell Signaling). Primary antibodies were detected with anti-rabbit antisera conjugated to HRP (Santa Cruz Biotechnology) and visualized by chemiluminescence.

TAP1-deficient (*Taptm1Arp*) mice were purchased from The Jackson Laboratory. The tails of the mice were skinned and cultured in DMEM with 10% FBS, 1% (vol/vol) penicillin/streptomycin. Fibroblasts were harvested after 7–10 d. Murine pre-B Cells were derived from bone marrow as described previously (25).

Microarray and ISGs. Microarrays were done on an Affymetrix 430.2 chip (University of California, Los Angeles Genotyping and Sequencing Core). Individual ISGs were provided by GeneCopoeia, Inc.

VSV Screening and Flow Cytometry. HEK293T cells were plated in 12-well collagen-coated plates of 0.5 mg/mL rat tail collagen I (BD Biosciences) in PBS. Individual ISG expression plasmids were transfected with DsRed construct (Clontech) at a 3:1 ratio with FuGENE 6 (Roche) transfection reagent. After 36 h, the cells were infected with VSV-GFP at a 0.01 multiplicity of infection (MOI) and collected at 9 hpi in 2% (vol/vol) paraformaldehyde solution in PBS. FACS was done with standard compensation (FACSCaliber; BD Biosciences), and the data were analyzed using CellQuest (BD Biosciences).

MHV-68 Screening. HEK293T cells were seeded in a 96-well plate overnight and transfected with individual ISG expression plasmids for 36 h. Cells were infected with MHV-68 at a 0.25 MOI for 1 h and lysed in 1× passive lysis buffer (Promega) at 9 hpi, and luciferase activity was measured.

Viral Plaque Assay. Plaque assays were done on Vero cells in 12-well plates at 2×10^5 and 2×10^4 cells per well for VSV and MHV-68 plaque assays, respectively. Supernatants from infected cells were serially diluted and infected in Vero cells for 1 h. The cells were then covered with growth medium containing 0.6% (mass/vol) low-melting point agarose. Plaques were counted after 16 h or 6 d for VSV and MHV-68, respectively.

VSV-G–Pseudotyped VSV-G Luciferase. VSV-G–pseudotyped VSV-G luciferase pseudovirus (VSVΔG-Luc/G) was a gift from Benhur Lee (University of California, Los Angeles, CA). The pseudovirus was generated by methods previously described (27) and concentrated by ultracentrifugation (>140,000 × *g*). The concentrations used to generate a linear range of luciferase signal were determined empirically.

MHV-68 Gene Expression Studies. RNA was isolated from MHV-68–infected cells at the indicated times. cDNA was generated with iScript (Bio-Rad). Primers used for quantitative PCR were RTA-forward 5′-GATTCCCCTTCAGCCGATAAG-3′, RTA-reverse 5′-CAGACATTGTAGAAGTTCAGGTC-3′, ORF57-forward 5′-GACCAAATGATGGAAGGAC-3′, ORF57-reverse 5′-GCAGAGGAGAGTTGTGGAC-3′. PCR conditions used were 95 °C for 3 min followed by 45 cycles of 95 °C for 15 s, 60 °C for 20 s, and 72 °C for 30 s.

Software and Graphing. Microarray analysis was performed using GeneSpring software (Agilent). All graphs were generated with GraphPad Prism. Heat maps were generated by using the web program Matrix2png (28).

ACKNOWLEDGMENTS. We thank Dr. Ting-Ting Wu for her advice on MHV-68 gene expression studies and Dr. Edward Fritsch for editing the paper. This work was supported by National Institutes of Health (NIH)/National Cancer Institute Tumor Immunology Training Grant 5T32CA009120, NIH Grants R01 AI078389 and AI069120, Warsaw Fellowship, and the Medical Scientist Training Program.

Supporting Information

Liu et al. 10.1073/pnas.1114981109

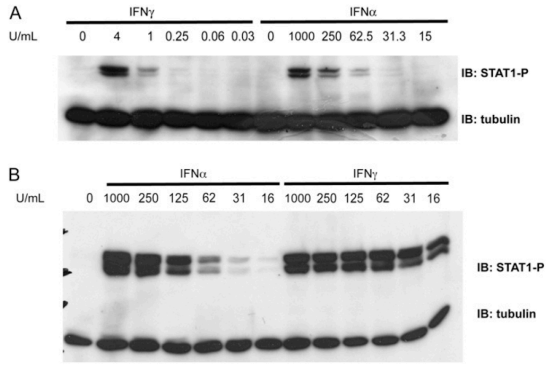

Fig. S1. (*A*) Bone marrow-derived macrophages were treated with IFNα and IFNγ at the indicated concentrations for 30 min and the cell lysates were subjected to immunoblotting (IB) for phospho-STAT1 and tubulin, which is a housekeeping gene. (*B*) Similar to *A*. Higher titrations of IFNα and IFNγ were used.

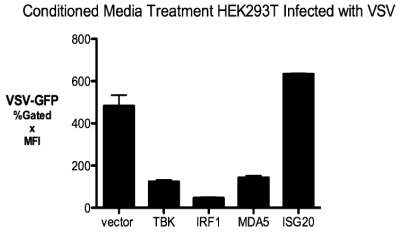

Fig. S2. Conditioned media from HEK293T cells overexpressing the indicated gene were used to treat freshly plated HEK293T cells. The cells were infected with vesicular stomatitis virus (VSV)-GFP 4 h after treatment, and VSV-GFP was measured by FACS. Values are represented as mean ± SEM. MFI, geometric mean of fluorescence index.

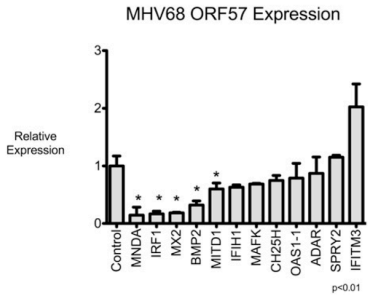

Fig. S3. HEK293T cells were transfected with selected IFN-stimulated genes (ISGs) that inhibited murine gammaherpes virus (MHV)-68 replication. Expression of MHV-68 ORF57 was measured by quantitative PCR at 4 h postinfection (hpi). Values are represented as mean ± SEM.

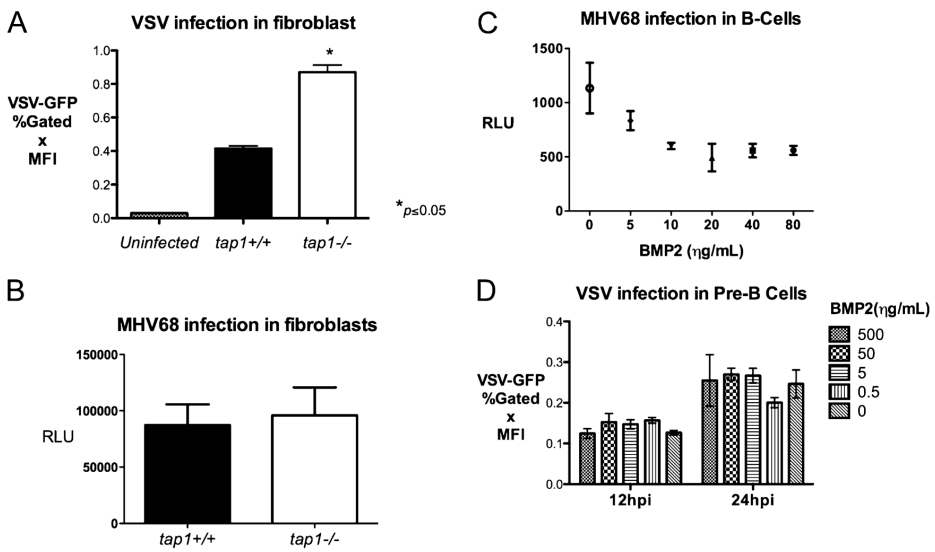

Fig. S4. (*A*) TAP$^{+/+}$ and TAP$^{-/-}$ tail-derived fibroblasts were infected with VSV-GFP at 0.1 MOI, and VSV-GFP was measured by FACs at 12 hpi. MFI, geometric mean fluorescence index. (*B*) TAP$^{+/+}$ and TAP$^{-/-}$ fibroblasts were infected the MHV-68 at 0.25 MOI, and MHV-68-Luc activity was measured at 9 hpi. (*C*) Immortalized pre-B cells were treated with hBMP2 at indicated concentration for 12 h and infected with MHV-68-Luc at 0.25 MOI. Luciferase activity in the cell lysates was quantified at 9 hpi. Values represent mean ± SD. (*D*) HEK293T and Pre-B cells treated with BMP2 at increasing concentrations for 12 h and infected with VSV at 0.01 and 1MOI respectively. VSV-GFP expression was measured by FACS at 9 hpi. Values represent mean ± SD.

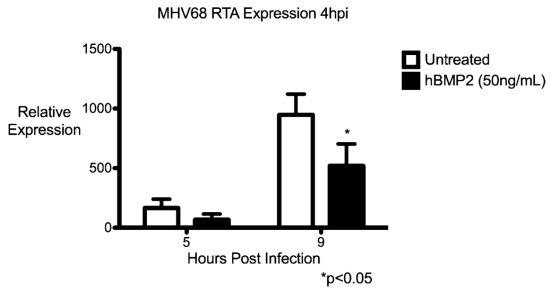

Fig. S5. HEK293T cells were treated with recombinant human BMP2 (hBMP2) at 50 ng/mL for 12 h and infected with 0.2 multiplicity of infection (MOI) of MHV-68. Expression of replication and transactivator protein (RTA) was measured at 4 hpi.

Table S1. List of IFNα-specific, IFN-γ specific, and commonly induced ISGs described in Fig. 1

Table S1 (DOCX)

Table S2. List of all ISGs that inhibited VSV-GFP replication when expressed with red fluorescent construct (DsRed) in HEK293T cells as measured by FACS

Table S2 (DOCX)

VSV-GFP was measured in DsRed^{+} cells and normalized to control transfected cells.

Table S3. Summary of selected 24 antiviral ISGs that inhibited VSV-GFP by FACS

Table S3 (DOCX)

Significant inhibitory effects observed by plaque assay and VSV-G-Luc–pseudotyped virus as shown in Figs. 4*A* and 5*A*, respectively, are indicated by (+) for inhibition and (–) for no inhibition.

Table S4. List of all ISGs that inhibited MHV-68 luciferase activity when expressed in HEK293T cells

Table S4 (DOCX)

Table S5. Summary of selected 12 antiviral ISGs that inhibited MHV-68 luciferase and plaque assay

Table S5 (DOCX)

Significant inhibitory effects by MHV-68 plaque assay or RTA expression as shown in Figs. 4*B* and 5*B*, respectively, are indicated by (+) for inhibition and (–) for no inhibition.

Supplementary Table T1

IFNα-Specific Genes

	IFNα Fold Induction	IFNγ Fold Induction
Whsc1l1	3.00	1.06
Zfp800	3.07	1.15
Glipr2	3.08	1.09
LOC100039742	3.11	1.16
Ms4a6b	3.11	-1.03
Plekha2	3.12	-1.15
Prpf4	3.14	1.21
Asb13	3.16	1.11
Rnf135	3.16	-1.05
Mxd1	3.18	-1.01
Mcm10	3.19	1.14
Klrg2	3.20	1.00
Creb5	3.21	1.01
Dennd1b	3.21	-1.05
LOC100044115 /// Rin2	3.26	-1.43
Cutc	3.27	-1.00
LOC100048247 /// Pcgf5	3.29	1.06
Tiparp	3.29	1.15
Tor1aip2	3.29	1.20
Sp100	3.35	1.17
Spry2	3.35	1.30
Mid1	3.36	1.32
Dusp28	3.37	1.27
Otud1	3.39	1.12
Aim2	3.39	-1.18
LOC100044383 /// Pnpt1	3.40	1.36
Bmp2	3.40	-1.52
Bambi-ps1	3.43	-1.33
Nr4a2	3.45	1.12
Peli1	3.47	1.09
Sertad3	3.49	1.17
Irf2	3.57	1.29
Nfxl1	3.58	-1.49
BC006779	3.58	-1.64
Ms4a4b	3.63	-1.00
Ch25h	3.66	1.46
D330050I23Rik	3.72	1.20
9530028C05	3.72	1.31
LOC100046817 /// Tbc1d1	3.76	1.23
Abcb1a	3.77	-1.04
Plekhf2	3.79	1.05
6330442E10Rik	3.80	1.46
Cbx4	3.81	1.27
Atp10a	3.86	1.06
Rgs2	3.86	1.44
Ccdc86	3.90	1.25
Hsh2d	3.91	1.08
A530023O14Rik	3.91	1.40
B4galt4	3.93	1.21
Socs2	3.95	1.31
Fndc3a	3.96	1.12
Oas1a	4.01	1.59
Gnb4	4.05	1.37
BC016423	4.07	-1.00
Pvrl4	4.12	1.22
Sp110	4.16	1.47
P4ha1	4.17	1.08
Lipg	4.18	1.30
Etnk1	4.20	1.47
B430306N03Rik	4.20	-1.27
Adar	4.27	1.63
2310016F22Rik /// BC020489	4.31	1.32
Ncoa7	4.34	1.08
Slc25a22	4.50	1.30
E330016A19Rik	4.50	1.55
Oas1b	4.57	1.62
Oas1c	4.60	1.34
Zcchc2	4.65	1.44
Ccl4	4.68	-1.00
Trim30	4.70	1.79
Dcp2	4.77	1.27
Gpsm2	4.79	-1.06
Ifi35	4.91	1.44
LOC640746 /// Trim34	4.97	1.68
Pfkfb3	5.01	1.85
Tmem171	5.06	-1.02
Abtb2	5.07	1.70
AW112010	5.08	-1.01
Grasp	5.10	1.06
Trim25	5.16	1.98
Oas3	5.40	1.91
Frmd4a	5.41	1.09
Lrch1	5.48	1.42
Ube2l6	5.49	1.60
Timeless	5.62	1.31
Trim34	5.69	1.64

Klrk1	5.76	1.48
Ly6e	5.79	2.14
Mov10	6.00	1.53
Oas2	6.04	2.15
Mthfr	6.07	1.34
Rtp4	6.27	2.06
LOC625360	6.35	1.17
Pols	6.41	1.41
Epsti1	6.50	1.96
Slfn3	6.63	1.37
AI451617 /// Trim30	6.63	2.16
Znfx1	6.68	1.20
Ccl7	6.73	2.22
LOC100047963 /// Tor3a	6.83	1.71
Cd69	6.96	1.03
Slfn9	7.07	1.94
2700019D07Rik	7.10	1.74
LOC677168	7.18	1.38
Eif2ak2	7.35	2.93
Aldh1b1	7.40	1.60
LOC100046469 /// LOC671535 /// Plec1	7.42	2.79
Tor3a	7.45	1.34
Daxx	7.48	2.33
Kif5c	7.69	2.33
Slfn4	8.01	1.20
Ifih1	8.01	1.39
Kdr	8.31	1.44
Setdb2	8.36	2.00
5730411F24Rik	8.38	1.35
Tpst1	8.44	3.18
D14Ertd668e	8.56	1.74
AI451617	8.56	2.04
Slfn8	8.66	2.46
Il15	8.72	3.38
Ccnj	8.86	1.30
Fbxo39	9.64	2.48
Oasl2	9.75	2.85
2010002M12Rik	9.83	1.34
Ms4a4c	9.87	1.64
Tlr3	10.10	2.37
Slfn3 /// Slfn4	10.20	1.89
Stat2	10.40	3.52
Dck	10.50	3.88
Nt5c3	10.80	1.58
Enpp4	11.00	3.34
Ppm1k	11.10	1.98

Dhx58	11.40	1.58
Herc5	11.60	1.78
Mmp13	12.00	-1.14
Slfn5	12.10	4.42
Il10	12.30	-1.56
Il6	12.40	-1.42
BC013672	12.70	1.58
Slfn1	12.80	2.60
Ifi44	13.10	1.42
Ddx58	13.90	1.75
Isg15 /// LOC100038882 /// LOC100044225 /// LOC677168	13.90	2.06
Il15ra	14.10	3.65
G530011O06Rik	14.70	3.23
Isg20	16.10	1.19
BC094916 /// LOC100048304 /// LOC637605 /// Pyhin1	17.40	2.54
LOC623121	18.30	2.37
Mx2	18.90	1.27
Ddx4	19.50	2.25
Irf7	19.60	2.85
Ifit2	23.60	2.64
E030037K03Rik	25.70	2.99
Lhx2	26.70	2.18
LOC100048304 /// Pyhin1	27.10	2.86
Oasl1	28.80	1.33
Ifit3	30.30	2.23
LOC100045707 /// Pou3f1	38.00	3.60
Ifit1	39.80	2.01
Rsad2	42.30	1.65
Tnfsf10	48.80	3.09
Tyki	49.20	2.09
Mx1	50.20	1.09
OTTMUSG00000016644	60.20	1.59
LOC100048346 /// Usp18	60.40	5.14

IFNα and IFNγ Commonly Induced Genes

	IFNα Fold Induction	IFNγ Fold Induction
Ccnj	3.05	1.300000
Rab19	3.13	1.300000
H2-T10 /// H2-T22 /// H2-T9 /// LOC100044190 /// LOC100044191	3.31	1.330000
Pex26	3.06	1.350000
Tmem67	3.09	1.350000
Isoc1	3.24	1.360000
Tera	3.04	1.370000
Dcp2	3.23	1.390000
Armcx6	3.26	1.410000
E330016A19Rik	3.36	1.410000
Mgat1	3.33	1.410000
Ube1l	3.08	1.410000
Aff1	3.46	1.440000
D330022A01Rik /// Ube1l	3.06	1.440000
Casp2	3.35	1.460000
Ch25h	3.08	1.460000
P2ry13	3.47	1.490000
Dhx58	3.27	1.560000
Samd9l	3.96	1.600000
Trim12	3.50	1.630000
LOC100046232 /// Nfil3	3.59	1.640000
AA960436	3.34	1.650000
Rnf213	3.75	1.650000
Trafd1	3.34	1.650000
C330023M02Rik	4.07	1.670000
Rbm43	4.02	1.700000
D14Ertd668e	3.16	1.740000
Usp12	4.30	1.750000
D16Ertd472e	3.17	1.760000
Ifitm6	3.08	1.760000
Rbl1	3.87	1.760000
Parp11	3.38	1.770000
Hist3h2a	3.28	1.780000
9230105E10Rik	3.36	1.790000
Slc30a1	3.28	1.810000
Parp12	3.75	1.850000
Nmi	3.63	1.870000
Fbxw17	3.05	1.920000
Epsti1	3.39	1.960000
Gadd45g	3.08	1.990000
Ifit1	3.72	2.010000
AI607873	3.01	2.050000
Isg15 /// LOC100038882 /// LOC100044225 /// LOC677168	3.91	2.060000
Kmo	3.47	2.070000
Ndn	3.38	2.080000
Mlkl	3.93	2.100000
Ly6e	5.22	2.140000
Enpp4	3.39	2.160000
Golga3	3.66	2.160000
Lhx2	4.36	2.180000
Ikzf1	4.53	2.210000
Ccl7	3.00	2.220000
Eif2ak2	3.37	2.220000
Ifit3	3.74	2.230000
Akap12	5.31	2.240000
Apobec3	3.48	2.240000
Ddx4	3.23	2.250000
Ibrdc2	5.13	2.260000
P2ry14	4.81	2.290000
LOC100045567 /// LOC667034 /// Pnp	4.34	2.310000
1600014C10Rik	5.68	2.320000
Daxx	3.21	2.330000
Kif5c	4.20	2.330000
Clec2d	3.32	2.370000
LOC623121	4.97	2.370000
Bach1	3.97	2.410000
1200015F23Rik	3.32	2.430000
A730095J18Rik	3.17	2.430000
Fbxo39	3.40	2.480000
Mafk	4.80	2.480000
H2-T24	5.85	2.500000
BC094916 /// LOC100048304 /// LOC637605 /// Pyhin1	2.86	2.540000
39500	4.14	2.550000
5730508B09Rik	4.39	2.630000

Ifit2	3.73	2.640000
Mitd1	5.89	2.720000
Axud1	3.65	2.730000
Pik3ip1	3.10	2.780000
LOC100046469 /// LOC671535 /// Plec1	4.60	2.790000
Ccl8 /// LOC100048554	5.47	2.840000
Irf7	3.91	2.850000
Oasl2	7.10	2.850000
LOC100048304 /// Pyhin1	4.79	2.860000
Ifi203 /// Ifi204 /// Ifi205 /// LOC100040462 /// LOC100044072 /// LOC100048634	5.01	2.870000
Ifi204 /// LOC100048309	5.41	2.890000
BC023892	5.54	2.900000
Parp14	6.01	2.930000
E030037K03Rik	3.35	2.990000
Casp12 /// LOC100044205	3.47	3.030000
BB146404	1.85	3.050000
Card6	1.93	3.050000
C230093N12Rik	1.43	3.060000
9630017O17	2.01	3.080000
Il15ra	3.84	3.120000
Psmb9	4.17	3.120000
Ccl2	6.37	3.180000
AW061234	1.41	3.190000
2610016C23Rik	5.86	3.200000
Brdt	2.45	3.220000
F3	1.81	3.220000
G530011O06Rik	3.45	3.230000
Tnfsf14	1.45	3.230000
Noc4l	2.43	3.240000
Abl2	2.26	3.250000
Il18rap	2.83	3.260000
AA467197	4.02	3.270000
Irf8	1.85	3.320000
Pbef1	3.11	3.360000
AI480535	3.08	3.370000

Il15	3.81	3.380000
Trex1	5.07	3.420000
9330175E14Rik	4.46	3.460000
Inpp5b	1.97	3.460000
Ifi205 /// Mnda	6.95	3.470000
AI447881	3.03	3.480000
Spsb1	2.30	3.560000
Nod1	4.81	3.570000
Arid4a	2.72	3.610000
4833411O04Rik	4.18	3.620000
Tmem173	2.65	3.650000
Il4ra	1.67	3.680000
Dtx3l	7.16	3.830000
LOC432459	2.78	3.850000
Dck	3.21	3.880000
2600010E01Rik	4.07	3.940000
Irf1	2.57	4.110000
Fcgr4	4.93	4.120000
Pml	9.35	4.130000
LOC100045519 /// Trim21	7.74	4.190000
AI451557	6.93	4.200000
1600021P15Rik	2.79	4.360000
Fcgr1	7.33	4.400000
Parp9	6.87	4.410000
Slfn5	10.30	4.420000
Tmem140	4.46	4.420000
Gpr171	5.66	4.470000
Cd300lf /// LOC100047115	3.75	4.480000
Trim21	7.79	4.520000
Crem	4.30	4.660000
Tap1	8.22	4.670000
Ifi203	10.30	4.790000
Sectm1a	5.28	4.810000
Gvin1 /// LOC100042856	8.26	4.970000
LOC100048346 /// Usp18	4.93	5.140000
Tppp3	5.45	5.150000
Tmem2	4.31	5.260000
Rhoh	7.93	5.270000
Zbp1	11.80	5.340000
BC013712	9.30	5.430000
Ppp1r3d	2.41	5.440000
Cxcl11	7.16	5.880000
Gdap10	4.69	6.490000

Ly6a	6.18	6.750000
Cxcl10 /// LOC100045000	8.56	7.060000
Gbp6 /// LOC100047881	8.80	7.090000
Gbp6	10.10	7.540000
Samhd1	8.83	7.600000
Gbp3	9.40	7.880000
Arid5a	10.30	7.950000
Stat1	8.70	8.760000
Fgl2	18.40	8.770000
5830443L24Rik	8.98	8.950000
LOC667597	4.40	9.490000
Cd274	14.90	11.900000
Gbp2	10.90	12.000000
Ifi47	14.00	12.200000
Batf2	8.33	12.400000
Irgm	12.70	13.100000
Iigp2	17.30	13.800000
Igtp	17.10	15.200000
A630077B13Rik	17.30	15.900000
	14.60	17.200000
Ccl12 /// LOC100048556	49.60	22.400000
LOC626578 /// Mpa2l	17.40	23.700000
Mpa2l	21.10	25.600000
Socs1	33.90	30.300000
LOC100039796 /// Tgtp	57.80	45.700000
Serpina3g	40.40	70.000000
Iigp1	99.30	118.000000
Slamf8	2.87	5.900000

IFNγ-specific genes

	IFNα Fold Induction	IFNγ Fold Induction
Cxcl9	39.80	169.00
Selp	1.38	11.90
Gpr146	1.71	7.85
Ahr	1.01	4.95
Ifitm1	1.88	4.83
Gpr18	-1.08	4.83
Trib3	1.20	4.75
Xrcc6bp1	-1.01	4.64
B4galt3	1.39	4.48
A230097K15Rik	1.23	3.67
Dna2l	1.31	3.37
Rapgef6	1.06	3.27
Bmf	-1.05	3.20
Fbxl5	1.01	3.18
AW548124 /// LOC100048505	-1.07	3.13
Trim16	-1.44	3.12
Slc5a6	-1.17	3.02

Supplementary Table T2

ISG	% VSV-GFP inhibition normalized to Control
Cholesterol Hydrolase 25	95.11%
IRF1	94.01%
IFIH1	90.35%
OAS1 -transcript variant 2	88.73%
PVRL4	83.68%
PARP12	82.51%
MGAT1 - var1	80.87%
ISG20	80.63%
TRIM31	79.67%
TRIM62	79.42%
MITD1	78.89%
OAS1 - variant 1	78.52%
USP2	78.01%
TRIM25	77.27%
LY6E	74.81%
IFITM3	74.59%
FCGR1A (CD64)	72.23%
INHBB	70.88%
DDX58	70.37%
SLFN12	69.72%
TAP1	69.06%
APOBEC3G	67.78%
APOBEC3F	67.26%
GPR146	67.20%
SOCS1	65.22%
PARP11	64.55%
SLFN11	64.32%
SELP	63.97%
PML	63.15%
UBE3A	62.72%
CASP2	61.88%
IFITM2	61.25%
TRAF3	60.86%
MAFK,MAFG,MAFF	60.78%
RHOH	59.04%
ABCC4	58.84%
APOBEC3C	56.69%
OASL	55.89%
SERPINA10	55.72%
GDF10	55.09%
GATA3	54.85%
MX2	54.54%
SERPINA5	53.42%
TBC1D1	52.18%
PNPT1	51.62%
SP110	50.56%
TAP2	50.49%
P2RY13	50.29%
AIM2	50.25%
MARK4	50.11%

Supplementary Table 3. Selected Anti-viral ISG against VSV					
ISG	**Full Name**	**VSV-GFP Inhibition by FACs (DsRed Population)**	**Significant Inhibition by Plaque Assay ($p<0.05$)**	**Inhibition of VSV-G-Luciferase Protein Expression**	**Anti-Viral Function**
IFIH1	interferon induced with helicase C domain 1 (MDA5)	98.9±0.3%	+	+	Activator of interferon
IRF1	interferon regulatory factor 1	97.8±0.1%	+	+	Activator of Interferon
CH25H	Cholesterol 25 Hydroxylase	89.0±1.9%	+	+	Unknown
ISG20	interferon stimulated exonuclease gene 20kDa	88.1±2.1%	+	-	3'-5' exonuclease that inhibits several members of RNA viruses including HCV, influenza, HIV.
DDX58	DEAD box polypeptide 58 (RIG-I)	87.3±5.3%	+	+	An intracellular sensor of dsRNA that activates interferon
OAS1-2	2'-5'-oligoadenylate synthetase 1 variant 2	83.8±1.3%	+	-	Activates RNaseL and leads to degradation of viral RNA
IFITM3	interferon induced transmembrane protein 3	82.2±4.7%	+	+	Inhibits entry HIV, VSV, WNV, influenza, Dengue
APOBEC3G	apolipoprotein B mRNA editing enzyme, catalytic polypeptide-like 3G	82.0±0.5%	+	-	A cytidine deaminase that Inhibits HIV by DNA editing
MGAT1	mannosyl (alpha-1,3-)-glycoprotein beta-1,2-N-acetylglucosaminyltransferase	77.5±6.0%	-	-	Unknown
APOBEC3F	apolipoprotein B mRNA editing enzyme, catalytic polypeptide-like 3F	76.3±0.7%	+	-	A cytidine deaminase that edits RNA or DNA. Has restrictive activity against several viruses including HIV.
GPR146	G protein-coupled receptor 146	74.7±2.5%	+	+	Unknown
LY6E	lymphocyte antigen 6 complex, locus E	73.7±3.6%	+	-	Unknown
TAP1	transporter 1, ATP-binding cassette	72.8±4.0%	+	+	Unknown
SLFN12	schlafen family member 12	72.2±5.9%	-	-	Unknown
FCGR1A(CD64)	Fc fragment of IgG, high affinity Ia, receptor	67.1±3.7%	+	-	Unknown
TRIM62	tripartite motif containing 62	64.7±8.6%	+	-	Unknown
USP2	ubiquitin specific peptidase 2	63.6±1.9%	-	-	Unknown
MAFK	v-maf musculoaponeurotic fibrosarcoma oncogene homolog K	63.4±3.8%	-	-	Unknown
PARP12	poly (ADP-ribose) polymerase family, member 12	62.9±5.1%	-	+	Unknown
TRIM25	tripartite motif containing 25	61.8±6.6%	-	+	Activates interferon through RIG-I
MITD1	microtubule interacting and transport, domain containing 1	56.3±3.3%	-	-	Unknown
OAS1-1	2'-5'-oligoadenylate synthetase 1 variant 1	48.7±5.3%	-	-	Activation of RNaseL leads to degradation of viral RNA
MX2	myxovirus (influenza virus) resistance 2	48.4±3.1%	-	-	GTPase that inhibits Orthomyxoviruses, paramyxoviruses, rhabdoviruses, togaviruses, bunyaviruses including HBV, influenza, coxackie virus
OASL	2'-5'-oligoadenylate synthetase-like	29.4±10.4%	-	-	Activation of RNaseL leads to degradation of viral RNA

Supplementary Table T4

	Average % Inhibition of MHV68 compared to control-transfected cells
IRF1	105%
MX1/MX2	65%
BMP2	51%
SPRY2	49%
IKZF1	48%
MNDA	47%
MX2	44%
MGAT1	42%
SLFN12	41%
MAFK,MAFG,MAFF	40%
CREB5	38%
FCGR1A (CD64)	38%
PML	37%
RNF213	36%
APOBEC3G	36%
PARP12	35%
LY6E	33%
ADAR	33%
Setdb1	32%
IFIT1	32%
LIPG	31%
ALDH1	30%
SOCS3	28%
ASB13	24%
PRPF4	24%

Supplementary Table 5. Selected Anti-viral ISG against MHV68					
ISG	**Full Name**	**MHV68 Inhibition by luciferase (9hpi)**	**Significant Inhibition by Plaque Assay ($p<0.05$)**	**Inhibition of Immediate Early RTA Expression 4hpi**	**Anti-Viral Function**
IRF1	interferon regulatory factor 1	52±20%	+	+	Activator of Interferon
DDX58	DEAD box polypeptide 58 (RIG-I)	40±28%	+	+	Activator of Interferon
OAS1-1	2'-5'-oligoadenylate synthetase 1 variant 1	48.7±5.3%	+	+	Activation of RNaseL leads to degradation of viral RNA
MX2	myxovirus (influenza virus) resistance 2	49.0±11%	+	+	GTPase that inhibits Orthomyxoviruses, paramyxoviruses, rhabdoviruses, togaviruses, bunyaviruses including HBV, influenza, coxackie virus
BMP2	bone morphogenetic protein 2	34±12%	+	+	unknown
ADAR	adenosine deaminase, RNA-specific	34±11%	+	-	Edits viral genome by deamination of RNA from adenosine to inosine. Different effects on growth of various viruses.
MNDA	myeloid cell nuclear differentiation antigen	31±10%	+	+	unknown
SPRY2	sprouty homolog 2	23±7%	+	-	unknown
MAFK	v-maf musculoaponeurotic fibrosarcoma oncogene homolog K	37±8%	+	-	unknown
CH25H	Cholesterol 25 Hydroxylase	0%	+	+	unknown
MITD1	microtubule interacting and transport, domain containing 1	0%	+	+	unknown
IFIH1	interferon induced with helicase C domain 1 (MDA5)	5%	+	+	Activator of interferon

REFERENCES

1. van den Broek MF, Müller U, Huang S, Zinkernagel RM, Aguet M (1995) Immune defence in mice lacking type I and/or type II interferon receptors. *Immunol Rev* 148(1):5–18.
2. Sadler AJ, Williams BRG (2008) Interferon-inducible antiviral effectors. *Nat Rev Immunol* 8:559–568.
3. Schroder K, Hertzog PJ, Ravasi T, Hume DA (2004) Interferon-γ: An overview of signals, mechanisms and functions. *J Leukoc Biol* 75(2):163–189.
4. Schoggins JW, et al. (2011) A diverse range of gene products are effectors of the type I interferon antiviral response. *Nature* 472:481–485.
5. Flaño E, Kim I-J, Woodland DL, Blackman MA (2002) γ-Herpesvirus latency is preferentially maintained in splenic germinal center and memory B cells. *J Exp Med* 196: 1363–1372.
6. Meraz MA, et al. (1996) Targeted disruption of the Stat1 gene in mice reveals unexpected physiologic specificity in the JAK-STAT signaling pathway. *Cell* 84:431–442.
7. Xie ZL, et al. (2011) Co-transfection and tandem transfection of HEK293A cells for overexpression and RNAi experiments. *Cell Biol Int* 35(3):187–192.
8. Yoneyama M, et al. (2005) Shared and unique functions of the DExD/H-box helicases RIG-I, MDA5, and LGP2 in antiviral innate immunity. *J Immunol* 175:2851–2858.
9. Miyamoto M, et al. (1988) Regulated expression of a gene encoding a nuclear factor, IRF-1, that specifically binds to IFN-β gene regulatory elements. *Cell* 54:903–913.
10. Hwang S, et al. (2008) Persistent gammaherpesvirus replication and dynamic interaction with the host in vivo. *J Virol* 82:12498–12509.
11. Park C, Li S, Cha E, Schindler C (2000) Immune response in Stat2 knockout mice. *Immunity* 13:795–804.
12. Takaoka A, et al. (2000) Cross talk between interferon-γ and -α/β signaling components in caveolar membrane domains. *Science* 288:2357–2360.
13. Müller U, et al. (1994) Functional role of type I and type II interferons in antiviral defense. *Science* 264:1918–1921.
14. Banerjee AK (1987) Transcription and replication of rhabdoviruses. *Microbiol Rev* 51 (1):66–87.
15. Barr JN, Whelan SP, Wertz GW (2002) Transcriptional control of the RNA-dependent RNA polymerase of vesicular stomatitis virus. *Biochim Biophys Acta* 1577:337–353.
16. Negrete OA, et al. (2005) EphrinB2 is the entry receptor for Nipah virus, an emergent deadly paramyxovirus. *Nature* 436:401–405.
17. Wu T-T, Usherwood EJ, Stewart JP, Nash AA, Sun R (2000) Rta of murine gammaherpesvirus 68 reactivates the complete lytic cycle from latency. *J Virol* 74:3659–3667.
18. Dutia BM, Allen DJ, Dyson H, Nash AA (1999) Type I interferons and IRF-1 play a critical role in the control of a gammaherpesvirus infection. *Virology* 261(2):173–179.
19. Sarawar SR, et al. (1997) γ interferon is not essential for recovery from acute infection with murine gammaherpesvirus 68. *J Virol* 71:3916–3921.
20. Taniguchi T, Takaoka A (2002) The interferon-α/β system in antiviral responses: A multimodal machinery of gene regulation by the IRF family of transcription factors. *Curr Opin Immunol* 14(1):111–116.
21. Wang X, Lybarger L, Connors R, Harris MR, Hansen TH (2004) Model for the interaction of gammaherpesvirus 68 RING-CH finger protein mK3 with major histocompatibility complex class I and the peptide-loading complex. *J Virol* 78:8673–8686.
22. Boname JM, de Lima BD, Lehner PJ, Stevenson PG (2004) Viral degradation of the MHC class I peptide loading complex. *Immunity* 20:305–317.
23. Yamaguchi K, et al. (1999) XIAP, a cellular member of the inhibitor of apoptosis protein family, links the receptors to TAB1-TAK1 in the BMP signaling pathway. *EMBO J* 18:179–187.
24. Brown HJ, et al. (2003) NF-κB inhibits gammaherpesvirus lytic replication. *J Virol* 77: 8532–8540.
25. Scherle PA, Dorshkind K, Witte ON (1990) Clonal lymphoid progenitor cell lines expressing the BCR/ABL oncogene retain full differentiative function. *Proc Natl Acad Sci USA* 87:1908–1912.
26. Zarnegar BJ, et al. (2008) Noncanonical NF-κB activation requires coordinated assembly of a regulatory complex of the adaptors cIAP1, cIAP2, TRAF2 and TRAF3 and the kinase NIK. *Nat Immunol* 9:1371–1378.
27. Takada A, et al. (1997) A system for functional analysis of Ebola virus glycoprotein. *Proc Natl Acad Sci USA* 94:14764–14769.
28. Pavlidis P, Noble WS (2003) Matrix2png: A utility for visualizing matrix data. *Bioinformatics* 19:295–296.

CHAPTER 3

The Interferon-Inducible Cholesterol-25-Hydroxylase Broadly Inhibits Viral Entry by Production of 25-Hydroxycholesterol

ABSTRACT

Interferons (IFN) are essential antiviral cytokines that establish the cellular antiviral state through upregulation of hundreds of interferon-stimulated genes (ISGs), most of which have uncharacterized functions and mechanisms. We identified Cholesterol-25-hydroxylase (Ch25h) as an antiviral ISG that can convert cholesterol to a soluble antiviral factor, 25-hydroxycholesterol (25HC). Ch25h expression or 25HC treatment in cultured cells broadly inhibits enveloped viruses including VSV, HSV, HIV, and MHV68 as well as acutely pathogenic EBOV, RVFV, RSSEV, and Nipah viruses under BSL4 conditions. As a soluble oxysterol, 25HC inhibits viral entry by blocking membrane fusion between virus and cell. In animal models, Ch25h-knockout mice were more susceptible to MHV68 lytic infection. Moreover, administration of 25HC in humanized mice suppressed HIV replication and rescued T-cell depletion. Thus, our studies demonstrate a unique mechanism by which IFN achieves its antiviral state through the production of a natural oxysterol to inhibit viral entry and implicate membrane-modifying oxysterols as potential antiviral therapeutics.

INTRODUCTION

Viruses are obligate intracellular pathogens that—despite having unique structure and function--undergo lifecycle stages of entry, replication, protein synthesis, assembly, and egress. Upon specific binding to cell surface molecules, non-enveloped virus can enter the cell directly while enveloped viruses undergo fusion process that requires specific interactions between the viral and cellular receptors and membranes. After entry, viral components are released into the cytoplasm and may enter the nucleus. Although incipient viral proteins may be sufficient to initiate early lifecycle processes, full viral replication, transcription and translation require utilization of cellular factors. The newly synthesized viral proteins and genome are then coordinately assembled into virions, which then exit the cell by lysis or budding.

While viruses exploit host factors to successfully replicate, the innate immune system produces interferons (IFN), essential antiviral cytokines that induce wide array of antiviral effectors. Individually, many of these IFN-stimulated genes (ISGs) work to inhibit virus at particular stages of its lifecycle. IFITM proteins block viral entry and ISG20, a 3-5' exonuclease, degrades single stranded viral RNA; PKR inhibits viral translation through suppression of eIF2a elongation factors and tetherin prevents release of virions from the cell(Degols et al., June; García et al., 2006; Brass et al., 2009; Perez-Caballero et al., 2009). These ISGs exemplifies only a few of the hundreds of confirmed ISGs; most of them are uncharacterized.

Cholesterol-25-hydroxylase (Ch25h) is an ISG conserved across mammalian species. The intronless gene encodes an endoplasmic-reticulum-associated enzyme that catalyzes oxidation of cholesterol to 25-hydroxycholesterol (25HC)(Holmes et al.,

2011). 25HC belongs to a diverse class of endogenous oxysterols, the oxidation products of cholesterol. It is widely understood to be a soluble factor that controls sterol biosynthesis through regulation of sterol-responsive element binding proteins (SREBP) and nuclear receptors (Kandutsch et al., 1978; Janowski et al., 1999). While oxysterols have unique roles in metabolism, studies have implicated their importance in immunity. Macrophages and B-cells express Ch25h robustly in response to various toll-like receptor (TLR) ligands and IFN(Bauman et al., 2009; Park and Scott, 2010). Ch25h suppresses IgA production in B-Cells and may promote intracellular bacterial growth by induction of prosurvival factors in macrophages (Bauman et al., 2009; Zou et al., 2011). Like immune mediators, dysregulation of 25HC is associated with immune pathology such as atherosclerosis (Andrew J and Jessup, 1999), which is partly attributed to its induction of the inflammatory cytokine, IL-8 (Wang et al., 2012). Although these studies support a conserved immunological role of Ch25h and 25HC, their functions in the immune system remain elusive.

We have found that Ch25h is important for the host immune response against viral infection. This study explores the antiviral properties of Ch25h, the mechanism of its viral inhibition, as well as its physiological significance during viral infections.

RESULTS

Ch25h is an IFN-dependent Gene with Antiviral Activity

In a microarray analysis of IFNα and IFNγ stimulated murine bone marrow-derived macrophages (BMMs), we found both IFNs induced expression of Ch25h within 3hrs (Fig. 3-1A). A subsequent RNAseq analysis showed the TLR4 agonist, lipidA, induced Ch25h expression. This induction was dependent on IFN receptor (IFNAR) but independent of IL-27, a cytokine that mediates IFN secondary gene expression, such as IL-10 (Fig. 3-1B). We further tested different TLR agonists and found dsRNA mimetic, polyI:C (TLR3 agonist), and lipidA induced Ch25h mRNA expression highly whereas Pam-3-Cys (TLR2 agonist) and CpG (TLR9 agonist) induced it less. IFNAR-deficient BMMs had abrogated Ch25h expression when treated with these agonists showing that Ch25h expression is IFN-dependent (Fig. 3-1C).

In a previous study, we sought antiviral ISGs against vesicular stomatitis virus (VSV) in a blinded and unbiased functional screen (Liu et al., 2012). Individual ISGs in expression plasmids were co-transfected with red fluorescent construct (DsRed) in HEK293T cells for 36h and subsequently infected with VSV coexpressing GFP (VSV-GFP) for 9 h and analyzed by FACS. Active viral replication was measured by percentage and geometric mean fluorescence index (%GFP+ X Geometric MFI) of GFP-positive cells in the DsRed population. TANK-binding kinase-1 (Tbk1), which is an activator of IFN production, was used as a positive control. The amount of infection was normalized to cells co-transfected with DsRed and control vector. Expression of Ch25h inhibited VSV-GFP replication by ~70% at 9hpi (Fig. 3-1 D and E). IFN activators like

Tbk1, Ifih1 (Mda5), and Irf1 strongly inhibited VSV as well as the RNA exonuclease, ISG20.

To validate the antiviral effect of Ch25h, we generated a doxycycline-inducible Ch25h-flag construct co-expressing a flourescent-red mCherry (Ch25h-mCherry). Doxycycline addition to HEK293T expressing this construct increased CH25H-flag expression (Fig. 3-2 A top) and mCherry expression in a dose-dependent manner (Fig. 3-2A, bottom). When infected with VSV-GFP, HEK293T expressing Ch25h-mCherry and treated with doxycycline exhibited a dose-dependent inhibition of VSV-GFP compared to vector control (Fig. 3-2 A, bottom). Taken together, Ch25h is sufficient to inhibit VSV.

Loss of function of Ch25h leads to Susceptibility to Viral Infections *in vitro*

We sought to determine whether Ch25h might play a necessary role in the viral infection. We generated Ch25h stable knockdown cell lines in murine macrophage cell line, RAW264.7, with two distinct shRNA sequences against Ch25h (Fig. 3-2B). Both knockdown cell lines demonstrated increased VSV replication compared to scramble control (Fig. 3-2C). To further validate these results, we derived B-Cells and macrophages from Ch25h-deficient (*ch25h-/-*) and matching wild-type (*ch25h+/+*) mice. In our experience, VSV-GFP can not establish infection in primary cells (unpublished). Hence, B-cells were immortalized with BCR-ABL virus and several stable clones were isolated. We observed about 100 fold increase in VSV-GFP replication in 3 different *Ch25h-/-* B-Cell clones at 48hpi compared to 2 *ch25h+/+* B-cell clones (Fig. 3-2D). In parallel, we performed VSV infection in BMMs immortalized by J2 virus (Fig. 3-2E).

Similarly, *ch25h-/-* J2 BMMs displayed 5-fold increased susceptibility to VSV infection compared to *ch25h+/+* J2 BMMs at 14hpi. These results show that Ch25h may be required for host antiviral immunity.

Ch25h produces a soluble antiviral factor that is not IFN

Based on the FACs analyses of HEK293T transfected with ISGs in Figure 1D, we separated our analyses to examine total, DsRed-positive (DsRed+), and DsRed-negative (DsRed-) populations (Fig. 3-3A). DsRed+ population should represent cells that highly expressed the ISG, whereas DsRed- population should represent the low expressing population. IFN activators such as Tbk1, Irf1, and Ifih1 inhibited VSV-GFP expression by >95% in all populations suggesting that the high expressers (DsRed+) confer viral resistance to low expressers (DsRed-) (Fig. 3-3B). This result is consistent with IFN-mediated induction of an antiviral response in naïve cells. In contrast, the cytoplasmic exo-nuclease ISG20 that degrades viral RNA, only inhibited VSV in DsRed+ population, but could not confer protection to DsRed- population. Overexpression of Ch25h also inhibited virus in both DsRed+ and DsRed- populations suggesting that Ch25h produced a soluble factor that could confer, *in trans,* antiviral activity onto other cells.

To determine if Ch25h produced a soluble antiviral factor, we tested whether conditioned media from cells overexpressing Ch25h had antiviral activity. HEK293T cells were transfected with vector, interferon activators (Tbk11, Irf1, and Ifih1) or ISGs, for 48hours and the conditioned media was filtered and transferred onto freshly plated HEK293T cells for 8h before infection with VSV-GFP (0.01MOI) for 9h. VSV-GFP

measured by FACs was significantly less in cells treated with conditioned media from Tbk1, Irf1, Ifih1, because they contain IFN. Compared to vector controls, Ch25h-conditioned media caused ~80% VSV-GFP inhibition (Fig. 3-3 C). On the other hand, conditioned-media from Isg20-transfected cells had no effect on VSV replication. Furthermore, we have observed inhibition of VSV growth by Ch25h conditioned media across several human and murine cell lines including HeLa, 3T3, BHK, Veros, MDCK, and Huh751 (Supp. Fig. S3-1 A). These results demonstrate that Ch25h produces a soluble antiviral factor.

IFN is well known to induce many ISGs that positively feedback and amplify IFN itself. Since there have been no soluble antiviral ISGs described aside from IFN, we tested whether Ch25h can induce IFN. Ch25h conditioned media had no detectable IFNβ by ELISA and did not induce an IFN-stimulated responsive element (ISRE) luciferase reporter (Supp. Fig. S3-1 B and C). More importantly, Ch25h-conditioned media inhibited VSV replication in both *ifnar-/-* fibroblasts and J2 BMMs. On the other hand, conditioned media from IFN activators, Irf1, Ifih1, and Rig-I, were unable to confer antiviral activity to *ifnar-/-* cell lines (Fig. 3-3 E and F). Taken together, Ch25h produces a soluble factor that is not IFN and can confer antiviral activity independent of IFNAR.

25-hydroxycholesterol, the cognate product of Ch25h, has antiviral activity

Ch25h catalyzes oxidation of cholesterol to 25-hydroxycholesterol (25HC), which is a soluble oxysterol that modulate cellular functions in an autocine and paracrine fashion (Fig. 3-4 A, top). We hypothesized that the soluble antiviral factor generated by Ch25h is 25-hydroxycholesterol. Treatment of HEK293T cells with 25HC for 8h

inhibited VSV-GFP expression by FACs in a dose-dependent manner with IC_{50} of ~1μM (Fig. 3-4 A, bottom). Some studies have shown 25HC as a weak ligand for LXR suggesting this nuclear receptor might play a role in the antiviral activity of 25HC (Janowski et al., 1999). Treatment of HEK293Ts with 22-(R)-hydroxycholesterol (22R-HC), an oxysterol that strongly activates LXR, however, did not confer antiviral effect and neither did 22-(S)-hydroxycholesterol (22S-HC), an inactive ligand for LXR (Fig 3-4. A, bottom). 25HC treatment of *ch25h+/+* and *ch25h-/-* J2 BMMs also reduced VSV replication (Fig. 3-4B).

We tested whether the antiviral activity of 25HC was attributed to cellular cytotoxicity. Treatment of 10μM of 25HC, which is10 fold higher than observed IC_{50}, did not increase LDH in supernatants of cells after 16h of treatment; LDH level increased only after 30-40h treatment at 40μM of 25HC (Supp. Fig. S3-2 A and B). Similarly, Ch25h-conditioned media did not alter cell viability as measured by cellular ATP levels (Supp. Fig. S3-2 C). These data show that Ch25h-conditioned media and the effective antiviral dose of 25HC are not cytotoxic. Therefore, these results suggest that the antiviral activity of Ch25h is carried out through its enzymatic product, 25HC. Its antiviral activity is not attributed to LXR function *per se* and---compared to the oxysterols tested—is specific.

Ch25h-conditioned media and 25HC is broadly antiviral

To determine the breadth of antiviral activity of Ch25h, we tested the effect of Ch25h-conditioned media and 25HC on various viruses. For HIV, primary peripheral blood mononuclear cells were treated with conditioned media or oxysterol and

subsequently infected with HIV NL4-3. At 3dpi, Ch25h- and Irf1- conditioned media caused ~75% reduction of HIV NL4-3 p24 expression (Fig. 3-4 C). Similarly, 25HC (1μM) inhibited p24 expression by ~80% at 3dpi compared to vehicle treatment, whereas 22S-HC had no effect (Fig. 3-4 D). Ch25h-conditioned media also inhibited herpes simplex virus 1 (HSV-1) by plaque assay (Fig. 3-4 E) and expression of Ch25h in HEK293T also inhibited MHV68 infection by plaque assay (Fig. 3-4 F).

HIV, HSV-1, and MHV68 are viruses that achieve chronically persistent infections. To determine whether Ch25h-induced 25HC can inhibit acutely pathogenic viruses, we tested the effect of 25HC on live Ebola virus (EBOV-Zaire), Nipah virus (Bangladesh), Russian Spring-Summer Encephalitis Virus (RSSEV), and Rift Valley fever virus RVFV (wild-type strain ZH501 and vaccine strain MP12) under BSL4 conditions. Figures 3-4 G, H, I, and J show that 1μM of 25HC inhibited replication of these live viruses. 25HC also inhibited replication of Nipah and RVFV (MP12) in a dose-dependent manner (Supp. Fig. S3-2 D and E). In contrast, a non-enveloped virus, adenovirus coexpressing GFP, was not affected by 25HC as measured by FACs (Fig. 3-4 K). Taken together, Ch25h-induced 25HC has antiviral activity against several types of enveloped DNA and RNA viruses, while they do not seem to have effect on non-enveloped virus.

25HC inhibits VSV entry

We took advantage of tools available for VSV and HIV to study the mechanism of Ch25h inhibition on the viral lifecycle. First, we utilized the pseudotyped VSVΔG-Luc reporter virus system that has the receptor-binding G gene (VSV-G) replaced with a

luciferase reporter gene (Negrete et al., 2006). When VSV-G is provided *in trans*, this pseudotyped VSV reporter virus is only capable of single-round infections because it cannot produce its own VSV-G. Hence, quantification of luciferase activity is indicative of viral lifecycle processes from entry to protein synthesis. We observed that Ch25h and Irf1 conditioned media inhibited virus reporter gene expression at the earliest time-point (8 hpi) we can detect luciferase activity in the infected cell lysate (Fig. 3-5A), suggesting Ch25h inhibits viral replication at an early stage.

Next, we performed a time-of-addition experiment to better elucidate the mechanism underlying the antiviral activity of 25HC. HEK293T cells were treated or pre-treated with 5μM 25HC at the indicated time points. For pretreated cells, they were infected with VSVΔG-Luc pseudovirus for 1h without 25HC; after washing, cells were replaced with regular media. We also added 25HC concurrently with infection (time 0) for 1h or added it at 1hpi. Interestingly, longer pre-treatment times correlated with greater inhibition of VSVΔG-Luc expression, compared to the ethanol vehicle treated controls. When 25HC was added concurrently with VSVΔG-Luc pseudovirus or 1 hpi, there was no significant inhibition of VSV-G-Luc (Fig. 3-5 B). These results suggest that 25HC does not inhibit VSV during infection or after infection has taken place. Rather, it is likely that 25HC establishes an antiviral state prior to infection.

Since these data implicate early viral lifecycle steps may be affected, we carried out experiments to determine whether 25HC affects attachment (Weidner et al., 2010). HEK293Ts were treated for 8h with ethanol (EtOH), 25HC (1μM), CPZ (10μg/mL), an endocytosis inhibitor that would have no effect on binding. To measure binding, VSV (1MOI) was incubated with HEK293T at 4°C for 1h to allow for binding but not cell entry.

After washing 3 times with cold PBS, total RNA was collected and VSV genomic RNA (gRNA) was reverse-transcribed with gRNA specific primer. 25HC and CPZ did not inhibit binding significantly ($P>0.05$) (Fig. 3-5 C).

To determine if 25HC affects efficiency of fusion, we established a VSV-G β-lactamase (Bla) entry assay based on the ability of VSV-G to be pseudotyped onto viral-like particles made from the Bla-Nipah virus matrix fusion protein, herein called VSV-G/BlaM (Wolf et al., 2009). VSV-G mediated fusion will result in cytoplasmic delivery of Bla-M; by addition of lipophilic fluorescent CCF2-AM substrate, the β-lactamase activity can be measured by the green (525nm) to blue (485 nm) fluorescence shift as a result of CCF2-AM cleavage (Zlokarnik et al., 1998). Hence, efficiency of virus-cell fusion can be measured by the increase in the ratio of blue to green (blue:green) fluorescence, which is reflective of the β-lactamase activity associated with BlaM that was been released into the cytoplasm after VSV-G mediated fusion (Cavrois et al., 2002; Wolf et al., 2009). Unlike the VSVΔG-Luc pseudotyped virus, this VSV-G/BlaM entry assay does not require transcription and translation of viral proteins for reporter gene expression.

HEK293T cells were transfected with several ISGs for 48 hours and infected with VSV-G/BlaM. Figure 3-5D showed that Ch25h and Irf1 reduced efficiency of VSV fusion. Compared to vector control, BlaM activity from Ch25h- and Irf1-transfected cells proceeded at a slower rate compared to vector-transfected cells (compare the respective slopes for the first 45 min) and plateaued at a lower level (compare blue:green ratio at 120 min). To a lesser extent, Ifitm3 also reduced VSV-G/BlaM entry, consistent with published results that showed it inhibits VSV-pseudovirus infection

(Brass et al., 2009). ISG20, a viral RNA exonuclease, had no effect on viral entry. Ch25h-conditioned media similarly inhibited VSV-G/BlaM entry, but with a more pronounced effect than Irf1-conditioned-media (Fig. 3-5 E). Finally, we also observed a dose-dependent inhibition on VSV-G/BlaM entry with treatment of 25HC at 1, 2.5, and 5μM (Fig. 3-5 F). These results demonstrate that the ISG, Ch25h, and its cognate product, 25HC, modulates the target cell membrane in a manner that inhibits efficiency of virus-cell fusion.

Since the viral entry step involves interactions between both the viral and cellular membranes, we then asked if the infectivity of the virions were affected when produced from 25HC treated cells. HEK293T were treated with and without 25HC (2.5μM) for 8h and infected with replication-competent VSV at 0.01 MOI. After a 1h infection period, the cells were washed and media with or without 25HC (2.5μM) was added. The viral supernatants from infected cells were collected at 24hpi, purified, and concentrated by ultracentrifugation through a 20% sucrose cushion, which also removed any residual 25HC. As expected, 25HC treatment caused >80% reduction in the amount of VSV produced compared to vehicle-treated controls as measured by qRT-PCR for the number of viral genome copies (Supp. Fig. S3-3 A). To assess infectivity, we measured the infectious titer of viruses produced from 25HC- or vehicle-treated cells after normalizing for the amount of viral gRNA as determined above. When the titer was quantified on Vero cells, viruses from 25HC treated cells had equivalent plaque forming units as viruses from vehicle-treated cells (Supp. Fig. S3-3 B), demonstrating that while 25HC exerts its antiviral effect by altering target cell membrane properties, this effect is not manifested in virions produced from those cells.

25-hydroxycholesterol is a suppressor of SREBP2, which controls sterol biosynthesis and can alter membrane sterol composition. Hence, we tested the hypothesis that 25HC inhibits viral infection through suppression of SREBP2. We tested whether overexpression of active (cleaved) form of SREBPs in HEK293T would overcome the anti-viral effect of 25HC. When we overexpressed the active forms of SREBP1a, SREBP1-c, and SREBP2 in HEK293Ts, however, 25HC inhibited viruses in all transfected cells (Supp Fig. S3-4 A). These data demonstrate that the antiviral effect of 25HC is SREBP independent.

Ch25h and 25HC inhibits HIV entry

We sought to validate Ch25h and 25HC antiviral mechanism on HIV. Unlike VSV, HIV is a retrovirus that undergoes pH-independent cellular entry. In CEM cells, 25HC inhibited >50% luciferase expression from single round infection of pseudovirus with HIV-IIIB envelope on a NL4-3 backbone coexpressing luciferase (pNL4-3.Luc.-R-E) (Fig. 3-6A). AZT, an inhibitor of reverse transcription, served as positive control and inhibited expression by ~70%. Hence, these data also suggest 25HC inhibits viral lifecycle prior to translation.

HIV initiates reverse transcription of its genomic RNA to DNA immediately after entry. Hence, we examined the effect of 25HC on the production of full-length, reverse-transcribed DNA (lateRT). CEM cells were infected with pseudotyped HIV-IIIB and lateRT was measured by qRT-PCR. 25HC inhibited lateRT expression >99% at 2hpi and ~70% at 6hpi (Fig. 3-6B). The HIV entry inhibitor, AMD3100, served as a positive control. Elvitegravir inhibits HIV at the step of DNA integration into the host genome

and served as negative control because it shouldn't inhibit lateRT formation. These results show that 25HC inhibits a stage of the HIV life cycle before reverse transcription of its genome.

We next asked whether Ch25h inhibits HIV similar to VSV at the level of entry. We coexpressed pNL4-3 with Bla-VPR fusion gene to produced virions containing Bla-VPR (NL4-3/Bla). CEM cells treated with Ch25h conditioned media exhibited ~60% reduction in viral entry compared to vector- and Isg20-conditioned media. AMD3100 abrogated NL4-3/Bla entry (Fig. 3-6C). We further confirmed our findings by FACS analysis and observed ~50% decrease in the number of cells expressing cleaved CCF2-AM substrate (blue population) in CEM treated with Ch25h conditioned media compared to control (supp. Fig. S3-5 A). Treatment of CEM cells with 25HC (5μM) caused ~60% decrease in NL4-3/Bla blue-green ratio at endpoint (Fig. 3-6D) and >85% reduction in cells expressing cleaved CCF2-AM by FACS analysis (Fig. 3-6E).

Since 25HC may have diverse cellular effects, we asked whether 25HC might affect other HIV life cycle processes. To assess 25HC effect on HIV transcription, we transfected HEK293Ts with pNL4-3 co-expressing GFP (NL4-3-GFP) and treated the cells with 25HC at 4h post transfection. The NL4-3-GFP expression after 24h was not suppressed suggesting that 25HC does not affect HIV transcription and translation (Supp. Fig. S3-5 B). Concurrently, treatment of with 25HC did not reduce budding of HIV virions from NL4-3-GFP transfected cells as measured by HIV p24 in the supernatants, while Nelfinavir, a known budding inhibitor, inhibited p24 expression by >50% at 24 and 48h post transfection (Supp. Fig. S3-5 C). Taken together, Ch25h and

25HC inhibits efficiency of HIV membrane fusion, while 25HC treatment does not seem to affect HIV transcription, translation, and budding processes.

25HC inhibits virus-cell membrane fusion

Although β-lactamase data demonstrate 25HC inhibits viral entry processes up to fusion, we sought to test whether 25HC inhibits the viral fusion process itself. Since we have observed 25HC inhibited live Nipah replication (Figure 3-4H), we sought to test whether it would also affect its fusion process. Expression of the Nipah fusion (F) and attachment (G) proteins by themselves induces pH-independent cell membrane fusion and syncytia formation. Hence, vero cells were transfected with recombinant Nipah F and G at equal ratios for 5h and refreshed with media containing 25HC or ethanol (vehicle). At 21h post transfection, cells were fixed and stained by Giemsa. Grossly, 25HC treatment led to less syncytia formation and fewer nuclei per syncytias compared to ethanol control (Fig. 3-6F). In a blinded count of numbers of nuclei per syncytia, a standard measure of fusion, 2μM of 25HC reduced fusion by ~50% and 10μM by ~60% relative to ethanol control (Fig. 3-6G). These data demonstrate that 25HC modifies the cellular membrane to inhibit viral membrane fusion.

25HC reduces HIV infection *in vivo*

To further determine the efficacy of 25HC against viral infection *in vivo*, we took advantage of HIV infection in a humanized mouse model. Humanized NOD-$Rag1^{null}Il2rg^{null}$ mice (NRG-hu) were administered 25HC (50mg/kg) 12h prior to infection with HIV NL4-R3A by intraperitoneal (i.p) injection. 25HC or the vehicle, 2-

hydroxypropyl-β-cyclodextrin (HβCD), was administered by i.p. every day and the serum was collected 7dpi. Quantification HIV RNA in the serum from 2 combined experiments showed >80% reduction of HIV RNA (copies/mL) in 25HC-treated mice compared to vehicle-treated mice ($P<0.0001$) (Fig. 3-7 A). At termination of the experiment on 14dpi, HIV p24 was significantly lower in CD4 T-cells from spleens of 25HC treated mice than control (Fig. 3-7 B). Moreover, at 10dpi, 25HC prevented HIV-mediated CD4+ T-cell depletion compared to vehicle control in CD3+(live T-cell) population in peripheral blood leukocytes ($P<0.05$); this effect was less significant in the spleen ($P=0.06$) (Fig. 3-7 C). These data show that administration of 25HC can cause antiviral effect against HIV *in vivo*.

Ch25h-deficient mice are more susceptible to viral infections

To determine whether Ch25h has a physiological role in host defense against viral infection, we tested whether *ch25h-/-* mice had increased susceptibility to matching wild-type mice (*ch25h+/+*). Since Ch25h expression inhibited MHV68 *in vitro*, we used MHV68 coexpressing luciferase (MHV68-Luc) to infect mice so that viral lytic growth kinetics could be measured in real time by bioluminescence. Eight-week old female *ch25h+/+* and *ch25h-/-* mice (N=4 in each group) were infected with 500pfu of MHV68-Luc i.p. and imaged every day after 3dpi. Average and maximal luminescence intensities from ventral, right, left, and dorsal side of every mouse were measured. We observed significantly higher MHV68-Luc activity in *ch25h-/-* mice over *ch25h+/+* mice starting 5 dpi and maximal differences between day 7 and 8 (Fig. 3-7 D and E). MHV68-Luc activity began to wane in both groups by 9dpi with significantly higher activity in

Ch25h-/- mice. To validate the imaging results, *Ch25h-/-* spleens had approximately ~3.5 fold higher MHV68 genomic DNA than spleens of *Ch25h+/+* mice at 10dpi (Fig. 3-7 F and G). These results show that Ch25h is a physiologically important antiviral factor.

DISCUSSION

We have identified the antiviral activity of an IFN-inducible gene, Ch25h, through a systematic, functional screen. Distinct from known IFN-mediated antiviral mechanisms, Ch25h inhibits growth of a wide range of enveloped viruses by production of a soluble oxysterol, 25-hydroxycholesterol. It also exemplifies the only soluble antiviral ISG that is not IFN itself. Independent of its known regulatory effect on metabolism, 25HC impairs viral entry at the step virus-cell fusion by inducing cellular membrane changes. In animal models, administration of 25HC reduces HIV infection in humanized mice. Moreover, the immune response against viral infections requires Ch25h *in vivo*. These findings illustrate an essential function of Ch25h in immunity.

Ifitm proteins are the only ISGs that have been described to inhibit viral entry, after endocytosis and before primary transcription (Brass et al., 2009; Weidner et al., 2010). The transmembrane protein inhibits only certain viruses, suggesting it has specific protein interactions with viral components. In contrast, 25HC is broadly inhibitory against enveloped viruses because it modifies the host cellular membrane and perturbs the virus-cell fusion process. Moreover, in our β-lactamase assays, overexpression of Ch25h inhibited VSV entry >2-fold higher than Ifitm3 (Fig. 3-5 D). Taken together, IFN induces these two ISGs to block viral entry likely by disparate mechanisms.

Oxysterols have multi-faceted physiological roles. Their permeability and solubility make them ideal rapid signaling regulators. Many oxysterols, like 7β-, 22-, 24-, 25-, and 27-hydroxycholesterol, redundantly regulate of sterol biosynthesis through suppression SREBP2 activity (Radhakrishnan et al., 2007). 25HC also increases

cellular cholesterol accessibility by directly mobilizing cholesterol from membranes(Lange et al., 2004). While the microbial effects of some oxysterols have been appreciated in chemistry, our study highlights the relationship between the host antiviral response and the oxysterol 25HC---illustrating that Ch25h-induced 25HC also acts as rapid, soluble viral fusion inhibitors (Moog et al., 1998; Pezacki et al., 2009). Therefore, 25HC has multiple functions in metabolism and in immunity.

Viruses enter cells with different types of fusion machinery, classified structurally and biochemically. 25HC's inhibition of virus is not specific to particular class of fusion proteins because HIV and Ebola have class-I fusion peptides, RVFV and RSSEV use class-II peptides, whereas VSV and HSV belong to class III (Kielian and Rey, 2006; Vaney and Rey, 2011). It also inhibits viruses that undergo either pH-dependent or pH-independent fusion as exemplified by VSV and HIV, respectively. These findings suggest that 25HC affect a more basic fusion process involving the viral and cellular membrane. Indeed, 25HC causes membrane expansion, increases solvent exposure of phospholipids, and prevents the membrane condensing effect of cholesterol in bilayers (Gale et al., 2009; Olsen et al., 2011). These changes can perturb viral fusion, which is fundamentally dependent on membrane properties such as spacing of lipid head groups, receptor accessibility, membrane curvature, and fluidity (Pécheur et al., 1998; Teissier and Pécheur, 2007). Studies on viral entry have predominantly focused on viral fusion components and their interactions with specific cellular receptors. How membrane properties modulate viral fusion remains subject of further research.

This study demonstrates how IFN inhibits viral fusion through the production of 25HC. Although 25HC have been associated with pathological conditions like

atherosclerosis and Alzheimers, it may have a beneficial role in innate immunity during viral infections. 25HC inhibited highly pathogenic viruses, which have no treatments are currently available, and short-term 25HC treatment suppressed HIV *in vivo*. These results encourage the exploration of antiviral oxysterols or cellular membrane modifiers as viral entry inhibitors against acute infections.

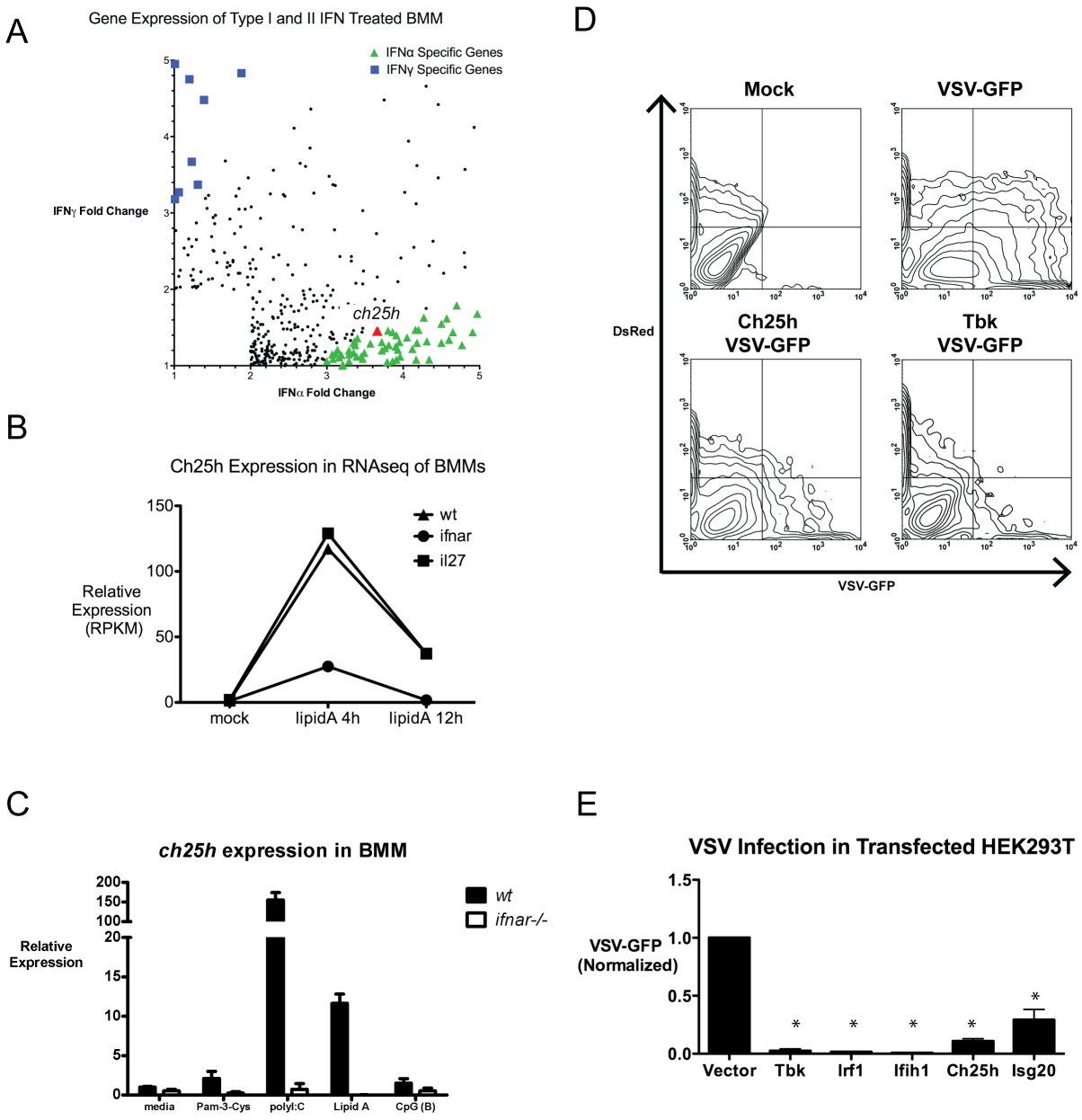

Figure 3-1.

A) Ch25h is IFN inducible. Gene expression profile of BMMs treated for 2.5 h with IFNα and IFNγ at 62 U/mL and 1 U/mL, respectively. Axes represent fold change in response to IFNα or IFNγ over untreated cells. IFNα-stimulated genes that were 3-fold higher than induction of IFNγ stimulated genes were categorized as IFNα-specific (green). Similarly, IFNγ stimulated genes were defined this way (blue). Ch25h is highlighted in red.

B) Wildtype, IFNAR-deficient and IL-27R (TCCR/WSX-1) deficient BMMs were stimulated with LipidA (100ng/mL) or saline control for 4hr and 12hr, respectively. CH25 expression values are presented as RKPM values
C) Ch25h gene expression measured by qPCR of wt and ifnar-/- BMMs stimulated with TLR agonists, Pam-3-Cys(100ng/mL), polyI:C(25ug/mL), lipidA(10ng/mL), CpG-B(100μM) for 4 hours.
D) HEK293T was co-transfected flourescent red marker (DsRed) and with individual plasmids encoding TBK, Ch25h, or vector for 36h and infected with VSV-GFP (0.01MOI) for 9h. VSV-GFP in DsRed+ and DsRed- populations was quantified by FACs.
E) Effect of overexpression of individual ISGs and Ch25h on VSV-GFP in DsRed-positive population normalized to vector control. VSV-GFP was quantified by the product of percent GFP-postive population and geometric mean of the fluorescence index (MFI). Mean±SEM; *P<0.01

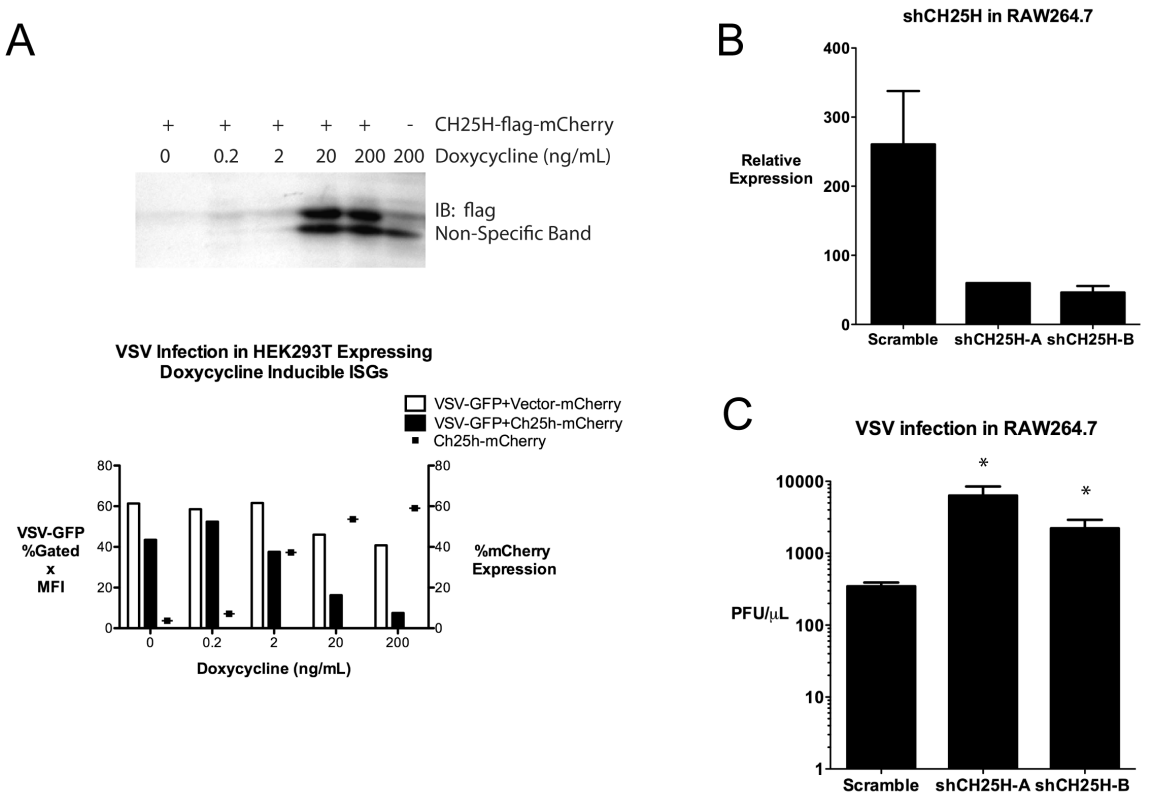

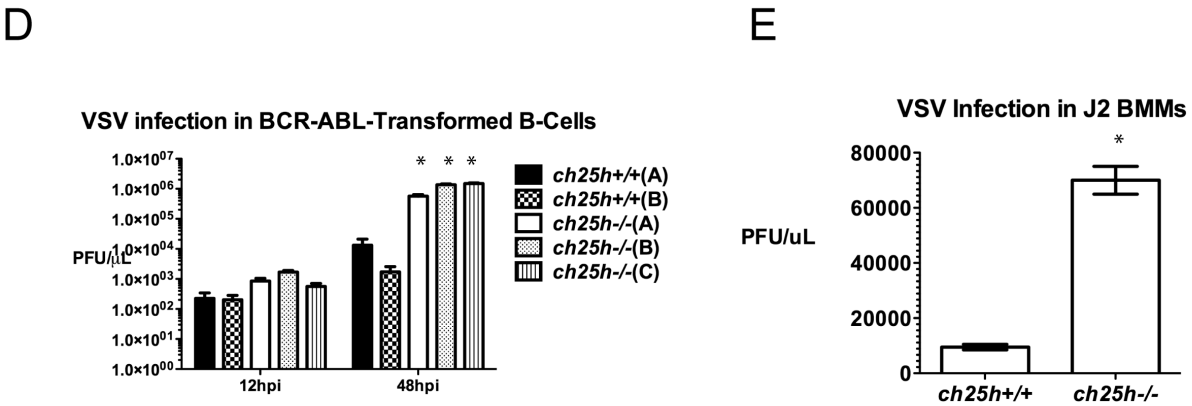

Figure 3-2

A) HEK293T expressing doxycycline-inducible construct coexpressing Ch25h-flag and red flourescent marker mCherry. HEK293T was transfected with vector or Ch25h encoding plasmids for 24h and doxycycline was added for 12h at indicated concentrations. After treatment, cells were infected with VSV-GFP (0.01MOI) for 9hrs and VSV-GFP was quantified by FACs. Dots represent percent positive mCherry. Expression of Ch25h-flag was confirmed by western blot (lower panel).

B) RAW264.7 stably knocked down the shRNA against Ch25h were generated by retro-viral infection. Two shRNA constructs were made (shCh25h-A and shCH25h-B) along with scramble control. Knockdown was confirmed by qPCR. *P<0.01
C) shCH25h-A, shCH25hB, and scrambled stable RAW264.7 were infected with VSV-GFP (0.1 MOI) and the VSV-GFP was measured by plaque assay 14hpi.
D) Individual clonal population of BCR-ABL transformed B-cells from *ch25h+/+* and *ch25h-/-* mice were infected with VSV-GFP (0.1MOI) in biological triplicates and the viral titers were measured by plaque assay at indicated times. *P<0.01
E) J2 BMM were derived from *ch25h+/+* and *ch25h-/-* mice and passaged for 2 weeks. The cells were infected VSV-GFP (0.1MOI) and viral titers 14hpi in the supernatants was quantified by plaque assay. *P<0.01

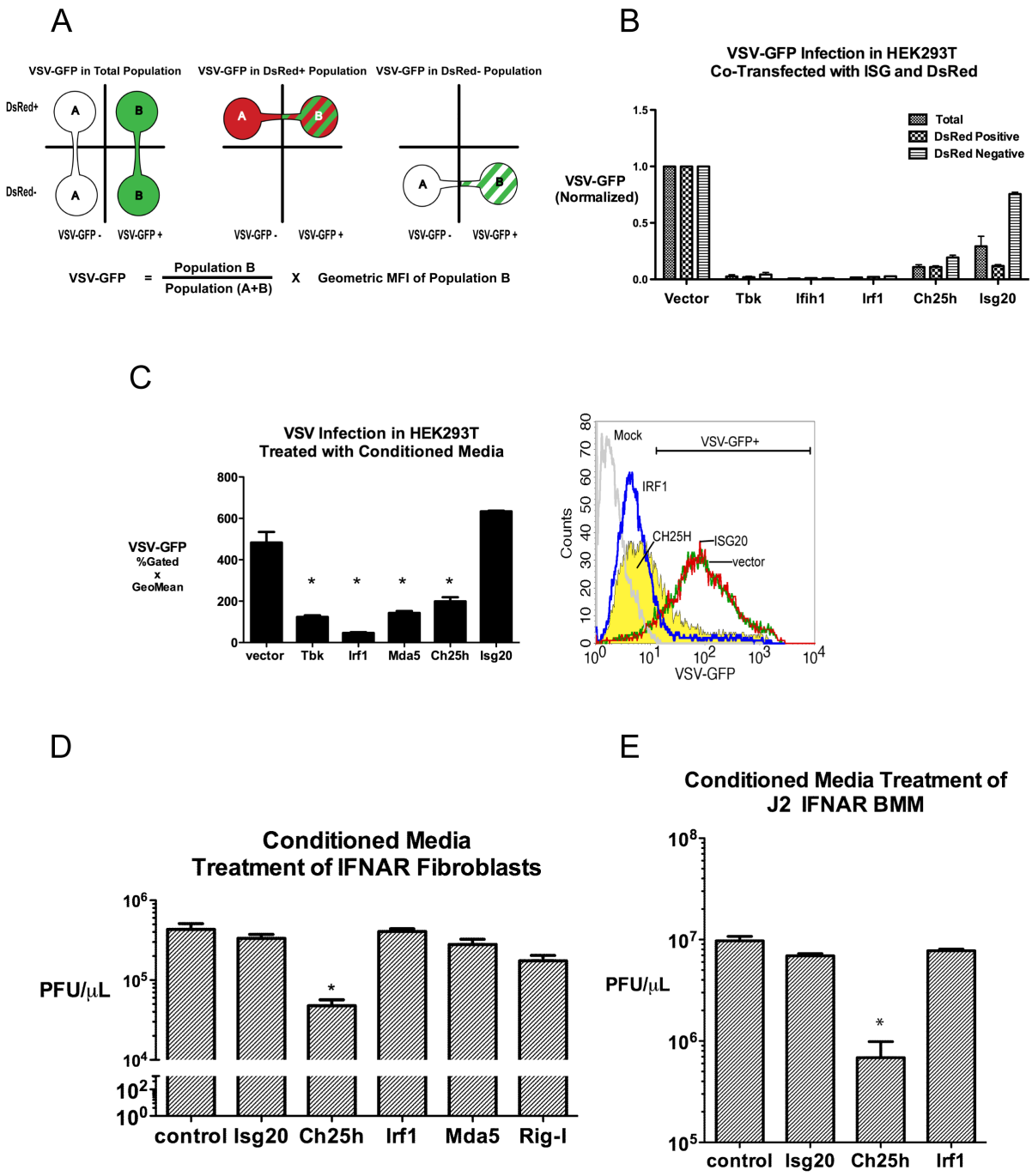

Figure 3-3

A) Schematic of FACs analysis of VSV-GFP in total, DsRed- VSV-GFP was defined as %postive GFP times the geometric mean fluorescence index (MFI). (DsRed+) and DsRed-negative (DsRed-) populations.
B) HEK293T transfected with DsRed and indicated expression vectors were infected with VSV-GFP and analyzed by FACs.
C) Media was collected from HEK293T after 48h transfection with indicated expression vector. Freshly plated HEK293T was treated with conditioned media for 12h and

infected with VSV-GFP (0.01MOI) for 9h. VSV-GFP was quantified by FACs similar to part A. Repesentative histogram of FACs data (right). *P<0.01

D) *Ifnar-/-* tail derived fibroblasts were treated with conditioned media for 12h from HEK293T transfected with indicated expression vector. The fibroblasts were infected with VSV-GFP (0.1 MOI) and the viral titer in the supernantant was measured by plaque assay. *P<0.05

E) *Ifnar-/-* derived J2 BMMs fibroblasts were treated with conditioned media for 12h from HEK293T transfected with indicated expression vector. The cells were infected with VSV-GFP (0.1 MOI) and the viral titer in the supernantant was measured by plaque assay. *P<0.05

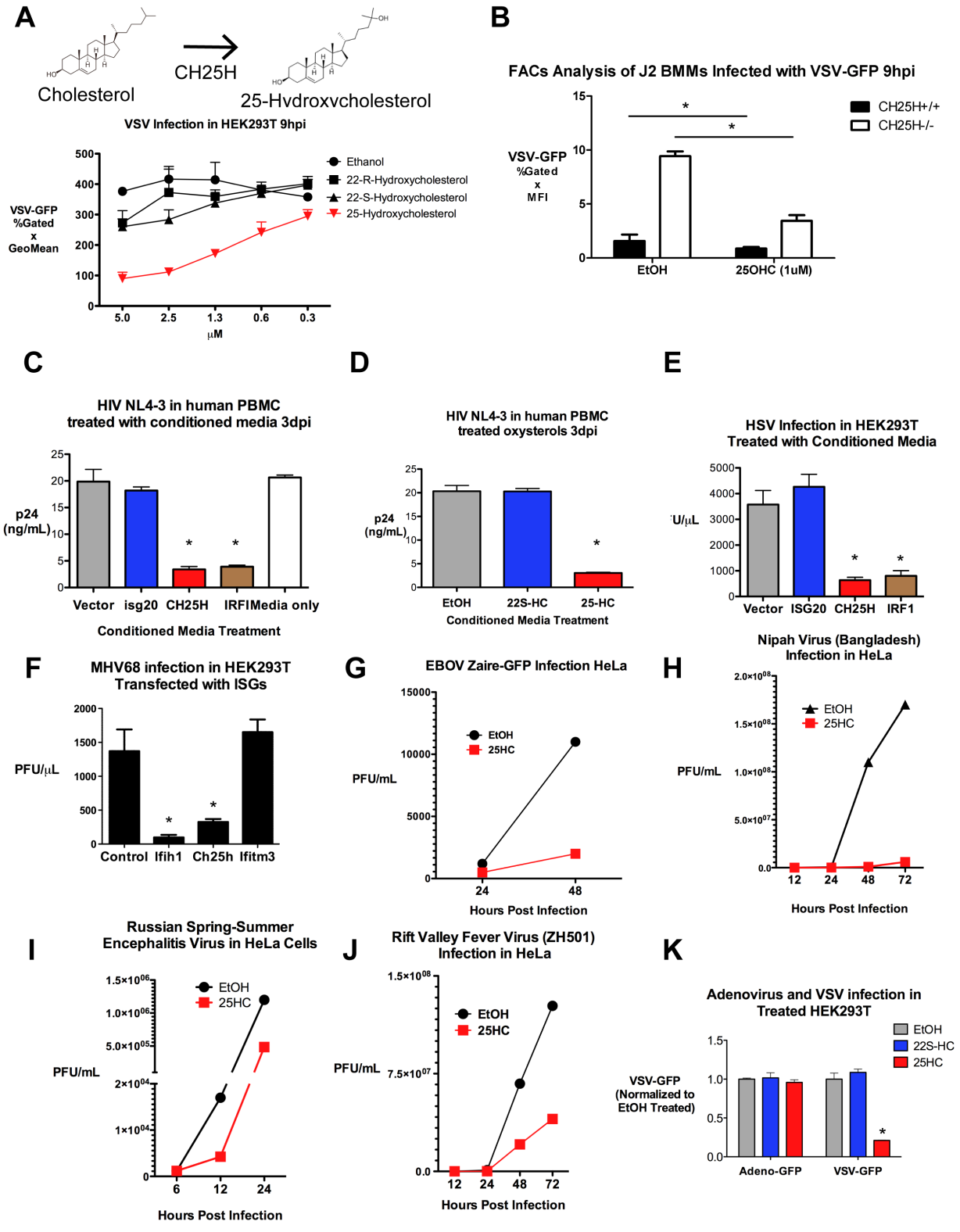
A
Cholesterol
CH25H
25-Hydroxycholesterol
VSV Infection in HEK293T 9hpi
VSV-GFP %Gated x GeoMean
Ethanol
22-R-Hydroxycholesterol
22-S-Hydroxycholesterol
25-Hydroxycholesterol
μM
B
FACs Analysis of J2 BMMs Infected with VSV-GFP 9hpi
VSV-GFP %Gated x MFI
CH25H+/+
CH25H-/-
EtOH
25OHC (1uM)
C
HIV NL4-3 in human PBMC treated with conditioned media 3dpi
p24 (ng/mL)
Vector
isg20
CH25H
IRFI
Media only
Conditioned Media Treatment
D
HIV NL4-3 in human PBMC treated oxysterols 3dpi
p24 (ng/mL)
EtOH
22S-HC
25-HC
Conditioned Media Treatment
E
HSV Infection in HEK293T Treated with Conditioned Media
U/μL
Vector
ISG20
CH25H
IRF1
F
MHV68 infection in HEK293T Transfected with ISGs
PFU/μL
Control
Ifih1
Ch25h
Ifitm3
G
EBOV Zaire-GFP Infection HeLa
PFU/mL
EtOH
25HC
Hours Post Infection
H
Nipah Virus (Bangladesh) Infection in HeLa
PFU/mL
EtOH
25HC
Hours Post Infection
I
Russian Spring-Summer Encephalitis Virus in HeLa Cells
PFU/mL
EtOH
25HC
Hours Post Infection
J
Rift Valley Fever Virus (ZH501) Infection in HeLa
PFU/mL
EtOH
25HC
Hours Post Infection
K
Adenovirus and VSV infection in Treated HEK293T
VSV-GFP (Normalized to EtOH Treated)
EtOH
22S-HC
25HC
Adeno-GFP
VSV-GFP

Figure 3-4

A) CH25H converts cholesterol to 25-hydroxycholesterol (25HC, top). HEK293T was treated with 22(S)-HC, 22(R)-HC, 25HC, and the vehicle, ethanol (EtOH) for 8h at the indicated concentrations and infected with VSV-GFP. VSV-GFP was quantified by FACs (%GFP+ X Geometric MFI).
B) *Ch25h+/+* and *Ch25h-/-* J2 BMMs were treated with 25HC(1μM) or EtOH and infected with VSV-GFP (0.01MOI). VSV-GFP was quantified by FACs at 12hpi. Mean±SD; *P<0.02
C) Costimulated PBMC were pre-incubated for 24h in conditioned media before infection with HIV NL4-3. At 3dpi, p24 in triplicate samples were quantified by ELISA. Mean±SEM; *P<0.001
D) Costimulated PBMC ($1x10^6$) were pre-incubated for 24h in 22(S)-HC (1μM), 25HC(1μM), and vehicle (EtOH) containing media before infection with HIV NL4-3 in triplicates (30 ng of HIV strain NL4-3). At 3dpi, p24 was quantified by ELISA. Mean±SEM; *P<0.001
E) HEK293T was treated with indicated conditioned media for 12h and infected with HSV (0.25MOI) for 24h. HSV titer in the supernatant was quantified by plaque assay. Mean±SEM; *P<0.001
F) HEK293Ts were transfected with indicated expression plasmids and infected with MHV68 (0.2MOI) for 24h. MHV68 titer in the supernatant was quantified by plaque assay. Mean±SEM; *P<0.001
G) HeLa cells were pretreated with 25HC (1μM) or EtOH containing media for 5h and infected with Ebola Zaire-GFP (EBOV) at 0.1MOI. At the indicated times, combined supernatants from biological triplicates was measured by plaque assay.
H) HeLa cells were pretreated with media containing indicated concentrations of 25HC or EtOH for 18h and infected with Nipah virus (Bangladesh strain) at 0.1MOI. At the indicated times, combined supernatants from biological triplicates was measured by plaque assay.
I) HeLa cells were pretreated as in Fig. 4H and infected with Russian Spring-Summer Encephalitis Virus (RSSEV) at 0.1MOI. At the indicated times, combined supernatants from biological triplicates was measured by plaque assay.
J) HeLa cells were pretreated with media containing indicated concentrations of 25HC or EtOH for 5h and infected with wildtype Rift Valley Fever Virus ZH501 (RVFV) at 0.1MOI. Viral titer at indicated time points was measured by plaque assay. Values represent means of samples from triplicates.
K) HEK293T were treated with EtOH, 22S-HC, and 25HC for 12h and infected with adenovirus-GFP and VSV-GFP and quantified by FACs (%GFP+ X Geometric MFI). Mean±SEM; *P<0.001

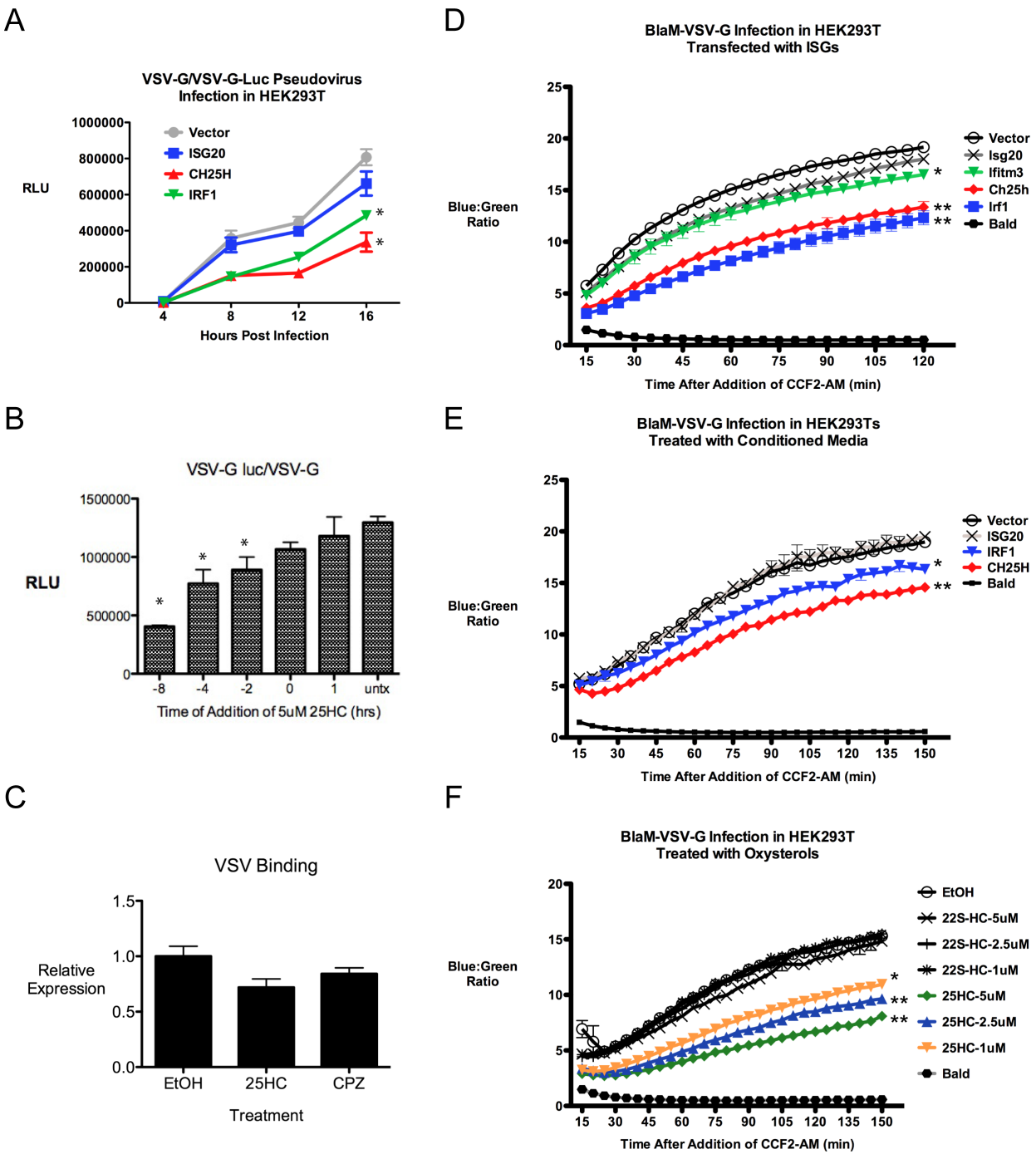

Figure 3-5

A) HEK293Ts were treated with conditioned media for 12h and infected with VSV-G pseudovirus encoding VSVΔG luciferase (VSVΔG-Luc/G). The cell lysates were collected at indicated times and measured for luciferase activity.

B) HEK293T were treated with 25HC (5μM) at different times relative to the VSVΔG-Luc/G infection. For time 0, VSVΔG-Luc/G and 25HC were added together to the cells for 1h. Negative numbers indicate addition of 25HC before infection; positive

number indicates addition after infection. Relative Light Units (RLU) is represented as Mean±SD *P<0.01

C) HEK293T were treated with respective agonists for 8h in triplicates. VSV was bound to cells at 4ºC, washed 3 times with PBS, and let sit for 30min before total RNA collection. VSV genomic RNA was quantified by qRT-PCR Mean±SEM; *P<0.05

D) HEK293T was transfected with indicated expression plasmids for 24h and infected with pseudovirus with encoding NipahM-β-lactamase inside VSV-G (VSV-G/BlaM) for 1.5h. β-lactamase activity was measured by blue:green ratio of the cleaved CCF2-AM. *P<0.01, **P<0.001

E) HEK293T was treated with indicated conditioned media for 12h and infected with VSV-G/BlaM. β-lactamase activity was measured by CCF2-AM cleavage. *P<0.01, **P<0.001

F) HEK293T was treated with indicated concentration of 22(S)-HC, 25HC, and equivalent volume of vehicle (EtOH) for 12h and infected with VSV-G/BlaM. β-lactamase activity was measured by CCF2-AM cleavage. *P<0.01, **P<0.001

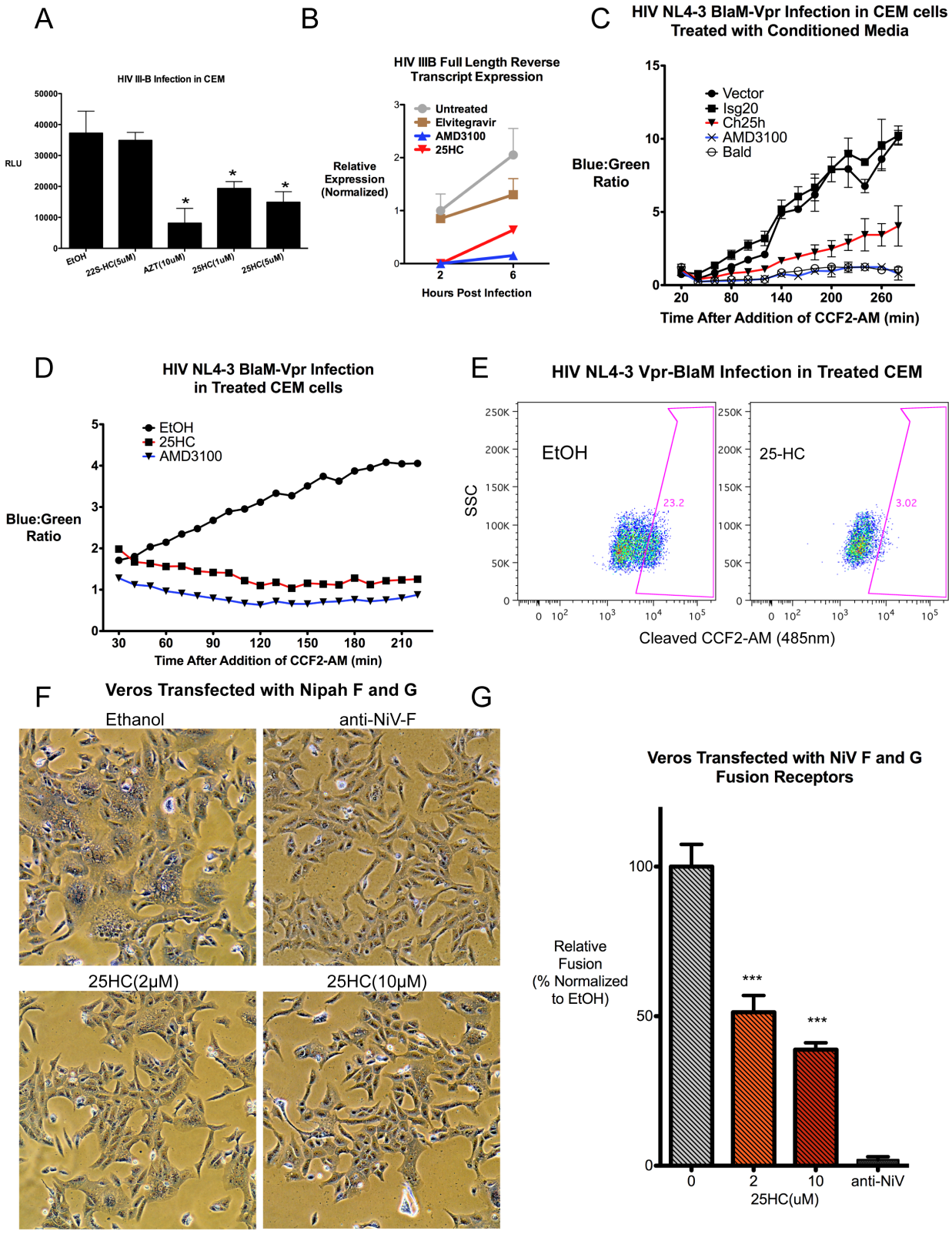
A
HIV III-B Infection in CEM
RLU
50000
40000
30000
20000
10000
0
EtOH
22S-HC(5uM)
AZT(10uM)
25HC(1uM)
25HC(5uM)
B
HIV IIIB Full Length Reverse Transcript Expression
Relative Expression (Normalized)
Untreated
Elvitegravir
AMD3100
25HC
Hours Post Infection
C
HIV NL4-3 BlaM-Vpr Infection in CEM cells Treated with Conditioned Media
Blue:Green Ratio
Vector
Isg20
Ch25h
AMD3100
Bald
Time After Addition of CCF2-AM (min)
D
HIV NL4-3 BlaM-Vpr Infection in Treated CEM cells
Blue:Green Ratio
EtOH
25HC
AMD3100
Time After Addition of CCF2-AM (min)
E
HIV NL4-3 Vpr-BlaM Infection in Treated CEM
EtOH
25-HC
23.2
3.02
SSC
Cleaved CCF2-AM (485nm)
F
Veros Transfected with Nipah F and G
Ethanol
anti-NiV-F
25HC(2μM)
25HC(10μM)
G
Veros Transfected with NiV F and G Fusion Receptors
Relative Fusion (% Normalized to EtOH)
***
***
0
2
10
anti-NiV
25HC(uM)

Figure 3-6

A) CEM cells were treated as indicated for 12h and underwent single-round infection with HIV-IIIB coexpressing luciferase. Cell lysates were collected after 24h and measured for luciferase activity. Relative Light Units (RLU) is represented as Mean±SD. *P<0.05
B) CEM cells were treated with elvitegravir (10μM), AMD3100(10μM), 25HC (1μM), and vehicle (EtOH) for 12h and infected with HIV III-B pseudovirus. At 2 and 6 hpi, total cellular DNA was collected and HIV full-length late reverse transcript (LateRT) was quantified by qRT-PCR with Taqman probe and normalized to mitochondrial DNA.
C) CEM cells were treated with indicated conditioned media or AMD3100 for 8h and infected with HIV NL4-3 encoding Vpr-BlaM (NL4-3/BlaM) in duplicates. β-lactamase activity was measured by cleavage of CCF2-AM by fluorescence plate reader. Mean±SD *P<0.01 by student's t-test for last time point.
D) Similar to Part C. CEM cells were treated with indicated 25HC(5μM) and vehicle (EtOH) for 8h and infected with HIV NL4-3/BlaM.
E) CCF2-AM cleavage from samples in Fig. 6D was confirmed by FACs. Numbers represent percentage of cells expressing cleaved form of CCF2-AM (485nm).
F) Vero cells were transfected with Nipah F and G receptors. 5h after transfection, the cells were treated with indicated conditions. The cells were fixed 21h after transfection and Giemsa stained.
G) Syncytias were defined by the presence of 4 or more nuclei in a common cell membrane. Relative fusion was determined by normalizing the number of nuclei per syncytia under the experimental conditions to the vehicle (ethanol) treated group, set to 100%.

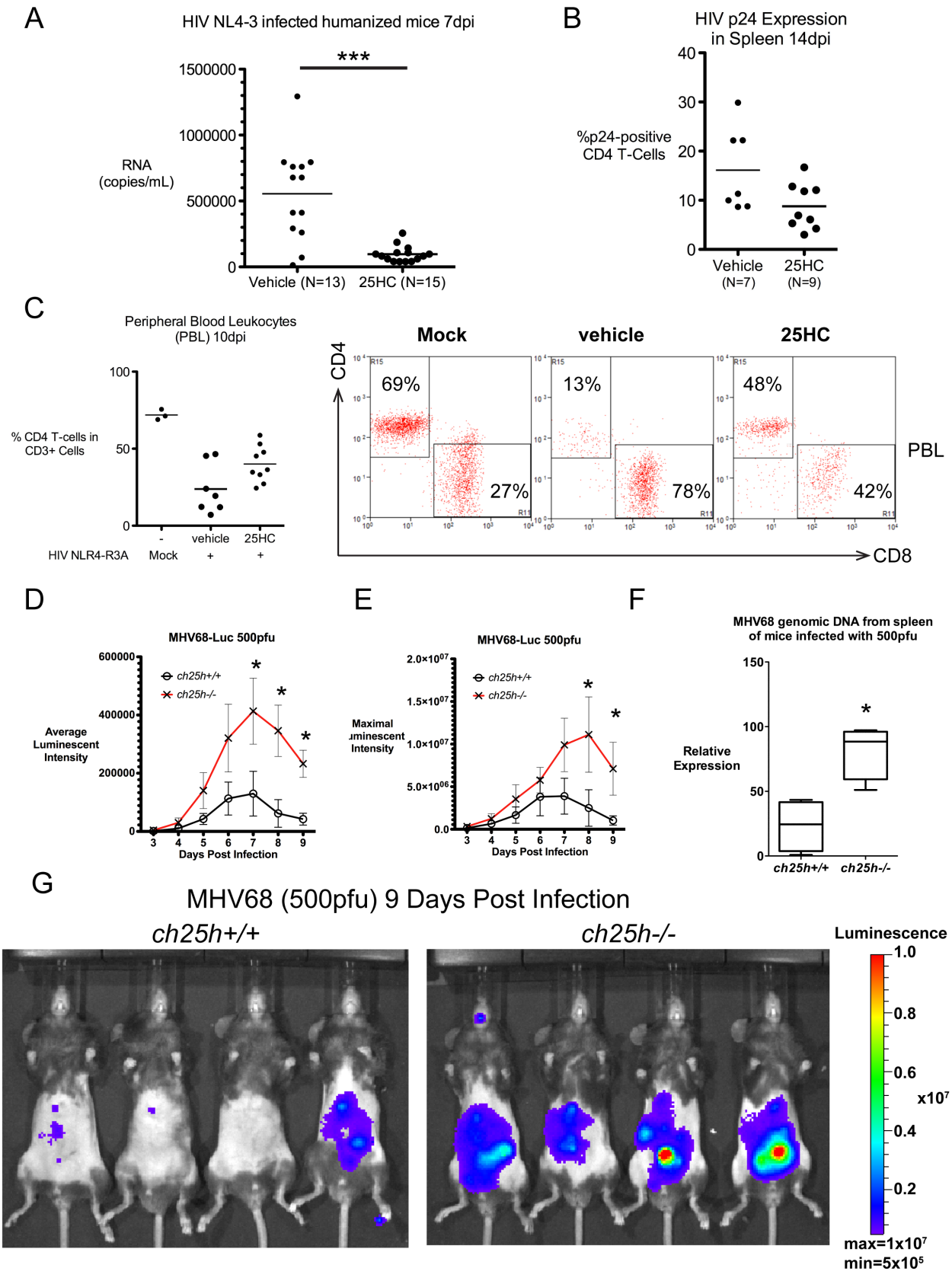
A
HIV NL4-3 infected humanized mice 7dpi
***
1500000
1000000
500000
0
RNA (copies/mL)
Vehicle (N=13)
25HC (N=15)
B
HIV p24 Expression in Spleen 14dpi
40
30
20
10
0
%p24-positive CD4 T-Cells
Vehicle (N=7)
25HC (N=9)
C
Peripheral Blood Leukocytes (PBL) 10dpi
100
50
0
% CD4 T-cells in CD3+ Cells
-
vehicle
25HC
HIV NLR4-R3A
Mock
+
+
Mock
vehicle
25HC
CD4
69%
27%
13%
78%
48%
42%
PBL
CD8
D
MHV68-Luc 500pfu
600000
400000
200000
0
Average Luminescent Intensity
ch25h+/+
ch25h-/-
3
4
5
6
7
8
9
Days Post Infection
E
MHV68-Luc 500pfu
2.0×10^07
1.5×10^07
1.0×10^07
5.0×10^06
0.0
Maximal Luminescent Intensity
ch25h+/+
ch25h-/-
3
4
5
6
7
8
9
Days Post Infection
F
MHV68 genomic DNA from spleen of mice infected with 500pfu
150
100
50
0
Relative Expression
ch25h+/+
ch25h-/-
G
MHV68 (500pfu) 9 Days Post Infection
ch25h+/+
ch25h-/-
Luminescence
1.0
0.8
0.6
x10^7
0.4
0.2
max=1x10^7
min=5x10^5

Figure 3-7

A) 25HC (50mg/kg) or vehicle (2-hydroxypropyl-β-cyclodextrin) was administered 12h before HIV NL4-3 infection in humanized mice (NRG-hu). Treatment was administered daily after infection. Viral titer in serum was measured by qRT-PCR 7dpi. Results are combined from 2 experiments. ***P<0.0001
B) Spleens from NRG-hu mice were harvested 14dpi and quantified by FACs after HIV p24 intracellular staining.
C) Percent CD4+ T-cells was compared by FACs in 25HC and EtOH treated group. Representative FACs plots are shown (right).
D) *ch25h+/+* and *ch25h-/-* mice were infected with MHV68-Luc (500pfu) and the amount of infection was quantified everyday by bioluminescence imaging. Average intensities (photons/sec/cm^2/steradian) from ventral, right, left, and dorsal sides were measured for all mice. *P<0.05 by student's t-test at indicated timepoint.
E) Similar to Fig. 7D, maximum intensities (photons/sec/cm^2/steradian) were averaged. *P<0.05 by student's t-test at indicated timepoint.
F) MHV68 genomic DNA from *ch25h+/+* and *ch25h-/-* infected mice 9dpi was quantified by qRT-PCR and normalized to a genomic promoter of ccl2 gene. *P<0.01
G) Bioluminescent images of *ch25h+/+* and *ch25h-/-* mice 9dpi.

A

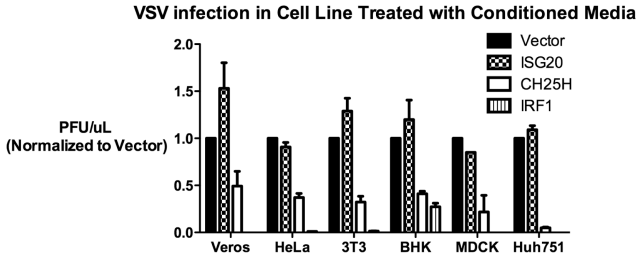

B

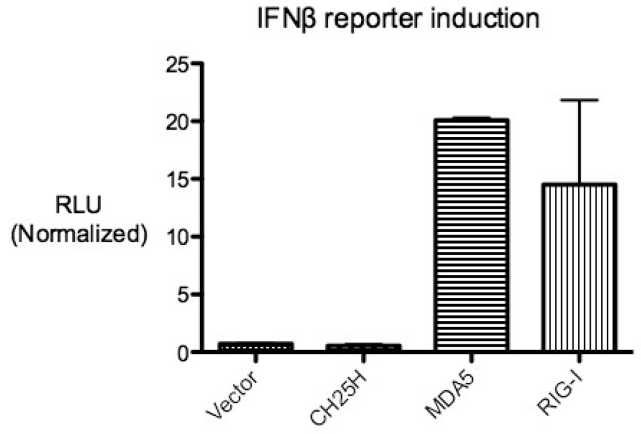

C

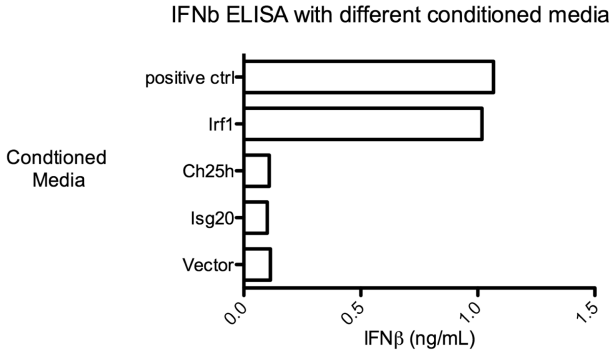

Fig. S3-1

A. Indicated cell lines were treated for 8-12h with conditioned media from HEK293T transfected with indicated expression vectors. They were infected with VSV at 0.01MOI for 9-14h, depending on the cell line. VSV-GFP was quantified by FACs (%GFP+ X Geometric MFI) and normalized to VSV-GFP in cell treated with vector-conditioned media

B. HEK293T was transfected with indicated expression vector and IFNβ-luciferase reporter. Luciferase activity was measured after 16h. RLU-relative light units.
C. IFNβ ELISA of conditioned media from HEK293T transfected with indicated expression vectors after 24h.

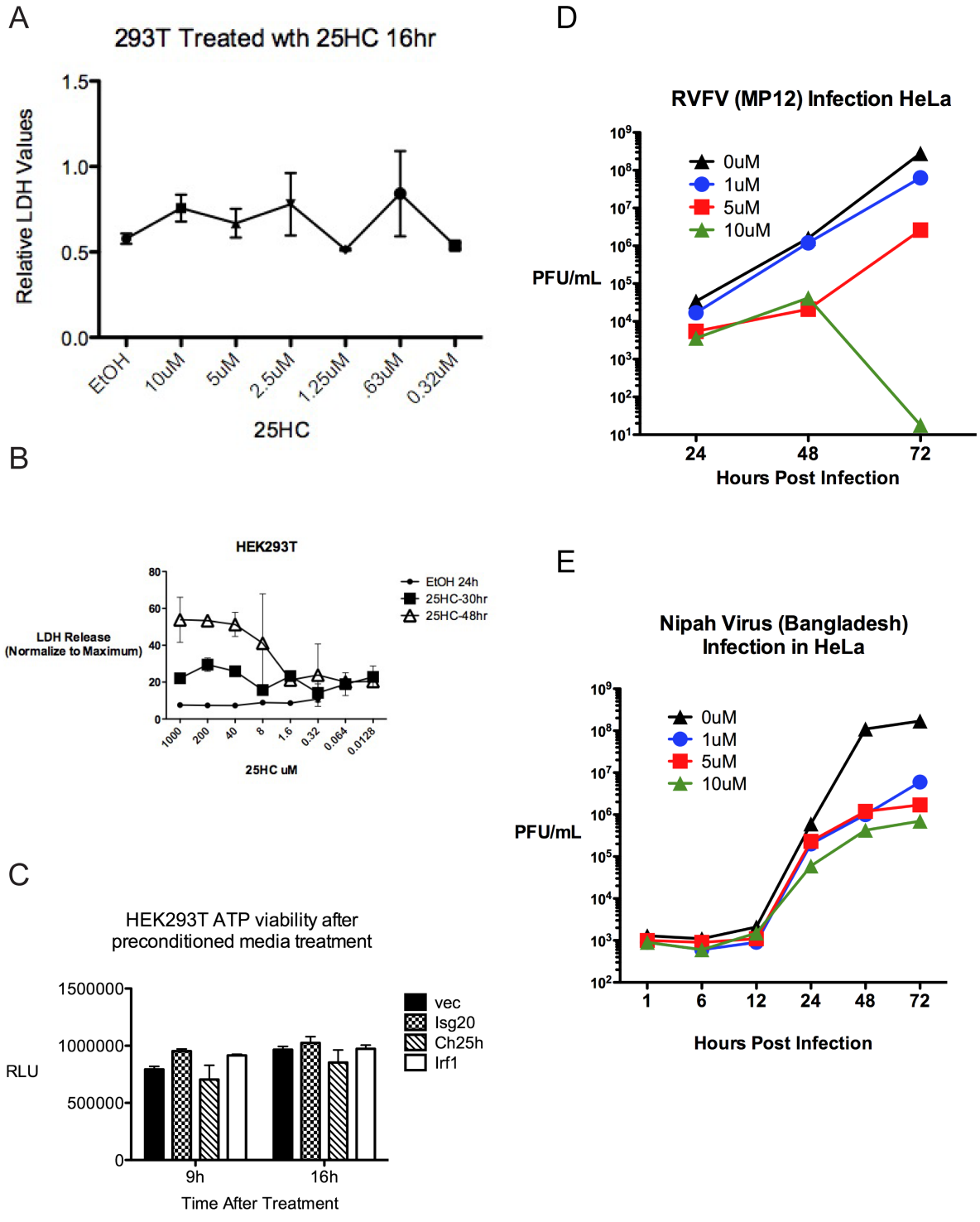
A
293T Treated wth 25HC 16hr
Relative LDH Values
1.5
1.0
0.5
0.0
EtOH
10uM
5uM
2.5uM
1.25uM
.63uM
0.32uM
25HC
B
HEK293T
LDH Release
(Normalize to Maximum)
80
60
40
20
0
1000
200
40
8
1.6
0.32
0.064
0.0128
25HC uM
EtOH 24h
25HC-30hr
25HC-48hr
C
HEK293T ATP viability after
preconditioned media treatment
RLU
1500000
1000000
500000
0
9h
16h
Time After Treatment
vec
Isg20
Ch25h
Irf1
D
RVFV (MP12) Infection HeLa
PFU/mL
0uM
1uM
5uM
10uM
24
48
72
Hours Post Infection
E
Nipah Virus (Bangladesh)
Infection in HeLa
PFU/mL
0uM
1uM
5uM
10uM
1
6
12
24
48
72
Hours Post Infection

Fig. S3-2

A. HEK293T were treated with increasing amount of 25HC and LDH values was measured after 16h
B. HEK293T were treated with increasing amount of 25HC and LDH was measured after 30 and 48h
C. HEK293T was treated with indicated condition media for 16h. Cell viability was measured by quantitation of ATP present in the cell by luminescent substrate.
D. HeLa cells were pretreated with media containing indicated concentrations of 25HC or EtOH for 18h and infected with RVFV (MP12 vaccine strain) at 0.1MOI. Viral titer at indicated time points was measured by plaque assay. Values represent means of samples from triplicates.
E. HeLa cells were pretreated with media containing indicated concentrations of 25HC or EtOH for 18h and infected with Nipah virus (Bangladesh strain) at 0.1MOI. Viral titer at indicated time points was measured by plaque assay. Values represent means of samples from triplicates.

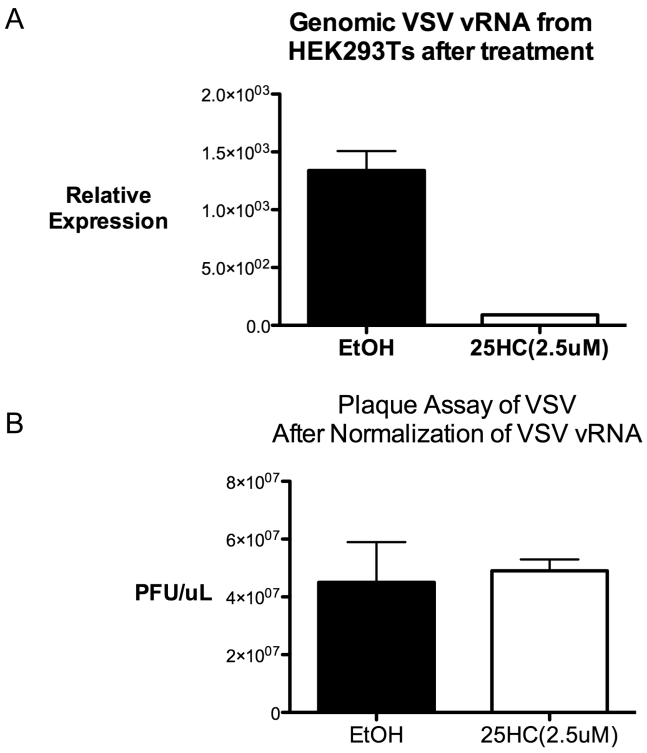

Fig. S3-3

A. HEK293T were treated with 25HC (2.5μM) and vehicle (EtOH) for 8h and infected with VSV-GFP at 0.01 MOI. The cells were treated against with 25HC after infection. Supernatants were collected 24hpi and virus was concentrated by centrifugation. For a part of the concentrated virus, VSV genomic RNA (gRNA) was quantified by qRT-PCR.
B. Concentrated virus from part A was normalized based on VSV gRNA and standard plaque assay was performed.

A

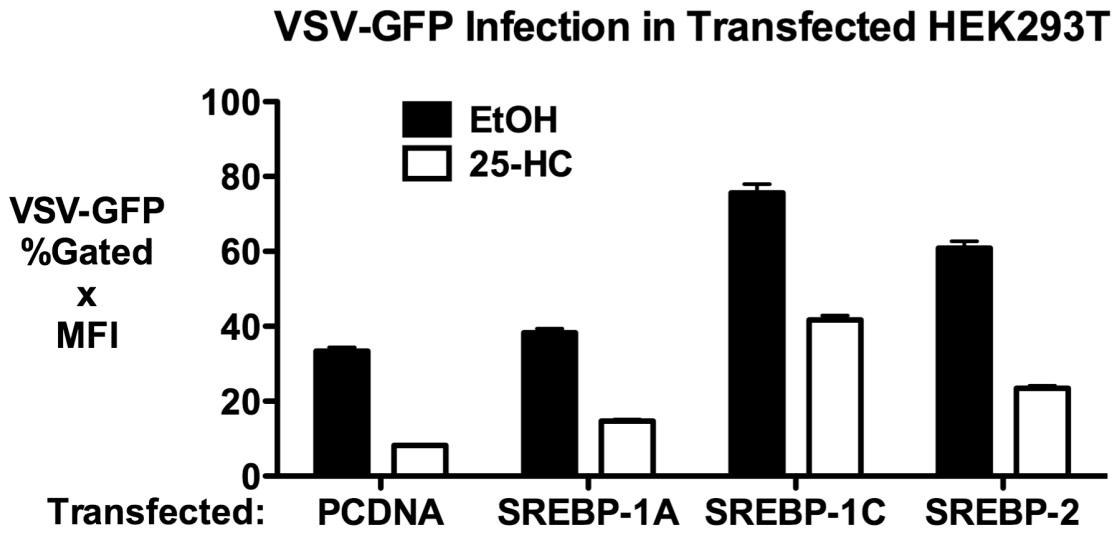

Fig. S3-4

A. HEK293T were transfected with mature form of SREBP1a, SREBP1c, and SREBP2 for 24 and treated with 25HC for 12h. The cells were infected with VSV-GFP(0.01MOI) and quantified by FACs.

A

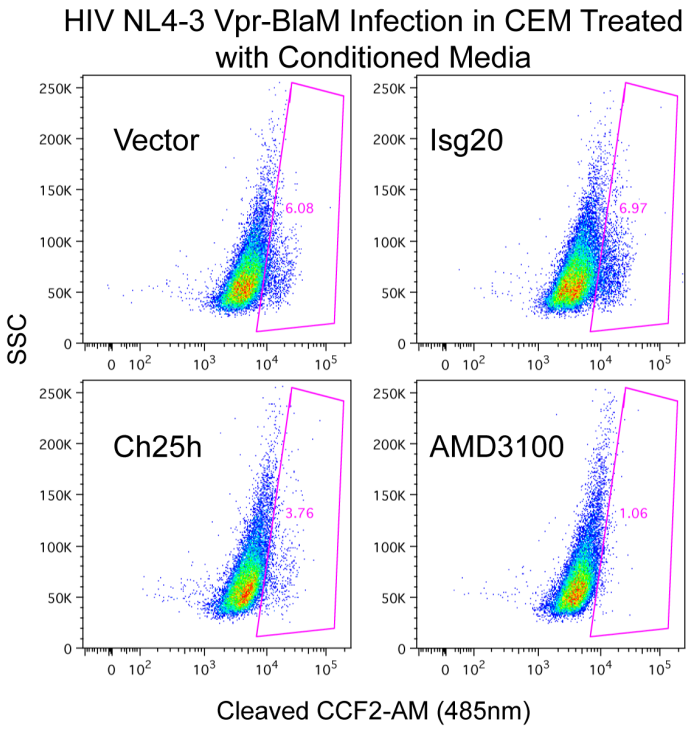
HIV NL4-3 Vpr-BlaM Infection in CEM Treated with Conditioned Media
Vector
Isg20
Ch25h
AMD3100
6.08
6.97
3.76
1.06
SSC
Cleaved CCF2-AM (485nm)

B

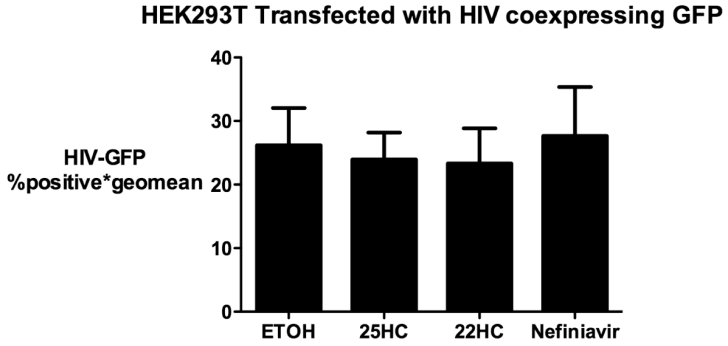
HEK293T Transfected with HIV coexpressing GFP
HIV-GFP %positive*geomean
ETOH
25HC
22HC
Nefiniavir

C

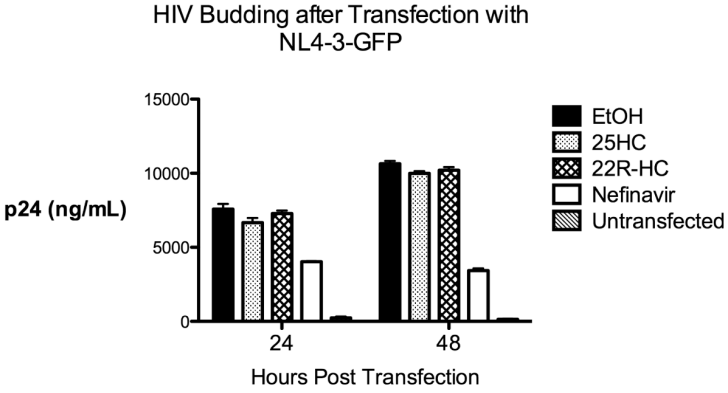
HIV Budding after Transfection with NL4-3-GFP
p24 (ng/mL)
EtOH
25HC
22R-HC
Nefinavir
Untransfected
Hours Post Transfection

Fig. S3-5

A. CEM cells were treated with indicated conditioned media for 8h and infected with HIV NL4-3 encoding Vpr-BlaM (NL4-3/BlaM) in duplicates. AMD3100 serve as postive control for entry inhibition. CCF2-AM cleavage was confirmed by FACs. Numbers represent percentage cells expressing cleaved form of CCF2AM (485nm)
B. HEK293T were transfected with proviral plasmid of HIV coexpressing GFP and treated with indicated agonists 6h after transfection. HIV-GFP was quantified by FACs after 48h.
C. Viral supernatants from part A were collected after 48h and p24 was quantified by ELISA.

MATERIALS AND METHODS

Cells and Reagents:

RAW and HEK293T cells were obtained from ATCC and grown in standard DMEM with 5% FBS, 1% Penicillin/Streptomycin (GIBCO). CEM cells were cultured in RPMI media supplemented with 10% fetal calf serum (Hyclone) and 1 % Pen/Strep (Invitrogen). Dr. Glen Barber (University of Miami, Florida) provided VSV-GFP. MHV-68-Luc was provided by Dr. Ren Sun in MIMG in UCLA. Luciferase activity was measured using firefly luciferase substrate kit (Promega).

To make bone marrow derived macrophages (BMMs), bone marrow was harvested from 6-8 week C57B/L6 mice (Jackson Labs) and differentiated with 10ng/mL of M-CSF in DMEM+10%FBS for 7 days. On day 6 the media was replaced and on day 7 the cells were stimulated with IFNα or IFNγ (PBL Interferon Source). The cells were treated for 2.5 hours and harvested in Trizol (Invitrogen). The RNA was isolated by isopropanol precipitation for microarray analyses. For J2 immortalized macrophages, bone marrow was infected with J2 retrovirus. A retrovirus expressing v-raf and c-myc expressing cell line was established (called GG2EE) and grown in RPMI (10mM Hepes ph7.8, 10%FBS, 1% Pen/strep). Virus containing supernatant was harvested and filtered through 0.45μM filter(Palleroni et al., 1991). For BCR-ABL transformed B-cells were derived by infecting bone marrow with BCR-ABL retrovirus as described previously(Scherle et al., 1990). Stable knockdown in RAW264.7 were generated using pSiren shRNA knockdown system (Clonetec) according to the published protocol. Knockdown primers sequences are available by request. Tail-derived fibroblasts were derived by skinning the tails of mice and incubating them

directly in culture dishes in DMEM 10%FBS. Cells were scraped and re-plated after 7 days.

Expression plasmids were obtained from Genecopoeia, Inc. Doxycycline inducible expression system was purchased from Clonetec. SREBP2 expression plasmids were a gracious gift from Dr. Elizabeth Tarling (UCLA).

VSV, HSV, and MHV68 Viral Plaque Assay

HEK293T and RAW264.7 were infected with VSV-GFP at 0.01 MOI for 1h and the media was changed with fresh media. For J2 BMMs and BCR-ABL B-cells, 1MOI VSV-GFP was used. Approximately 150uL of supernatants were collected at various timepoints between 8-16hpi for plaque assay. For HSV and MHV68, 0.25MOI was used for infection and supernatants were collected at 24hpi.

Plaque Assays were done on Vero cells in 12-well plates at $2x10^5$ and $2x10^4$ cells per well for VSV and MHV-68 plaque assay, respectively. Supernatants from infected cells were serially diluted and infected on Veros for 1hr. The cells were then covered with growth medium containing 0.6% low-melting point agarose. Plaques stained with crystal violet 0.5% (m/v) in 20% ethanol (v/v) and were counted after 16hrs or 6 days for VSV and MHV-68, respectively.

VSV Screening and Flow-cytometry:

HEK293T cells were plated 12 wells on collagen coated plates 0.5mg/mL rat-tail collagen I (BD Biosciences) in PBS. Individual ISGs expression plasmid was transfected with DsRed construct (Clontech) at 3:1 ratio Fugene 6 (Roche) transfection reagents. After 36 hours, the cells were infected as described above. At 9hpi, cells were collected in 2% paraformaldehyde solution in PBS. FACs was done with standard

compensation (FACSCaliber, BDBiosciences) and the data was analyzed using CellQuest (BDBiosciences).

Ebola, RSSEV, and RVFV Infections

HeLa cells were pre-treated with 25HC (1μM) or EtOH containing medium for 5hrs prior infection with Ebola-Zaire-GFP (EBOV) or Rift Valley fever virus (RVFV) wild type strain ZH501 (MOI 0.1), respectively. Cell culture supernatant aliquots were harvested at the indicated time points and pooled from biological triplicates, prior virus titration by plaque assay. For infection with RVFV vaccine strain MP-12, Nipah virus Bangladesh strain or Russian Spring-Summer encephalitis virus Sofjin strain (RSSEV), HeLa cells were pre-treated with 25HC (1μM) or EtOH containing medium for 18hrs prior infection. Plaque Assays were performed on Vero cells (for EBOV, Nipah, and RVFV) in 12-well plates or BHK-SA cells (for RSSEV) in 6 well plates. Cells were infected for 1hr at 37ºC with serial 10-fold dilutions of supernatant aliquots from infected cells. The cells were then overlain with growth medium containing 0.6% methyl cellulose (for EBOV, Nipah, and RVFV) or 0.5% tragacanth gum (for RSSEV). After 3 days (RVFV, Nipah), 4 days (RSSEV) and 10 days (EBOV), cells were fixed with 10% buffered formalin, stained with crystal violet and plaques counted. All work involving EBOV, Nipah, RSSEV and wild-type RVFV, were performed at the Robert E. Shope BSL-4 laboratory at UTMB.

HIV Infections in hPBMCs

Human peripheral blood mononuclear cells (PBMC) were obtained from the UCLA Virology Core. These cells were cultured in RPMI Medium 1640 (Invitrogen) containing 10% FBS, 100 units/ml of Penicillin + 100 μg/ml of Streptomycin (Pen/Strep,

Invitrogen), and 20 units/ml of interleukin-2 (Roche). PBMC were costimulated for 3 days with plate-bound anti-CD3 and soluble anti-CD28 antibodies as previously described(Korin and Zack, 1999). Costimulated PBMC were pre-incubated for 24h at a density of $3x10^6$ cells/ml in conditioned media before infection with HIV. Infections were set-up in 200 μl volumes of conditioned media containing 10^6 cells, 30 ng of HIV strain NL4-3 (as determined by p24 antigen ELISA [Beckman Coulter]), and 10 μg/ml of polybrene. The mixture was incubated for 2h at 37°C on a rocking platform. Following infection, cells were washed twice with media and then split into triplicate 2ml cultures in conditioned media, each containing $3.3x10^5$ cells. At various post-infection timepoints, 100 μl of cell-free supernatant was removed and added to 2% Triton-x-100 in PBS for storage at 4°C before quantitation of p24 concentration by ELISA.

VSV-G pseudotyped VSV-G Luciferase pseudovirus production

VSV-G pseudotyped VSV-G luciferase pseudo-virus (VSVΔG-Luc/G) was generated by methods previously described(Takada et al., 1997) and concentrated by ultracentifugation on 20% sucrose cusion. The VLPs were resuspended in NTE buffer (100 mM NaCl; 10 mM Tris–HCl, pH 7.5; 1 mM EDTA) and stored in -80C. The concentrations used to generate linear range of luciferase signal were determined empirically.

VSV-G/BlaM Production

A previously described construct encoding NipahM1 fusion with beta-lactamase (BlaM) was used to package inside VSV-G(Wolf et al., 2009). HEK293Ts were transfected with constructs encoding BlaM and VSV-G or BlaM alone (bald) at 3:1 ratio

in 10cm dishes by PEI transfection reagent. The viral supernatants were collected, clarified, and concentrated by ultracentrifugation at >75,000g on 20% sucrose cushion,

HIV IIIB pseudotyped virus production

Envelopes and backbone were obtained through the NIH AIDS and Research and Reference Reagent Program. Pseudovirons were generated by cotransfection of 293T cells with envelope deleted LucRE- vector and envelope expressing vector at a 3:1 µg ratio with Bioline Bio T transfection reagent. 72 hours post transfection viral supernatant was collected, clarified by low speed centrifugation and stored at -80c. The number of infectious virus particles was determined by serial dilution assay on Ghost HI-X4 cells, cells that express GFP controlled by a HIV LTR promoter. Briefly, 4 X 10^4 Ghost HI-X4 cells were seeded into a 48 well dish. 24 hour later, cells are infected with 2 fold serially diluted psuedovirons. 48 hours later, cells were collected and percent positive cells were determined using flow cytometry.

CEM Infection with pseudotyped IIIB Virus

CEMs cells were treated with 25HC, 22HC or EtOH for a minimum of six hours. Prior to infection previously untreated cells were incubated with AMD3100, AZT, Elvitegravir or Nelfinavir at a concentration of 10um or 20um for a minimum of 15 minutes. IIIB pseudovirus was used to infect treated and untreated CEM cells at 0.1MOI. Infections were spin inoculated for 60 minutes at 2,000RPM, at 37C. After spin inoculation, cells were transferred into a 37C incubator. 48 hours post infection cells were lysed with 1% triton-X 100 and assayed for luciferase activity. P24 Assay was done in with PerkinElmer's HIV-1 P24 Elisa kit (NEK050B). Accompanied protocol was followed.

Generation of VPR-BlaM Fusion Gene

VPR-BlaM was generated by overlapping pcr and cloned into PCDNA3.1. VPR was amplified from SG3Δ. Catalytically optimized beta lactamase described previously in (cite) was amplified with primers (3,4). The two pcr products were used in the overlapping pcr using primers (1,4) to generate VPR-BlaM. VPR-BlaM pcr product was cloned into pcdna3.1 expression vector previously cut with BamHI and XhoI using the Infusion system (CloneTech).

NL4-3 VPR-BlaM Virus Production

NL4-3 VPR-BlaM was produced in according to the methods outlined previously(Cavrois et al., 2002). Briefly, 2 ug of VPR BlaM, 1ug of padvantage (Promega) and 8 ug of NL4-3 were cotransfected into 293Ts in 10cm plate with PEI reagent. 48 hours post transfection viral supernatant was collected, clarified by low speed centrifugation, and concentrated on 20% sucrose cushion. VLPs were resuspended in small volume of NTE and stored at -80c.

NL4-3 VPR-BlaM Infection of CEM cells

CEMs cells were treated with 25HC or EtOH for a minimum of six hours. Prior to infection previously untreated cells were incubated with AMD3100 at a concentration of 20um for a minimum of 15 minutes. Concentrated NL4-3 BlaM or Bald virus was added to treated CEM cells . Infections were spin inoculated for 60 minutes at 2,000RPM, at 37 degrees Celsius. After spin inoculation, cells were transferred into a 37 degree incubator for 2 hours. Free floating virus was inactivated and CEM cells were washed twice. CCF2-AM (Invitrogen) was added according to manufacture's protocol. Kinetic readings were taken for 1-3 hours. After the kinetic reading the cells were washed with

FACS Buffer, fixed with 2 % paraformaldehyde and examined by flow cytometry. Data was analyzed using FlowJo.

PCR

Cells were collected in trizol and RNA was isolated by standard isopropanol precipitation. RNA was quantitated and 1 µg of RNA was reversed transcribed using IScript (BioRad) according to the manufacturer's instructions with either random hexamer as primers. Q-PCR analysis was done using the iCycler thermocycler (Bio-Rad). Q-PCR was conducted in a final volume of 20 µL containing: Native Taq polymerase (Invitrogen), 1× Taq buffer (Stratagene), 125 µM dNTP, SYBR Green I (Molecular Probes), and Fluoroscein (Bio-Rad), and 1% cDNA. Amplification conditions were: 95°C (3 min), 40 cycles of 95°C (20 s), 55°C (30 s), 72°C (20 s). Expression values were normalized to L32 control and fold induction was normalized to untreated control.qPCR of Ch25h was done with primers: Ch25h fwd: 5'-TGCTACAACGGTTCGGAGC-3'. Ch25h rev: 5'-AGAAGCCCACGTAAGTGATGAT-3'. L32 fwd: 5'-AAGCGAAACTGGCGGAAAC-3'; L32 rev: 5'-TAACCGATGTTGGGCATCAG-3'.

For detection of VSV genomic RNA, cells infected with VSV was collected in Trizol and RNA was isolated and reverse transcribed with VSV specific primer N1-5' GATAGTACCGGAGGATTGACGACTA using Superscript II (Invitrogen) according to manufacturer's protocol. Real time PCR with Taqman probe with conditions described above. VSV fwd: 5′-GATAGTACCGGAGGATTGACGACTA-3′; VSV rev: 5′-TCAAACCATCCGAGCCATTC-3; VSV Probe: 5' (FAM)-TGCACCGCCACAAGGCAGAGA-(TAMRA)-3'.

CEM cells were infected with HIV IIIB expressing GFP and or Luciferase. After spinoculation, the cells were collected at indicated time and total DNA was extracted with DNAeasy Blood &Tissue Kit (Qiagen). Full length LateRT was measured by Taqman qPCR as described previously (Butler et al., 2001) and normalized to mitochondria DNA. Primers used: late RT forward: 5'-TGTGTGCCCGTCTGTTGTGT-3'; late RT reverse: 5'-GAGTCCTGCGTCGAGAGAGC-3';
late RT probe, 5'-(FAM)-CAGTGGCGCCCGAACAGGGA-(TAMRA)-3'; Mitochondrial forward primer, 5'-ACCCACTCCCTCTTAGCCAATATT-3'; mitochondrial reverse primer, 5'-GTAGGGCTAGGCCCACCG-3'

RNA isolation and RNAseq of Bone Marrow Derived Macrophage Stimulation

$5x10^5$ BMMs from wildtype (C57BL/6), IFNAR-deficient and IL-27R (TCCR/WSX-1) deficient mice were stimulated with Lipid A (100ng/mL) or saline control for 4hr and 12hr, respectively. Cells were harvested in Trizol (Invitrogen) and RNA was isolated via chloroform extraction.

Prior to cDNA library construction for RNA-Seq analyses, RNA was quantified and assessed for quality (RNA Integrity Value) using an Agilent 2100 Bioanalyzer (Santa Clara, CA). 1ug of RNA per condition was used for library construction using TruSeq SBS Kit v3 (FC-401-3001) according to the manufacturers guidelines (Illumina, San Diego, CA). Multiplex Sequence Analysis was performed using a Illumina HiSeq2000 Single End 100bp read parameters according to the manufacturers guidelines (www.illumina.com). Sequencing was performed by the Southern California Genotyping Consortium (SCGC) in the Epigenetics and Genetics Core at UCLA. Sequence reads

from each cDNA library (100 bp, single-read) were trimmed to 80 bp long and mapped onto the mouse genome build NCBI37/mm9 using Bowtie (bowtie-0.12.1, http://bowtie-bio.sourceforge.net/index.shtml) with setting '-v 2 -k 11 -m 10 -t–best–strata'. The mappable data were then processed by the ERANGE v. 3.3 RNA-seq analysis program(Mortazavi et al., 2008). Assuming total transcriptional activity is comparable between different cell types, the obtained data (data units in RPKM, reads per kilobase exon model per million mapped reads) were first $\log_2$ transformed and linearly normalized between individual samples, then averaged among biological replicates or triplicates. At the same time, in order to find genes that were changed in expression between two populations to a statistically significant degree, ERANGE processed data were analyzed by the Bioconductor DEGseq program (Wang et al., 2010) (http://www.bioconductor.org/packages/2.6/bioc/html/DEGseq.html) (data units in RPM, reads per million mapped reads, method = "MARS," $p < 0.001$). Data is presented using RPKM values.

HIV infection in NRG-hu mice

We used an HIV molecular clone with a highly pathogenic dual tropic envelope, R3A in NL4-3 Backbone for infection. HIV-1 viral stocks were produced in 293T cells, and titered on Hela-CD4-LTR-gal cells (NIH AIDS Research and Reference Reagent Program, Division of AIDS, NIAID). NRG-hu mice with stable human leukocyte reconstitution were administered 50mg/kg of 25HC or the vehicle control (2-hydroxypropyl)-β-cyclodextrin (HBCD) intraperitonial (i.p.) injection for 12h before infection with HIV NL4-R3A at 5ng of p24/mouse by intravenously injection (i.v.). Mice were administered 50mg/kg of 25HC or HBCD control every day. NRG-hu mice

infected with mock supernatant were included as control groups. RNA was extracted by Qiagen RNA extraction mini plus kit(Cat#52904) and HIV replication (genome copy/ml in the plasma) was measured using TaqMan One step RT PCR Master Mix Reagents Kit from Roche (Cat # 4309169). Intracellular staining and FACs analysis were done as previously described (Zhang et al., 2011).

Mouse Infections and Bioluminescence Imaging

C57BL/6 and *ch25h-/-* mice were purchased from Jackson. Mice were first anaesthetized by intraperitoneal (*i.p.*) injection with 200 mg/kg ketamine, 4 mg/kg xylazine in PBS. MHV68 (500 pfu) in 200uL of PBS was administered by i.p. On days 3 following infection, mice were imaged using the in vivo imaging system (IVIS, Xenogen). Briefly, mice were anaesthetized by intraperitoneal injection with 200 mg/kg ketamine, 4 mg/kg xylazine in PBS, followed by intraperitoneal injection of 3mg D-luciferin/mouse prior to imaging. Grayscale photographs and color images of imaged mice were superimposed with LivingImage (Xenogen) and Igor (Wavemetrics) programs, similar to that previously described. The mice were imaged on dorsal, ventral, right, and left side until the maximal luminescence has passed. The average and maximum photon flux value was measured for each mouse at every angle and expressed as photons/sec/cm^2/steradian. These values were averaged for all the mice. At 9dpi, mice were euthanized the spleens were extracted and homogenized in DMEM. Total DNA was extracted using DNeasy Blood & Tissue Kit (Qiagen) and MHV68 DNA was quantified by qPCR.

REFERENCES

Andrew J, and Jessup, W. (1999). Oxysterols and atherosclerosis. Atherosclerosis *142*, 1–28.

Bauman, D.R., Bitmansour, A.D., McDonald, J.G., Thompson, B.M., Liang, G., and Russell, D.W. (2009). 25-Hydroxycholesterol secreted by macrophages in response to Toll-like receptor activation suppresses immunoglobulin A production. Proceedings of the National Academy of Sciences *106*, 16764 –16769.

Brass, A.L., Huang, I.-C., Benita, Y., John, S.P., Krishnan, M.N., Feeley, E.M., Ryan, B.J., Weyer, J.L., van der Weyden, L., Fikrig, E., et al. (2009). The IFITM Proteins Mediate Cellular Resistance to Influenza A H1N1 Virus, West Nile Virus, and Dengue Virus. Cell *139*, 1243–1254.

Butler, S.L., Hansen, M.S.T., and Bushman, F.D. (2001). A quantitative assay for HIV DNA integration in vivo. Nat Med *7*, 631–634.

Cavrois, M., de Noronha, C., and Greene, W.C. (2002). A sensitive and specific enzyme-based assay detecting HIV-1 virion fusion in primary T lymphocytes. Nat Biotech *20*, 1151–1154.

Degols, G., Eldin, P., and Mechti, N. (June). ISG20, an actor of the innate immune response. Biochimie *89*, 831–835.

Gale, S.E., Westover, E.J., Dudley, N., Krishnan, K., Merlin, S., Scherrer, D.E., Han, X., Zhai, X., Brockman, H.L., Brown, R.E., et al. (2009). Side Chain Oxygenated Cholesterol Regulates Cellular Cholesterol Homeostasis through Direct Sterol-Membrane Interactions. Journal of Biological Chemistry *284*, 1755 –1764.

García, M.A., Gil, J., Ventoso, I., Guerra, S., Domingo, E., Rivas, C., and Esteban, M. (2006). Impact of Protein Kinase PKR in Cell Biology: from Antiviral to Antiproliferative Action. Microbiology and Molecular Biology Reviews *70*, 1032 –1060.

Holmes, R., VandeBerg, J., and Cox, L. (2011). Genomics and proteomics of vertebrate cholesterol ester lipase (*LIPA*) and cholesterol 25-hydroxylase (*CH25H*). 3 Biotech *1*, 99–109.

Janowski, B.A., Grogan, M.J., Jones, S.A., Wisely, G.B., Kliewer, S.A., Corey, E.J., and Mangelsdorf, D.J. (1999). Structural requirements of ligands for the oxysterol liver X receptors LXRα and LXRβ. Proceedings of the National Academy of Sciences *96*, 266 – 271.

Kandutsch, A., Chen, H., and Heiniger, H. (1978). Biological activity of some oxygenated sterols. Science *201*, 498 –501.

Kielian, M., and Rey, F.A. (2006). Virus membrane-fusion proteins: more than one way to make a hairpin. Nat Rev Micro *4*, 67–76.

Korin, Y.D., and Zack, J.A. (1999). Nonproductive Human Immunodeficiency Virus Type 1 Infection in Nucleoside-Treated G0 Lymphocytes. Journal of Virology *73*, 6526 –6532.

Lange, Y., Ye, J., and Steck, T.L. (2004). How cholesterol homeostasis is regulated by plasma membrane cholesterol in excess of phospholipids. Proceedings of the National Academy of Sciences of the United States of America *101*, 11664 –11667.

Liu, S.-Y., Sanchez, D.J., Aliyari, R., Lu, S., and Cheng, G. (2012). Systematic identification of type I and type II interferon-induced antiviral factors. Proceedings of the National Academy of Sciences *109*, 4239 –4244.

Moog, C., Aubertin, A., Kim, A., and Luu, B. (1998). Oxysterols, but not cholesterol, inhibit human immunodeficiency virus replication in vitro. Antiviral Chemistry & Chemotherapy *9*, 491–496.

Mortazavi, A., Williams, B.A., McCue, K., Schaeffer, L., and Wold, B. (2008). Mapping and quantifying mammalian transcriptomes by RNA-Seq. Nat Meth *5*, 621–628.

Negrete, O.A., Wolf, M.C., Aguilar, H.C., Enterlein, S., Wang, W., Mühlberger, E., Su, S.V., Bertolotti-Ciarlet, A., Flick, R., and Lee, B. (2006). Two Key Residues in EphrinB3 Are Critical for Its Use as an Alternative Receptor for Nipah Virus. PLoS Pathog *2*, e7.

Olsen, B.N., Schlesinger, P.H., Ory, D.S., and Baker, N.A. (2011). 25-Hydroxycholesterol Increases the Availability of Cholesterol in Phospholipid Membranes. Biophysical Journal *100*, 948–956.

Palleroni, A.V., Varesio, L., Wright, R.B., and Brunda, M.J. (1991). Tumoricidal alveolar macrophage and tumor infiltrating macrophage cell lines. Int. J. Cancer *49*, 296–302.

Park, K., and Scott, A.L. (2010). Cholesterol 25-hydroxylase production by dendritic cells and macrophages is regulated by type I interferons. Journal of Leukocyte Biology *88*, 1081 –1087.

Pécheur, E.-I., Sainte-Marie, J., Bienvenüe, A., and Hoekstra, D. (1998). Lipid Headgroup Spacing and Peptide Penetration, but Not Peptide Oligomerization, Modulate Peptide-Induced Fusion†. Biochemistry *38*, 364–373.

Perez-Caballero, D., Zang, T., Ebrahimi, A., McNatt, M.W., Gregory, D.A., Johnson, M.C., and Bieniasz, P.D. (2009). Tetherin Inhibits HIV-1 Release by Directly Tethering Virions to Cells. Cell *139*, 499–511.

Pezacki, J., Sagan, S., Tonary, A., Rouleau, Y., Belanger, S., Supekova, L., and Su, A. (2009). Transcriptional profiling of the effects of 25-hydroxycholesterol on human hepatocyte metabolism and the antiviral state it conveys against the hepatitis C virus. BMC Chemical Biology *9*, 2.

Radhakrishnan, A., Ikeda, Y., Kwon, H.J., Brown, M.S., and Goldstein, J.L. (2007). Sterol-regulated transport of SREBPs from endoplasmic reticulum to Golgi: Oxysterols

block transport by binding to Insig. Proceedings of the National Academy of Sciences *104*, 6511 –6518.

Scherle, P.A., Dorshkind, K., and Witte, O.N. (1990). Clonal lymphoid progenitor cell lines expressing the BCR/ABL oncogene retain full differentiative function. Proceedings of the National Academy of Sciences *87*, 1908 –1912.

Takada, A., Robison, C., Goto, H., Sanchez, A., Murti, K.G., Whitt, M.A., and Kawaoka, Y. (1997). A system for functional analysis of Ebola virus glycoprotein. Proceedings of the National Academy of Sciences *94*, 14764 –14769.

Teissier, É., and Pécheur, E.-I. (2007). Lipids as modulators of membrane fusion mediated by viral fusion proteins. European Biophysics Journal *36*, 887–899.

Vaney, M.-C., and Rey, F.A. (2011). Class II enveloped viruses. Cellular Microbiology *13*, 1451–1459.

Wang, F., Xia, W., Liu, F., Li, J., Wang, G., and Gu, J. (2012). Interferon regulator factor 1/retinoic inducible gene I (IRF1/RIG-I) axis mediates 25-hydroxycholesterol-induced interleukin-8 production in atherosclerosis. Cardiovascular Research *93*, 190 –199.

Wang, L., Feng, Z., Wang, X., Wang, X., and Zhang, X. (2010). DEGseq: an R package for identifying differentially expressed genes from RNA-seq data. Bioinformatics *26*, 136 –138.

Weidner, J.M., Jiang, D., Pan, X.-B., Chang, J., Block, T.M., and Guo, J.-T. (2010). Interferon-Induced Cell Membrane Proteins, IFITM3 and Tetherin, Inhibit Vesicular Stomatitis Virus Infection via Distinct Mechanisms. Journal of Virology *84*, 12646 –12657.

Wolf, M., Wang, Y., Freiberg, A., Aguilar, H., Holbrook, M., and Lee, B. (2009). A catalytically and genetically optimized beta-lactamase-matrix based assay for sensitive, specific, and higher throughput analysis of native henipavirus entry characteristics. Virology Journal *6*, 119.

Zhang, L., Jiang, Q., Li, G., Jeffrey, J., Kovalev, G.I., and Su, L. (2011). Efficient infection and impairment of pDC in the bone marrow and peripheral lymphoid organs during early HIV-1 infection in humanized rag2-/-γC-/- mice in vivo. Blood.

Zlokarnik, G., Negulescu, P.A., Knapp, T.E., Mere, L., Burres, N., Feng, L., Whitney, M., Roemer, K., and Tsien, R.Y. (1998). Quantitation of Transcription and Clonal Selection of Single Living Cells with β-Lactamase as Reporter. Science *279*, 84 –88.

Zou, T., Garifulin, O., Berland, R., and Boyartchuk, V.L. (2011). Listeria monocytogenes Infection Induces Prosurvival Metabolic Signaling in Macrophages. Infection and Immunity *79*, 1526 –1535.

CHAPTER 4

Retinoid-X-Receptor Modulates Host Response Against Viral Infections

ABSTRACT

Immune activation during viral infections causes host cells to suppress expression of Retinoid-X-Receptors (RXR), which is a nuclear hormone essential for cellular and whole-body metabolism. Here, we describe a novel immunological role for RXR in which it acts as a negative regulator of host anti-viral response. Activation of RXR increased host cell susceptibility to vesicular stomatitis virus (VSV), murine gamma-herpes virus (MHV68), and herpes simplex virus (HSV-1). Functional absence of RXR or treatment with RXR antagonists inhibited viral growth and replication. Further studies indicated that RXR activation in macrophages significantly repressed the expression of multiple anti-viral genes including IFNβ, ISG15, ISG20, IRF7, and OAS2. These data suggest that downregulation of RXR during viral infection alleviates suppression of anti-viral gene expression and illustrates a potential novel pathway of immune regulation during viral infections.

INTRODUCTION

Pattern recognition receptors (PRRs), such as Toll-like receptors or RIG-I like receptors, are sensors of microbial components and are highly expressed in macrophages and dendritic cells. Classically, they activate transcription factors NFκB and IRF3 to induce expression of primary anti-viral genes such as IFNβ, ISG15, and IFIT1 (Kawai and Akira, 2008). IFNβ is a type-I interferon that activate expression of antiviral genes through autocrine and paracrine action (Baum and García-Sastre, 2010). The IFN-induced antiviral state also causes changes in cell metabolism as shown by studies that implicate viral infections may lead to metabolic diseases like atherosclerosis and Reye's Syndrome (Castrillo et al., 2003; Chow et al., 2006). Conversely, activation of metabolic pathways can also regulate immune processes, the classic example being the suppression of inflammatory genes by glucocorticoid receptors. The relationship and outcome of immune and metabolic regulation during viral infection---although important for understanding of disease pathogenesis and therapeutic development--remain unclear.

In a study with viral infection and liver metabolism, we unexpectedly found that immune activation by viruses suppresses expression of retinoid-X-receptor (RXR), which is a nuclear hormone receptor critical for cellular metabolism, differentiation, and apoptosis(Mangelsdorf and Evans, 1995; Chow et al., 2006). This observation led to a potential role of RXR in the immunological response against viral infection.

RXR belongs to a class of ligand-activated nuclear hormone receptors and is critical in embryogenesis, development, and essential metabolic processes. It exist in three isoforms (RXRα,RXRβ, and RXRγ) with RXRα and RXRβ most widely expressed

(Mangelsdorf and Evans, 1995). RXR dimerizes with other nuclear hormone receptors at specific target promoters, where it requires ligand binding for full transcriptional activation. Vitamin A-derived retinoid, 9-*cis*-retinoic acid (9*cis*RA), is an endogenous ligand that binds and activates RXR (Allenby et al., 1993). Other retinoid compounds, such as all-*trans*-retinoic acid (ATRA) and 13-*cis*-retinoic acid (13*cis*RA), can activate RXR dimers at higher concentrations and possibly through isomerization to 9*cis*RA (Mangelsdorf et al., 1992; Tsukada et al., 2000; Armstrong et al., 2005). These retinoids and synthetic RXR-specific agonists, called rexinoids, are used for various cancers and skin diseases(Altucci et al., 2007).

Our previous study has demonstrated an IFN-independent and IRF3-dependent pathway that lead to down-regulation of RXR expression. IRF3 up-regulates transcriptional repressor, Hes1, which suppresses RXR expression by binding to its promoter(Chow et al., 2006). We hypothesized that suppression of RXR may be beneficial to the immune response against viral infection. Indeed, we found RXR activation increases susceptibility of host cells to viral infection and suppresses important host anti-viral factors. Our data suggest that host cell down-regulates RXR to alleviate its broad suppressive effect on host anti-viral response.

RESULTS

The purpose of this study was to investigate the potential role of RXR in modulation of host innate immune response against viral infections. In previous gene expression study, viral infection causes downregulation of RXR expression in bone marrow macrophages (BMMs) and dendritic cells(Chow et al., 2006; Ng et al., 2009). To test whether this response is general for RNA and DNA viruses, BMMs were infected with 1MOI of vesicular stomatitis virus expressing GFP(VSV, RNA virus), herpes simplex virus-1 (HSV-1, DNA virus), and murine gamma herpes virus (MHV68, DNA virus) and RNA was collected for qPCR analysis (Wu et al., 2001; Fernandez et al., 2002). RXR expression was reduced after infection by all these viruses (Fig. 4-1 A). This suppression was specific because there was no change in L32 control gene. RXR expression was also significantly suppressed in BMMs treated with dsRNA mimetic, poly(I:C), consistent with published data (Fig. 4-1 B). To investigate whether RXR play a role in viral infection, RAW264.7 (RAW), a macrophage cell line, stably expressing human-RXRα (hRXRα) and pBABE vector control were generated by retroviral infection and then infected with VSV coexpressing GFP (VSV-GFP) at 0.01 MOI. Supernatants were collected at 14h.p.i and the titer was quantitated by standard plaque assay. VSV-GFP viral load in RAW264.7 stably expressing hRXRα was 10-fold higher than that of pBABE-vector control (Fig.4-1 C and D). The result was consistent across different populations and single cell clones that stably overexpressed hRXRα. These data show that RXR expression cause susceptibility to viral infections.

To determine whether RXR has a functional role in host response against viral infection, wild-type and RXR-null F9 embryonal carcinoma were infected with VSV at

0.01MOI. RXR-null infected cells were more resistant to VSV infection compared to wild-type cells as determined by plaque assay (Fig. 4-1 E and F). To show that this difference is RXR-dependent, RXR-null F9 cells stably expressing RXRα and pBABE control were generated by retroviral infection. VSV infection in three separate hRXRα overexpressing populations produced significantly higher viral titers than pBABE control cell lines (Fig.4-1 G and H). Taken together, these result show that RXR increases host cell to viral infections.

RXR is a nuclear receptor that requires ligand binding for its activity. To investigate whether ligand activation of RXR can affect viral infection, RAW264.7 were treated with two RXR-specific agonist LG268 (100nM) and AGN194204 (100nM) for 16hours and infected with VSV for 14 hours. Consistent with previous data, activation of RXR with either agonist increased VSV viral load (Fig. 4-2A). In RAW264.7 overexpressing hRXRα, AGN194204 treatment further increased the viral load (supplementary Fig. S4-1 A). Ligand treatment on Vero cells did not affect viral burden indicating that the agonist carried over from supernatant did not affect quantification of viral titer (data not shown). Similarly, treatment with 100nM of 9-*cis*-retinoic acid, an endogenous ligand for RXR, also increased susceptibility RAW264.7 to VSV infection in a dose-dependent manner (Fig. 4-2 B-C and supplementary. Fig. S4-1 B). Conversely, RAW264.7 were more resistant to VSV infection after treatment with a specific RXR antagonist, HX531(Fig. 4-2B and C) (Ebisawa et al., 1999). In the F9 cell line, AGN194204 also increased susceptibility of wild-type cell to VSV infection, whereas it had no effect on RXR-null cells suggesting that ligand response is RXR-specific (Fig. 4-2D). To further confirm this specific ligand response, hRXRα was reconstituted stably

into RXR-null F9 cells and single cell clones were selected. In three single cell clones, RXR-null cell lines stably expressing hRXRα were more susceptible to viral infections after treatment with AGN194204 (Fig. 4-2E).

Vesicular stomatitis virus is a negative-strand RNA virus that undergoes replication and production of its viral components in the cytoplasm. To study whether RXR modulate expression of VSV protein production, RAW264.7 stably expressing hRXRα were treated with 9*cis*RA and HX531 and then infected with replication-incompetent VSV pseudovirus containing a VSV-G-renilla reporter. Treatment with 9*cis*RA increased VSV reporter expression and HX531 caused decrease in expression (Fig. 4-3A). Since the pseudovirus is incapable of replication, the increase in reporter expression infers an increase in efficiency of viral protein production upon RXR activation. To validate this finding, RAW264.7 pre-treated with DMSO and 9*cis*RA were infected with wild-type VSV, and the lysates were collected and VSV-G protein was quantitated by immunoblot. At 4 and 8h.p.i, VSV-G level in RAW264.7 overexpressing hRXRα was higher compared to pBABE control. Treatment with 9*cis*RA dramatically increased VSV-G levels (Fig. 4-3B). These data show RXR increases VSV proteins and may affect translational processes.

Genomic replication is another critical process required for successful viral replication. To test whether RXR activation affects VSV genome replication, RNA from VSV infected RAW264.7 pre-treated with 9*cis*RA were collected and the negative-stranded genomic RNA (vRNA) was quantitated by qPCR. RAW264.7 treated with 9*cis*RA showed increase vRNA levels within 2h.p.i and the difference was more significant at 4h.p.i (Fig. 4-3C). These results show that RXR activation modulates viral

genomic RNA production and viral protein production. Although these two processes may be related, the data implies that RXR may affect multiple viral lifecycle processes.

There are several possible mechanisms for the regulation of RXR on viral growth. First, RXR may promote VSV growth by directly activating viral genes. For example, RAR and RXR can activate early enhancer elements of human cytomegalovirus (hCMV)(Ghazal et al., 1992; Angulo et al., 1996). However, this possibility was unlikely because RXR did not affect viral growth in other cell types like Veros or 293Ts (data not shown). Second, RXR may up-regulate a particular host factor that promotes VSV growth or act as a suppressor of host anti-viral response. The former hypothesis was unlikely because RXR appeared to affect multiple viral lifecycle processes, which suggested multiple factors are mediating this effect. Also, RXR did not induce or regulate known host factors that promote VSV replication such as casein kinase 2 (data not shown) (Barik and Banerjee, 1992). Hence, we hypothesized that RXR may act as a negative regulator of anti-viral response.

To test this hypothesis, RAW264.7 were pre-treated with RXR agonist 9*cis*RA and antagonist HX531 for 16 hours and then stimulated with dsRNA mimetic, poly(I:C) (1ug/mL). At various times, RNA was collected for gene expression analysis. RXR activation with 9*cis*RA significantly suppressed primary anti-viral genes, *ifn*β and *isg15* within 2 hours after poly(I:C) treatment (Fig. 4-3 D). Expression of secondary interferon-stimulated genes (ISGs) with anti-viral activity, such as *oas2, gbp1, irf7, and isg20* were also suppressed in 9*cis*RA treated cells (Fig. 4-3 E). The RXR antagonist, HX531, significantly increased expression of some but not all anti-viral genes tested. 9*cis*RA and HX531 treatment modulated basal expression of some of these genes, suggesting

that RXR activation during normal physiological states may suppress anti-viral gene activation. These data suggest that activation of RXR cause suppression of anti-viral host factors.

We sought to understand the breadth and specificity of RXR inhibition on immune antiviral response by gene expression profile. We hypothesized that RXR activation by *9cis*RA may suppress IFN and antiviral genes that are activated by specific immune pathways. IFN activation can occur through TLR3/4 via TRIF-dependent pathways or through intracellular receptors, RIG-I and MDA5, in an IPS-1-dependent pathway. Hence, we treated RAW264.7 with 9cisRA (100nM) for 16h and subsequently transfected poly(I:C)(6ug) or treated the cells with lipidA (1ug/mL) for 2h--- which would activate IPS-1 and TRIF pathways, respectively. Total RNA was collected for gene expression profiling by microarray. Of the many genes induced by poly(I:C) and lipidA, large subsets were suppressed by 9cisRA. Induction of several forms of interferons, Ifnβ, Ifnα2, Ifnα4, and Ifnα5, by lipidA and poly(I:C) was down-regulated in 9cisRA-treated cells (Fig. 4-4). Likewise, we observed suppression of many poly(I:C) induced IFN-stimulated genes (ISGs), including, Socs3, Ifnα4, Cxcl10, and Rsad2 (Fig. 4-4 A, asterisks). Similarly, many lipidA-induced genes suppressed by 9cisRA were anti-viral genes (Fig. 4-4B). Another subset were induced by both ligands and also suppressed by RXR (Fig. 4-4 C). In total, RXR inhibited 89 out of 222 poly(I:C)-induced genes (40%) and 150 out of 693 (21%) lipidA-induced genes, showing that RXR inhibited gene activation by poly(I:C) more than lipidA. These results suggested that RXR might inhibit common signaling pathway activated by these ligands. Since poly(I:C) predominantly activate IPS→TBK→IRF3 cascade and lipidA activates TRIF→TBK→IRF3, RXR may

affect activation of TBK and IRF3 (Table. T1-T5). Taken together, RXR broadly inhibits gene expression by poly(I:C) and lipidA with greater inhibition on poly(I:C) induced genes.

Gene expression profiling suggests that induction of primary genes, such as IFN, is suppressed by RXR. In other words, RXR suppression would be upstream of IFN activation and not downstream of IFN signaling. To test this hypothesis, IFN receptor deficient (*ifnar-/-*) BMMs were pretreated with 9*cis*RA and HX531 and stimulated with poly(I:C). 9*cis*RA significantly downregulated poly(I:C)-induced IFNβ and ISG15 in *ifnar-/-* BMMs (Fig. 4-5A). To test the functional effect of primary antiviral gene suppression, *ifnar-/-* BMMs were pre-treated with 9*cis*RA and HX531 and infected with VSV. RXR activation by 9*cis*RA significantly increased viral load and HX531 reduced viral load (Fig. 4-5 B). Taken together, activation of RXR by 9*cis*RA suppresses primary anti-viral genes and cause susceptibility to viral infections.

We hypothesized that RXR inhibits activation of IFN-luciferase reporter (IFN-Luc) by various upstream signaling factor. In stable RXR-overexpressing cell lines, RXR activation by 9cisRA inhibited poly(I:C) induced IFN-Luc activity (Fig. 4-6 A). In HEK293T, overexpression of RXR inhibited TRIF, RIG-I, IPS-1, TBK, and IRF3 activation of IFN-Luc (Fig. 4-6 B, C, and D). RXR, not GFP control, specifically inhibited IRF3 activation of IFNβ reporter showing that this inhibition was not a general overexpression effect (Fig. 4-6 E). Of the IFN activators tested, IRF3 is farthest in the IFN activation pathway and can directly activate IFNβ; hence, RXR may inhibit IRF3 activity.

To further validate the overexpression findings, we examined whether functional loss of RXR would modulate IFN activation. In IFN-Luc transfected HEK293T, siRNA and shRNA knockdown of RXR increased IPS-1 and TBK-1 activation of the reporter (Fig. 4-6 F and G). Hence, transient loss of RXR enhanced induction of IFN.

Previous studies have implicated RXR to suppress NFκB, another essential activator of IFNβ (Motomura et al., 2001; Dheen et al., 2005). Hence, we tested whether RXR inhibits activity of NFκB. In HEK293T, RXR overexpression inhibited MyD88 and P65 activation of a NFκB-luciferase reporter (Fig. 4-6 H). Consistently in RAW264.7, expression of RXR with 9cisRA stimulation inhibited P65 activation of NFκB-Luc reporter (Fig. 4-6 I). Hence, RXR activation can inhibit NFκB reporter activation. Taken together, RXR activation may inhibit upstream IRF3 and NFκB activation.

We sought to test the effect of 9cisRA on the activation of endogenous IRF3, which undergoes phosphorylation and dimerization before activation of IFN. Treatment of RAW264.7 with 9cisRA caused reduction in poly(I:C) induced IRF3 dimerization within 2h (Fig. 4-6 J). IRF3 and TBK1 phosphorylation was also suppressed by 9cisRA (Fig. 4-6 K). These results show that 9cisRA can inhibit the efficiency of IRF3 phosphorylation either directly or indirectly inhibit upstream signaling factors.

The observation that ligand activation of RXR inhibits many anti-viral genes suggests that RXR may suppress general host anti-viral response in macrophages. To this end, the effect of RXR activation on different viral infections was compared. RAW264.7 were treated with RXR-specific agonist, AGN194204, and infected with murine gamma-herpes virus 68 expressing luciferase reporter (MHV68-luc) and Herpes

simplex virus 1 (HSV1). Compared to DMSO treated controls, AGN194204 treated RAW264.7 displayed >20 fold increase in MHV68 luciferase reporter expression (Fig. 4-7 A). The RXR agonist increased HSV viral titer by more than 3 fold as measured by plaque assay (Fig. 4-7 B). Overexpression hRXRα alone slightly increased MHV68 reporter expression and HSV1 viral load, whereas treatment with 9*cis*RA increased susceptibility of cells to these viruses (Fig. 4-7 C and D). Moreover, inhibition of RXR with HX531 suppressed viral load. These results show RXR activation increase sensitivity to both RNA and DNA viruses and are consistent with a suppressive role of RXR on host anti-viral genes.

Retinoids have been commonly used as drug treatments for skin diseases and various cancers. Isoretinoin, 13*cis*RA, is most widely used and has also shown to increase VSV infection in RAW264.7 (Supp. Fig. S4-1 C). Some reports show that 13*cis*RA may be associated to herpes infection(Baxter and Cunliffe, 2001). To test whether retinoids can affect HSV-1 infection *in vivo*, 13-*cis*-retinoic acid (1mg/kg) or vehicle control were administered by intraperitoneal (i.p.) injection to age and sex-matched mice for 3 days every 24 hours. The mice were infected with HSV-1 at 10^7 pfu by intraperitoneal injection (*i.p.*) on day 4 and the livers were harvested on 5 days post infection. Mice treated with 13*cis*RA had significantly higher HSV titer in livers in two independent experiments (Fig. 4-7 E). These data provide physiological support for negative role of retinoids on host anti-viral response.

DISCUSSION

In this study, we sought to understand the immunological role of RXR during viral infections. Genetic and pharmacological data demonstrate that RXR is a suppressor of host anti-viral response and its activation suppresses many primary anti-viral genes including IFN. RXR cause inhibition of IRF3 and NFκB activity. The observation that host cell down-regulates RXR expression during viral infection suggests that this response is protective and may represent a novel anti-viral strategy.

Our results illustrate how immune and metabolic processes are intertwined. On one hand, viral infection causes IRF3-dependent downregulation of RXR resulting in lower metabolic activity. Since RXR is an essential heterodimer of many nuclear hormone receptors, suppression of RXR hinders drug and lipid metabolism and may lead to clinical disease like asprin toxicity and atherosclerosis(Castrillo et al., 2003; Chow et al., 2006). On the other hand, the present work shows that the immune response to downregulates RXR may further enhance defense mechanisms against viral infections. Our data show that RXR overexpression or activation promotes viral infection whereas RXR deficiency or antagonisms reduce viral growth. Thus, while RXR downregulation may have metabolic consequences, its suppression may be beneficial for the host defense against virus.

On a molecular level, our model suggests that RXR is constitutively expressed and activated by trace amount of endogenous ligands, such as 9*cis*RA, during a normal metabolic state and may suppress unnecessary anti-viral gene activation. However, during a viral infection, IRF3 and NFκB are activated to induce primary anti-viral genes like IFNβ, ISG15, and IFIT. In addition, IRF3 indirectly inhibits RXR expression,

possibly through induction of the repressor Hes1(Chow et al., 2006). This suppression of RXR will then alleviate inhibition of anti-viral genes allowing for their optimal expression (Fig. 4-7 F). This system allows for fine modulation of anti-viral genes and may be particularly important in macrophages because they are primary responders of viral infections.

Our initial studies of how RXR activation increases susceptibility of host cells to viral infection implicated that multiple VSV lifecycle processes were affected. Hence we hypothesized that downregulation of host anti-viral factors would lead to this broad effect. Gene profiling studies of known anti-viral genes showed that RXR-ligand activation significantly suppressed poly(I:C) induced genes, including Ifnβ, Isg15, Isg20, Gbp-1, Oas2, and Irf7. Further analyses in *ifnar-/-* BMMs also show that ligand activation of RXR also increased susceptibility to viral infection, suggesting an interferon-independent effect. This observation is consistent with suppression of primary induced anti-viral genes Ifnβ and Isg15 by RXR activation in *ifnar-/-* BMMs. Our data support previous studies showing a repressive role of RXR on NFκB activity (Aukrust et al., 2000; Motomura et al., 2001; Xu and Drew, 2006; Lee et al., 2008). In addition, we showed that RXR also inhibits phosphorylation and dimerization of IRF3, which is believed to be the dominant activator of IFN. TBK phosphorylation was also inhibited. Together, RXR may have multiple inhibitory action activation of IFN. Although it may exhibit specific transrepression of inflammatory and antiviral genes analogous to other nuclear hormone receptors such as LXR and PPARγ (Joseph et al., 2003; Welch et al., 2003; Ogawa et al., 2005; Ghisletti et al., 2007; Glass and Saijo, 2010), it is likely to have specific effect on the signaling factors that activate IFN.

Retinoids are frequently used in the clinical setting as treatment for cancer, inflammatory skin diseases, and acne (Kang and Voorhees; Van De Kerkhof, 2006; Altucci et al., 2007). Aside from their teratogenic effects, retinoids are generally well tolerated because their levels are well controlled in normal physiology. Dominant vitamin A derivatives, 9*cis*RA and ATRA, readily induce their own metabolism through induction of CYP26 enzymes (Taimi et al., 2004). On the other hand, 13*cis*RA is slowly metabolized through different P450 enzymes (Tsukada et al., 2000; Taimi et al., 2004; Muindi et al., 2008). Our results show that 13*cis*RA treatment increases susceptibility to HSV-1 infection in mice and support clinical reports of association of 13*cis*RA with herpetic infections (Baxter and Cunliffe, 2001; Stetson et al., 2003; Yazici et al., 2006). Even though other counter-regulatory processes may mask retinoid-mediated suppression of anti-viral genes, our results suggest that certain retinoid compounds may be contraindicated in patients with high risk of viral infections.

While RXR activation can negatively regulate anti-viral response, downregulation of RXR may be a beneficial to host cells during viral infection. Our data show RXR antagonism by treatment with HX531 moderately increased induction anti-viral genes. More importantly, HX531 treatment in macrophages and RXR-null cells displayed increase resistance to various viral infections. It is possible that RXR antagonism may also inhibit viral replication through suppression of metabolic processes that are required for viral growth. The potential role for RXR antagonism in viral therapeutics encourages comprehensive analyses of various RXR antagonists on different viral infections *in vitro* and *in vivo.*

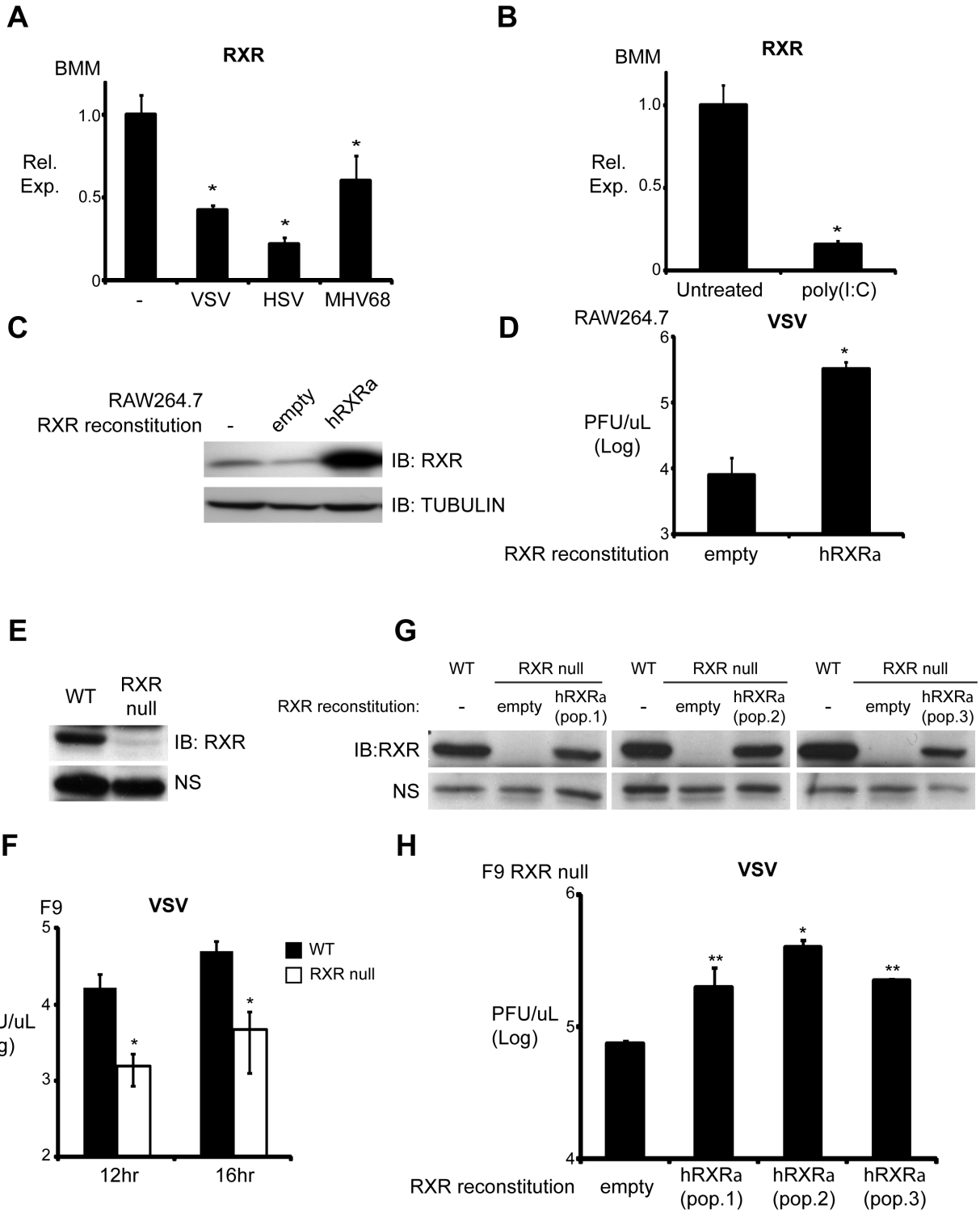
A
RXR
BMM
Rel. Exp.
1.0
0.5
0
-
VSV
HSV
MHV68
B
RXR
BMM
Rel. Exp.
1.0
0.5
0
Untreated
poly(I:C)
C
RAW264.7
RXR reconstitution
-
empty
hRXRa
IB: RXR
IB: TUBULIN
D
RAW264.7
VSV
PFU/uL (Log)
6
5
4
3
RXR reconstitution
empty
hRXRa
E
WT
RXR null
IB: RXR
NS
G
WT
RXR null
RXR reconstitution:
-
empty
hRXRa (pop.1)
hRXRa (pop.2)
hRXRa (pop.3)
IB:RXR
NS
F
F9
VSV
PFU/uL (Log)
5
4
3
2
WT
RXR null
12hr
16hr
H
F9 RXR null
VSV
PFU/uL (Log)
6
5
4
RXR reconstitution
empty
hRXRa (pop.1)
hRXRa (pop.2)
hRXRa (pop.3)

Figure 4-1. RXR expression modulates host cell sensitivity to VSV infection

(A) RXR expression in BMMs infected with 1 MOI of VSV for 4 hours, HSV-1 and MHV68 for 8 hours. Relative gene expression data are represented as mean ± SD for biological triplicates normalized to uninfected control. *, significant ($p \leq 0.05$), **, very significant ($p \leq 0.01$).
(B) RXR expression in BMMs treated with poly(I:C) 1ug/mL for 4hours and the RNA was collected. *, significant ($p \leq 0.01$). Relative gene expression data are represented as mean ± SD for biological triplicates normalized to untreated control.
(C) RXR protein expression in cell lysates from Wild-type RAW264.7 cells and RAW264.7 stably expressing pBABE vector control and RXR were detected by immunoblot.
(D) RAW264.7 cells stably overexpressing hRXRα or pBABE control were infected with VSV at 0.01 MOI. Supernantants were collected at 14h.p.i and viral titer was quantitated by standard plaque assay. *, significant ($p \leq 0.01$). Pfu/uL is represented as mean ± SD in biological triplicates. Data is representative of 3 experiments.
(E) Immunoblot of RXR in WT and RXR-null F9 Embryonal Carcinoma cell lines.
(F) Wild-type and RXR null F9 embryonal carcinoma cell line were infected with VSV at 0.01MOI and the viral titer of supernantant was quantified at various time points. Pfu/uL is represented as mean ± SD in biological triplicates. *, significant ($p \leq 0.05$). Data is representative of 3 experiments.
(G) RXR-null F9 cells were reconstituted with hRXRα or pBABE control by retroviral infection. Three independent RXR overexpressing populations were made, RXR (pop.1), RXR(pop.2), RXR(pop.3), and pBABE control. RXR expression in these cell lines was confirmed by immunoblot.
(H) RXR-null F9 cells were reconstituted with hRXRα or pBABE control as described in part G were infected with VSV at 0.01 MOI. Supernatants were collected 12h.p.i and quantitated for by plaque assay. Pfu/uL is represented as mean ± SD in biological triplicates. *, significant ($p \leq 0.06$), very significant ($p \leq 0.01$). Data is representative of 2 experiments.

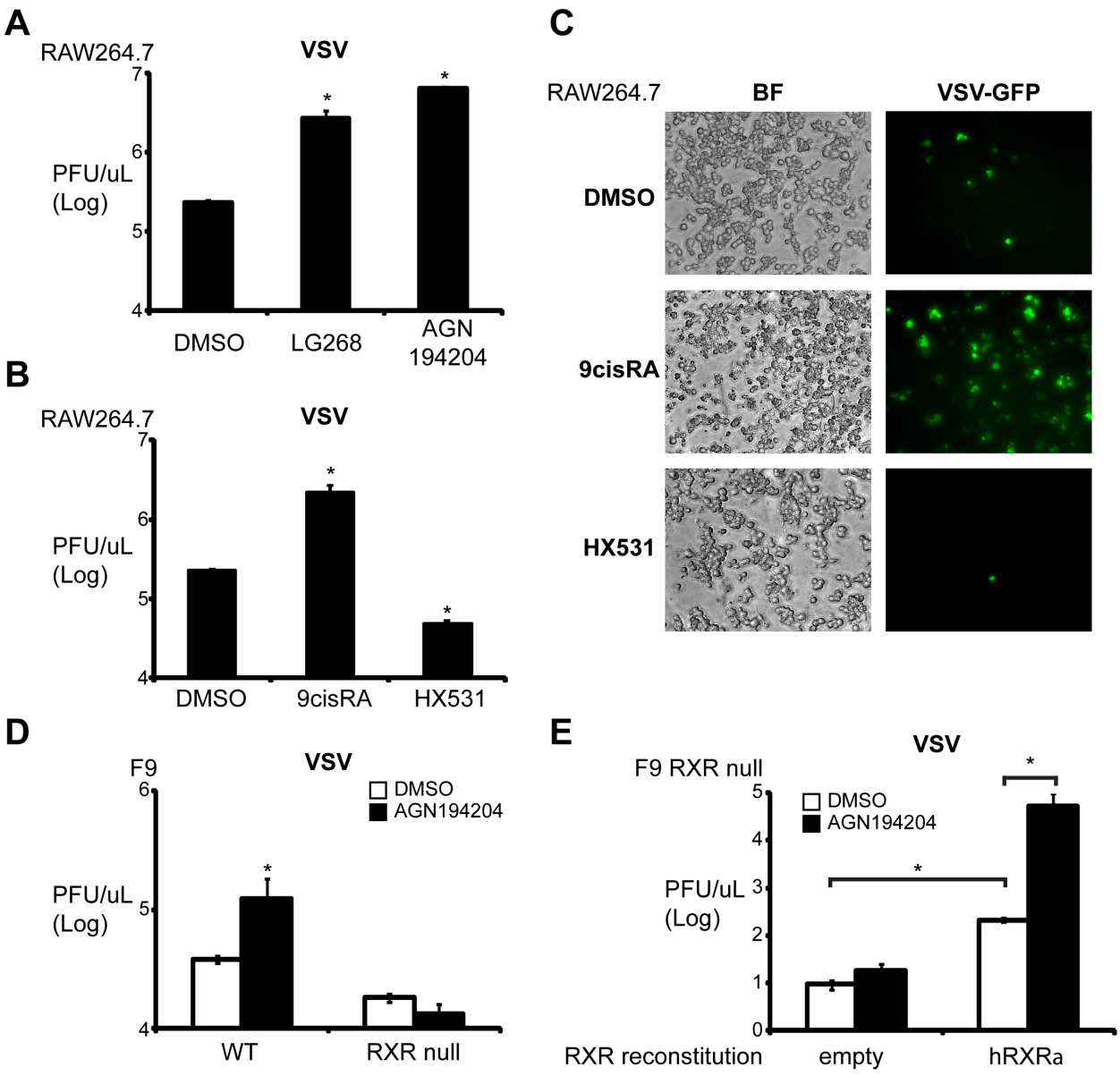

Figure 4-2. RXR-specific agonists and anatagonist modulate host cell sensitivity to VSV infection.
(A) RAW264.7 cells were treated with DMSO vehicle control or RXR-specific ligands, LG268 (100nM) and AGN194204 (100nM) for 16 hours. The cells were subsequently infected with VSV at 0.01 MOI and the supernatant was collected 14h.p.i and quantified by plaque assay. Pfu/uL is represented as mean ± SD in biological triplicates. *, significant ($p \leq 0.01$). Data is representative of 3 experiments.
(B) RAW264.7 were treated with endogenous RXR ligand, 9*cis*RA, and an RXR antagonist HX531 and subsequent infected with VSV at 0.01MOI. The titer was quantitated by plaque assay. Pfu/uL is represented as mean ± SD in biological triplicates. . *, significant ($p \leq 0.01$). Data is representative of 3 experiments.
(C) Representative fluorescence image of VSV-GFP in RAW264.7 treated with DMSO, 9*cis*RA, and HX531 at 9h.p.i.

(D) Wild-type and RXR null F9 cells were treated with AGN194204, infected with VSV at 0.01MOI, and titered by plaque assay. Pfu/uL is represented as mean ± SD in biological triplicates. *, significant ($p \leq 0.05$)
(E) Single cell clones from RXR-null F9 cells stably expressing RXR were treated with DMSO or AGN194204 and infected with VSV at 0.01MOI. The VSV viral load was quantitated 12h.p.i. Result is representative of 1 out of 3 single cell clonal populations. Pfu/uL is represented as mean ± SD.

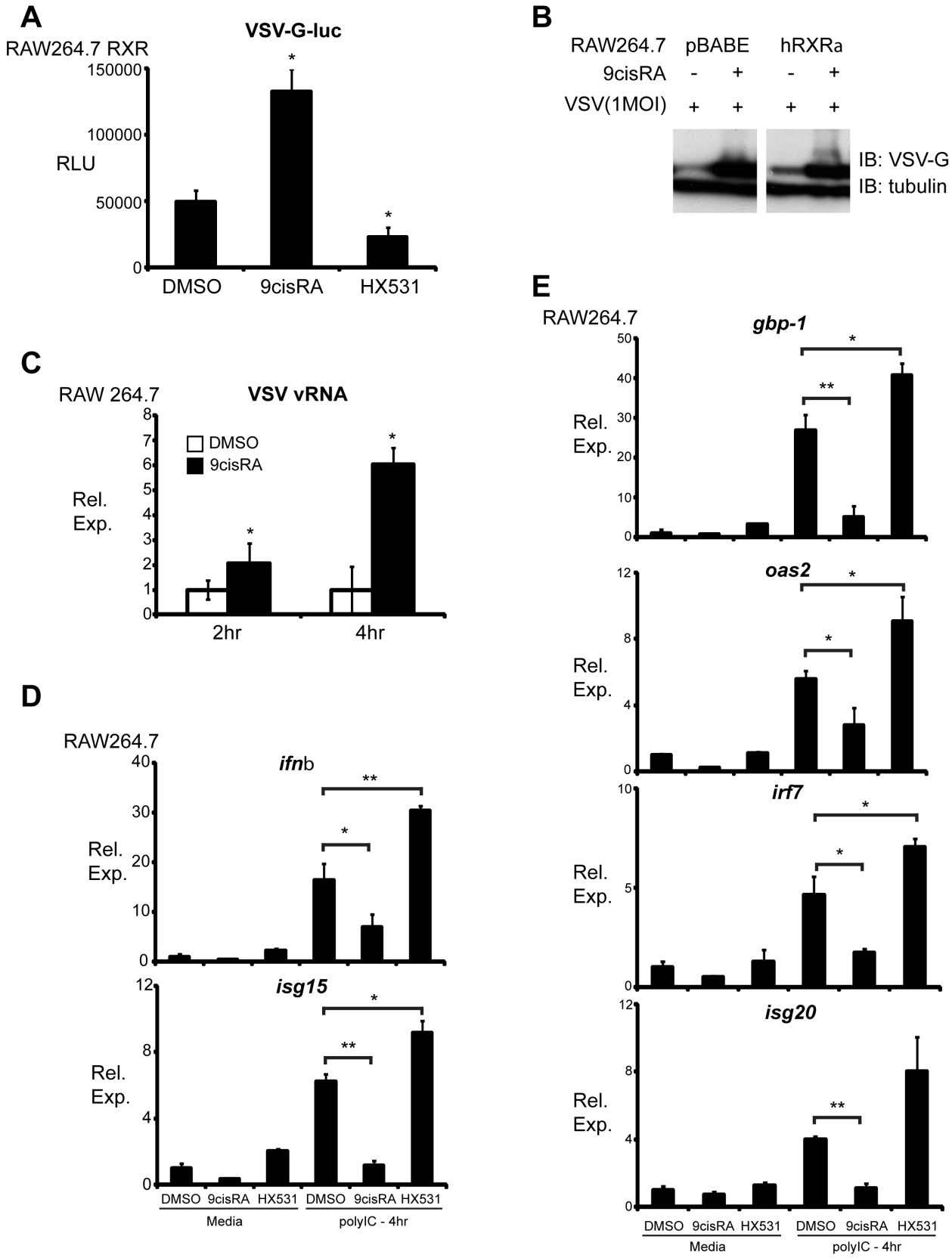
A
RAW264.7 RXR
VSV-G-luc
150000
100000
RLU
50000
0
DMSO
9cisRA
HX531
B
RAW264.7
pBABE
hRXRa
9cisRA
VSV(1MOI)
IB: VSV-G
IB: tubulin
C
RAW 264.7
VSV vRNA
DMSO
9cisRA
Rel. Exp.
2hr
4hr
D
RAW264.7
ifnb
isg15
Rel. Exp.
DMSO 9cisRA HX531 DMSO 9cisRA HX531
Media
polyIC - 4hr
E
RAW264.7
gbp-1
oas2
irf7
isg20
Rel. Exp.
DMSO 9cisRA HX531 DMSO 9cisRA HX531
Media
polyIC - 4hr

Figure 4-3. RXR modulates host anti-viral gene expression.

(A) RAW264.7 overexpressing hRXRα were treated with DMSO, 9*cis*RA and HX531 infected with replication-incompetent VSV pseudovirus encoding VSV-G luciferase reporter. The lysates were collected at 24h.p.i and the luciferase activity was quantitated. RLU is represented as mean ± SD in biological quadruplicates. *, significant (p≤0.01). Data is representative of 3 experiments.

(B) RAW264.7 expressing pBABE control or RXR were pretreated 9*cis*RA and infected with VSV. At 8h.p.i, cell lysates were collected and VSV-G protein level was detected by immunoblot.

(C) Relative genomic VSV RNA was quantiated at 2 and 4h.p.i. Relative gene expression data are represented as mean ± SD for biological triplicates normalized to DMSO treated samples. *, significant (p≤0.01).

(D) RAW264.7 cells were pretreated with 9*cis*RA or HX531 for 16hours and subsequently stimulated with poly(I:C) at a final concentration of 1ug/mL. RNA was collected 2 hours after stimulation and the level of primary induced *ifn*β and *isg15* was assessed by qPCR. Relative gene expression data are represented as mean ± SD for biological triplicates normalized to DMSO and media treated samples. *, significant (p≤0.05). **, very significant (p≤0.01).

(E) Expression of interferon-induced factors with known anti-viral activity, *gbp-1*, *isg20*, *oas2*, and *irf7*, were quantitated by qPCR on samples described from part D. Relative gene expression data are represented as mean ± SD for biological triplicates normalized to DMSO- and media-treated control. Data is representative of 3 experiments. . *, significant (p≤0.05). **, very significant (p≤0.01).

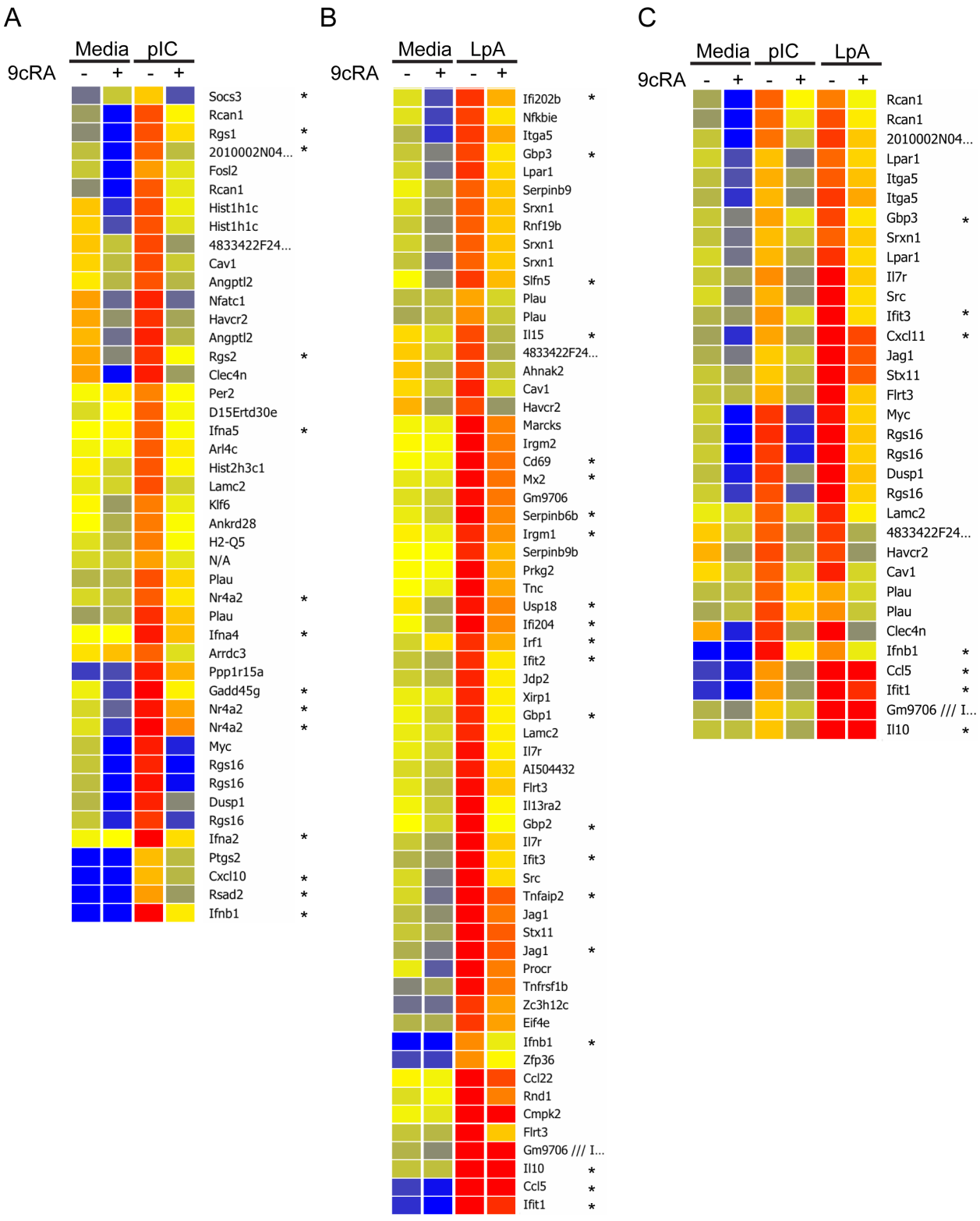
A
Media
pIC
9cRA
- + - +
Socs3 *
Rcan1
Rgs1 *
2010002N04... *
Fosl2
Rcan1
Hist1h1c
Hist1h1c
4833422F24...
Cav1
Angptl2
Nfatc1
Havcr2
Angptl2
Rgs2 *
Clec4n
Per2
D15Ertd30e
Ifna5 *
Arl4c
Hist2h3c1
Lamc2
Klf6
Ankrd28
H2-Q5
N/A
Plau
Nr4a2 *
Plau
Ifna4 *
Arrdc3
Ppp1r15a
Gadd45g *
Nr4a2 *
Nr4a2 *
Myc
Rgs16
Rgs16
Dusp1
Rgs16
Ifna2 *
Ptgs2
Cxcl10 *
Rsad2 *
Ifnb1 *
B
Media
LpA
9cRA
- + - +
Ifi202b *
Nfkbie
Itga5
Gbp3 *
Lpar1
Serpinb9
Srxn1
Rnf19b
Srxn1
Srxn1
Slfn5 *
Plau
Plau
Il15 *
4833422F24...
Ahnak2
Cav1
Havcr2
Marcks
Irgm2
Cd69 *
Mx2 *
Gm9706
Serpinb6b *
Irgm1 *
Serpinb9b
Prkg2
Tnc
Usp18 *
Ifi204 *
Irf1 *
Ifit2 *
Jdp2
Xirp1
Gbp1 *
Lamc2
Il7r
AI504432
Flrt3
Il13ra2
Gbp2 *
Il7r
Ifit3 *
Src
Tnfaip2 *
Jag1
Stx11
Jag1 *
Procr
Tnfrsf1b
Zc3h12c
Eif4e
Ifnb1 *
Zfp36
Ccl22
Rnd1
Cmpk2
Flrt3
Gm9706 /// I...
Il10 *
Ccl5 *
Ifit1 *
C
Media
pIC
LpA
9cRA
- + - + - +
Rcan1
Rcan1
2010002N04...
Lpar1
Itga5
Itga5
Gbp3 *
Srxn1
Lpar1
Il7r
Src
Ifit3 *
Cxcl11 *
Jag1
Stx11
Flrt3
Myc
Rgs16
Rgs16
Dusp1
Rgs16
Lamc2
4833422F24...
Havcr2
Cav1
Plau
Plau
Clec4n
Ifnb1 *
Ccl5 *
Ifit1 *
Gm9706 /// I...
Il10 *

Figure 4-4. The effect of RXR activation on poly(I:C) and lipidA induced gene expression profile.

(A) Gene expression array of RAW264.7 (triplicates combined) showing representative genes that induced by poly(I:C)(6ug) by more than 2-fold and suppressed by 9cisRA (100nM) by more than 2-fold. *IFN-stimulated genes (ISGs).
(B) Gene expression array of RAW264.7 (triplicates combined) showing representative genes that induced by lipidA(1ug/mL) by more than 2-fold and suppressed by 9cisRA (100nM) by more than 2-fold. *ISGs
(C) Gene expression array of RAW264.7 (triplicates combined) showing representative genes that induced by poly(I:C) and lipidA and suppressed by more than 2-fold. *IFN-stimulated genes. *ISGs

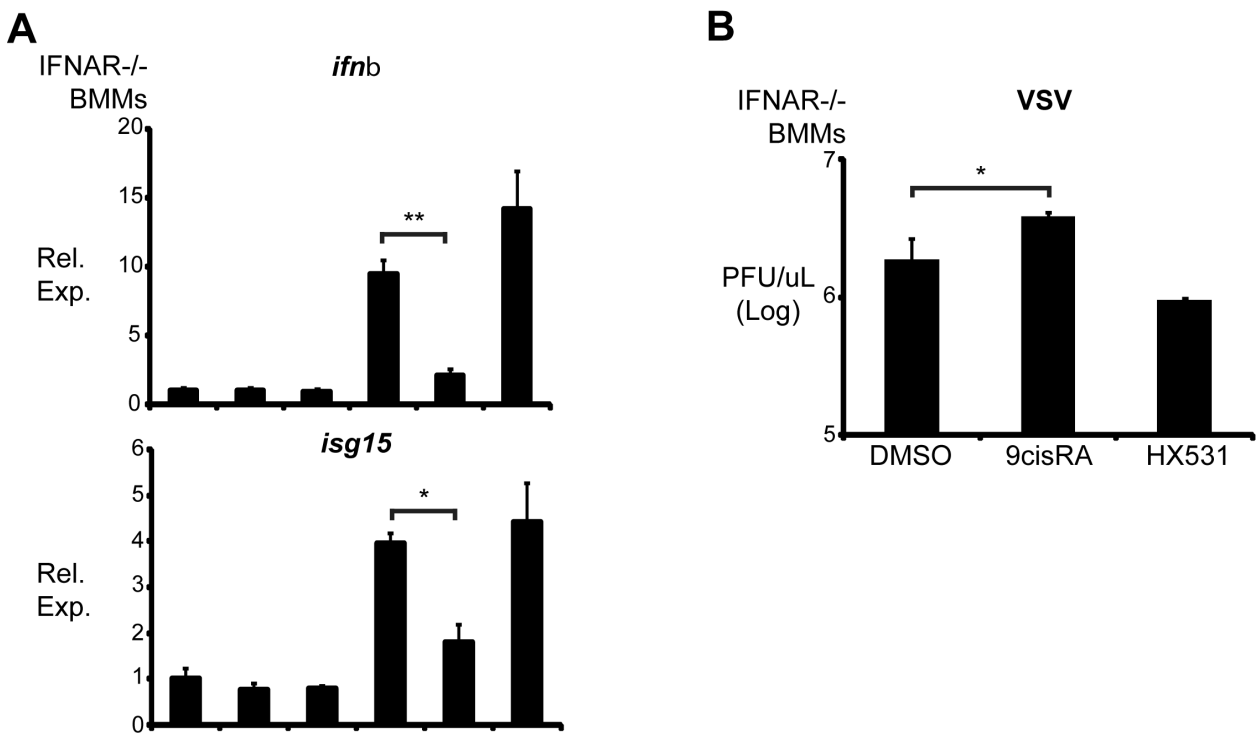

Figure 4-5. RXR activation suppress primary anti-viral gene expression and NFκB activity

(A) *IFNAR-/-* BMMs were pretreated with 9*cis*RA or HX531 for 16 hours and stimulated with poly(I:C) (1ug/mL). Level of IFNβ (upper panel) and ISG15 (lower panel) was quantitated by qPCR. Relative gene expression data are represented as mean ± SD for biological triplicates normalized to DMSO- and media-treated control. Data is representative of 3 experiments. *, significant (p≤0.05). **, very significant (p≤0.01).
(B) IFNAR-deficient BMMs were pre-treated with 9*cis*RA and HX531 for 16 hours and infected with VSV at 0.01 MOI. The titers of supernatant 12h.p.i were quantitated by plaque assay. Pfu/uL is represented as mean ± SD in biological triplicates. Data is representative of 3 experiments. . *, significant (p≤0.05)

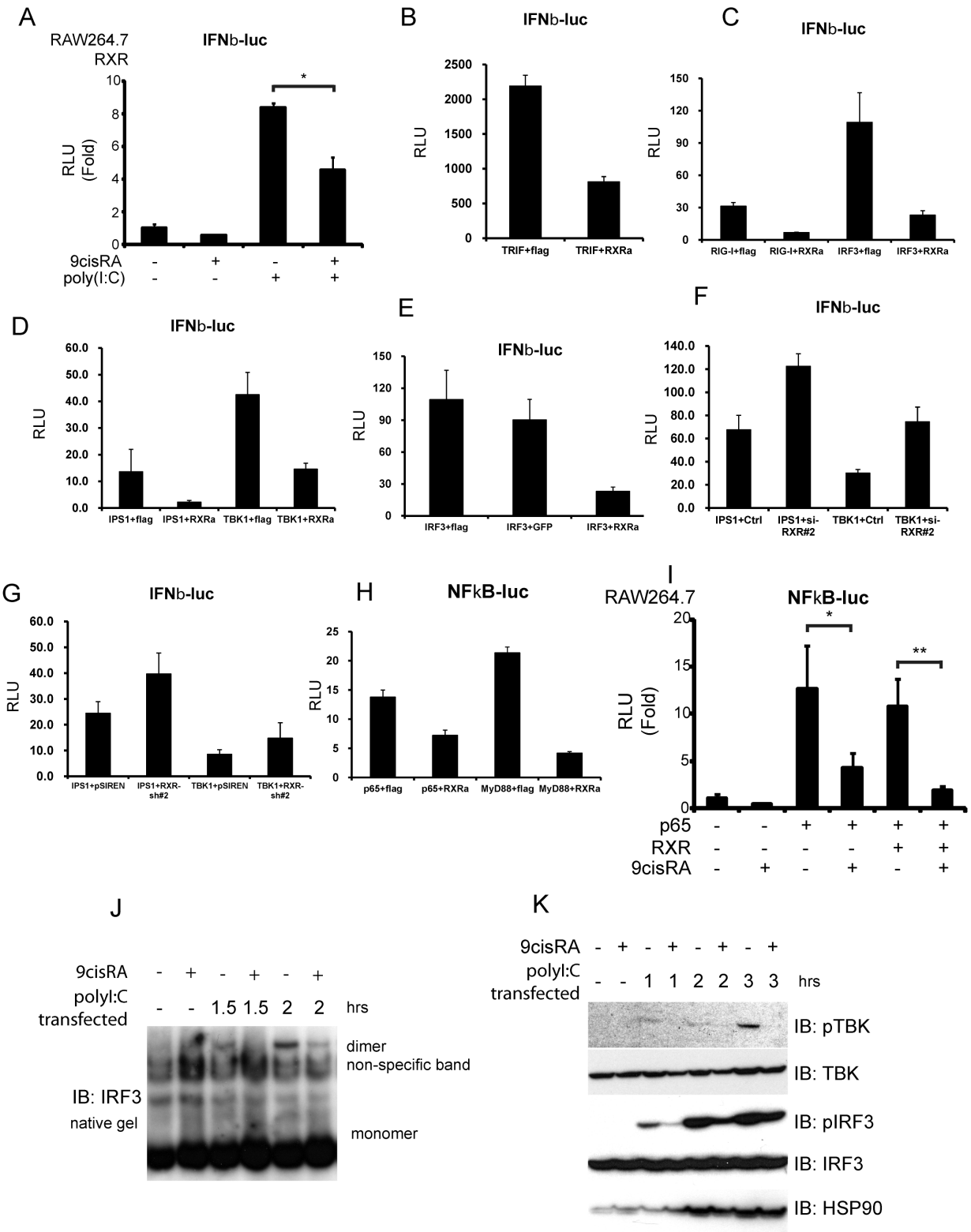
A
RAW264.7
RXR
IFNb-luc
RLU (Fold)
9cisRA
poly(I:C)
B
IFNb-luc
RLU
TRIF+flag
TRIF+RXRa
C
IFNb-luc
RLU
RIG-I+flag
RIG-I+RXRa
IRF3+flag
IRF3+RXRa
D
IFNb-luc
RLU
IPS1+flag
IPS1+RXRa
TBK1+flag
TBK1+RXRa
E
IFNb-luc
RLU
IRF3+flag
IRF3+GFP
IRF3+RXRa
F
IFNb-luc
RLU
IPS1+Ctrl
IPS1+si-RXR#2
TBK1+Ctrl
TBK1+si-RXR#2
G
IFNb-luc
RLU
IPS1+pSIREN
IPS1+RXR-sh#2
TBK1+pSIREN
TBK1+RXR-sh#2
H
NFkB-luc
RLU
p65+flag
p65+RXRa
MyD88+flag
MyD88+RXRa
I
RAW264.7
NFkB-luc
RLU (Fold)
p65
RXR
9cisRA
J
9cisRA
polyI:C transfected
hrs
IB: IRF3
native gel
dimer
non-specific band
monomer
K
9cisRA
polyI:C transfected
hrs
IB: pTBK
IB: TBK
IB: pIRF3
IB: IRF3
IB: HSP90

Figure 4-6. The effect of RXR activation on signaling pathways that activate IFN.

(A) RAW264.7 stably expressing RXR were transfected with IFN-Luc and RXR and treated with 9cisRA. Luciferase activity was measured 24h post transfection. Relative light units (RLU). Mean±SD.
(B) HEK293T were transfected with IFN-Luc and TRIF-flag with and without RXR. Luciferase activity was measured 24h post transfection. Relative light units (RLU); Mean±SD.
(C) HEK293T were transfected with IFN-Luc, RIG-I, IRF3, and with and without RXR. Luciferase activity was measured 24h post transfection. Relative light units (RLU); Mean±SD.
(D) HEK293T were transfected with IFN-Luc, IPS-1, TBK1, and with and without RXR. Luciferase activity was measured 24h post transfection. Relative light units (RLU); Mean±SD.
(E) HEK293T were transfected with IFN-Luc, IRF3, with GFP or RXR. Luciferase activity was measured 24h post transfection. Relative light units (RLU); Mean±SD.
(F) HEK293T were transfected with IFN-Luc, IPS1 or TBK1, and RXR siRNA. Luciferase activity was measured 24h post transfection. Relative light units (RLU); Mean±SD.
(G) HEK293T were transfected with IFN-Luc, IPS1 or TBK1, and RXR shRNA. Luciferase activity was measured 24h post transfection. Relative light units (RLU); Mean±SD.
(H) HEK293T were transfected with NFκB-luciferase reporter, P65 or MyD88, with or without RXR. Luciferase activity was measured 24h post transfection. Relative light units (RLU); Mean±SD.
(I) RAW264.7 cells were transfected with NFκB luciferase reporter with vector control or NFκB subunit P65. The cells were treated with DMSO or 9*cis*RA for 24 hours and the reporter activity was quantitated. *p≤0.05, **p≤0.01.
(J) RAW264.7 were pre-treated with 9cisRA and transfected with poly(I:C) (1ug/mL) for the indicated times. Cell lysates were collected in non-reducing buffers and separate in native gel.
(K) RAW264.7 was treated with 9cisRA for 16h and transfected with poly(I:C) (6ug) for the indicated time. Cell lysates were collected, separated on standard SDS-PAGE, and immunoblotted with indicated antibodies.

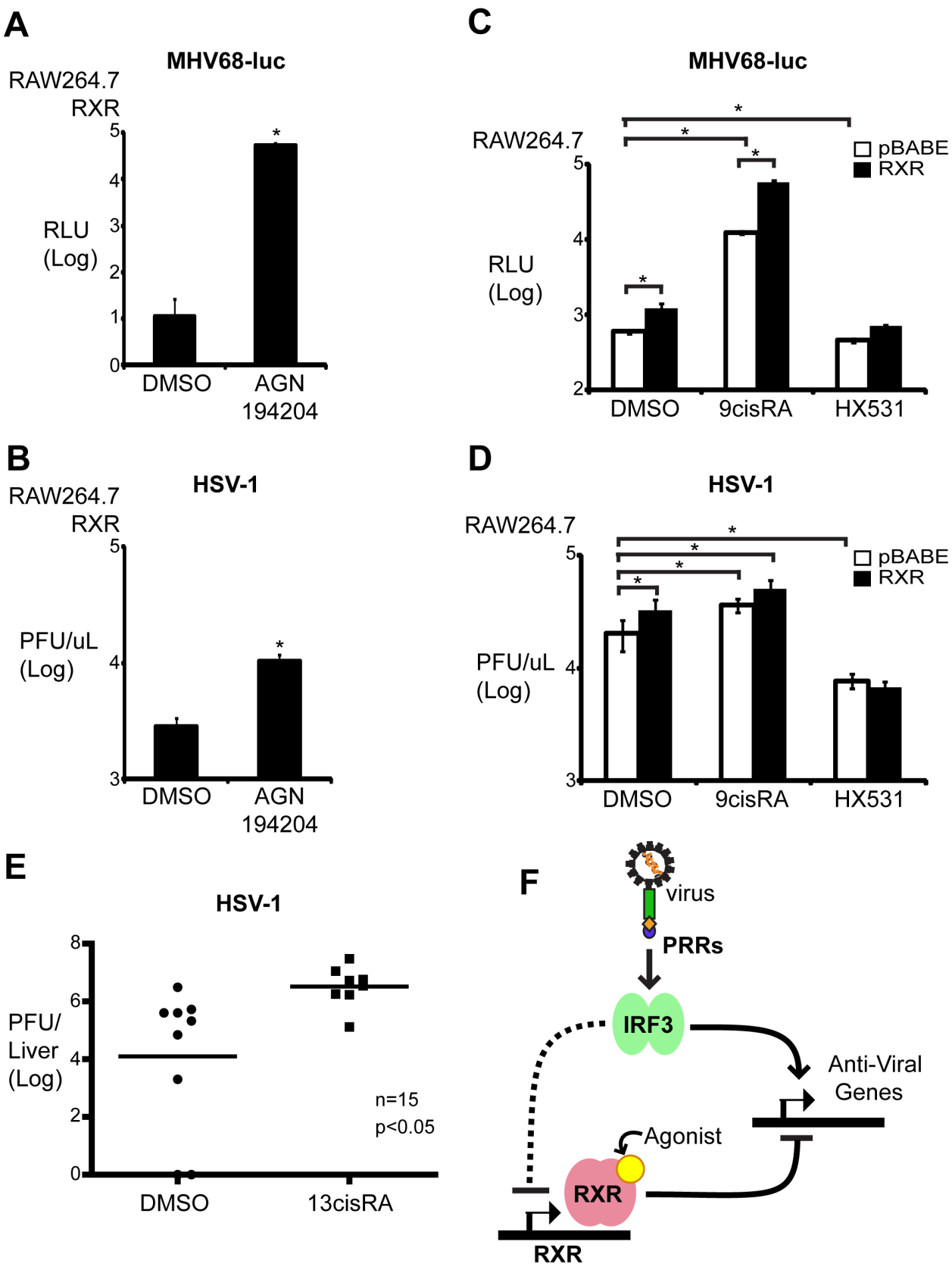
A
MHV68-luc
RAW264.7
RXR
RLU
(Log)
DMSO
AGN
194204
B
HSV-1
RAW264.7
RXR
PFU/uL
(Log)
DMSO
AGN
194204
C
MHV68-luc
RAW264.7
pBABE
RXR
RLU
(Log)
DMSO
9cisRA
HX531
D
HSV-1
RAW264.7
pBABE
RXR
PFU/uL
(Log)
DMSO
9cisRA
HX531
E
HSV-1
PFU/
Liver
(Log)
n=15
p<0.05
DMSO
13cisRA
F
virus
PRRs
IRF3
Anti-Viral
Genes
Agonist
RXR
RXR

Figure 4-7. RXR expression modulate host response against DNA viruses
A) RAW264.7 overexpressing RXRα were treated with DMSO, AGN19420 for 16 hours. The cells were then infected with MHV68 expressing luciferase (0.5MOI). Cells were lysed in passive lysis buffer at 24h.p.i and the luciferase activity was quantitated by luminescence assay. RLU is represented as mean ± SD and is representative of 2 experiements. *, significant ($p \leq 0.01$).

(B) RAW264.7 overexpressing RXRα pretreated with AGN19424 were infected with HSV-1 KOS strain (0.25MOI). Supernatants were collected at 24h.p.i and the viral titer was quantitated by standard plaque assay. Pfu/uL is represented as mean ± SD in biological triplicates. Data is representative of 2 experiments. *, significant ($p \leq 0.05$)

(C) RAW264.7 stably expressing pBABE vector or hRXRα were pretreated with 9*cis*RA and HX531 for 16 hours and infected with MHV68-luc (0.5MOI). Cells were lysed in passive lysis buffer at 24h.p.i and the luciferase activity was quantitated by luminescence assay. RLU is represented as mean ± SD and is representative of 3 experiements. *, significant ($p \leq 0.01$).

(D) RAW264.7 stably expressing pBABE vector or hRXRα were pretreated with 9*cis*RA and HX531 for 16 hours and infected with HSV-1 KOS Strain (0.25MOI). Supernatants were collected at 24h.p.i and the viral titer was quantitated by standard plaque assay. Pfu/uL is represented as mean ± SD in biological triplicates. Data is representative of 2 experiments. *, significant ($p \leq 0.05$)

(E) Mice were injected i.p. with DMSO (n=7) or 13*cis*RA (1mg/kg) (n=8) solubilized in corn oil every 24hours for 3 days and infected with 10^7 pfu of HSV-1(Strain 17) on day 4. Mice were sacrificed 5dpi and the livers were harvested, homogenized in media, and quantiated for viral titers by standard plaque assay. Data is representative of 2 experiments.

(F) Proposed model of how viral infection suppresses RXR and thereby release inhibition on anti-viral gene activation. RXR activation by endogenous agonists suppress unnecessary anti-viral gene expression. Viral infection trigger pattern recognition receptor and activates IRF3. IRF3 induces expression anti-viral genes but also indirectly inhibits RXR. Downregulation of RXR allows for optimal expression of anti-viral genes.

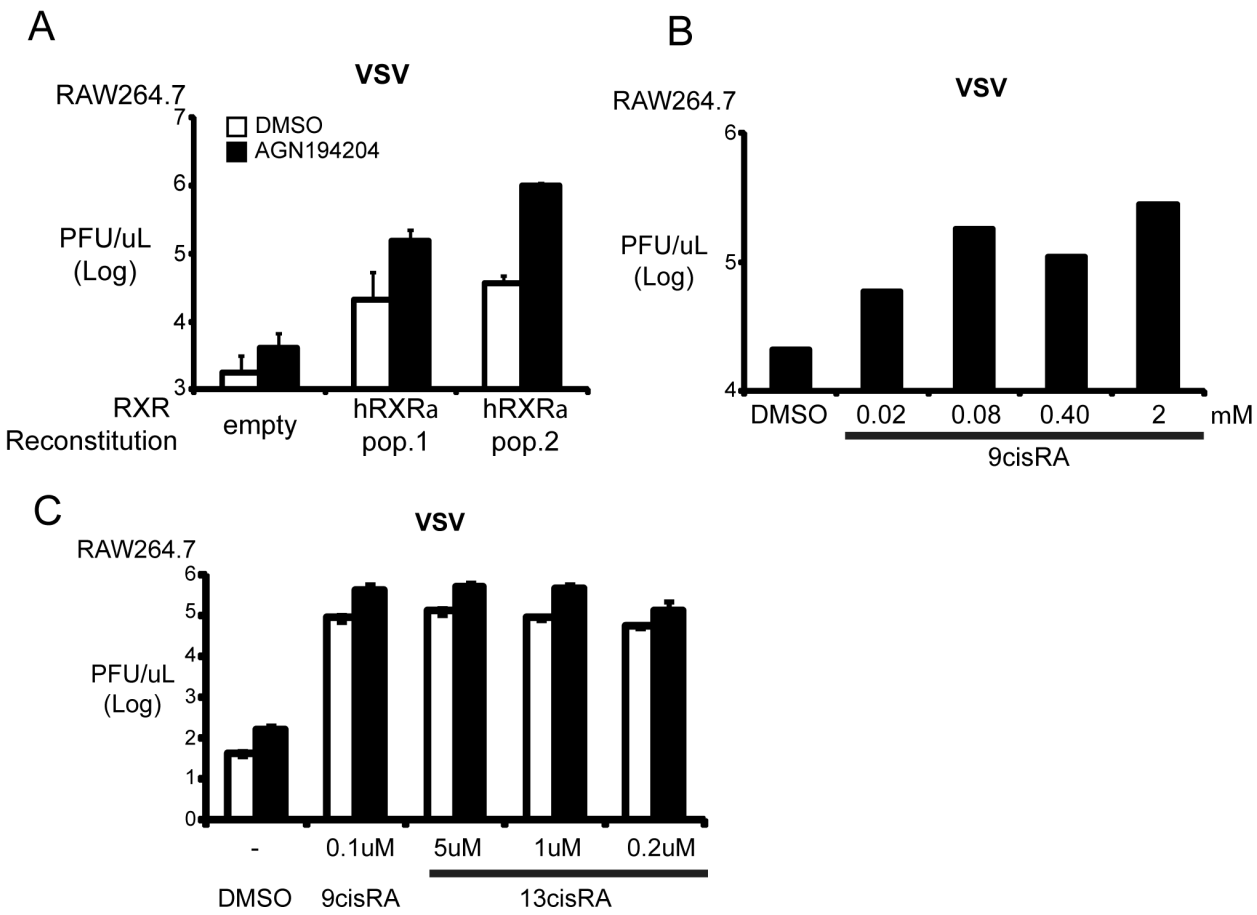

Supplementary Figure S4-1

A. RAW264.7 stably expressing hRXRα were treated with AGN194204(100nM) for 16h before infection with VSV(0.01MOI). Viral titer was collected at 14hpi and quantified by standard plaque assay.

B. RAW264.6 was treated with 9cisRA for 16h at indicated concentrations and infected with VSV (0.01MOI). Viral titer was collected at 14hpi and quantified by standard plaque assay.

C. RAW264.6 was treated with 9cisRA or 13cisRA for 16h at indicated concentrations and infected with VSV (0.01MOI). Viral titer was collected at 14hpi and quantified by standard plaque assay.

Supplementary Table T4-1
Lipid and poly(I:C) Induced by >2-fold and Suppressed by 9cisRA >2-fold (Normalized Log Values)

Gene Symbol	[DMSO]	[9cisRA]	[pIC]	[9cRA+pIC]	[LpA]	[9cRA+LpA]
Ifnb1	-2.95	-3.07	2.37	0.16	1.13	-0.16
Rgs16	-0.55	-3.24	2.06	-2.13	3.09	0.55
Myc	-0.47	-2.55	1.98	-1.90	2.31	0.47
Clec4n	0.83	-2.17	1.97	-0.83	2.55	-1.09
Dusp1	-0.60	-2.21	1.91	-1.02	2.96	0.60
Rgs16	-0.49	-2.52	1.91	-2.20	3.19	0.49
Plau	-0.81	-0.64	1.81	0.51	1.09	-0.51
Havcr2	0.76	-0.92	1.78	-0.76	1.79	-0.98
Rgs16	-0.47	-1.91	1.71	-1.65	2.89	0.47
4833422F24Rik	0.49	-0.49	1.58	-0.86	1.90	-0.77
Cav1	0.38	-0.54	1.57	-0.43	2.19	-0.38
Rcan1	-0.83	-2.70	1.54	0.07	1.26	-0.07
Lamc2	-0.17	-0.35	1.54	-0.38	2.11	0.17
Plau	-0.62	-0.62	1.51	0.38	0.84	-0.38
Rcan1	-0.96	-3.28	1.45	-0.18	1.74	0.18
2010002N04Rik	-0.54	-2.56	1.38	-0.54	1.93	0.54
Il7r	-0.49	-0.92	1.12	-1.08	2.94	0.49
Ifit3	-0.71	-1.00	1.02	-0.35	2.71	0.35
Ccl5	-1.85	-2.32	1.01	-1.01	4.91	3.17
Ifit1	-2.02	-3.02	0.94	-0.94	4.22	2.04
Gbp3	-0.53	-1.21	0.90	-0.27	1.84	0.27
Cxcl11	-0.88	-2.04	0.88	-0.92	3.32	1.79
Itga5	-0.59	-1.68	0.77	-0.88	1.60	0.59
Flrt3	-0.55	-0.68	0.75	-0.82	4.00	0.55
Src	-0.35	-1.27	0.75	-1.07	2.73	0.35
Itga5	-0.70	-1.99	0.70	-1.10	1.95	0.86
Lpar1	-0.39	-1.35	0.70	-0.84	2.01	0.39
Srxn1	-0.55	-1.34	0.64	-0.51	1.54	0.51
Lpar1	-0.43	-1.74	0.60	-1.29	1.49	0.43
Il10	-0.56	-0.61	0.56	-0.82	4.98	3.13
Gm9706 /// Isg15	-0.71	-1.11	0.52	-0.52	4.22	3.20
Stx11	-0.51	-0.85	0.51	-0.66	2.95	1.59
Jag1	-0.75	-1.28	0.50	-0.50	2.89	1.65

Supplementary Table T4-2
poly(I:C) Induced >2-fold and suppressed by 9cisRA by 2-fold (Normalized Log Values)

Gene Symbol	[DMSO]	[9cisRA]	[pIC]	[9cRA+pIC]
Ifna2	-0.06	0.01	3.63	0.29
Gadd45g	-0.11	-1.64	2.49	0.11
Ifnb1	-2.95	-3.07	2.37	0.16
Nr4a2	-0.24	-1.71	2.22	1.01
Rgs16	-0.55	-3.24	2.06	-2.13
Nr4a2	-0.33	-1.33	2.04	0.80
Ifna4	0.00	0.00	2.00	0.57
Myc	-0.47	-2.55	1.98	-1.90
Clec4n	0.83	-2.17	1.97	-0.83
Ppp1r15a	-1.67	-1.53	1.96	0.66
Angptl2	0.63	-1.22	1.94	-0.63
Nfatc1	0.82	-1.28	1.92	-1.29
Dusp1	-0.60	-2.21	1.91	-1.02
Rgs16	-0.49	-2.52	1.91	-2.20
Plau	-0.81	-0.64	1.81	0.51
Havcr2	0.76	-0.92	1.78	-0.76
Rgs2	0.76	-1.01	1.77	-0.01
Rgs16	-0.47	-1.91	1.71	-1.65
4833422F24Rik	0.49	-0.49	1.58	-0.86
Cav1	0.38	-0.54	1.57	-0.43
Hist1h1c	0.49	-1.79	1.56	-0.14
Rcan1	-0.83	-2.70	1.54	0.07
Lamc2	-0.17	-0.35	1.54	-0.38
Rgs1	-0.98	-2.39	1.53	0.31
Plau	-0.62	-0.62	1.51	0.38
Hist1h1c	0.41	-1.52	1.51	-0.25
Angptl2	0.19	-0.59	1.49	-0.60
Hist2h3c1	0.13	-0.37	1.47	0.07
Rcan1	-0.96	-3.28	1.45	-0.18
Nr4a2	-0.33	-0.54	1.41	0.20
Arl4c	-0.06	-0.06	1.41	0.16
2010002N04Rik	-0.54	-2.56	1.38	-0.54
D15Ertd30e	-0.28	0.05	1.38	-0.05
Arrdc3	0.26	0.55	1.36	-0.26
Ifna5	0.01	0.09	1.36	-0.01
Ankrd28	0.01	-0.68	1.14	-0.01
H2-Q5	-0.25	-0.61	1.12	-0.01
Il7r	-0.49	-0.92	1.12	-1.08
Klf6	0.06	-0.83	1.12	-0.15
Per2	-0.03	0.17	1.07	0.03
Bcar3	-0.51	-2.08	1.05	-0.82
Ifit3	-0.71	-1.00	1.02	-0.35
Ccl5	-1.85	-2.32	1.01	-1.01

Il6	-1.33	-1.14	1.00	-1.00
Ifit1	-2.02	-3.02	0.94	-0.94
Serpine1	-1.77	-1.75	0.91	-0.91
Gbp3	-0.53	-1.21	0.90	-0.27
Cxcl11	-0.88	-2.04	0.88	-0.92
Pdgfb	-1.20	-2.78	0.86	-0.86
Pdgfa	-0.26	-1.35	0.86	-0.52
Fosl2	-0.47	-2.42	0.85	-0.21
Rsad2	-3.51	-2.88	0.84	-0.84
Rsad2	-2.54	-1.82	0.82	-0.82
	-0.32	-0.46	0.81	-0.20
2210403K04Rik	-0.32	-2.46	0.80	-1.07
Plekhf1	-0.81	-1.28	0.78	-0.46
Itga5	-0.59	-1.68	0.77	-0.88
Pdgfb	-0.76	-2.02	0.76	-0.86
Pdgfa	-0.45	-1.29	0.76	-0.76
Flrt3	-0.55	-0.68	0.75	-0.82
Src	-0.35	-1.27	0.75	-1.07
Tnfaip3	-2.48	-2.06	0.72	-0.72
Traf1	-1.02	-1.22	0.71	-0.71
	-0.71	-0.57	0.71	-0.51
Itga5	-0.34	-0.69	0.71	-0.56
Itga5	-0.70	-1.99	0.70	-1.10
Lpar1	-0.39	-1.35	0.70	-0.84
Pmepa1	-1.78	-1.70	0.65	-0.65
Srxn1	-0.55	-1.34	0.64	-0.51
Pmepa1	-2.21	-1.89	0.63	-0.63
Flnb	-0.89	-1.21	0.62	-0.39
Rsad2	-1.79	-1.83	0.62	-0.62
Cxcl10	-2.34	-3.46	0.60	-0.60
Lpar1	-0.43	-1.74	0.60	-1.29
Adora2b	-1.42	-1.75	0.58	-0.58
Gadd45b	-0.65	-1.51	0.57	-0.57
Gadd45b	-0.57	-1.36	0.57	-0.57
Ptgs2	-3.11	-4.41	0.57	-0.57
Socs3	-1.20	-0.56	0.56	-1.45
Rnf19b	-0.51	-1.23	0.56	-0.44
Il10	-0.56	-0.61	0.56	-0.82
Dusp4	-1.02	-2.18	0.55	-0.55
Dusp5	-1.18	-1.56	0.54	-0.54
Traf1	-0.52	-2.08	0.52	-1.34
Adora2b	-1.17	-1.54	0.52	-0.52
Gm9706 /// Isg15	-0.71	-1.11	0.52	-0.52
Stx11	-0.51	-0.85	0.51	-0.66
Jag1	-0.75	-1.28	0.50	-0.50
Socs3	-1.21	-0.46	0.46	-1.49

Supplementary Table T4-3
poly(I:C) Induced genes greater than 2-fold AND less than 2-fold suppression by 9cisRA

Gene Symbol	[DMSO]	[9cisRA]	[pIC]	[9cRA+pIC]
Egr1	-1.8127813	-0.14469719	1.4774923	1.8717041
Smad6	-0.6662922	0.17661762	1.468442	1.3483353
Egr2	-1.8753452	-4.1085005	1.4341202	0.9591799
Jun	-0.28845215	0.001195908	1.3874931	1.2215214
Ptger4	-0.1531601	-0.33108902	1.3683023	1.1160507
Hist1h3d	-0.34356785	-0.16893578	1.3356915	0.98874474
Tgfbr1	-0.04660988	-0.21147346	1.318883	0.55684566
Ptger4	-0.31085396	-0.5035615	1.3039603	0.58136845
Slc30a1	-0.47568703	-0.6148968	1.2952709	0.62358475
Id2	-0.024709702	0.024709702	1.2724133	0.82199097
Id2	-0.13337994	0.13337994	1.2590647	0.8578453
Cxcr4	0.11232996	-0.11232996	1.2350144	0.8495898
Spry2	-0.037979603	-0.47756958	1.2198043	1.500639
	0.10245037	-0.8435588	1.2196198	0.2511015
Trib1	-0.17504835	-0.6793537	1.1346464	0.17504883
Etv1	-0.23415709	-0.75581264	1.1245217	0.5416479
Egr2	-1.9832678	-4.0331593	1.053832	0.78166294
Hist2h2bb	-0.02609253	-0.13144255	1.0215812	0.39590645
	-0.9932494	-1.1470942	1.0204353	0.050872803
Hist1h3f	-0.98308086	-0.24992609	0.9282398	0.9558754
Nr4a2	-0.11221504	0.101732254	0.89218235	0.46865177
Jun	-0.25189972	0.07191563	0.8882437	0.6977825
Nfe2l2	-0.2905116	-0.31796217	0.87754345	0.8618355
Etv1	-0.22475243	-0.9618273	0.8256998	0.29969025
BC049807	-0.23931932	-0.7878151	0.7775221	0.10115385
Smad7	-0.34918952	-0.51779747	0.7560847	0.021808386
Ifit2	-0.5355592	-0.79529333	0.74972296	-0.23303461
Malat1	-0.27000427	-0.84395695	0.74926853	-0.071930885
Nr4a1	-0.6233187	-0.5289674	0.7466774	0.929121
Slc30a1	-0.6110263	-0.7586622	0.7462883	0.4282627
Aff1	-0.407506	-0.8073664	0.7222185	-0.27602386
Atf3	-1.419198	-2.1735353	0.63565063	-0.35678768
Id3	-1.3141909	-0.9421358	0.61059475	-0.026169777
Prdm1	-0.40137506	-0.20451379	0.6043105	0.011841297
Filip1l	-0.6852493	-1.567625	0.57934284	0.07937145
Socs3	-0.92110825	-0.63805485	0.49849796	-0.49849796
Pdcd1	-0.7526927	-1.5160313	0.493649	-0.49364853
	-0.74513674	-0.9959178	0.4897728	-0.3421769
Ptgs2	-3.2237208	-3.1114616	0.4879117	-0.48791122
Zc3h12c	-1.1787872	-2.1613803	0.4877882	-0.4877882
Ccrn4l	-0.78907585	-1.0893793	0.47957897	-0.47957897
Cxcl2	-5.096919	-5.8662124	0.4458332	-0.44583416
Plaur	-0.9592085	-1.2856522	0.43384743	-0.43384743

Sqstm1	-0.59196854	-1.2734041	0.42711353	-0.42711353
Fosl1	-1.2853503	-2.2203918	0.42570114	-0.42570114
Adora2b	-1.108428	-1.975769	0.41120958	-0.4112091
Armc8	-0.68965673	-0.006660461	0.40534735	0.20105839
Jag1	-0.6171589	-1.0755339	0.39836073	-0.39836025
Tnfrsf12a	-1.4242086	-1.6889334	0.38375568	-0.38375568
Id1	-2.5806546	-0.9782448	0.3815279	0.45401
LOC100503807	-0.79146767	-0.7690501	0.3725276	-0.13777876
Trib3	-0.7182188	0.01936245	0.3663907	0.64252424
Tnfrsf12a	-1.4100838	-1.3578176	0.3512478	-0.3512478
Gna13	-0.7530966	-0.49594784	0.34497356	-0.2034502
Zc3h12c	-1.4850578	-1.9386759	0.3329239	-0.3329239
	-0.71714497	-0.93397284	0.32178402	-0.11341429
Fosl1	-0.8532791	-1.2920289	0.30848932	-0.30848885
Agpat9	-1.0020409	-1.5460377	0.30002737	-0.3000269
Klf9	-1.0085983	-0.42668724	0.29195976	0.8659477
Zc3h12c	-1.3785315	-1.4006348	0.2768569	-0.27685738
Plk3	-1.6857247	-0.82684374	0.27298355	1.3438807
Relb	-0.7781186	-1.1155334	0.2699337	-0.2699337
Ptgir	-0.81153107	-1.0238848	0.25684595	-0.25684595
Ier2	-1.0343189	-0.91924	0.25511932	0.55048084
Klf9	-0.85216284	-0.24065924	0.24065876	1.0209775
Klf9	-0.88866615	-0.22373295	0.22373295	0.847929
Bcor	-1.0871553	-1.1969948	0.21769524	-0.21769524
Klf9	-0.9192362	-0.2769041	0.21539974	0.87304115
C78513	-1.1675372	-1.204503	0.21150446	-0.21150494
Map3k8	-0.8872585	-0.9915371	0.21037531	-0.21037579
Junb	-1.3074179	-1.9967928	0.20840168	-0.20840168
Phlda1	-1.8182144	-1.9410577	0.19710541	-0.19710541
Bcl3	-0.8153496	-0.2976184	0.19561958	-0.1956191
Prkab2	-0.8654008	-0.853395	0.18961048	0.22276592
Tlr2	-1.1319885	-1.4611063	0.17900372	-0.15359497
Irg1	-2.7365675	-2.0316563	0.17647266	-0.17647266
Sertad1	-1.4600992	-1.7561884	0.17029953	-0.028589249
Nfkbia	-0.98803616	-0.4733219	0.1695919	-0.16959286
Abtb2	-0.9694309	-0.6362395	0.15066624	-0.15066624
Gadd45a	-1.1981125	-1.3277464	0.14592743	-0.14592695
1200016E24Rik	-1.0373912	-0.72849846	0.14406872	-0.14406872
Zfp36	-1.7851229	-1.8534431	0.14390755	-0.067349434
Saa3	-0.99758387	-0.31257153	0.1394062	-0.1394062
Tnfrsf1b	-1.1635818	-0.804934	0.13273048	-0.13273048
Olr1	-2.383833	-1.2039995	0.09959173	-0.09959173
5033430I15Rik	-1.1739945	-0.80647373	0.08689594	-0.06426954
Gpbp1	-0.97706795	-0.07754612	0.07754612	-0.32486248
Tnf	-2.427473	-1.9901457	0.059308052	-0.0593071
Arc	-0.95406437	-0.95729494	0.05578804	1.0620465
Bhlhe40	-2.0032206	-1.3824997	0.049526215	-0.049526215

Lif	-1.4367228	-1.02456	0.04526615	-0.04526615
Ccl7	-1.812182	-1.6310701	0.035818577	0.20356989
Cd83	-2.8836842	-1.4407177	0.031514168	-0.031514168
Hmox1	-0.9739628	-0.77713966	0.031066895	-0.031066895
Nfkbiz	-2.915906	-2.214079	0.024181366	-0.024181366
Rasgef1b	-1.8289123	-0.8928499	0.01985073	0.6016102
Cflar	-1.1095982	-0.96916485	0.018942833	-0.018942833
Ccl4	-2.7957516	-1.9051266	0.014246941	-0.014247894
Nfkbiz	-1.8854399	-1.6251631	0.013878346	-0.013878822
Skil	-1.77458	-1.1975794	0.006307602	0.0951004
Cldn12	-1.0245085	-0.34492493	-0.019414425	1.2442055
Maff	-1.7124109	-1.9685874	-0.020110607	0.020110607
Nfkbiz	-1.0470428	-0.9177375	-0.02917099	0.02917099
Ccrl2	-2.3346767	-1.5085168	-0.07650185	0.07650185
Ccl2	-4.6286683	-2.3698645	-0.09770393	0.6533165
Kdm6b	-1.446001	-1.3144178	-0.10076237	0.10076237
C3ar1	-1.2340703	-0.37316608	-0.10128832	0.10128832
Pdlim7	-1.3370109	-0.5570011	-0.11379337	0.11379337
Kdm6b	-1.4960876	-1.1711326	-0.13017464	0.13017464
Niacr1	-1.6440558	-2.212141	-0.15962982	0.15962982
Dusp2	-1.6973858	-1.6540537	-0.16347408	0.16347408
Tcf7l2	-1.1822948	0.17221689	-0.17221642	0.87712145
Kdm6b	-2.0376544	-1.6442623	-0.17662334	0.17662334
C3ar1	-1.5949712	-0.38973045	-0.18148947	0.18148947
Ptger2	-1.2905335	-0.93182325	-0.20931864	0.20931864
Ier3	-1.5579796	-0.22029877	-0.2782135	0.22029781
Dusp16	-1.6702805	-1.3629241	-0.28219318	0.28219318
Skil	-1.4122319	-0.83447313	-0.2878623	0.2878623
Egr3	-3.7702556	-2.4073772	-0.29693508	0.6525049
C3ar1	-1.5358524	-0.6658225	-0.30266476	0.30266476
Ccl3	-1.6883793	-0.60601234	-0.3099079	0.3099079
Gm6377	-3.2131512	-2.5459738	-0.34552097	1.3123102
Sgk1	-2.108673	2.2829084	-0.4028349	2.0346537
	-1.477911	0.042441368	-0.42476463	-0.042441368
Hivep3	-1.5593433	-0.1895256	-0.43034554	0.1895256
Zswim6	-1.6827908	0.37673092	-0.61186314	0.61506367
Plk2	-1.8409	0.57961845	-0.6375866	0.6763487
Fam20c	-1.8884068	1.4718819	-0.7736912	1.5909739
Abca1	-2.7256804	1.278408	-1.4378166	0.9524307
Tgm2	-3.198288	1.3112841	-2.0158682	1.5733185
Tgm2	-3.1936798	1.3334246	-2.1012163	1.6293621
Tgm2	-3.3607836	1.4147263	-2.1767483	1.5420246

Supplementary Table T4-4
LipidA induced genes greater than 2-fold and suppressed by 9cisRA greater than 2-fold (Normalized Log Values)

Gene Symbol	[DMSO]	[9cisRA]	[LpA]	[9cRA+LpA]
Il10	-0.56	-0.61	4.98	3.13
Ccl5	-1.85	-2.32	4.91	3.17
Ifit1	-2.02	-3.02	4.22	2.04
Gm9706 /// Isg15	-0.71	-1.11	4.22	3.20
Flrt3	-0.55	-0.68	4.00	0.55
Areg	-0.50	-2.49	3.87	1.08
Cmpk2	-0.09	-0.25	3.81	2.70
Ccl22	0.10	-0.10	3.72	1.80
Rnd1	-0.31	-0.09	3.40	1.24
Cxcl11	-0.88	-2.04	3.32	1.79
Rgs16	-0.49	-2.52	3.19	0.49
Rgs16	-0.55	-3.24	3.09	0.55
Il13ra2	-0.09	-0.50	3.00	0.09
Dusp1	-0.60	-2.21	2.96	0.60
Stx11	-0.51	-0.85	2.95	1.59
Il7r	-0.49	-0.92	2.94	0.49
Rgs16	-0.47	-1.91	2.89	0.47
Jag1	-0.75	-1.28	2.89	1.65
Serpinb6b	-0.16	-0.45	2.85	1.16
Marcks	-0.07	-0.14	2.77	1.23
Jag1	-0.62	-1.08	2.73	1.33
Src	-0.35	-1.27	2.73	0.35
Ifit3	-0.71	-1.00	2.71	0.35
Prkg2	0.03	-0.04	2.67	0.75
Tnfaip2	-0.35	-1.36	2.65	1.63
Procr	-0.17	-1.57	2.62	1.26
Ifi204	-0.03	-0.79	2.60	1.15
Irgm2	0.04	-0.04	2.57	1.26
Cd69	-0.01	-0.11	2.55	1.39
Clec4n	0.83	-2.17	2.55	-1.09
Gbp2	0.00	-0.42	2.53	0.00
Tnc	0.02	-0.15	2.47	0.85
Mx2	-0.21	-0.26	2.47	1.37
Tnfrsf1b	-1.16	-0.80	2.43	1.26
Flrt3	-0.22	-0.61	2.41	0.53
Gm9706	-0.29	-0.44	2.39	1.33
Il7r	-0.17	-0.42	2.37	0.17
Vegfc	0.92	-2.29	2.32	-0.88
Myc	-0.47	-2.55	2.31	0.47
Vegfc	1.13	-3.42	2.31	-0.91
Usp18	0.25	-0.85	2.31	1.19

AI504432	-0.33	-0.52	2.23	0.39
Clec4n	0.70	-2.04	2.23	-1.41
Cav1	0.38	-0.54	2.19	-0.38
Jdp2	-0.46	-0.66	2.14	0.19
Xirp1	-0.14	-0.23	2.13	0.18
Lamc2	-0.17	-0.35	2.11	0.17
Irgm1	0.14	-0.14	2.10	1.04
Serpinb9b	0.01	-0.01	2.10	0.68
Gbp1	-0.11	-0.43	2.09	0.14
Vegfc	0.45	-2.63	2.07	-0.43
Ifit2	-0.54	-0.80	2.06	0.23
Irf1	-0.39	0.29	2.03	0.79
Lpar1	-0.39	-1.35	2.01	0.39
Igsf3	0.12	-1.19	2.00	-0.12
Ifi202b	-0.28	-1.73	1.99	0.78
Fbxo15	-0.35	-2.63	1.99	0.86
Tnc	0.27	-1.06	1.97	-0.20
Itga5	-0.70	-1.99	1.95	0.86
Zc3h12c	-1.38	-1.40	1.94	0.92
Eif4e	-0.72	-0.78	1.94	0.91
Slfn5	-0.01	-1.15	1.94	0.66
Nfkbie	-0.31	-2.26	1.94	0.31
Opn3	0.00	-0.08	1.93	0.00
2010002N04Rik	-0.54	-2.56	1.93	0.54
4833422F24Rik	0.49	-0.49	1.90	-0.77
Ifi202b	-0.31	-1.78	1.89	0.56
Nfkbie	-0.26	-1.82	1.88	0.26
Igsf3	-0.04	-0.95	1.88	0.04
Gbp3	-0.53	-1.21	1.84	0.27
Gbp2	-0.24	-0.32	1.84	0.24
AI504432	-0.29	-0.50	1.83	0.46
Tmem2	-0.35	-0.40	1.80	0.19
Havcr2	0.76	-0.92	1.79	-0.98
Gbp6	-0.25	-0.21	1.79	0.10
Il15	0.36	-0.36	1.78	-0.70
Cd274	-0.47	-0.42	1.78	0.43
Ahnak2	0.56	-0.70	1.78	-0.56
Rcan1	-0.96	-3.28	1.74	0.18
Ripk2	-0.03	-0.31	1.69	0.62
2500002B13Rik	0.13	-1.87	1.69	-0.13
Flrt2	-0.08	-2.19	1.68	0.08
Gbp6	-0.35	-0.48	1.67	0.35
Lpar1	-0.17	-0.13	1.65	0.13
Gm11545	0.35	-1.97	1.65	-0.35
Pyhin1	-0.11	-0.44	1.64	0.25
Ptpre	0.06	-1.22	1.63	0.10
Srxn1	-0.29	-1.03	1.61	0.58

Plat	-0.22	0.07	1.60	0.20
Itga5	-0.59	-1.68	1.60	0.59
Trps1	-0.27	-0.24	1.60	0.23
Srxn1	-0.42	-1.04	1.59	0.56
	0.05	-0.49	1.58	-0.05
Rnf19b	-0.49	-1.12	1.58	0.54
Fam171b	-0.33	0.08	1.57	0.24
Itgav	-0.33	-0.63	1.56	0.50
Tm7sf4	0.33	-3.16	1.56	-0.33
Sgms2	-0.04	-0.36	1.55	0.52
Serpinb9	-0.12	-0.85	1.55	0.53
Tmem2	-0.58	-0.49	1.55	0.37
Srxn1	-0.55	-1.34	1.54	0.51
Nqo1	-0.02	-1.92	1.52	0.12
Sdc1	0.17	-0.83	1.51	-0.17
Shisa3	-0.14	0.14	1.51	0.31
Ptpre	0.14	-0.78	1.49	0.04
Lpar1	-0.43	-1.74	1.49	0.43
Oasl2	-0.16	-0.48	1.47	0.29
Src	-0.09	-0.27	1.46	0.09
Flrt2	0.17	-1.67	1.46	-0.17
	-0.15	-0.44	1.46	0.43
Dnajb4	0.01	-0.76	1.43	-0.01
Tcfec	-0.01	-0.49	1.43	0.40
Myo10	0.03	-1.41	1.42	-0.03
Trps1	-0.14	-0.49	1.40	0.14
Hmga2	-0.16	-1.48	1.39	0.16
Akap13	0.17	-1.16	1.38	-0.17
Cd44	-0.03	-1.30	1.38	0.03
Sdc1	0.13	-0.78	1.35	-0.13
Lamc1	0.29	-0.61	1.33	-0.29
Ifi205 /// Mnda	-0.06	-0.46	1.31	0.06
LOC634012	0.08	-1.19	1.31	-0.08
Isg20	-0.14	-0.60	1.30	0.14
Ifi204 /// Ifi205 /// Mnda /// Mndal	-0.01	-0.49	1.28	0.01
Atp2b1	0.11	-0.55	1.28	-0.11
Sdc1	0.16	-0.61	1.28	-0.16
Flrt2	0.13	-3.16	1.27	-0.13
Rcan1	-0.83	-2.70	1.26	-0.07
Mndal	0.11	-0.56	1.25	-0.11
Ifi203 /// LOC100044071	0.20	-0.34	1.24	-0.08
Dnajb4	-0.12	-0.66	1.24	0.12
Cd207	0.06	-0.67	1.24	-0.06
Lims2	-0.36	-0.27	1.24	0.16
Arhgap23	0.10	-0.58	1.23	-0.10
Myo10	-0.01	-1.27	1.21	0.01
Gm7609	0.04	-0.08	1.21	-0.04

Sdc1	0.03	-0.35	1.17	-0.03
Hmga2-ps1	0.15	-1.02	1.17	-0.15
Klra2	0.07	-1.04	1.16	-0.07
Akap13	-0.02	-0.52	1.16	0.02
Cd44	0.04	-1.33	1.15	-0.04
Nrp2	0.11	-0.43	1.15	-0.11
Myo10	-0.02	-1.38	1.14	0.02
Slc22a4	-0.07	-0.65	1.14	0.07
Mndal	0.05	-0.42	1.13	-0.05
Hmga2	-0.12	-1.26	1.13	0.12
Ifnb1	-2.95	-3.07	1.13	-0.16
Trps1	-0.05	-0.55	1.10	0.05
Plau	-0.81	-0.64	1.09	-0.51
Zfp36	-1.79	-1.85	1.08	0.07
Plau	-0.62	-0.62	0.84	-0.38

Supplementary Table T4-5
LipidA Induced >2-fold and suppressed by 9cisRA by less than 2-fold(Normalized Log Values)

Gene Symbol	[DMSO]	[9cisRA]	[LpA]	[9cRA+LpA]
Il1b	-0.46	-0.49	6.54	5.67
Csf3	-0.41	-0.33	5.58	6.07
Lif	-1.44	-1.02	5.11	6.25
Serpinb2	-0.07	0.07	5.02	4.02
Socs3	-1.21	-0.46	4.59	4.40
Socs3	-0.92	-0.64	4.58	4.20
Socs3	-1.20	-0.56	4.39	4.31
Il1a	-0.23	-0.69	4.21	4.71
Oasl1	-0.50	-0.67	4.12	3.72
Ptger2	-1.29	-0.93	3.95	4.68
1200016E24Rik	-1.04	-0.73	3.87	3.95
C78513	-1.17	-1.20	3.73	3.25
Ifih1	-0.14	-0.36	3.72	3.53
Ptgs2	-3.22	-3.11	3.70	3.20
Zc3h12a	-0.55	-0.58	3.64	3.50
Pim1	-0.50	-0.89	3.62	3.18
Pim1	-0.37	-0.75	3.55	2.95
Rsad2	-3.51	-2.88	3.53	2.54
Rsad2	-1.79	-1.83	3.51	2.52
Gadd45b	-0.65	-1.51	3.45	3.47
Il6	-1.33	-1.14	3.44	2.59
Lif	-0.64	-0.14	3.38	5.02
Gadd45b	-0.57	-1.36	3.22	3.04
Serpine1	-1.77	-1.75	3.20	3.00
Tpbg	-0.07	-0.10	3.15	3.04
Cxcl10	-2.34	-3.46	3.07	2.69
Ptgs2	-3.11	-4.41	3.06	2.64
Traf1	-0.52	-2.08	3.06	2.53
Rsad2	-2.54	-1.82	3.06	2.14
Abtb2	-0.97	-0.64	3.06	2.39
Phlda1	-1.82	-1.94	3.04	3.16
Csrnp1	-0.65	-0.83	3.02	2.33
Malt1	-0.05	-0.55	3.00	2.78
Bcl2l11	-0.25	-0.43	2.92	1.97
Mtmr7	-0.21	-0.53	2.92	2.03
Dusp5	-1.18	-1.56	2.92	2.32
Nfkbiz	-1.89	-1.63	2.86	3.42
Pde4b	-0.33	-0.36	2.85	2.90
Irg1	-2.74	-2.03	2.85	2.81
Saa3	-1.00	-0.31	2.85	2.76
Fabp4	0.00	-0.17	2.82	2.04
Il1rn	-0.17	-1.13	2.79	2.17

Olr1	-2.38	-1.20	2.75	3.34
Fabp4	0.05	-0.23	2.75	1.92
	-0.39	-0.99	2.74	2.53
Peli1	-0.63	-0.51	2.73	2.61
Sdc4	-0.27	-0.83	2.71	1.89
Pde4b	-0.75	-0.12	2.71	2.81
Peli1	-0.43	-0.26	2.69	2.63
Malt1	-0.42	-0.19	2.67	2.25
Il1rn	-0.26	-1.91	2.64	2.07
Gadd45a	-1.20	-1.33	2.63	3.64
Slc7a11	-0.65	-0.24	2.62	2.11
Pde4b	-0.38	-0.22	2.61	2.79
Ccl4	-2.80	-1.91	2.60	2.50
Traf1	-1.02	-1.22	2.59	2.32
Slc7a11	-0.19	-0.77	2.56	1.88
Malt1	-0.14	-0.56	2.55	2.22
9530028C05	0.10	-1.44	2.52	1.61
Peli1	-0.52	-0.34	2.51	2.57
Cd40	-0.63	-0.20	2.47	1.53
Arl5b	-0.51	-0.30	2.47	2.97
Rsbn1	-0.21	-0.50	2.45	1.60
Clec2d	0.22	-0.22	2.44	1.52
Cd40	-0.38	-0.01	2.40	1.53
Stat1	-0.19	-0.26	2.39	1.79
Tsc22d1	-0.19	-2.39	2.38	2.15
Cflar	-0.36	-0.45	2.38	1.97
Nlrp3	-0.66	-0.76	2.36	1.86
Tsc22d1	-0.17	-2.46	2.34	2.18
Nfkbiz	-2.92	-2.21	2.33	2.71
Tpbg	0.00	-0.34	2.33	2.26
Pdgfb	-1.20	-2.78	2.30	2.19
Fas	-0.15	-0.70	2.29	1.34
Atrip /// Trex1	0.23	-0.73	2.28	1.44
Arg2	-0.27	-0.37	2.24	1.90
Dusp2	-1.70	-1.65	2.23	2.27
Cdc42ep2	-0.57	-0.23	2.22	1.94
Cflar	-0.29	-0.36	2.22	1.68
Rel	-0.80	-0.89	2.22	2.37
Cdk5r1	-0.31	-0.25	2.20	2.27
9530028C05	-0.07	-1.25	2.18	1.25
Pdgfb	-0.76	-2.02	2.18	2.25
Il1rn	-0.36	-1.75	2.17	1.67
Il33	-0.02	-0.12	2.17	1.37
Marcksl1	-0.93	-0.48	2.17	2.10
Odc1	-0.22	-0.28	2.15	1.50
Il4i1 /// Nup62-il4i1	0.04	-0.64	2.15	1.31
Stx11	-0.22	-0.67	2.13	1.22

Tsc22d1	-0.15	-2.35	2.13	1.93
Cdk5r1	-0.14	-0.11	2.11	2.06
Cd40	-0.32	-0.14	2.11	1.13
Rsbn1	-0.44	-0.09	2.11	1.61
Arhgef3	-0.80	-0.36	2.10	2.17
Plaur	-0.96	-1.29	2.10	1.63
Tnf	-2.43	-1.99	2.09	2.08
Irf7	0.08	-0.64	2.06	1.60
Gpr84	-1.22	-0.13	2.05	1.97
Marcksl1	-0.82	-0.44	2.05	1.94
Jak2	-0.15	-0.59	2.05	1.61
Arg2	-0.38	-0.06	2.03	1.32
Slfn2	-0.47	-1.43	2.01	2.00
Cflar	-1.11	-0.97	2.00	1.76
Ier3	-1.56	-0.22	2.00	2.51
Parp14	0.17	-0.17	2.00	1.58
Kdm6b	-2.04	-1.64	1.98	2.07
Cmpk2	-0.03	-0.03	1.98	1.15
Slfn8	0.00	-0.40	1.98	1.16
Marcksl1	-0.97	-0.60	1.97	1.93
	-0.05	0.00	1.96	1.74
Hdc	-0.17	-0.25	1.96	1.76
Zbp1	-0.07	-0.51	1.95	0.95
Rsbn1	-0.48	-0.34	1.94	1.31
Tnfaip2	-0.27	-1.26	1.93	1.41
Bcl2l11	-0.34	-1.42	1.93	1.10
Niacr1	-1.64	-2.21	1.92	1.88
Bcl2l11	-0.42	-0.47	1.92	0.96
Tnfaip3	-2.48	-2.06	1.91	1.62
Marcksl1	-0.96	-0.19	1.90	1.74
4933432I03Rik	-0.34	-0.07	1.90	1.30
Clec4e	-0.49	-1.41	1.88	1.57
Rtp4	0.09	-0.92	1.88	1.32
H28	0.15	-0.42	1.86	1.70
Cxcl3	-0.25	-0.20	1.84	3.30
Cflar	-0.52	-0.77	1.84	1.74
Kdm6b	-1.45	-1.31	1.84	1.77
Cebpd	-0.04	-0.52	1.83	1.00
BC006779	-0.03	-0.10	1.83	1.73
Ddx60	0.04	-0.41	1.83	1.05
H28	0.11	-0.53	1.81	1.71
Calcrl	0.06	-0.06	1.81	1.65
Serpinb1b	-0.02	-1.37	1.80	0.99
Zc3h12c	-1.18	-2.16	1.80	0.91
Slc7a2	-0.16	-0.05	1.80	0.87
Bcl2l11	-0.44	-1.17	1.79	0.86
Cxcl2	-5.10	-5.87	1.78	1.78

Xaf1	0.04	-0.58	1.78	0.94
Tnip1	-0.16	-0.80	1.77	1.31
Samd9l	-0.04	-1.69	1.77	0.81
Slc31a2	-0.26	-0.51	1.77	1.64
Ccrl2	-2.33	-1.51	1.76	3.15
Mtmr7	0.03	-0.37	1.75	1.29
Zc3h12c	-1.49	-1.94	1.75	1.15
Cd83	-2.88	-1.44	1.74	1.74
Edn1	-0.24	-0.07	1.74	0.88
Tmem171	-0.18	-0.21	1.73	1.18
Igtp	0.12	-0.22	1.72	0.74
Plagl2	-0.31	-0.24	1.72	1.63
	-0.01	-0.51	1.71	0.89
Gadd45b	-0.51	-0.71	1.71	1.51
C030046G05	-0.85	-0.85	1.71	1.80
Errfi1	-0.48	-0.78	1.71	1.79
	-0.19	0.16	1.69	1.59
Adora2b	-1.42	-1.75	1.67	1.14
Rab11fip1	-0.39	-0.51	1.67	1.47
Ccl3	-1.69	-0.61	1.66	1.78
Kdm6b	-1.50	-1.17	1.64	1.87
Tslp	-0.03	-0.33	1.64	1.54
Sdc4	-0.12	-0.81	1.63	1.27
Timp1	-0.36	-0.44	1.63	1.49
Arl5b	-0.60	-0.66	1.63	1.94
Il10ra	-0.05	0.05	1.62	1.24
Icam1	-0.25	-0.90	1.62	1.02
3930401B19Rik /// A130040M12Rik /// E430024C06Rik	0.02	-0.15	1.61	1.51
Cpd	0.01	-0.35	1.60	1.61
Ptprj	-0.53	0.02	1.60	0.92
Jak2	-0.20	-0.59	1.60	1.36
Nfkbia	-0.99	-0.47	1.57	1.41
Bcl2l11	-0.39	-1.28	1.56	0.62
	-0.17	-0.26	1.55	0.86
Ddx58	0.14	-0.14	1.55	0.88
Peli1	-0.03	-0.38	1.55	0.70
Cpd	0.06	-0.92	1.54	0.91
Plek	-0.59	-0.79	1.53	0.74
Ifi44	0.09	-0.61	1.53	0.91
Fam82a1	0.13	-0.27	1.53	0.99
Pion	-0.41	-0.96	1.52	0.70
Frmd6	-0.49	-0.75	1.51	0.97
Metrnl	-0.29	-0.43	1.50	1.72
1200003I10Rik	-0.03	-0.07	1.49	1.25

/// 1200015M12Rik /// A130040M12Rik /// E430024C06Rik				
Abtb2	-0.59	-0.61	1.49	0.76
Slc31a2	0.01	-0.23	1.49	1.24
Plagl2	-0.35	-0.25	1.48	1.27
Pdcd1	-0.75	-1.52	1.48	1.23
Ereg	-0.10	-0.10	1.48	2.14
Bcl3	-0.82	-0.30	1.46	1.07
H2-T24	0.28	-0.50	1.45	1.09
Klf7	-0.30	-0.38	1.45	0.84
A630072M18Rik	-0.83	-0.06	1.45	2.64
Gch1	-0.29	-0.60	1.44	1.19
Tnfaip3	-0.54	-0.45	1.44	1.10
Dusp4	-1.02	-2.18	1.44	1.62
	-0.15	-0.40	1.43	0.64
Adora2b	-1.11	-1.98	1.42	1.10
Itga5	-0.14	-0.14	1.42	0.57
Hivep3	-1.56	-0.19	1.42	2.01
Fam82a1	-0.13	-0.17	1.41	1.13
Rab11fip1	-0.25	-0.15	1.41	1.18
Adora2b	-1.17	-1.54	1.41	0.87
Map3k8	-0.89	-0.99	1.41	0.90
	-0.06	-0.05	1.40	1.00
1200009I06Rik	-0.16	-0.83	1.40	0.86
Gp49a /// Lilrb4	-0.21	-1.31	1.40	0.89
Dcbld2	0.01	-0.03	1.39	1.79
Ccrn4l	-0.79	-1.09	1.39	1.02
Rnf19b	-0.51	-1.23	1.38	0.44
Tiparp	-0.70	-0.25	1.37	0.87
Phldb1	-0.32	-1.06	1.37	1.13
	-0.17	-0.30	1.36	0.86
Mir155	-0.21	-0.46	1.36	1.48
Lgals9	-0.09	0.09	1.36	1.03
Csf2	-0.09	-0.22	1.36	4.26
Rhbdf2	-0.46	-0.16	1.36	1.25
Trim30a	-0.22	-0.03	1.35	0.77
Maff	-1.71	-1.97	1.35	1.74
Klf7	-0.18	-0.44	1.35	1.00
Micall2	-0.05	0.05	1.35	1.05
1200015M12Rik /// A130040M12Rik /// E430024C06Rik	-0.05	0.05	1.35	1.35

Klf7	-0.36	-0.58	1.35	0.73
Ddx6	-0.25	0.25	1.34	1.49
Gfod1	0.12	-0.20	1.34	1.45
Pdlim5	-0.32	-0.22	1.32	1.37
Cpd	0.06	-0.64	1.32	1.09
Rap2b	-0.28	-1.09	1.31	0.74
Trim21	0.07	-0.09	1.31	0.44
Zbtb7a	-0.08	-0.26	1.31	0.98
Tgtp1 /// Tgtp2	-0.10	0.10	1.31	0.68
Trim30a /// Trim30d	-0.40	-0.17	1.31	0.51
Vps37a	-0.10	-0.38	1.31	0.77
Stk40	-0.34	-0.58	1.31	0.65
Cpd	-0.05	-0.73	1.30	1.17
C130026I21Rik /// LOC100041885	-0.07	0.05	1.30	1.24
2210403K04Rik	-0.32	-2.46	1.30	0.32
Sp110	0.08	-0.08	1.29	0.72
Dhx58	0.11	-0.89	1.29	0.60
Pmepa1	-2.21	-1.89	1.29	1.27
D530037H12Rik	-0.26	0.01	1.29	0.52
Nupr1	-0.92	-0.23	1.28	0.67
Plagl2	-0.05	-0.05	1.28	1.11
Lrrc16a	-0.09	-0.98	1.28	0.64
Tiparp	-1.00	-0.36	1.28	0.91
Slc11a2	-0.32	-0.07	1.28	0.76
Fosl1	-0.85	-1.29	1.28	1.35
Slc4a7	-0.14	-0.35	1.27	0.39
Pdpn	-0.02	0.02	1.27	0.87
Sqstm1	-0.59	-1.27	1.27	0.80
AW555355	-0.18	-0.50	1.27	1.14
Itga5	-0.34	-0.69	1.26	0.34
Tor3a	0.05	-0.34	1.25	0.65
LOC100505088	0.03	-0.15	1.24	0.64
	-1.48	0.04	1.23	0.98
Odc1	-0.13	-0.12	1.23	0.99
Cpd	0.01	-0.48	1.23	0.91
Fgr	-0.05	-1.15	1.23	0.29
Rap2b	-0.20	-0.72	1.23	0.99
	-0.71	-0.57	1.22	0.51
Nfkb2	-0.21	-0.62	1.22	0.76
Txnrd1	-0.06	-0.33	1.21	0.56
Bbc3	-0.33	-0.16	1.21	0.85
Zfand5	-0.68	-0.77	1.20	0.81
Adar	0.02	-0.04	1.20	0.95
Sod2	-0.06	0.06	1.20	1.22
Parp14	-0.20	0.02	1.20	0.71

Nupr1	-0.92	-0.16	1.19	0.54
Ets2	-0.60	-0.12	1.18	1.43
Trim13	-0.37	-0.21	1.18	1.01
Eid3	-0.23	-0.22	1.18	0.56
Slc2a1	-0.20	-0.58	1.18	0.98
Peli1	-0.36	-0.04	1.17	0.94
	-0.36	-1.33	1.17	0.58
Npnt	-0.05	-0.37	1.16	0.26
6330409N04Rik	-0.08	-0.25	1.16	0.40
Nfkb1	-0.24	-0.35	1.16	1.15
Slc20a1	-1.09	-0.42	1.16	1.59
Ifrd1	-0.75	-0.07	1.16	1.01
Pik3r5	-0.06	-0.59	1.16	0.46
Trim25	0.02	-0.02	1.15	0.57
	-0.14	-0.05	1.15	0.45
Nfkbiz	-1.05	-0.92	1.15	1.87
Micall2	-0.12	-0.09	1.15	1.29
Ell2	-0.33	-1.27	1.15	1.09
Mmp14	-0.21	-0.01	1.14	0.67
Calcrl	-0.03	0.03	1.14	0.92
Slc4a7	-0.09	-0.47	1.14	0.30
Stim2	-0.03	-0.11	1.14	0.96
Cdkn1a	-0.47	-0.69	1.14	1.02
	-0.19	-0.35	1.13	0.42
Fosl1	-1.29	-2.22	1.13	1.30
Prkg2	-0.16	-0.03	1.13	0.77
Blcap	-0.30	-0.45	1.13	0.58
Slc11a2	-0.64	-0.04	1.13	0.72
	-0.05	0.04	1.12	0.88
Socs1	-0.09	0.01	1.12	0.71
Ptprj	0.06	-0.06	1.12	0.67
Mdm2	-0.67	-0.57	1.11	0.80
2310079F09Rik	0.01	-0.01	1.11	1.02
Fbxo11	-0.66	-0.34	1.11	1.56
Klf7	-0.46	-0.62	1.11	0.71
Plek	-0.76	-0.78	1.11	0.58
F10	0.10	-0.14	1.11	0.81
Pcdh7	-0.07	-1.85	1.11	0.28
Gdap10	0.02	-0.02	1.11	0.38
Nfkbib	-0.18	-0.25	1.10	0.84
Txnrd1	-0.10	-0.42	1.10	0.47
F3	-0.35	-0.66	1.10	1.99
Rap2b	-0.24	-0.88	1.10	0.90
Zswim4	-0.31	-0.75	1.10	0.34
Ddx58	0.00	-0.53	1.09	0.43
AI607873	-0.15	-1.66	1.09	0.49
Clec4e	-0.39	-1.47	1.09	0.82

Pmepa1	-1.78	-1.70	1.09	0.93
LOC432459	-0.09	-0.56	1.09	0.63
Kdm6b	-0.45	-0.55	1.08	1.00
Pdlim5	-0.13	-0.60	1.08	1.29
Glrx	-0.15	-1.80	1.08	0.39
Fgr	-0.09	-0.92	1.08	0.11
Micall1	-0.24	-0.62	1.08	0.39
3110043O21Rik	-0.64	-0.73	1.07	0.49
Slfn4	-0.25	-0.39	1.07	0.70
Relb	-0.78	-1.12	1.06	0.81
Slfn10-ps	-0.40	-1.80	1.06	0.78
Hmga2	-0.09	-1.38	1.06	0.09
Slc2a1	-0.24	-0.60	1.05	0.88
Ppfia3	0.00	-0.17	1.05	0.82
Zfand5	-0.75	-0.72	1.05	0.94
Rapgef2	-0.35	-0.80	1.05	1.17
LOC624295	-0.16	-0.49	1.04	0.35
Slfn3 /// Slfn4	-0.31	-0.41	1.04	0.88
Slc2a1	-0.25	-0.42	1.04	0.86
Nfkbia	-0.78	-0.25	1.03	0.98
Gvin1	-0.49	0.07	1.03	0.96
Apol9a /// Apol9b	-0.13	-0.11	1.02	0.13
Smox	-0.24	-0.86	1.01	0.62
Igf2bp2	-0.27	0.05	1.01	1.20
Ampd3	-0.08	-0.23	1.01	0.40
Afp	-0.03	-0.55	1.01	0.83
Junb	-1.31	-2.00	1.00	1.06
Cdc42ep4	-0.06	-1.10	1.00	1.04
Usp27x	-0.10	-0.38	1.00	0.89
Zfand5	-0.69	-0.60	0.99	0.70
Odc1	-0.40	-0.01	0.99	0.85
Tsc22d1	-0.13	-0.27	0.99	1.12
C3ar1	-1.54	-0.67	0.98	1.19
Afp	-0.06	-0.07	0.97	0.25
Agpat4	-0.34	-0.79	0.97	0.70
Errfi1	-0.38	-0.46	0.97	1.49
Zbtb7a	-0.10	-0.83	0.97	0.22
Hmox1	-0.97	-0.78	0.97	1.15
Slc39a14	-0.08	-0.55	0.97	0.08
Pvr	-0.81	-0.46	0.97	0.64
Itpkb	-0.59	0.00	0.97	1.03
Zyx	-0.34	-0.44	0.96	1.21
Gspt1	-0.71	-0.62	0.96	0.14
Arl5b	-0.89	-0.91	0.96	1.40
Znfx1	-0.12	-0.43	0.95	0.12
Ifi47	-0.30	0.03	0.95	0.25
Nfkbid	-0.76	-0.90	0.95	1.09

Ets2	-0.71	-0.18	0.95	1.14
Glrx	-0.18	-1.78	0.95	0.26
Rtp4	-0.39	-0.26	0.95	1.21
Tiparp	-0.84	-0.38	0.94	0.60
Adora2b	-0.48	-0.33	0.94	0.33
Mcl1	-0.28	-0.26	0.94	0.90
Med13	-0.13	-0.18	0.93	0.75
Jund	-0.18	-0.83	0.93	0.77
Jag1	-0.13	-0.03	0.93	0.39
Sertad2	-0.23	-0.74	0.93	0.48
Gclm	-0.43	-0.84	0.92	0.27
	-0.44	0.06	0.92	0.24
Cdc42ep4	-0.10	-0.99	0.92	1.05
Gch1	-0.77	-1.14	0.91	0.43
Plek	-0.65	-0.63	0.91	0.47
Mdm2	-0.50	-0.47	0.90	0.77
Coq10b	-0.97	-0.85	0.90	0.95
Aff1	-0.41	-0.81	0.90	0.28
Ptgir	-0.81	-1.02	0.89	0.29
Tgfb1	-0.31	-0.31	0.89	1.07
Pvr	-0.76	-0.64	0.88	0.38
Nfkbia	-0.75	-0.36	0.88	0.87
	-0.49	-0.46	0.88	1.58
Tet2	-0.18	-1.55	0.88	0.18
Fzd5	-0.44	-0.37	0.87	0.75
Zc3hav1	-0.30	-0.20	0.87	0.26
C3ar1	-1.23	-0.37	0.87	0.92
Bcar3	-0.51	-2.08	0.86	0.51
Zcchc2	-0.37	-0.02	0.86	0.69
Rc3h1	-0.37	-0.21	0.86	0.79
Pion	-0.23	-0.74	0.86	0.23
Rabgef1	-0.20	-0.40	0.86	0.66
	-0.39	-0.45	0.85	0.37
Itgav	-0.17	-0.50	0.85	0.09
2810474O19Rik	-0.21	-0.68	0.84	0.21
Vgf	-0.27	-0.46	0.84	0.32
Tmeff1	-0.31	-0.19	0.84	0.07
Enpp4	-0.41	0.07	0.84	0.72
Ddx58	-0.36	-0.14	0.83	0.59
Dnmt3l	-0.88	-0.52	0.83	0.65
Nfkbia	-0.82	-0.49	0.83	0.68
Zfp568	-0.43	-0.32	0.83	0.45
Car13	-0.25	0.25	0.82	0.53
4632427E13Rik	-0.30	-0.03	0.82	0.03
Gigyf2	-0.29	-0.33	0.82	0.49
2810474O19Rik	-0.20	-0.57	0.82	0.20
Ltb	-0.47	0.31	0.81	1.08

Ankrd57	-1.21	-0.05	0.80	1.15
Cdkn1a	-0.55	-0.75	0.79	0.85
Pdlim5	-0.27	-0.61	0.79	0.30
Mrpl52	-0.27	-0.24	0.78	0.90
Sertad2	-0.28	-0.72	0.78	0.33
Agpat4	-0.41	-0.77	0.78	0.41
	-1.08	-0.01	0.77	1.03
Pvr	-0.46	-0.47	0.77	0.47
Skil	-1.41	-0.83	0.77	1.62
Pdgfa	-0.45	-1.29	0.76	0.45
Bcl6b	-0.77	-0.01	0.76	1.77
Plekhf1	-0.81	-1.28	0.75	0.46
Bcl2a1a /// Bcl2a1b /// Bcl2a1d	-0.64	-0.11	0.75	1.18
Flnb	-0.89	-1.21	0.75	0.39
Pdlim7	-1.34	-0.56	0.75	1.42
Taok1	-0.38	-0.05	0.75	0.05
D13Ertd787e	-0.39	-0.42	0.74	0.37
Prdm1	-0.40	-0.20	0.74	-0.01
AI845619	-0.46	-0.57	0.74	0.64
Aff1	-0.32	-0.38	0.74	0.38
Igf2bp2	-0.31	0.00	0.73	1.15
Spty2d1	-0.63	-0.45	0.73	0.96
Atf3	-1.42	-2.17	0.72	0.36
Osm	-1.61	-0.81	0.72	1.94
Col5a3	-0.34	-0.05	0.72	-0.02
	-0.75	-1.00	0.72	0.34
Osgin2	-0.45	-0.28	0.71	0.69
Sash1	-1.01	-0.40	0.71	0.63
Zcchc2	-0.41	0.04	0.70	0.34
Bcl2l1	-0.54	-0.07	0.70	0.75
LOC100503807	-0.79	-0.77	0.69	0.14
Nfkbia	-0.63	-0.28	0.69	0.64
Bcor	-0.63	-0.73	0.68	0.82
Osgin2	-0.61	-0.51	0.67	0.60
Coq10b	-0.88	-0.85	0.67	0.97
Top1	-0.35	0.06	0.67	0.42
Gclm	-0.45	-0.80	0.67	0.22
Agpat9	-1.00	-1.55	0.67	0.36
Zc3hav1	-0.35	-0.25	0.66	0.36
Ehd1	-1.26	-0.06	0.66	0.63
Gtpbp4	-0.39	-0.05	0.65	0.51
Akap12	-0.40	0.08	0.65	0.54
Hdc	-0.51	-0.46	0.65	0.68
Gm11428	-0.38	-0.10	0.65	0.65
1110028C15Rik	-0.45	-0.41	0.64	0.44
Ptar1	-0.41	-0.13	0.64	-0.02

Plekho2	-0.39	-0.69	0.63	0.46
Zdhhc18	-0.60	-0.34	0.63	0.22
Tlr2	-1.13	-1.46	0.62	0.15
Anxa7	-0.57	-1.03	0.62	0.11
C3ar1	-1.59	-0.39	0.62	0.83
Lima1	-0.75	-0.42	0.60	0.72
Ndel1	-0.42	-0.62	0.59	0.38
Dusp16	-1.67	-1.36	0.59	1.10
Pvr	-0.48	-0.46	0.58	0.39
2610030H06Rik	-0.43	-0.02	0.57	0.92
Rasgef1b	-1.83	-0.89	0.57	-0.02
Plxna2	-0.47	-0.15	0.57	0.84
Nfkbib	-0.49	-0.18	0.56	0.23
Ehd1	-1.12	0.03	0.56	0.72
Gna13	-0.75	-0.50	0.55	0.20
Tnfrsf12a	-1.42	-1.69	0.54	0.60
Ehd1	-1.24	0.01	0.53	0.72
Btg2	-1.05	-1.24	0.53	0.59
	-0.49	-0.44	0.52	0.31
Nab2	-0.51	-0.66	0.52	1.13
Rhob	-0.68	-0.91	0.52	-0.16
Tnfrsf12a	-1.41	-1.36	0.51	0.67
Ehd1	-1.17	-0.01	0.51	0.54
Zfand5	-0.76	-0.93	0.51	0.10
Pvr	-0.58	-0.46	0.49	0.22
Gpbp1	-0.98	-0.08	0.48	0.28
Ezr	-0.61	-0.03	0.46	0.58
Gab2	-0.57	-0.72	0.46	0.05
Lima1	-0.88	-0.37	0.44	0.82
Ppard	-0.58	-0.36	0.44	0.38
Mex3c	-0.65	-0.64	0.44	0.30
Prrg4	-0.94	-0.01	0.43	0.41
Enpp4	-0.84	0.11	0.41	0.70
Mcts2	-0.66	-0.68	0.41	0.24
Car13	-0.67	0.08	0.39	0.23
Ppp1r15a	-1.67	-1.53	0.38	-0.38
Lonrf1	-0.82	-0.82	0.38	0.25
Eda2r	-0.66	-0.44	0.37	-0.13
Bcor	-1.09	-1.20	0.36	0.33
Zfp719	-0.67	-0.37	0.35	0.94
Kctd12	-2.00	-0.16	0.35	1.39
Gm6377	-3.21	-2.55	0.35	1.89
Slc15a3	-1.87	-0.15	0.33	1.66
Filip1l	-0.69	-1.57	0.32	-0.08
Lima1	-0.83	-0.30	0.30	0.66
Egr3	-3.77	-2.41	0.30	1.15
Slc25a33	-0.82	-0.28	0.28	0.67

Rem2	-0.73	-0.15	0.28	0.00
	-0.99	0.30	0.23	0.99
Arl2bp	-0.80	-0.44	0.21	0.31
Bhlhe40	-2.00	-1.38	0.20	0.51
Fbxo30	-0.81	-0.27	0.19	0.29
Egr2	-1.88	-4.11	0.19	-0.19
Cd86	-0.91	-0.18	0.18	0.96
Jarid2	-1.49	0.11	0.16	0.17
Adamts1	-0.87	-0.33	0.15	0.20
Egr2	-1.98	-4.03	0.14	-0.14
	-0.99	-1.15	0.12	-0.05
Zwint	-0.92	-0.94	0.12	0.05
Ubtd2	-1.03	-0.10	0.11	0.27
Pla2g5	-1.18	0.03	0.10	1.48
Ccl2	-4.63	-2.37	0.10	1.61
Id1	-2.58	-0.98	0.09	-0.09
Jarid2	-1.61	0.03	0.08	0.07
5033430I15Rik	-1.17	-0.81	0.06	0.49
Jarid2	-1.77	-0.02	0.05	0.02
Sertad1	-1.46	-1.76	0.03	0.05
Id3	-1.31	-0.94	0.03	0.71
Cldn12	-1.02	-0.34	0.02	1.14
Phf15	-1.02	0.14	0.01	0.57
Rffl	-1.19	0.00	0.00	1.07
Skil	-1.77	-1.20	-0.01	0.29
Notch1	-1.29	0.05	-0.01	0.27
Ccl7	-1.81	-1.63	-0.04	0.76
Btg3 /// Gm7334	-1.37	0.04	-0.04	0.78
Mt2	-2.56	0.06	-0.05	0.86
Klf3	-1.89	0.47	-0.06	0.11
Hipk2	-1.33	0.09	-0.09	0.10
Klf3	-1.32	0.13	-0.10	0.10
Adap2	-1.41	1.49	-0.24	0.24
Plk3	-1.69	-0.83	-0.27	0.72
Ikbke	-2.46	0.32	-0.29	1.32
C5ar1	-1.84	0.33	-0.33	0.92
C5ar1	-1.88	0.34	-0.34	1.03
Slc7a8	-1.36	0.35	-0.35	0.50
Zswim6	-1.68	0.38	-0.38	0.40
Plk2	-1.84	0.58	-0.58	2.57
Rbpms	-1.86	0.58	-0.58	1.47
Abca1	-2.73	1.28	-0.95	1.05
Tgm2	-3.20	1.31	-1.31	1.91

MATERIALS AND METHODS

Cells and Reagents

RAW264.7 were acquired for ATCC and cultured in standard 5% FBS in DMEM. Wild-type and IFNAR-deficient bone marrow macrophages (BMMs) were differentiated as described previously(Chin et al., 2002). BMMs were grown for 7 days in 2% 14-12 conditioned medium. Wild-type and RXR null embryonal carcinoma cells were obtained from Dr. Peter Tontonoz. Cells were treated with agonist and antagonists for 16-24 hours before infection or stimulation with poly(I:C). RXR specific agonists AGN194204 and LG268 was obtained from Dr. Peter Tontonoz. RXR antagonists, HX531, was obtained from Dr. Hiroyuki Kagechika. 9-*cis*-RA and 13-*cis*-RA were purchased from Sigma-Aldrich Inc. All compounds were resuspended in DMSO.

Stable Cell Lines

RXRa was cloned into pBABE-puromycin retroviral vector and expressed with packaging vectors psiA in 293T cells for 48hours. The supernatants were infected on to RAW 264.7 or F9 embryonal carcinoma cells and the selected for transformants by puromycin selection (2ug/mL).

Viral Infection and plaque assay:

RAW264.7 were plated in 6-well format at 6x105 and treated with DMSO control or agonists or antagonists for 16-24 hours. Replication competent VSV-GFP was graciously provided by Dr. Glen Barber and MHV68-luc was a gift from Dr. Ren Sun. Viruses were propagated as described previously(Doyle et al., 2002a). Cells were infected with VSV (0.01MOI) in media for 1 hour and replenished with DMEM with 1% FBS. Supernatants were collected between 12-16 h.p.i. Standard plaque assay was performed on monolayer of Vero cells. Briefly, Vero cells were seeded at $2.5x10^5$ cells

per well in standard 12-well plates. Ten-fold serial dilutions of viral supernatants were made. Vero cells were infected with diluted supernatants for 1 hour and resuspended in 1% FBS with 0.6% low-melt point agarose in DMEM overnight. The agarose was reomvoed by suction and stained with 0.05% crystal violet, 40% EtOH, in PBS. HSV-KOS (0.25MOI), MHV68-luc(1MOI), and WSN (1MOI) infections were done in the same way. HSV-1 plaque assay took 60hrs. for plaques to form and were stained the same way. MHV68-luc infection was quantitated by Firefly luciferase assay kit (Promega). VSV-G pseudotyped virus containing renilla luciferase reporter was a gift from Dr. Benhur Lee. Infections were performed similarly and quantitated by renilla luciferase kit (Promega). Student T-test (unpaired, 2-tailed) was used for used for statistical analyses on biological triplicates.

Real-time PCR and western blotting

Biological triplicates of RAW264.7 were pre-treated with 9*cis*RA (100nM) or HX531 (1uM) for 12hours and subsequent stimulated with poly(I:C) (1ug/mL). Cells were collected in trizol and RNA was isolated by standard isopropanol precipitation. RNA was quantitated and 1 µg of RNA was reversed transcribed using IScript (BioRad) according to the manufacturer's instructions with either random hexamer or VSV N1 (5’ GATAGTACCGGAGGATTGACGACTA) as primers. Q-PCR analysis was done using the iCycler thermocycler (Bio-Rad). Q-PCR was conducted in a final volume of 20 µL containing: Native Taq polymerase (Invitrogen) , 1× Taq buffer (Stratagene), 125 µM dNTP, SYBR Green I (Molecular Probes), and Fluoroscein (Bio-Rad), and 1% cDNA. Amplification conditions were: 95°C (3 min), 40 cycles of 95°C (20 s), 55°C (30 s), 72°C (20 s). Expression values were normalized to L32 control and fold induction was

normalized to untreated control. Student T-test (unpaired, 2-tailed) was used for used for statistical analyses on biological triplicates. Gene primer sequences used were:

GBP-1: 5'-CAGGGTAGACAATGGGCAGT; 5'-CACAGTAGGCTGGAGCATGA

IL-1b: 5'-GAGCTGAAAGCTCTCCACCTCA; 5'-TCGTTGCTTGGTTCTCCTTGTAC

TNFa: 5'-GGTGCCTATGTCTCAGCCTCTT; 5'-CGATCACCCCGAAGTTCAGTA

OAS2: 5'-GGTGAGGGTCCCATAACCTT; 5'-AGTCCACCAGAGCCTGCTTA

IRF7: 5′-ACAGGGCGTTTTATCTTGCG; 5′-TCCAAGCTCCCGGCTAAGT;

ISG15: 5′-CAGGACGGTCTTACCCTTTCC; 5′-AGGCTCGCTGCAGTTCTGTAC;

IFIT1: 5′-GGCAGGAACAATGTGCAAGAA; 5′-CTCAAATGTGGGCCTCAGTT;

*IFN*β: 5′-AGCTCCAAGAAAGGACGAACAT; 5′-GCCCTGTAGGTGAGGTTGATCT;

ISG20: 5'-CCATGGACTGTGAGATGGTG; 5'-CTCGGGTCGGATGTACTTGT

L32: 5'-AAGCGAAACTGGCGGAAAC; 5'-TAACCGATGTTGGGCATCAG

Cells lysis and Immunoblotting was done by methods described previously (Doyle et al., 2002b). Anti-RXRα and Anti-VSV-G antibodies were purchased from Santa Cruz Biotechnology.

Mouse Infections

Wild-type C57/BL6 mice were purchased from Jackson Laboratory. They were Mice were injected i.p. with DMSO (n=7) or 13*cis*RA (1mg/kg) (n=8) solubilized in corn oil every 24hours for 3 days and infected with 10^7 pfu of HSV-1(Strain 17) on day 4. Mice were sacrificed 5dpi and the livers were harvested, homogenized in media, and quantiated for viral titers by standard plaque assay.

REFERENCES

Allenby, G., Bocquel, M.T., Saunders, M., Kazmer, S., Speck, J., Rosenberger, M., Lovey, A., Kastner, P., Grippo, J.F., and Chambon, P. (1993). Retinoic acid receptors and retinoid X receptors: interactions with endogenous retinoic acids. Proceedings of the National Academy of Sciences of the United States of America *90*, 30 –34.

Altucci, L., Leibowitz, M.D., Ogilvie, K.M., de Lera, A.R., and Gronemeyer, H. (2007). RAR and RXR modulation in cancer and metabolic disease. Nat Rev Drug Discov *6*, 793–810.

Angulo, A., Suto, C., Heyman, R., and Ghazal, P. (1996). Characterization of the sequences of the human cytomegalovirus enhancer that mediate differential regulation by natural and synthetic retinoids. Mol Endocrinol *10*, 781–793.

Armstrong, J.L., Redfern, C.P.F., and Veal, G.J. (2005). 13-*cis* Retinoic acid and isomerisation in paediatric oncology--is changing shape the key to success? Biochemical Pharmacology *69*, 1299–1306.

Aukrust, Müller, Ueland, Svardal, Berge, and Frøland (2000). Decreased vitamin A levels in common variable immunodeficiency: vitamin A supplementation in vivo enhances immunoglobulin production and downregulates inflammatory responses. European Journal of Clinical Investigation *30*, 252–259.

Barik, S., and Banerjee, A.K. (1992). Phosphorylation by cellular casein kinase II is essential for transcriptional activity of vesicular stomatitis virus phosphoprotein P. Proceedings of the National Academy of Sciences of the United States of America *89*, 6570 –6574.

Baum, A., and García-Sastre, A. (2010). Induction of type I interferon by RNA viruses: cellular receptors and their substrates. Amino Acids *38*, 1283–1299–1299.

Baxter, K.F., and Cunliffe, W.J. (2001). Retinoid herpeticum. Clin Exp Dermatol *26*, 557–557.

Castrillo, A., Joseph, S.B., Vaidya, S.A., Haberland, M., Fogelman, A.M., Cheng, G., and Tontonoz, P. (2003). Crosstalk between LXR and Toll-like Receptor Signaling Mediates Bacterial and Viral Antagonism of Cholesterol Metabolism. Mol Cell *12*, 805–816.

Chin, A.I., Dempsey, P.W., Bruhn, K., Miller, J.F., Xu, Y., and Cheng, G. (2002). Involvement of receptor-interacting protein 2 in innate and adaptive immune responses. Nature *416*, 190–194.

Chow, E.K., Castrillo, A., Shahangian, A., Pei, L., O'Connell, R.M., Modlin, R.L., Tontonoz, P., and Cheng, G. (2006). A role for IRF3-dependent RXRα repression in hepatotoxicity associated with viral infections. The Journal of Experimental Medicine *203*, 2589 –2602.

Van De Kerkhof, P.C.M. (2006). Update on retinoid therapy of psoriasis in: an update on the use of retinoids in dermatology. Dermatologic Therapy *19*, 252–263.

Dheen, S.T., Jun, Y., Yan, Z., Tay, S.S., and Ang Ling, E. (2005). Retinoic acid inhibits expression of TNF-α and iNOS in activated rat microglia. Glia *50*, 21–31.

Doyle, S.E., Vaidya, S.A., O'Connell, R., Dadgostar, H., Dempsey, P.W., Wu, T.-T., Rao, G., Sun, R., Haberland, M.E., Modlin, R.L., et al. (2002a). IRF3 Mediates a TLR3/TLR4-Specific Antiviral Gene Program. Immunity *17*, 251–263.

Doyle, S.E., Vaidya, S.A., O'Connell, R., Dadgostar, H., Dempsey, P.W., Wu, T.-T., Rao, G., Sun, R., Haberland, M.E., Modlin, R.L., et al. (2002b). IRF3 Mediates a TLR3/TLR4-Specific Antiviral Gene Program. Immunity *17*, 251–263.

Ebisawa, M., Umemiya, H., Ohta, K., Fukasawa, H., Kawachi, E., Christoffel, G., Gronemeyer, H., Tsuji, M., Hashimoto, Y., Shudo, K., et al. (1999). Retinoid X receptor-antagonistic diazepinylbenzoic acids. Chemical and Pharmaceutical Bulletin *47*, 1778–1786.

Fernandez, M., Porosnicu, M., Markovic, D., and Barber, G.N. (2002). Genetically Engineered Vesicular Stomatitis Virus in Gene Therapy: Application for Treatment of Malignant Disease. J. Virol. *76*, 895–904.

Ghazal, P., DeMattei, C., Giulietti, E., Kliewer, S.A., Umesono, K., and Evans, R.M. (1992). Retinoic acid receptors initiate induction of the cytomegalovirus enhancer in embryonal cells. Proceedings of the National Academy of Sciences of the United States of America *89*, 7630 –7634.

Ghisletti, S., Huang, W., Ogawa, S., Pascual, G., Lin, M.-E., Willson, T.M., Rosenfeld, M.G., and Glass, C.K. (2007). Parallel SUMOylation-Dependent Pathways Mediate Gene- and Signal-Specific Transrepression by LXRs and PPAR^3. Mol Cell *25*, 57–70.

Glass, C.K., and Saijo, K. (2010). Nuclear receptor transrepression pathways that regulate inflammation in macrophages and T cells. Nat Rev Immunol *10*, 365–376.

Joseph, S., Castrillo, A., Laffittee, B., Mangelsdorf, D., and Tontonoz, P. (2003). Reciprocal regulation of inflammation and lipid metabolism by liver X receptors. Nature Medicine *9*, 213–219.

Kang, S., and Voorhees, J. Chapter 217. Topical Retinoids. In Wolff K, Goldsmith LA, Katz SI, Gilchrest B, Paller AS, Leffell DJ: Fitzpatrick's Dermatology in General Medicine, p.

Kawai, T., and Akira, S. (2008). Toll-like Receptor and RIG-1-like Receptor Signaling. Annals of the New York Academy of Sciences *1143*, 1–20.

Lee, H.-C., Headley, M.B., Iseki, M., Ikuta, K., and Ziegler, S.F. (2008). Cutting Edge: Inhibition of NF-{kappa}B-Mediated TSLP Expression by Retinoid X Receptor. J Immunol *181*, 5189–5193.

Mangelsdorf, D.J., Borgmeyer, U., Heyman, R.A., Zhou, J.Y., Ong, E.S., Oro, A.E., Kakizuka, A., and Evans, R.M. (1992). Characterization of three RXR genes that mediate the action of 9-*cis* retinoic acid. Genes & Development *6*, 329 –344.

Mangelsdorf, D.J., and Evans, R.M. (1995). The RXR heterodimers and orphan receptors. Cell *83*, 841–850.

Motomura, K., Ohata, M., Satre, M., and Tsukamoto, H. (2001). Destabilization of TNF-{alpha} mRNA by retinoic acid in hepatic macrophages: implications for alcoholic liver disease. Am J Physiol Endocrinol Metab *281*, E420–429.

Muindi, J.R., Roth, M.D., Wise, R.A., Connett, J.E., O'Connor, G.T., Ramsdell, J.W., Schluger, N.W., Romkes, M., Branch, R.A., Sciurba, F.C., et al. (2008). Pharmacokinetics and Metabolism of All-trans- and 13-*cis*-Retinoic Acid in Pulmonary Emphysema Patients. The Journal of Clinical Pharmacology *48*, 96 –107.

Ng, S.S.M., Tailor, P., Chang, T.-H., Ozato, K., and Kino, T. (2009). Viral infection alters mRNA expression of nuclear hormone receptors (NRs) and their coregulators in mouse dendritic cells (DCs). J Immunol *182*, 131.1.

Ogawa, S., Lozach, J., Benner, C., Pascual, G., Tangirala, R.K., Westin, S., Hoffmann, A., Subramaniam, S., David, M., Rosenfeld, M.G., et al. (2005). Molecular Determinants of Crosstalk between Nuclear Receptors and Toll-like Receptors. Cell *122*, 707–721.

Stetson, C.L., Butler, D.F., and Rapini, R.P. (2003). Herpetic whitlow during isotretinoin therapy. Int J Dermatol *42*, 496–498.

Taimi, M., Helvig, C., Wisniewski, J., Ramshaw, H., White, J., Amad, M., Korczak, B., and Petkovich, M. (2004). A Novel Human Cytochrome P450, CYP26C1, Involved in Metabolism of 9-*cis* and All-trans Isomers of Retinoic Acid. Journal of Biological Chemistry *279*, 77 –85.

Tsukada, M., Schroder, M., Roos, T.C., Chandraratna, R.A.S., Reichert, U., Merk, H.F., Orfanos, C.E., and Zouboulis, C.C. (2000). 13-*cis* Retinoic Acid Exerts its Specific Activity on Human Sebocytes through Selective Intracellular Isomerization to All-trans Retinoic Acid and Binding to Retinoid Acid Receptors. *115*, 321–327.

Welch, J.S., Ricote, M., Akiyama, T.E., Gonzalez, F.J., and Glass, C.K. (2003). PPARγ and PPARδ negatively regulate specific subsets of lipopolysaccharide and IFN-γ target genes in macrophages. Proceedings of the National Academy of Sciences of the United States of America *100*, 6712 –6717.

Wu, T.-T., Tong, L., Rickabaugh, T., Speck, S., and Sun, R. (2001). Function of Rta Is Essential for Lytic Replication of Murine Gammaherpesvirus 68. J. Virol. *75*, 9262–9273.

Xu, J., and Drew, P.D. (2006). 9-*Cis*-retinoic acid suppresses inflammatory responses of microglia and astrocytes. Journal of Neuroimmunology *171*, 135–144.

Yazici, A., Baz, K., and Ikizoglu, G. (2006). Recurrent herpes labialis during isotretinoin therapy: is there a role for photosensitivity? J Eur Acad Dermatol Venerol *20*, 93–95.

CHAPTER 5

Live Attenuated Vaccine Design by Functional Genome Profiling of Influenza M-gene

ABSTRACT

Live attenuated viruses are attractive vaccine candidates because they are strongly and broadly immunogenic. Using a reverse genetics system for influenza as a model, we introduced >10^5 random mutations in the M-gene and identified a map of mutations that are permissive and non-permissive for influenza growth under *in vitro* and *in vivo* selection. We hypothesized attenuated influenza mutants could establish initial infection but could not persist in the host. Hence, we monitored the growth profile of the entire mutant population during the course of infection in mice and found mutations that exhibited this attenuated growth profile. We identified one unique mutant, W7-791, that exhibited attenuated growth in mice and did not cause any signs of sickness at more than 100 times LD50. When used as a live-attenuated vaccine, a single, safe dose of W7-791 conferred full protection against lethal infection of H1N1 influenza of two subtypes, WSN and PR8, and a heterosubtypic strain, H3N2/Victoria.

INTRODUCTION

Vaccination has been the most effective way to prevent spread of viral infections. Live attenuated vaccines have been shown to be more effective and broadly immunogenic than inactivated vaccines likely because it stimulates both humoral and cell-mediated immune responses (Belshe et al., 2007). The challenges of attenuated vaccine design are not only to balance immunogenicity and safety but also to have a system to generate novel live, attenuated vaccines to address the continual emergence of new strains of viruses.

Traditionally, attenuated vaccines, such as the presently available measles, mumps, or influenza vaccines, have been made by a forward genetics approach through mutagenesis followed by rounds of selection in abnormal conditions. For example, temperature-sensitive flu vaccine was derived from serial passages of A/Ann Arbor/6/60 (H2N2) and B/Ann Arbor/1/66 at low temperatures(Neumann et al., 2009) and seasonal influenza vaccines are made by re-assortment of circulating HA and NA subtypes into this master donor viral strain(Cox et al., 2004). The underlying assumption of this process was that a cold-adapted virus would be attenuated at normal body temperature. The process of generating these types of attenuated vaccines is slow and inefficient because each one has to be made empirically. Hence, a systematic way to *directly* find live-attenuated mutations in virus for vaccine development would be particularly beneficial.

Reverse genetics systems for generating viruses by *in vitro* expression of viral genomic material have been an invaluable tool in viral vaccine design. It permits targeted mutations for vaccine development and efficient production of viruses *in vitro*

cell culture(Hoffmann et al., 2000). When the World Health Organization (WHO) issued a pandemic alert against H5N1 in 2003, deletion of polybasic motif in the HA or truncations of NS1 using a reverse genetics system led to novel vaccine candidates(Webby et al., 2004; Steel et al., 2009). While rational designs of vaccines has been proposed, they have not capture the entire space of possible attenuating domains in a viral genome. We sought to combine the versatility of reverse genetics system and a systematic approach to comprehensively identify potential attenuating mutations. In order to fit the basic requirement of an attenuated vaccine, candidate mutants must also be grown to high titer *in vitro* and be safe and immunogenic *in vivo*.

We used the reverse genetics system available for influenza as a model for systematic identification candidate live attenuated virus. Influenza A virus is an enveloped, single negative-strand RNA virus in the family of Orthomyxoviridae and consists of an eight-segmented genome, PB2, PB1, PA, HA, NP, NA, M, and NS(Lamb et al., 1981). The virion consists of envelope, matrix protein, and core. PB2, PB1, PA, and NA are essential for viral replication and transcription, where as HA and NA are surface proteins required for binding and budding processes. The 1027bp M-gene, or segment 7, encodes the 262aa M1 and the 97aa M2 proteins. M1 coats the nucleocapsid and is required for viral assembly processes and M2 forms a homotetrameric proton channel that is required for pH-dependent endocytosis. Unlike HA and NA which mutate rapidly, both M1 and M2 have evolved very slowly in all lineages of influenza, implicating their critical functions in viral growth(McCown and Pekosz, 2006). The M1 protein is also the most highly expressed protein in the influenza virion and the M2 protein is expressed on cell surface 2-fold higher than HA in

infected cells(Zebedee and Lamb, 1988; McCown and Pekosz, 2005; Iwatsuki-Horimoto et al., 2006). For these reasons, the M proteins have been evaluated as targets for vaccine development (Tompkins et al., 2007; Ilyinskii et al., 2008; Schnell and Chou, 2008). Given the critical role of the M gene in the viral lifecycle and its high expression level and conservation, we hypothesized it would be suitable target for modification as a way to attenuate influenza growth regardless of strain.

In this study, we generated high-density insertional mutations at nearly every nucleotide of the H1N1 influenza A/WSN/33 (WSN) M gene and profiled essential and non-essential regions that are required for viral growth *in vitro* and *in vivo*. We then profiled kinetics of mutant population growth and found mutations that exhibited attenuated-growth profiles. We isolated one unique attenuated influenza mutant that is safe and effective against lethal infections of several strains of influenza *in vivo* in murine models.

RESULTS

We utilized a plasmid-based system described previously by Hoffman et al., to generate replication competent influenza A/WSN/33 (WSN). Briefly, eight individual plasmids that encode the individual 8 segments of the viral genome and transcripts were co-transfected into transformed human embryonic kidney cells (HEK293T) to generate wild-type WSN, which were further amplified in Madin-Darby Canine Kidney (MDCK) cells (Hoffmann et al., 2000). This system allowed for manipulation of individual or all segments of the genome. Our approach, as outlined in Figure 5-1, was to identify essential and non-essential regions in the M-gene for viral growth as a way to find potential attenuating mutations. We used Mu-transposon mutagenesis to randomly insert a 15 nucleotide sequence, 5'-NNNNNTGCGGCCGCA-3', in the plasmid encoding the M-gene with a method previously described for functional profiling of hepatitis C virus (Arumugaswami et al., 2008). The mixed library of mutants was co-transfected with the 7 plasmids that encodes other segments of WSN to generate a mixed pool of viral mutants. To identify the location of the insertion for each mutant in a population, we generated cDNA from the infected cells and used a fluorescent-labeled primer against the 15-nucleotide insertion and a M-gene specific primer to amplify mutant gene fragments by PCR. Capillary electrophoresis resolved the sizes of the fragments corresponding to the approximate positions of the 15-nucleotide insertion. This genotyping method permitted rapid mapping of viable and non-viable mutants under a particular selection pressure (Figure. 5-2). In this study, the genotyping data were used to perform targeted search of mutants for desired growth characteristics for vaccine development.

We generated approximately >10^5 mutant clones by transposon mutagenesis in the plasmid encoding the influenza M-gene, which produced a mutant library of plasmids that contained more than 10 insertions per base pair. Genotyping of this mixed pool of plasmid showed a high number of mutations across the M-gene (Fig. 5-3 A, positive control). We then generated a mixed mutant virus population by transfecting the entire mutant M library with the 7 other wild-type plasmids into HEK293Ts. The newly formed virions were collected after 48hrs and passaged in MDCK cells. Mutations that were not deleterious to influenza would generate viable infectious viruses capable of multiple rounds of infection. We detected similar genotyping patterns in 3 biological replicates after one round of infection in MDCK cells (Supplementary Fig. S5-1A) whereas only a few non-specific peaks appeared in the negative control with cDNA from uninfected MDCK cells (Fig. 5-3A, negative control). To identify viable and stable mutant populations, we passaged the viruses for 4 generations in MDCK cells and genotyped each generation (Fig. 5-3B). Genotyping of viral particles in cell lysates from each round of infection showed three major clusters of viable mutations in positions 250-400nt, 525-600nt, and 725-825nt, referred herein as cluster A, B, and C respectively. Mutations in these regions are presumably permissive for WSN growth, hence, not essential for survival *in vitro*. Conversely, regions with no fluorescent peaks correspond to mutations that were deleterious to the virus and hence essential for viral growth.

To gain insight on where the mutations are in relation to conserved sites in the M gene, we compared the M gene across more than 300 influenza strains found in NCBI Influenza Database with the mutations identified by genotyping. Regions where

structural information was not publicly available were not mapped (Fig. 5-4A). Fully conserved regions in the M1 and M2 gene were mapped on the primary amino acid sequence and available M1 and M2 structures (Fig. 5-4B, blue box and Fig 5-4C, green). Insertional mutations in clusters A, B, and C were also mapped (Fig. 5-4B, red box and Fig 5-4C, red). Primary sequence alignment showed approximately 80% of the viable mutations did not overlap with conserved regions. In the M1 protein, cluster A and B were located in the outer helices, whereas no viable mutations were found in the central three helices (Fig. 5-4C, Helix 1,2 3) suggesting that structural integrity of these helices play important function for influenza survival. The M2 protein is a homotetramer and the helical transmembrane domain is clearly conserved. Mutations permissive to survival (cluster C) lied in N-terminus near the opening of the proton-channel to the cytosol (Fig. 5-4C, Helix 4). Taken together, most viable mutations identified through genotyping in M1 and M2 were located in non-conserved regions.

In order to satisfy the basic requirements of a live-attenuated virus, the virus must establish infection and not be virulent enough to cause sickness. In a population of mutants that infect a host, we hypothesized that individual mutants would exhibit three types of growth profiles. Virulent mutants, like wild-type virus, would undergo rapid growth followed by a stationary phase, which usually would cause host demise. Some mutants may not be able to establish productive infection at all. Attenuated mutants would exhibit initial growth like wild-type virus, but would eventually be suppressed by the host and cleared (Fig. 5-5 A).

Based on this hypothesis, we sought to find mutants with attenuated growth profiles in mice. Eight mice were given intratracheal (i.t.) injection of a concentrated

mixed pool of M-gene mutants, and cDNA was synthesized from RNA of lung homogenates collected 2, 4, 6, and 8 days post infection (Fig. 5-5 B). By genotyping, we observed mutant growth that corresponded with cluster A and cluster C from *in vitro* growth profile in Fig. 5-3B, herein called cluster A* and C*. The observed Cluster B from *in vitro* genotyping, called cluster B* *in vivo,* was absent in mice, suggesting that this cluster could not establish infection. When the maximal intensity from each region was measured and plotted against time, we observed that cluster A* had growth profile similar to a virulent strain, cluster B* similar to an innocuous strain, and cluster C* to an attenuated strain (Fig. 5-5C). These results suggest that mutants in Cluster C* would exhibit attenuated growth *in vivo*.

A second basic requirement of an attenuated virus is that it must be viable *in vitro* and *in vivo* for production. Mutants in cluster C and C* fit these criteria and hence, we sought to find individual mutants in this region. We isolated 67 single mutant clones with insertions distributed across the M-gene and transfected them individually with the complementary 7 segments to generate mutant viruses (Fig. 5-6 A). To measure the presence of infectious virions in the supernatants, we re-infected the supernatants onto HEK293T expressing a Gaussia luciferase reporter (gLuc) driven by the influenza PA-promoter. Expression of gLuc indicated viable virus. While several mutants were viable after initial transfection, mutants W7-757, W7-791, and W7-797 had mutations corresponding to C* region (Fig. 5-6B, highlighted area). Based on structural comparison described above, W7-757, W7-791, and W7-797 had insertions in the N-terminus near the cytoplasmic domain of the M2 channel; other mutants, W7-565 and W7-757, had mutations in the non-conserved regions of M1 (Supplementary Fig. S5-

2A). For comparison, W7-829 was not viable and had the insertion in the transmembrane domain, consistent with published data showing that this region is critical for proton activity (Supplementary Fig. S5-2B) (Schnell and Chou, 2008). When these selected mutants were serially passaged in MDCK cells, W7-791 grew to high titer.

The mutant clone W7-791 had the insertion, RHCGRI, after the 26th amino acid of M2 (Supplementary Fig. S5-3). The insertion is located on the cytoplasmic portion of the proton channel at the start of transmembrane region, which spans 25-46aa (Fig. 5-7A)(Schnell and Chou, 2008). It grew well *in vitro* but more slowly than the wild-type WSN virus (WT-WSN) (Fig. 5-7B) and caused less cell death in MDCK cells by LDH viability assay (Fig. 5-7C). These characteristics support our hypothesis that W7-791 might be attenuated compared to wild-type virus. Hence, we infected mice with WT-WSN or W7-791 at 4x10^4 pfu, which is 40-fold higher than the LD50 of wild-type virus. WT-WSN infected mice started to lose weight 3 days post infection (dpi) and all died or met criteria for euthanasia at 6 dpi. The W7-791 infected mice were healthy and did not lose any weight (Fig. 5-7D). At 6dpi, W7-791 infected mice had 10 times less viral load in their lungs compared to WT-WSN infected mice ($P<0.001$) (Fig. 5-7E). To determine whether W7-791 displayed attenuated growth or had an abortive infection, we measured the kinetics of viral growth of W7-791 and wild-type virus *in vivo*. WT-WSN viral titers in lungs of mice increased by 5 fold starting from day 2. The titer of W7-791 increased initially but persisted around the same titer levels past day 4 (Fig. 5-7F). We also observed less IL-1β production in W7-791 infected mice but no difference in TNFα production, suggesting that W7-791 causes less inflammation than WT-WSN infection

(Fig. 5-7G). Subsequent experiments demonstrated that mice showed no sign of sickness when infected with W7-791 at 10^5 plaque-forming units (pfu), which is more than 100 times LD50 of WT-WSN by intratracheal injection (Fig. 5-10A). Taken together, we directly found attenuating mutations by genotyping and found that W7-791 mutant did not cause persistent infection or sickness *in vivo*.

To test whether W7-791 can act as a live attenuated influenza vaccine, we infected wild-type mice with low dose of virus and subsequently challenged them with lethal dose of WT-WSN virus. During the vaccination phase, we infected the mice by intra-tracheal injection with PBS (mock vaccination), or 5000pfu of WT-WSN or W7-791. None of the W7-791 infected mice lost weight or appeared sick, but all WT-WSN infected mice lost weight and 4 mice died. Of the WT-WSN infected mice that survived, they recovered in about 2-3 weeks (Fig. 5-8A). After one month, the mice were challenged with lethal injection of 10^4 pfu of WT-WSN virus. The mock vaccinated group all lost weight and succumbed to the infection. The WT-WSN and W7-791 vaccinated groups did not lose weight and survived (Fig. 5-8 B and C). These results showed that vaccination with WT-WSN and W7-791 both could confer resistance against lethal WT-WSN infection. Importantly, W7-791 infection did not cause overt sickness or weight change during vaccination, satisfying a basic requirement of a vaccine.

We further tested whether W7-791 can protect against another mouse adapted H1N1 influenza virus in the same phylogenetic group, PR8. Similar to previous results, vaccination with a sub-lethal dose of WT-WSN led to sickness and weight-loss whereas W7-791 vaccinated mice did not cause any signs of sickness (Fig. 5-9A). Mock

vaccinated mice completely succumbed to lethal infection with 10^4 pfu of WSN or 200pfu of PR8, but W7-791 or WT-WSN vaccinated mice survived without weight loss or signs of sickness (Fig. 5-9 B and C). Mock-vaccinated mice had high viral titers in the lung homogenates whereas the vaccinated mice had no detectable viruses in their lungs 14 days after infection, when the experiment was terminated (Fig. 5-9 D and 7E). In conclusion, W7-791 is an attenuated virus that can generate effective immunity against different types of H1N1 influenza viral infections.

We hypothesized that vaccination of W7-791 conferred protection against WT-WSN and PR8 through a common antibody response against viral surface antigens, such as HA or NA. To test whether W7-791 elicited a common anti-HA response against PR8 and WSN, we assessed the presence of anti-HA antibody in the serum the lethally challenged mice. The HA-inhibition assay is a common way to titer anti-HA antibody by empirically measuring the concentration of serum titer that inhibits HA-agglutination of red blood cells (RBCs). As expected, when WSN was used to agglutinate the RBCs, WT-WSN- and W7-791-vaccinated mice had ~100 fold higher anti-HA antibody after WT-WSN challenge compared to mock-vaccinated mice with WT-WSN challenge. These vaccinated mice also produced anti-HA antibodies against WSN after PR8 challenge (Fig. 5-9 F). Unexpectedly, when PR8 was used to agglutinate the RBCs, we could not detect the presence of anti-HA antibody against PR8 in all groups of mice (Fig. 5-9 G). These results showed that WT-WSN and W7-791 vaccinated mice produced anti-HA antibodies specifically against WSN strain but not PR8 strain. It also demonstrated that W7-791 vaccination generated immunity against PR8 independent of cross-reactive anti-HA antibodies.

Live-attenuated vaccines are thought to generate broad immunogenicity through activation of humoral and cell-mediated immune responses. Since W7-791 vaccination did not induce cross-reactive anti-HA antibodies against PR8, we tested whether immunogenicity could be extended to influenza of another phylogenetic group, H3N2 A/Victoria/3/75. Two vaccine regimens were tested. One group of mice received a single dose of 10^5 pfu of W7-791 and was challenged with a lethal dose of H3N2/Victoria 5 weeks later (No booster Group). The second group was given 10^5 pfu of W7-791 two weeks after the initial dose and was lethally challenged 3 weeks after the last injection (Booster Group). W7-791 vaccinated mice did not lose any weight compared to mock controls (Fig. 5-10 A). Upon lethal H3N2 challenge, both groups of mice survived whereas mock-vaccinated group succumbed to the infection (Fig. 5-10 B and D). Interestingly, W7-791 vaccinated mice lost about 10% of their weight from 3-5 dpi and then recovered (Fig. 5-10 C and E). The booster group lost less weight, but the difference was not significant ($p>0.05$). All together, these results illustrate the capacity of a minimally modified live attenuated virus, W7-791, to generate broad immunogenicity and confer cross protection against different species of influenza.

DISCUSSION

We generated a mixed M-gene mutant population by transposon mutagenesis and profiled—by genotyping-- essential and non-essential regions for viral growth *in vitro* and *in vivo*. We then generated kinetic growth profile the entire mutant population *in vivo* and searched for mutations with attenuated growth profile. Hence, we identified a region near the cytoplasmic end M2 gene, where mutations might cause growth attenuation. From this region, we isolated the W7-791 mutant and showed that it is a safe and effective vaccine against influenza of different phylogenetic groups in mouse models.

Using random mutagenesis that can be easily tracked in a reverse genetics system offers an unbiased framework to find live-attenuated virus. Traditional approach to generate live attenuated viruses is done by empirical, trial-and-error processes. Current reverse genetics approaches use common master donor strains that may be insufficiently immunogenic. We hypothesized that attenuated virus would establish infection and be cleared by the host. The genome-wide genotyping method allowed for identification of regions with this attenuated growth profile in comprehensive way. Since the targeted mutations do not grossly modify the virus, immunogenicity would be well preserved.

The results from this study may have direct implication on generation of novel attenuated vaccines for influenza. The M1 and M2 proteins are conserved and essential for influenza growth, hence viable regions described here may serve as targets of attenuation in other influenza strains. Several individual mutants grew in vitro that have insertions in clusters A, B, and C from the genotyping data (Fig. 5-3B). Some

mutants did not correspond to these clusters suggesting that they represented micro-domains that are permissible to mutagenesis. They may be capable of growth individually but were not represented highly in by genotyping because they were out-competed in a mixed pool of mutants. Mutants in cluster C grew well *in vitro* and *in vivo*, from which W7-791 was subsequently identified to be a safe and effective attenuated vaccine. It remains unclear how the specific defect in the virus causes attenuated growth. Since the mutation exists the outer pore of the M2 channel, a defect in the proton pump function is possible. Defective M2 protein not incorporated into virions may be presented more efficiently on the cell surface to stimulate more robust immune response. The identification of this novel region in the M-gene to attenuate influenza introduces a possible new approach for flu vaccine development. One approach would be to generate attenuated vaccine by re-assorting W7-791 into virulent seasonal influenza.

The mechanism by which W7-791 elicits cross-protection against different strains of influenza appears to be mediated by a broad immune response. W7-791 vaccinated mice generated anti-HA antibodies against its parental strain, WT-WSN, but not a related H1N1 virus, PR8. W7-791-vaccinated mice did not exhibit any signs of sickness to lethal WT-WSN or PR8 infection, suggesting an immediate immune response that prevented an active infection, such as the production of another common cross-reactive antibody. On the other hand, there seems to be a different mechanism for cross-protection against H3N2. In this case, the W7-791 vaccinated mice lost about 10% of their weight and then fully recovered, suggesting that there was an active infection followed by clearance. This result implies a slower memory response involving clonal

expansion of smaller population B-cells against common epitopes or a memory T-cell response. In support of the latter possibility, seasonal H1N1 vaccines induced heterosubtypic memory T-cell responses that are important in cross-protection against H5N1 and H3N2 viruses(Lee et al., 2008).

Reversion is a common concern with live-attenuated viruses, although statistically it has not been a health concern with current LAIV. Current temperature-sensitive viruses contain point mutations and can potentially revert back to wild-type virus. The system described in this study utilized a 15nt random insertion that would less likely to revert by random point mutations. Reversions by non-homologous and homologous recombination events are extremely rare in influenza(Boni et al., 2010). Using the same approach to find other potential attenuated positions would allow one to generate combination of mutations that should further decrease rate of reversion or re-assortment.

Conceptually, this approach could be implemented to find attenuated viruses in reverse genetic systems that are currently available for many RNA and DNA viruses. It would require no working knowledge of specific gene function of the virus, which would make it more ideal for vaccine design for less understood or emergent viruses. The systematic approach requires the initial establishment of a comprehensive profiling of the entire genome *in vitro* and *in vivo*, but should subsequently expedite the process of finding new candidate live attenuated vaccines.

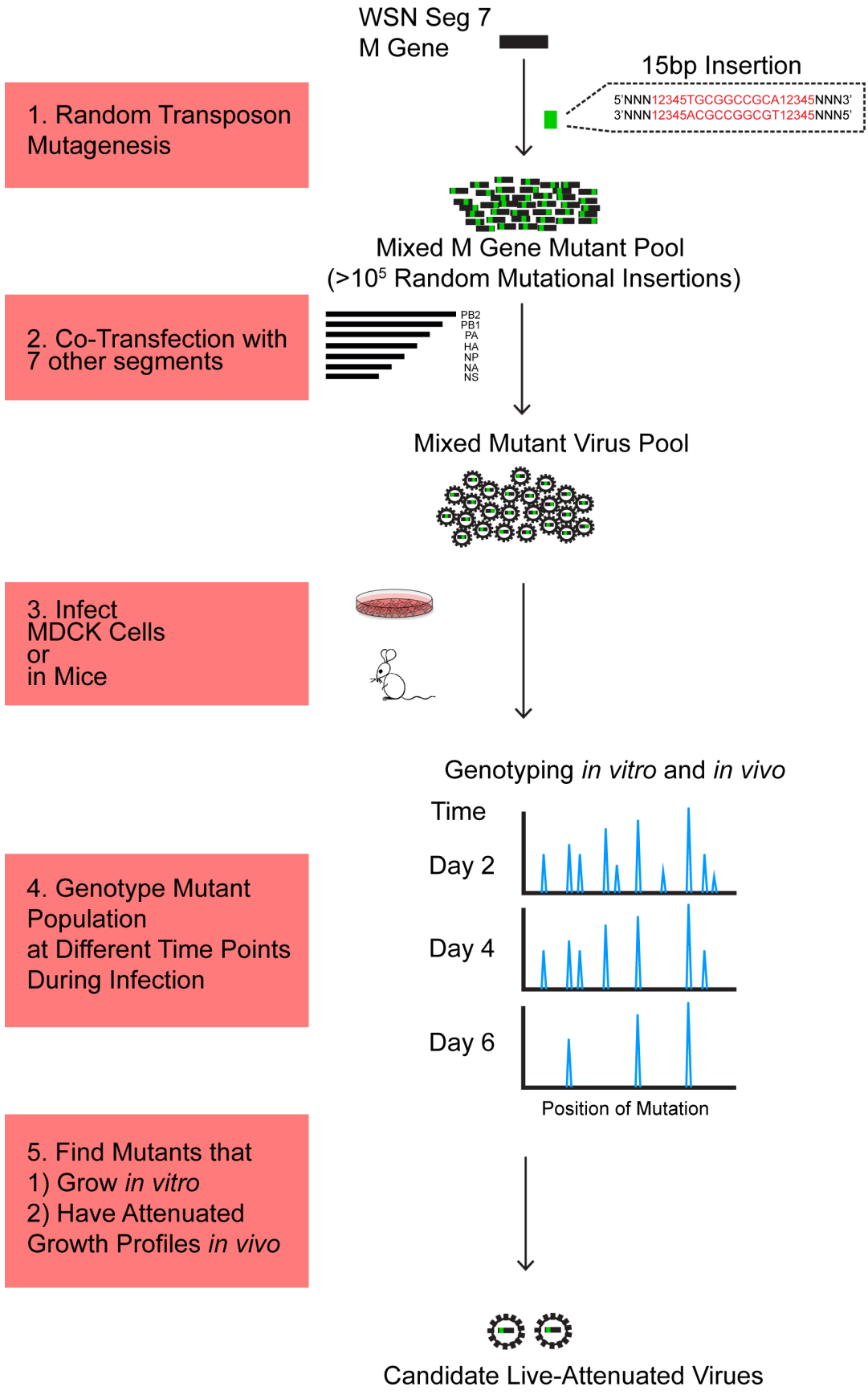
WSN Seg 7
M Gene
15bp Insertion
5'NNN12345TGCGGCCGCA12345NNN3'
3'NNN12345ACGCCGGCGT12345NNN5'
1. Random Transposon Mutagenesis
Mixed M Gene Mutant Pool
(>10^5 Random Mutational Insertions)
2. Co-Transfection with 7 other segments
PB2
PB1
PA
HA
NP
NA
NS
Mixed Mutant Virus Pool
3. Infect MDCK Cells or in Mice
Genotyping in vitro and in vivo
Time
Day 2
Day 4
Day 6
Position of Mutation
4. Genotype Mutant Population at Different Time Points During Infection
5. Find Mutants that
1) Grow in vitro
2) Have Attenuated Growth Profiles in vivo
Candidate Live-Attenuated Virues

Figure 5-1

Outline of Approach for Live-Attenuated Virus Design. (1) High-density mutations were made in the M-gene of influenza (A/WSN/33) with random insertion of 15nt by transposon mutagenesis. (2) Mutant viruses were generated by transfection with plasmids encoding other segments of WSN. Location of all mutations in the unselected pool can be determined by genotyping. (3) By infecting the mutant population in cells or mice, non-essential and essential regions in the M-gene required for viral growth *in vitro* and *in vivo* can be mapped. (4) The growth profile of the entire mutant population is tracked during an infection. We hypothesized attenuated mutants have growth profile in which it establishes initial infection, grows, and then clears. (5) Mutants with mutations in the M-gene that lead to this mutant growth are isolated as candidate attenuated-vaccine strains.

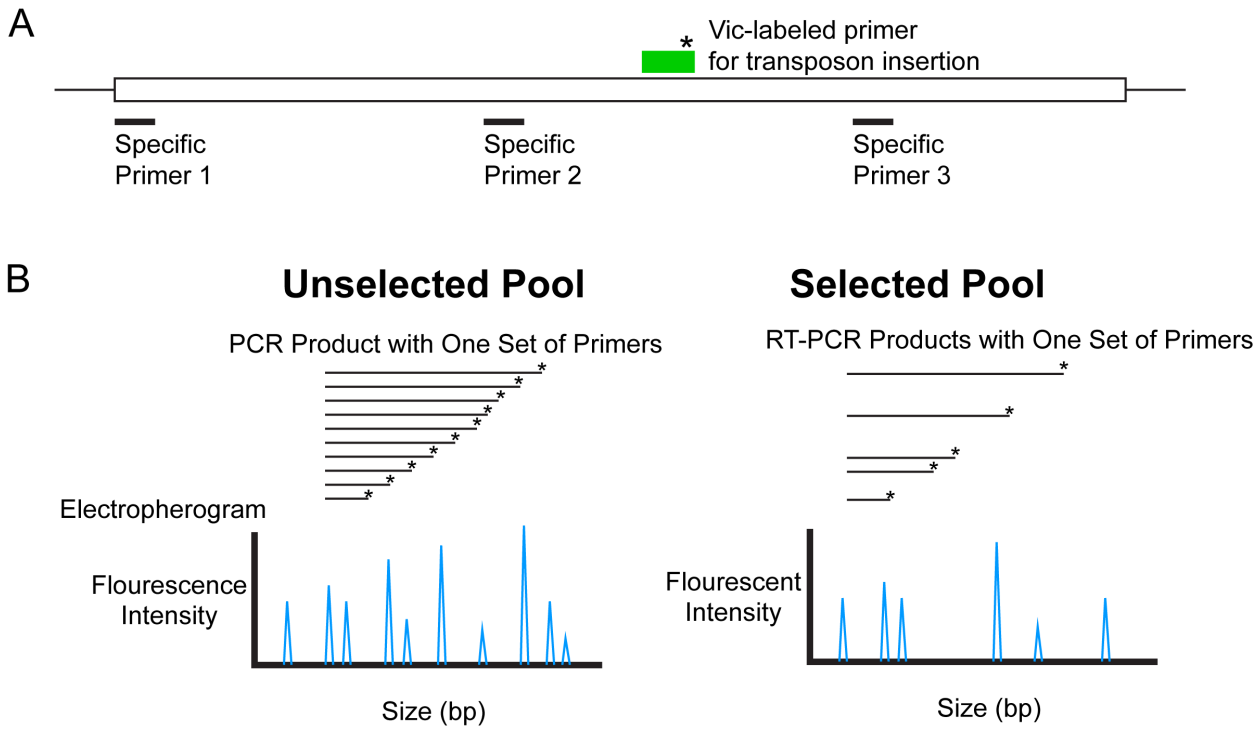

Figure 5-2

A. Individual mutation can be genotyped by PCR amplification with gene-specific primer and a primer against the 15nt insertion sequence.
B. The mutant pool library can be put through selection such as growth *in vitro* or *in vivo*. The selected pool is collected and genotyped. Essential and non-essential regions in the genome required for growth can be determined by comparing genotyping data from the unselected pool (total mutant library) and selected pool.

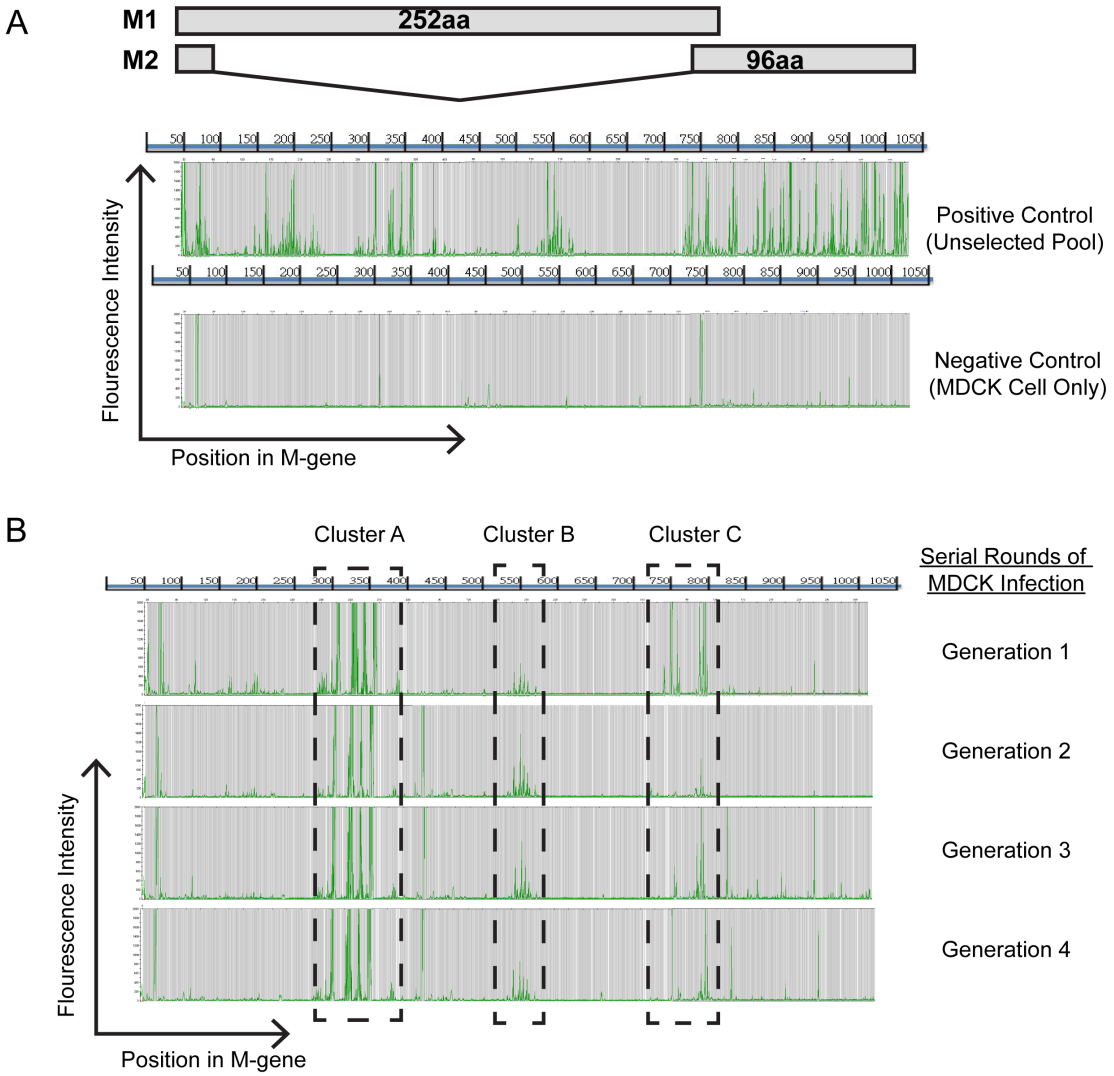

Figure 5-3

A. Schematic of M1 and M2 gene (top). Genotyping data the total mutant library containing all insertions (top) and for the unselected pool M-gene mutants in the negative control from MDCK cells (bottom).
B. Genotyping data of from mutant viruses that were passaged in MDCK cells for 4 generations, labeled G1,G2,G3, and G4, respectively. Dashed boxes indicate dominant clusters (A, B, and C).

A

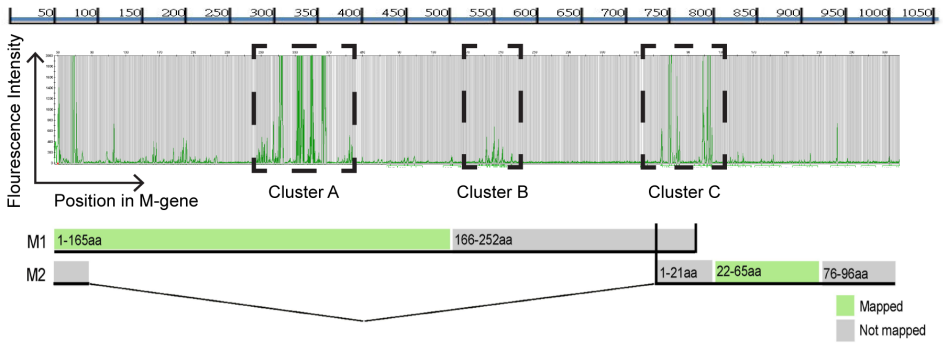
50 100 150 200 250 300 350 400 450 500 550 600 650 700 750 800 850 900 950 1000 1050
Flourescence Intensity
Position in M-gene
Cluster A
Cluster B
Cluster C
M1
1-165aa
166-252aa
M2
1-21aa
22-65aa
76-96aa
Mapped
Not mapped

B

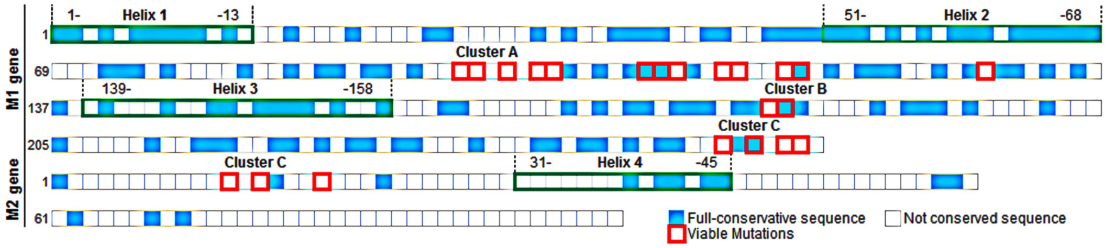
M1 gene
M2 gene
1-
Helix 1
-13
51-
Helix 2
-68
Cluster A
139-
Helix 3
-158
Cluster B
Cluster C
Cluster C
31-
Helix 4
-45
Full-conservative sequence
Viable Mutations
Not conserved sequence

C

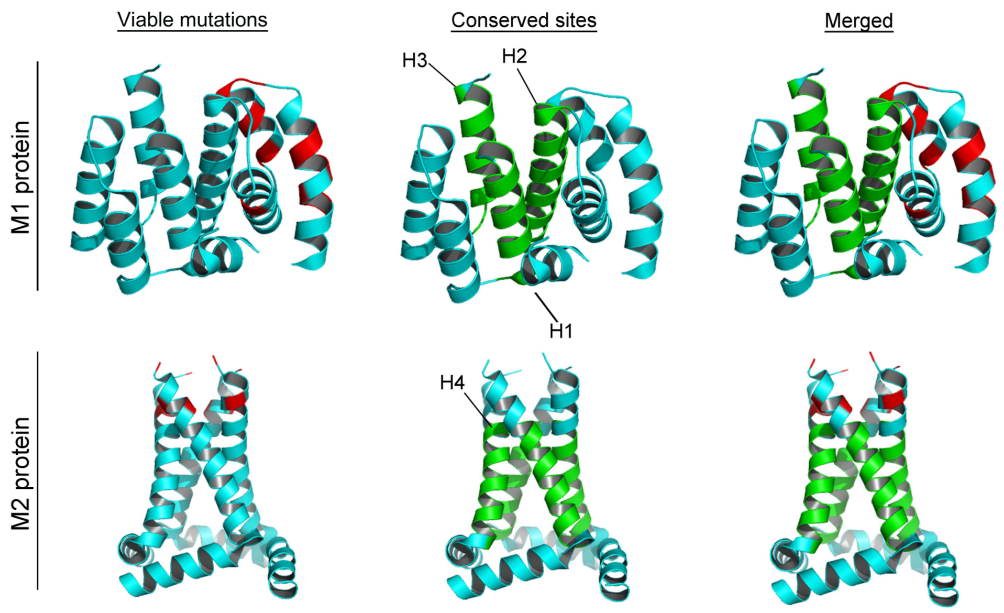
Viable mutations
Conserved sites
Merged
M1 protein
M2 protein
H1
H2
H3
H4

Figure 5-4

A. Regions in the M-gene permissible for growth are delineated in clusters A, B, and C. Regions where structural information is available and mapped are shown in green. Regions where structural information was unavailable are colored grey.
B. M1 and M2 across 300 strains of influenza in the NCBI influenza database were compared by sequence alignment. Red box indicate clusters A, B, and C identified through *in vitro* genotyping that were permissible to viral growth. Fully conserved amino acid against all known human H1N1 M1 and M2 genes are shown in blue, whereas not fully conserved are shown in white. Conserved helices are boxed in green (Helix 1,2,3, and 4).
C. Conserved and viable mutations in the M-gene were mapped to crystal structure of the monomeric M1 gene (PDB accession ID, 2Z16) and the tetrameric M2 gene (PDB accession ID, 2L0J). Mutations permissive to viral growth, selected from the genotyping profile, are shown in red. Conservative sites (Helix1, 2, 3 and 4) from the M1 and M2 genes are shown in green.

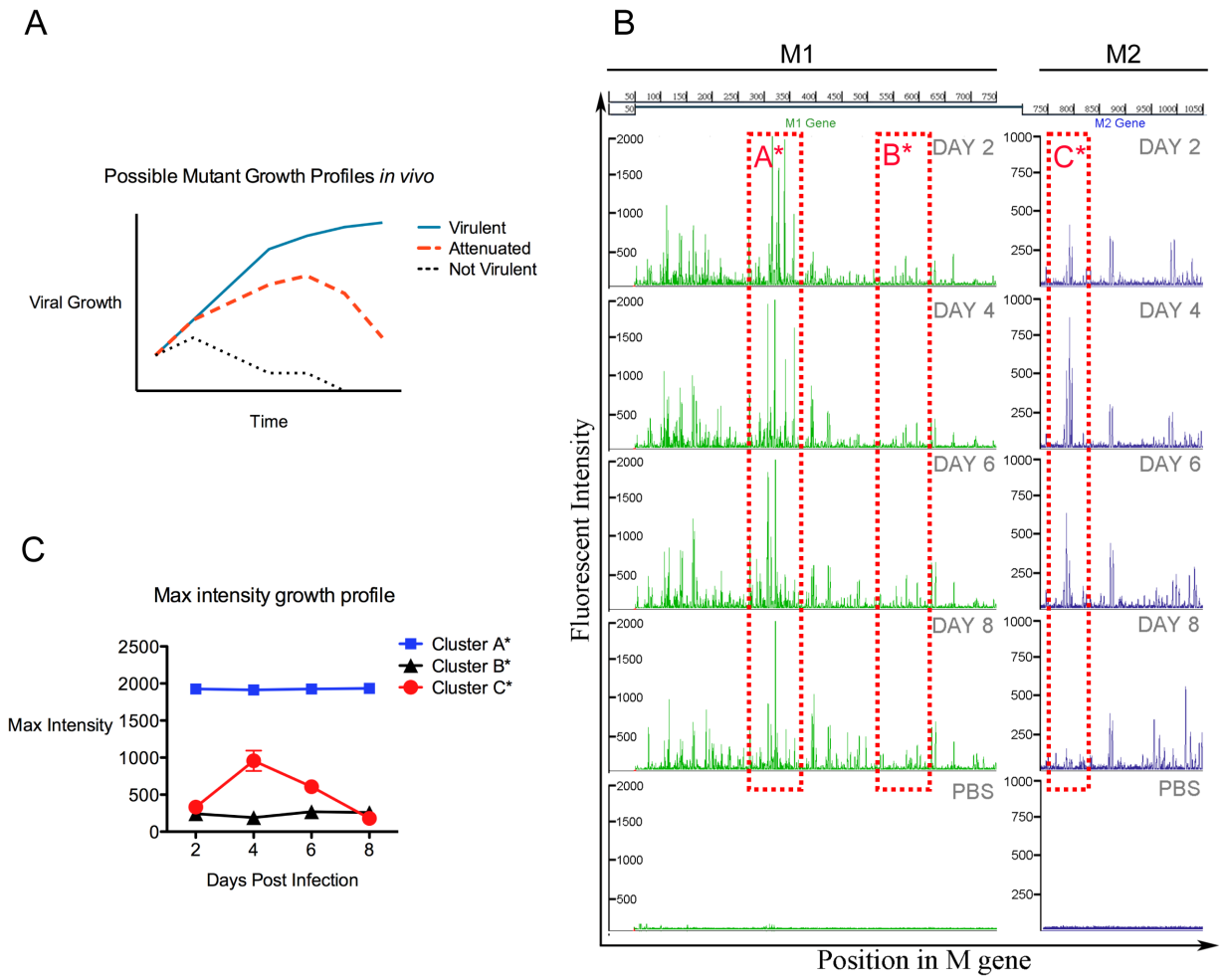

Figure 5-5

A. Schematic of hypothetical growth profiles of virulent, attenuated, and non-virulent viruses
B. Mice were infected with total mixed pool of M-gene mutants by i.t. Lungs were harvested at indicated days post infection and processed for genotyping. Lung homogenates from PBS-injected mice served as negative control. Clusters A*, B*, and C* correspond to Cluster A, B, and C from Fig. 5-3B.
C. The max intensity of Cluster A*, B*, and C* in part B were plotted with respect to time.

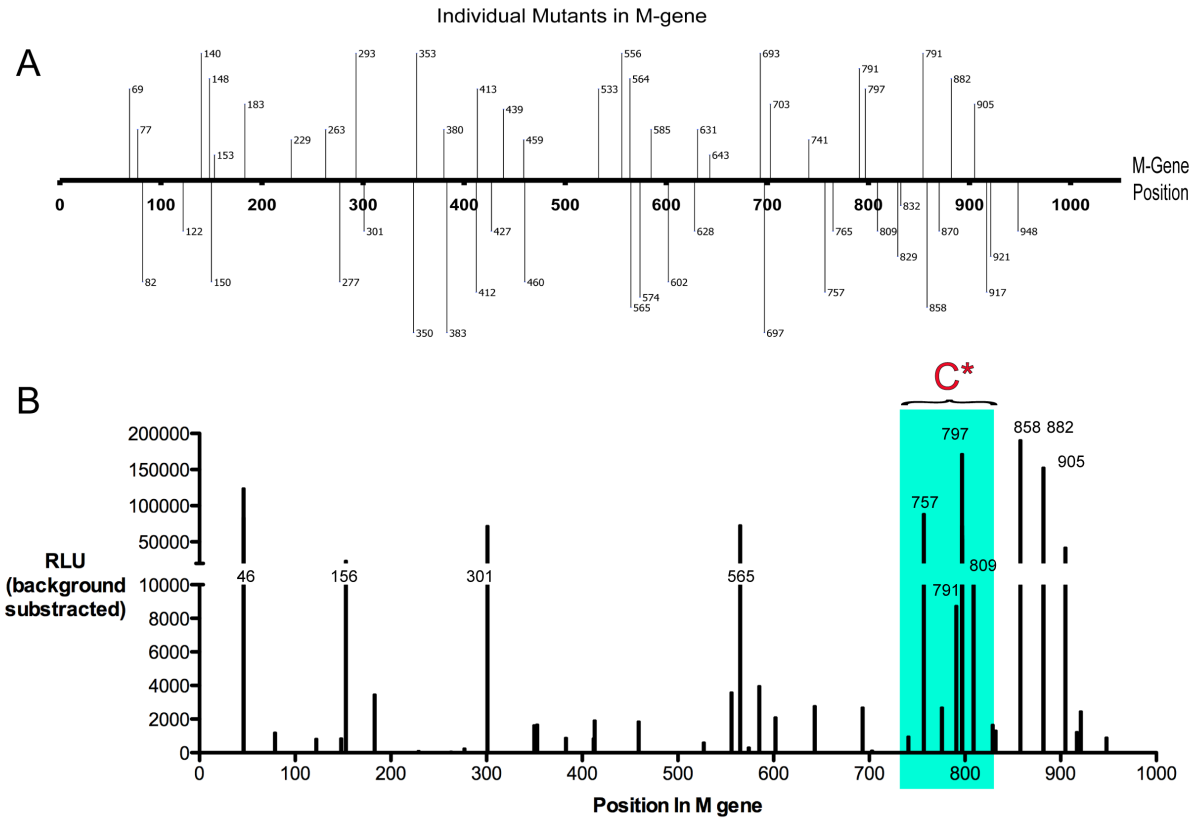

Figure 5-6

A. Schematic of position of 67 individual mutant clones that were isolated across the M-gene during initial mutagenesis.
B. 67 individual mutants were transfected with 7 other plasmids in HEK293Ts. Supernatants were collected after 48hrs and re-infected onto a reporter cell line that expresses Gaussia luciferase (gLuc) under a flu PA-promoter, which is an indirect a measure of infectious mutant flu (See methods).

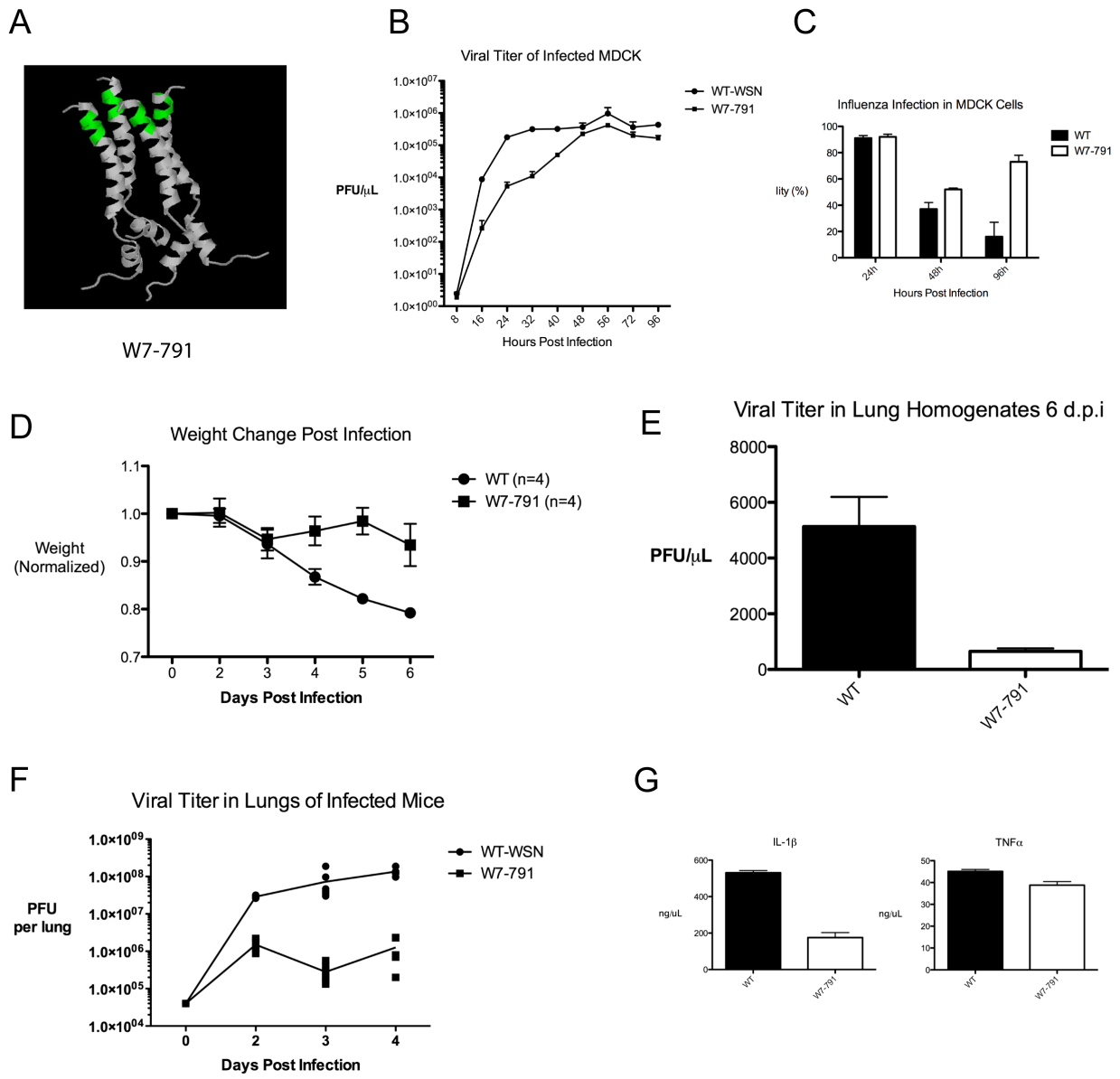

Figure 5-7

A. The insertion position of W7-791 was mapped on to the known M2 structure
B. *In vitro* characterization of WT-WSN and W7-791. MDCK cells were infected at equal MOI (0.25) of both viruses and the titer of virus at various time points was determined.
C. Cell viability of WT-WSN and W7-791 infected MDCK cells was determined by LDH assay.
D. Mice were infected with $4x10^4$ pfu of WT-WSN or W7-791. Weight of mice infected with WT-WSN and W7-791 ($4x10^4$pfu) were measured at indicated days after infection
E. All WT-WSN infected mice died after 6 days. Viral titer of lung homogenates from WT-WSN and W7-791 infected mice was determined 6 days post infection.

F. Viral titer in lung homogenates was determined in the first 4 days of infection (n=4 in each group).
G. Serum IL-1β and TNF-α from mice 6dpi was measured by ELISA.

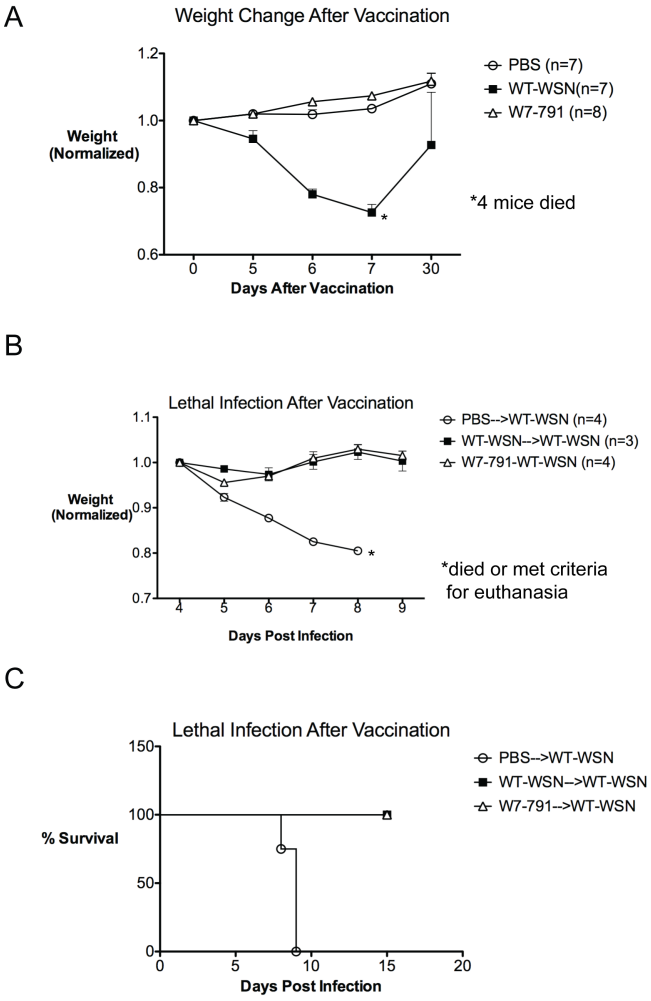

Figure 5-8

A. Mice were infected with 5000pfu of WT-WSN or W7-791 as a vaccination regimen. The weights of the mice were measured at indicated days after infection.
B. One month after initial vaccination, mice were infected with lethal dose of WT-WSN (10^4pfu). The weight of mice were recorded on indicated days after infection
C. Survival curve of mock- and vaccinated mice after lethal challenge with WT-WSN

A

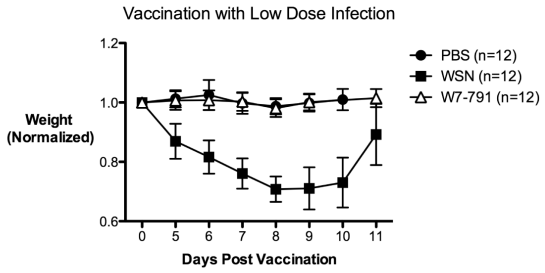
Vaccination with Low Dose Infection
Weight (Normalized)
Days Post Vaccination
PBS (n=12)
WSN (n=12)
W7-791 (n=12)

B

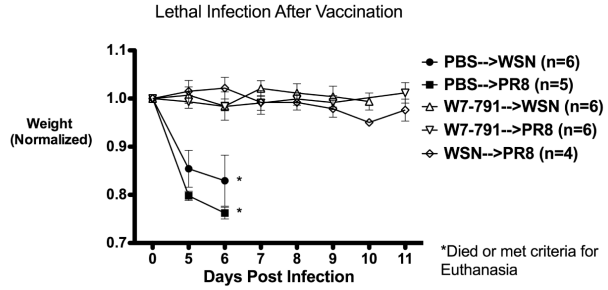
Lethal Infection After Vaccination
Weight (Normalized)
Days Post Infection
PBS-->WSN (n=6)
PBS-->PR8 (n=5)
W7-791-->WSN (n=6)
W7-791-->PR8 (n=6)
WSN-->PR8 (n=4)
*Died or met criteria for Euthanasia

C

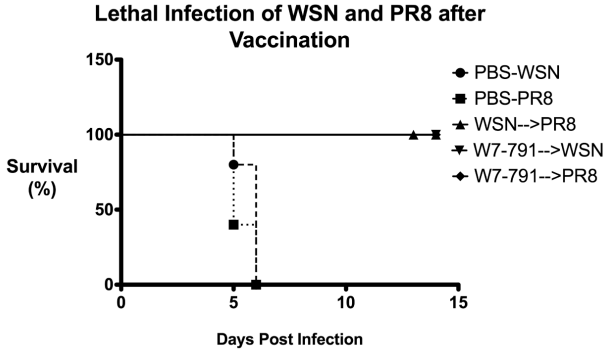
Lethal Infection of WSN and PR8 after Vaccination
Survival (%)
Days Post Infection
PBS-WSN
PBS-PR8
WSN-->PR8
W7-791-->WSN
W7-791-->PR8

D

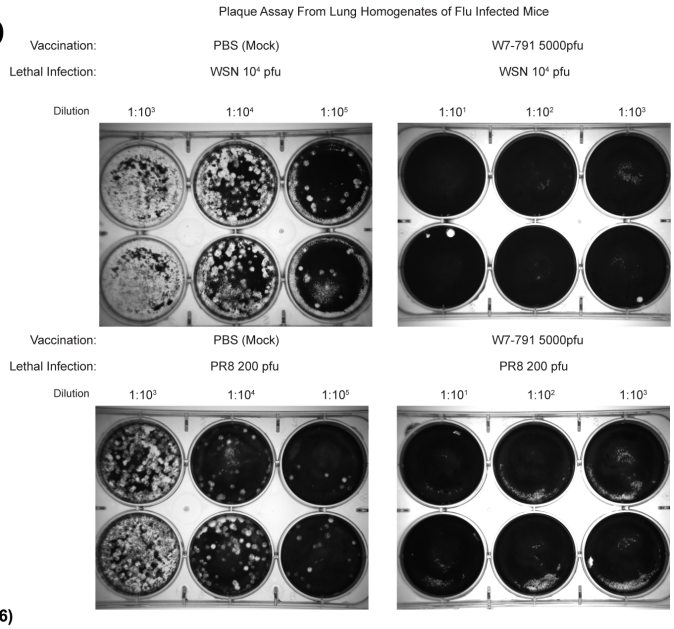
Plaque Assay From Lung Homogenates of Flu Infected Mice
Vaccination: PBS (Mock)
Lethal Infection: WSN 10⁴ pfu
Vaccination: W7-791 5000pfu
Lethal Infection: WSN 10⁴ pfu
Dilution 1:10³ 1:10⁴ 1:10⁵ 1:10¹ 1:10² 1:10³
Vaccination: PBS (Mock)
Lethal Infection: PR8 200 pfu
Vaccination: W7-791 5000pfu
Lethal Infection: PR8 200 pfu
Dilution 1:10³ 1:10⁴ 1:10⁵ 1:10¹ 1:10² 1:10³

E

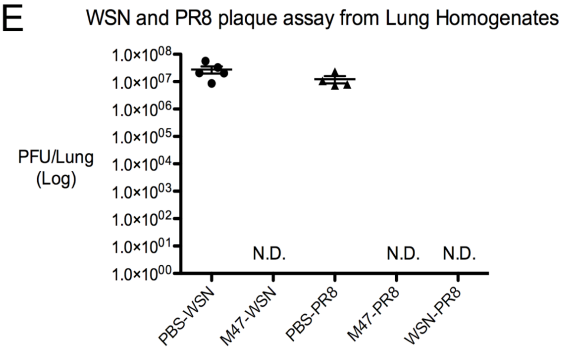
WSN and PR8 plaque assay from Lung Homogenates
PFU/Lung (Log)
N.D.
N.D.
N.D.
PBS-WSN
M47-WSN
PBS-PR8
M47-PR8
WSN-PR8

F

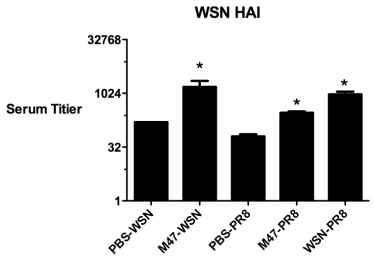
WSN HAI
Serum Titier
PBS-WSN
M47-WSN
PBS-PR8
M47-PR8
WSN-PR8

G

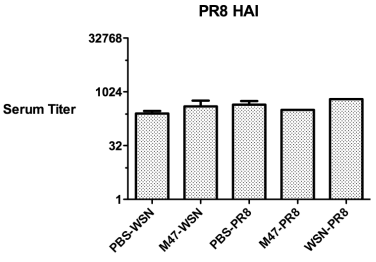
PR8 HAI
Serum Titer
PBS-WSN
M47-WSN
PBS-PR8
M47-PR8
WSN-PR8

Figure 5-9

A. Mice were infected with 5000pfu of WT-WSN or W7-791 as a vaccination regimen. The weights of the mice were measured at indicated days after infection.
B. Vaccinated mice were subsequently challenged with lethal dose of WT-WSN (10000pfu) or PR8 (200pfu) influenza strains. The weights of the mice were measured at indicated days after infection.
C. Survival curve of mock- and vaccinated mice after lethal challenge with WT-WSN or PR8
D. Lung of mock- and vaccinated- mice after lethal challenge were collected at the time of death or euthanasia. Viral titer was determined by plaque assay and representative images are shown.
E. Viral titer in lung homogenates of individual mice was quantified by plaque assay.
F. HA-inhibition assay against WSN. Serum from all groups of infected mice was tested for presence of anti-HA antibodies that inhibit WSN-agglutinated RBCs.
G. HA-inhibition assay against PR8. Serum from all groups of infected mice was tested for presence of anti-HA antibodies that inhibit PR8-agglutinated RBCs.

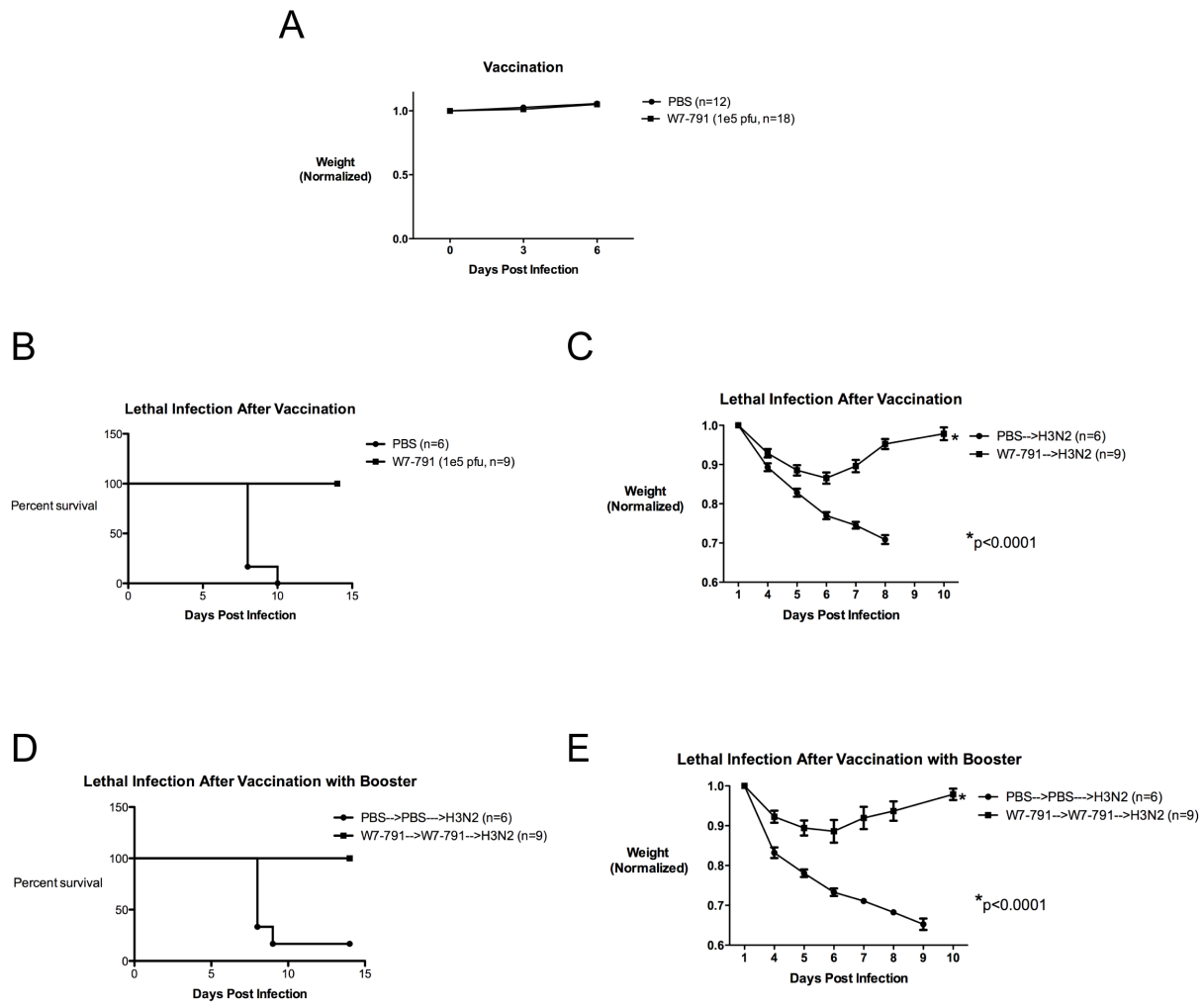

Figure 5-10

A. Weight of mice after mock vaccination or vaccination with 10^5 PFU of W7-791.
B. Survival of mice that were challenged with lethal infection of H3N2/Victoria 5 weeks after vaccination.
C. Weight change of mice described in part B
D. Survival of mice lethally challenged with H3N2 5 weeks after vaccination and also received a booster of 10^5 PFU of W7-791 on day 14.
E. Weight change of mice described in part D.

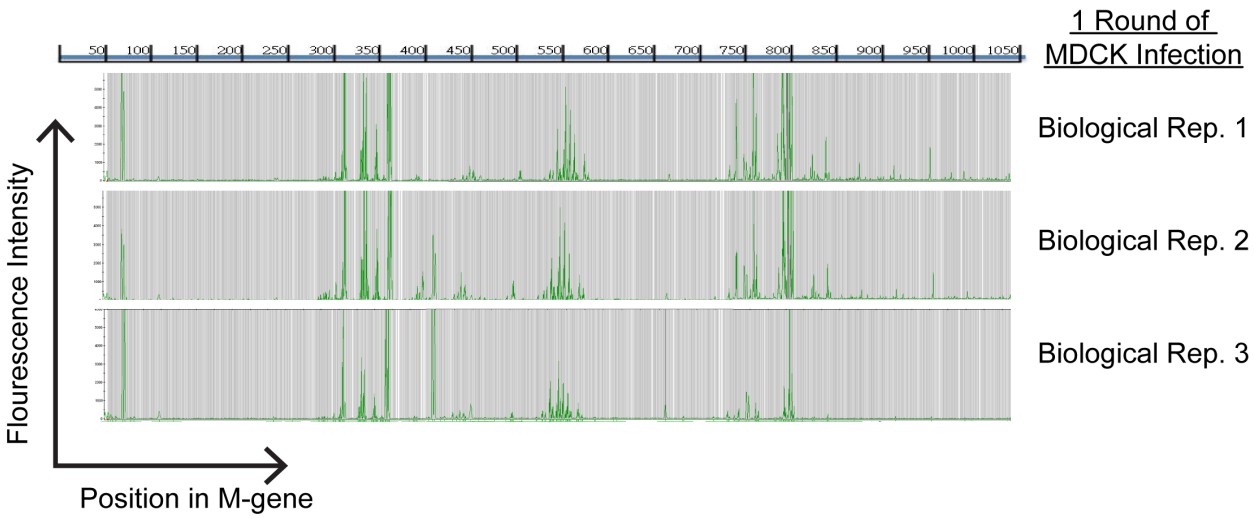

Supplementary Figure S5-1

Total mutant library was transfected with other segments of the influenza genome into HEK293T and subsequently passaged for 2 generations in MDCK. Here, genotyping data from three biological repeats are shown (G2-T1, G2-T2, and G2-T3).

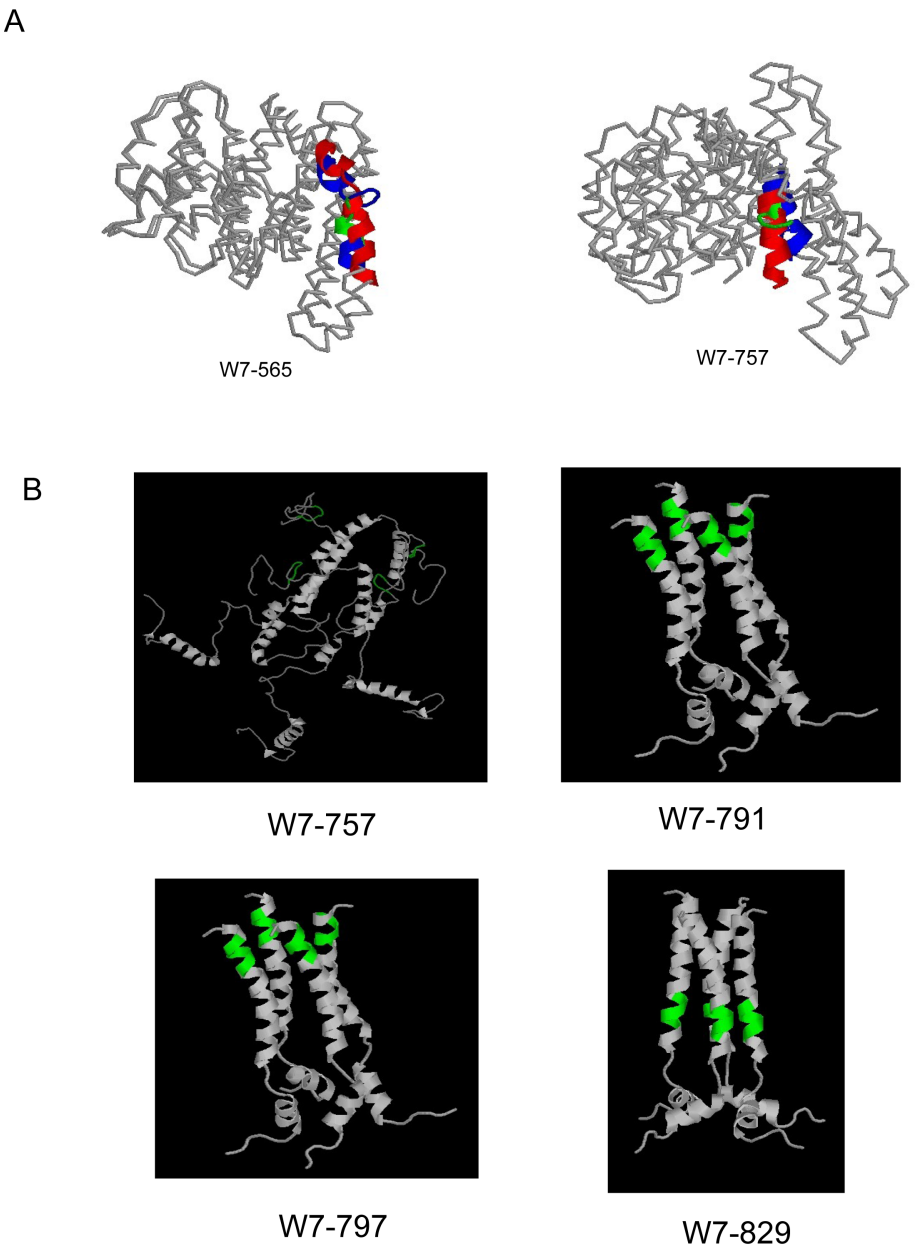

Supplementary Figure S5-2

A. W7-565 and W7-757 were mapped on to structure of influenza M1 protein. Red regions correspond to wild-type structure. Green region represents the 15nt insertion. Blue region represent the mutant structure after insertion.
B. Modeling of W7-757, W7-791, W7-797, W7-809, and W7-829 on the structure of influenza M2 protein. The green region represents the insertion location.

A

```
WT-M2              1 ATGAGTCTTCTAACCGAGGTCGAAACGCCTATCAGAAACGAATGGGGGTG     50
                     ||||||||||||||||||||||||||||||||||||||||||||||||||
W7-791             1 ATGAGTCTTCTAACCGAGGTCGAAACGCCTATCAGAAACGAATGGGGGTG     50

WT-M2             51 CAGATGCAACGATTCAAGTGATCCTC---------------TCGTCATTG     85
                     |||||||||||||||||||||||||               |||||||||
W7-791            51 CAGATGCAACGATTCAAGTGATCCTCgtcattgcggccgcaTCGTCATTG    100

WT-M2             86 CAGCAAATATCATTGGAATCTTGCACTTGATATTGTGGATTCTTGATCGT    135
                     |||||||||||||||||||||||||||||||||||||||||||||||||||
W7-791           101 CAGCAAATATCATTGGAATCTTGCACTTGATATTGTGGATTCTTGATCGT    150

WT-M2            136 CTTTTTTTCAAATGCATTTATCGTCGCCTTAAATACGGTTTGAAAAGAGG    185
                     |||||||||||||||||||||||||||||||||||||||||||||||||||
W7-791           151 CTTTTTTTCAAATGCATTTATCGTCGCCTTAAATACGGTTTGAAAAGAGG    200

WT-M2            186 GCCTTCTACGGAAGGAGTGCCAGAGTCTATGAGGGAAGAATATCGAAAGG    235
                     |||||||||||||||||||||||||||||||||||||||||||||||||||
W7-791           201 GCCTTCTACGGAAGGAGTGCCAGAGTCTATGAGGGAAGAATATCGAAAGG    250

WT-M2            236 AACAGCAGAATGCTGTGGATGTTGACGATGGTCATTTTGTCAACATAGAG    285
                     |||||||||||||||||||||||||||||||||||||||||||||||||||
W7-791           251 AACAGCAGAATGCTGTGGATGTTGACGATGGTCATTTTGTCAACATAGAG    300

WT-M2            286 CTGGAGT    292
                     |||||||
W7-791           301 CTGGAGT    307
```

B

```
WT-M2              1 MSLLTEVETPIRNEWGCRCNDSSDP-----LVIAANIIGILHLILWILDR     45
                     |||||||||||||||||||||||||     :||||||||||||||||||||
W7-791             1 MSLLTEVETPIRNEWGCRCNDSSDPRHCGRIVIAANIIGILHLILWILDR     50

WT-M2             46 LFFKCIYRRLKYGLKRGPSTEGVPESMREEYRKEQQNAVDVDDGHFVNIE     95
                     ||||||||||||||||||||||||||||||||||||||||||||||||||||
W7-791            51 LFFKCIYRRLKYGLKRGPSTEGVPESMREEYRKEQQNAVDVDDGHFVNIE    100

WT-M2             96 LE     97
                     ||
W7-791           101 LE    102
```

Supplementary Figure S5-3

A. M2 Nucleotide sequence alignment of wild-type (WT) and W7-791 M2-gene
B. M2 Protein sequence alignment of WT and W7-791 M2.

MATERIALS AND METHODS

Cell culture and Reagents

HEK293T cells were cultured in Dulbecco's modified Eagle's medium supplemented with 5% heat-inactivated fetal bovine serum (FBS). Madin-Darby canine kidney (MDCK) cells were maintained in Dulbecco's minimal essential medium (DMEM) containing 5% fetal bovine serum, penicillin/streptomycin (100 units/ml and 50 μg/ml, respectively), and 1 mM sodium pyruvate at 37°C with 5% CO2. Bone marrow macrophages were derived from bone marrow of mice grown in RPMI-1640 containing 10ng/mL M-CSF, 10% FBS and penicillin/streptomycin after 7 days.

Animals

C57BL/6 mice were purchased from the Jackson Laboratory. All animals were housed in specific pathogen–free conditions within the UCLA animal facilities. All experiments of animals were performed according to NIH policies about the human care and use of laboratory animals and were approved by the UCLA Animal Research Committee.

Virus generation and Titer Measurement:

A DNA transfection system in generating influenza A/WSN/33 from eight plasmids was applied(Hoffmann et al., 2000). The 8 plasmids in generating influenza A virus and GFP reporter vector were obtained from Dr. Yuying Liang(Emory University). The 8 plasmids containing the cDNA of the influenza virus A/WSN/33 (H1N1) transfected into HEK293Ts with TransIT LT-1 (Panvera, Madison, WI) by manufacture's protocol.

H3N2 A/Victoria/3/75 was a gift from Dr. Ioanna Skountzou at Dept. of Microbiology and Immunology in Emory University.

Viral titer was determined by luminescence assay or by plaque assay. For the luminescence assay, a luciferase reporter under the influenza PA promoter was designed. The reverse complementary sequence of the Gaussia luciferase (gLuc) coding region was inserted between a human RNA polymerase I promoter and a murine RNA polymerase I terminator. The gLuc coding sequence was flanked by the UTRs from the PA segment of influenza virus A/WSN/33 strain so that gLuc expression is dependent on influenza virus infection. The gLuc reporter was transfected into HEK293Ts for 24hours and the supernatants containing mutant or wild-type flu was infected onto the reporter cells. Upon active infection, gLuc is released into the supernatants and can be quantified with renilla luciferase substrate (Promega). Plaque assay was performed MDCK cells and calculated as plaque forming unit per uL (pfu/uL) of supernatant. The viral samples were serially diluted in dilution buffer (PBS with 10% BSA, $CaCl_2$, 1% DEAE-dextran, and $MgCl_2$). Diluents were infected onto monolayer of MDCK cells 6-well plates for 1 hour at 37°C and then covered with a growth medium containing 0.6% low-melting agarose and TPCK-treated trypsin (0.7 μg/ml). Infected cells were stained by after 48 hours (1% crystal violet, 20% ethanol, in PBS) to visualize the plaques.

Generation of M gene mutant Plasmid Library and Functional Profiling

To create the mutant plasmid library of M gene of influenza A virus /WSN/33, 15-nt insertion randomly was carried out *in vitro* by Mu-transposon mediated mutagenesis (MGS kit, Finnzymes) according to manufacturer's instructions. This resulted in a mutant library having a15-nt sequent insertion, 5'-NNNNNTGCGGCCGCA-3' (N: duplicated 5 nucleotides from target DNA), inserted randomly in the M gene plasmid of

influenza A virus. The M-gene mixed mutant pool was transfected by electroporation DH10B by Electroporation (ElectroMax ^{TM} DH10B,Invitrogen) at 2.0kV, 200Ω, 25μF.

Mutant M gene and other seven plasmids were transfected concomitantly to the HEK293T for virus generation. Three days after transfection, the supernatant was collected and re-infected to the MDCK cell for two days. The process was repeated for four generation. RNA was isolated with the TRIzol reagent (Invitrogen) after each generation. For infection *in vivo,* the mutant virus pool was titered, concentrated by ultra-centrifugation and infected in mice. After 2 days, the lungs were harvested, homogenized, and resuspended in TRIzol for RNA. After RNA isolation, reverse transcription-PCR was carried o by iScript^{TM} cDNA Synthesis kit (Bio-Rad). Three gene-specific forward primers approximate 400bp apart in the M-gene (5'-AGCAAAAGCAGGTAGATATT-3', 5'-GGGGCCAAAGAAATAGCACT-3', 5'-TCCTAGCTCCAGTGCTGGTC-3') and Vic-labeled insertion-specific mini-primer (5'-TGCGGCCGCA -3') were used to amplify fragments containing the 15nt insert with KOD Hot-Start polymerase (Novagen). The PCR conditions were set on 95℃ for 10 min (1 cycle), 95℃ for 45sec, 52℃ for 30sec and 72℃ for 90sec (30 cycles), and 72℃ for 10 min (1 cycle). The fluorescent labeled PCR products were analyzed in duplicate with Liz-500 size standard (Applied Biosystems) by using a 96-capillary genotyper (3730xl DNA Analyzer, Applied Biosystems) at the UCLA GenoSeq Core facility

Intra-trachea(i.t.) inoculation.

Mice were anesthetized by intraperitoneal (i.p.) injection of ketamine and xylazine mixture. The trachea was surgically exposed and 30 µl of inoculums was administered into the tracheal with a sterile 27-gauge needle(Shahangian et al., 2009).

Cell Viability Assays

Cell viability was measured by CytoTox 96 Non-Radioactive Cytotoxicity Assay (Promega) according to manufacture's instructions.

ELISA

IL-1β and TNF ELISA kits were purchased from R&D Biosciences and the cytokine levels were evaluated according to the manufacturer's instructions.

Hemagglutination inhibition (HI) assay.

WSN and PR8 at a concentration high enough to cause agglutination of sheep RBCs. Serial dilutions of serum are then added to agglutinated RBCs. Higher anti-HA antibody in the serum would inhibit agglutination at a higher dilution. Antibody titer is represented as the inverse of the dilution factor (Katz et al., 2009).

REFERENCES

Arumugaswami, V., Remenyi, R., Kanagavel, V., Sue, E.Y., Ngoc Ho, T., Liu, C., Fontanes, V., Dasgupta, A., and Sun, R. (2008). High-Resolution Functional Profiling of Hepatitis C Virus Genome. PLoS Pathog *4*, e1000182.

Belshe, R.B., Edwards, K.M., Vesikari, T., Black, S.V., Walker, R.E., Hultquist, M., Kemble, G., and Connor, E.M. (2007). Live Attenuated versus Inactivated Influenza Vaccine in Infants and Young Children. New England Journal of Medicine *356*, 685–696.

Boni, M.F., de Jong, M.D., van Doorn, H.R., and Holmes, E.C. (2010). Guidelines for Identifying Homologous Recombination Events in Influenza A Virus. PLoS ONE *5*, e10434.

Cox, R.J., Brokstad, K.A., and Ogra, P. (2004). Influenza Virus: Immunity and Vaccination Strategies. Comparison of the Immune Response to Inactivated and Live, Attenuated Influenza Vaccines. Scandinavian Journal of Immunology *59*, 1–15.

Hoffmann, E., Neumann, G., Kawaoka, Y., Hobom, G., and Webster, R.G. (2000). A DNA transfection system for generation of influenza A virus from eight plasmids. Proc Natl Acad Sci U S A *97*, 6108–6113.

Ilyinskii, P.O., Gambaryan, A.S., Meriin, A.B., Gabai, V., Kartashov, A., Thoidis, G., and Shneider, A.M. (2008). Inhibition of influenza M2-induced cell death alleviates its negative contribution to vaccination efficiency. PLoS One *3*, e1417.

Iwatsuki-Horimoto, K., Horimoto, T., Noda, T., Kiso, M., Maeda, J., Watanabe, S., Muramoto, Y., Fujii, K., and Kawaoka, Y. (2006). The cytoplasmic tail of the influenza A virus M2 protein plays a role in viral assembly. J Virol *80*, 5233–5240.

Katz, J., Hancock, K., Veguilla, V., Zhong, W., Lu, X., Sun, H., Butler, E., Dong, L., Liu, F., Li, Z., et al. (2009). Serum cross-reactive antibody response to a novel influenza A (H1N1) virus after vaccination with seasonal influenza vaccine. MMWR Morb Mortal Wkly Rep *58*, 521–524.

Lamb, R.A., Lai, C.J., and Choppin, P.W. (1981). Sequences of mRNAs derived from genome RNA segment 7 of influenza virus: colinear and interrupted mRNAs code for overlapping proteins. Proc Natl Acad Sci U S A *78*, 4170–4174.

Lee, L.Y.-H., Ha, D.L.A., Simmons, C., de Jong, M.D., Chau, N.V.V., Schumacher, R., Peng, Y.C., McMichael, A.J., Farrar, J.J., Smith, G.L., et al. (2008). Memory T cells established by seasonal human influenza A infection cross-react with avian influenza A (H5N1) in healthy individuals. J Clin Invest *118*, 3478–3490.

McCown, M.F., and Pekosz, A. (2005). The influenza A virus M2 cytoplasmic tail is required for infectious virus production and efficient genome packaging. J Virol *79*, 3595–3605.

McCown, M.F., and Pekosz, A. (2006). Distinct domains of the influenza a virus M2 protein cytoplasmic tail mediate binding to the M1 protein and facilitate infectious virus production. J Virol *80*, 8178–8189.

Neumann, G., Noda, T., and Kawaoka, Y. (2009). Emergence and pandemic potential of swine-origin H1N1 influenza virus. Nature *459*, 931–939.

Schnell, J.R., and Chou, J.J. (2008). Structure and mechanism of the M2 proton channel of influenza A virus. Nature *451*, 591–595.

Shahangian, A., Chow, E.K., Tian, X., Kang, J.R., Ghaffari, A., Liu, S.Y., Belperio, J.A., Cheng, G., and Deng, J.C. (2009). Type I IFNs mediate development of postinfluenza bacterial pneumonia in mice. J Clin Invest *119*, 1910–1920.

Steel, J., Lowen, A.C., Pena, L., Angel, M., Solorzano, A., Albrecht, R., Perez, D.R., Garcia-Sastre, A., and Palese, P. (2009). Live Attenuated Influenza Viruses Containing NS1 Truncations as Vaccine Candidates against H5N1 Highly Pathogenic Avian Influenza. J. Virol. *83*, 1742–1753.

Tompkins, S.M., Zhao, Z.S., Lo, C.Y., Misplon, J.A., Liu, T., Ye, Z., Hogan, R.J., Wu, Z., Benton, K.A., Tumpey, T.M., et al. (2007). Matrix protein 2 vaccination and protection against influenza viruses, including subtype H5N1. Emerg Infect Dis *13*, 426–435.

Webby, R., Perez, D., Coleman, J., Guan, Y., Knight, J., Govorkova, E., McClain-Moss, L., Peiris, J., Rehg, J., Tuomanen, E., et al. (2004). Responsiveness to a pandemic alert: use of reverse genetics for rapid development of influenza vaccines. The Lancet *363*, 1099–1103.

Zebedee, S.L., and Lamb, R.A. (1988). Influenza A virus M2 protein: monoclonal antibody restriction of virus growth and detection of M2 in virions. J Virol *62*, 2762–2772.

CONCLUSIONS

We set out to understand the basis of IFN antiviral function in a comprehensive way. We began with identification of type-I and -II IFN-stimulated genes by microarray study showing that they induce common and distinct sets of ISGs. Under an equivalent biological input, type-I IFN induced more ISGs than type-II IFN. To further understand the basis of their anti-viral function, we functionally screened through 288 ISGs for their antiviral effect against a RNA and DNA virus. No ISG was capable of inhibiting viruses more than IFN, suggesting that many ISGs are induced to create a cumulative anti-viral effect. Moreover, the antiviral effect of ISGs is specific toward certain viruses. Specifically, we showed that BMP2 inhibited growth of MHV68 but not VSV, whereas Tap1 suppressed VSV growth and not MHV68.

Based on the screen, cholesterol-25-hydroxylase emerged as an ISG inhibitory against VSV and MHV68 replication. Ch25h inhibited viral infection by production of a soluble anti-viral factor that is not IFN but rather an oxysterol, 25-hydroxycholesterol. It was broadly inhibitory against various enveloped viruses including HIV, VSV, HSV, EBOV, and RVFV. Further mechanistic study showed that 25HC inhibited viral entry in VSV and HIV. Functional loss of Ch25h cause increased susceptibility to viral infections *in vitro* and *in vivo*. Moreover, administration of 25HC reduced HIV viral load and T-cell-depletion in humanized mice, introducing oxysterols and membrane-modifying compounds as potential therapeutics against acute viral infections.

We have also explored the regulation of retinoid-X-receptors on host response against viral infection. Previous study has shown that viral infection causes host cell to down-regulate RXR expression, yet it remains unclear what is the purpose of RXR

down-regulation during infection. Under the hypothesis that RXR may act as a suppressor of immune response against viral infection, we found that overexpression and ligand-activation of RXR promoted viral infection. By gene expression profile study, we observed that RXR activation suppressed many types of IFN and IFN-induced genes. Moreover, RXR inhibited critical IFN activators, IRF3 and NFκB. These results demonstrated RXR as negative regulator of IFN and inflammatory signaling pathways as well as a suppressor of host anti-viral response.

While the mains studies focused host response against viral infections, we further utilized tools in molecular virology to improve antiviral immunity. The last study described an approach to develop novel attenuated vaccines. Unlike traditional selection processes that select for the mutants in non-physiological conditions, this vaccine strategy directly finds attenuated mutants. We generated high-density mutations in influenza M-gene and tracked the growth of the mutant pool population *in vivo* and searched for specific populations that exhibited an expected attenuated growth profile. This method led us to find the mutant clone W7-791, which did not cause sickness in mice at 100 times LD50. Most importantly, it conferred protection against similar and disparate phylogenic groups of influenza. This unbiased strategy may be particularly useful for finding new live-attenuated vaccines for emerging strains of virus.

Future Directions and Perspectives

The effector functions of interferon-stimulated genes are still an emerging subject in the field innate immunity. Their diverse functions that have co-evolved with viruses lend opportunities to understand basic host-pathogen interactions. Moreover, they introduce novel antiviral strategies. The identification of the antiviral function of 25-hydroxycholesterol introduces the potential for new class of viral entry inhibitors. Chemical screens have identified compounds that inhibit viral membranes, however, cellular membrane modifiers as antiviral agents remain unexplored. The use of natural oxysterols, or their derivatives, may be broadly effective while relatively non-toxic compared to artificial compounds. Detailed studies on the functions of other ISGs and their antiviral specificity may eventually lend to therapies that circumvent the need for interferon and its negative side effects.

The crosstalk between innate immunity and cellular metabolism is appreciated but also complex. While the mechanism of nuclear hormone receptor, RXR, in regulation of host antiviral response remain subject of further study, its suppressive effect on IFN is likely multifold. RXR inhibits IRF3 and NFκB activation of IFNβ promoter suggesting there may be direct interactions with these transcriptional factors. At the same time, activation of RXR seems to inhibit upstream signaling factors such as TBK phosphorylation suggesting an effect on upstream signaling factors. Further study on RXR interaction with signaling factors of IFN would provide insight on metabolic regulation of antiviral immune pathways.

Our approach for live-attenuated vaccine design would need to be validated with reverse genetic systems for other viruses. Mapping of essential and non-essential

regions required for viral growth may provide insight into basic knowledge of individual viruses. By the comprehensive identification of attenuating mutations, one would be able to incorporate combinations of mutations to optimize for vaccine safety and effectiveness.